Redox-Active α-Diimines and Novel Schiff Base Ligands for Uranium Coordination Chemistry

by

Julie E. Niklas

A dissertation submitted to the Graduate Faculty of
Auburn University
in partial fulfillment of the
requirements for the Degree of
Doctor of Philosophy

Auburn, Alabama
May 2, 2020

Keywords: actinide, uranyl, salophen, redox-active, diimine, Schiff base

Approved by

Anne E. V. Gorden, Chair, Associate Professor, Department of Chemistry and Biochemistry
J. V. Ortiz, Ruth W. Molette Professor, Department of Chemistry and Biochemistry
Christian R. Goldsmith, Associate Professor, Department of Chemistry and Biochemistry
Byron H. Farnum, Assistant Professor, Department of Chemistry and Biochemistry
Xinyu Zhang, Associate Professor, Department of Chemical Engineering

Abstract

The use of nuclear power for electricity generation plays a large role in our highly energy-dependent economy, and provides a source of low-emission, renewable energy that is used worldwide. Despite the positive impacts that it has had in lessening our dependence on fossil fuels, it is still a controversial energy source as any accidents that occur in storage, transportation, or on-site at facilities could result in large-scale environmental contamination requiring extensive remediation efforts. Thus, the continued exploration of the chemistry of the actinides is imperative to developing technologies which can improve the safety of nuclear power generation and waste storage. In this context, the coordination chemistry of uranyl (UO_2^{2+}), the most prevalent and environmentally relevant uranium species, is of great interest, especially its selective coordination and bonding interactions. Towards this end, mixed-donor ligands such as salophens have been investigated for the sensing and extraction of uranyl. The need to further investigate fundamental properties of actinide species, such as their redox properties, has prompted the study of several ligand frameworks presented here. The α-diimine ligand “phen-BIAN”which integrates a redox-active backbone with a salophen-like binding pocket, was developed, and its bonding interactions with uranyl studied and compared to uranyl complexes of less-conjugated analogues. These species have rich electrochemistry and intriguing solid-state interactions, indicative of the contribution of ligand conjugation to supporting covalent bonding with uranium. Studies of the ligand “naphthylsalophen” demonstrate that the extension of the π-system leads to an increase in metal-ligand communication, and actinide complexes of bis-salophen ligands have also been characterized. The latter complexes are unique supramolecular actinide complexes, including a dinuclear uranyl species and trinuclear thorium helicate. Another avenue that has been pursued is the use of the hexadentate pyrrole-containing

Schiff base system “pyrrophen” as a softer-donor ligand for favorable coordination of uranyl over other metal ions. This work has shown that this ligand is very well-suited to the linear geometry of the uranyl ion, and its modularity can be exploited for further improvements in its molecular recognition. The findings of these studies provide insight into the some of the unique behaviors exhibited by uranyl that may inform strategic coordination of tetravalent or transuranic actinide species.

Acknowledgments

This dissertation and the years of research which amounted to it do not exist in a vacuum. The past five years have been fueled by the insights, encouragements, and company of others, and were made possible by those who shaped and enabled me long before I started this journey.

I want to extend thanks first and foremost to my parents, Cindy and Frank, who raised me to question my world and have always given me their unconditional love and support. Thank you for everything you have done to help me, and for being on the other end of the phone almost every day for five years. And to my best friend and chosen sister, Bonnie Zimmerman—you have done more over the past decade than you may ever know or give yourself credit for to get me where I am today, and I am so immensely thankful for that. I also want to thank my aunt, Cindy, who likes to remind me to take care of myself first, and my late uncle, Mark, who always inspired me to stay three steps ahead and to never dismiss an opportunity to learn something new. I am also enormously grateful for my four-legged family who gave me a reason to come home from the lab each night, Tounces, who was a life-long friend, and Lewis, who has been my 'island of stability' in her absence.

Before starting my Ph.D., I was lucky enough to have teachers and advisors who were unendingly patient with me, and who helped shape and foster my love for chemistry. I want to thank Zach Matson, my high school chemistry teacher, who still roots for me from the reaches of social media and pings me chemistry jokes and interesting questions about dipoles, and Dr. Colin Abernethy, who incited my love of inorganic chemistry, and has always had advice and encouragement on hand. I am so grateful for their support and for the time they invested in me. Since being at Auburn, I have been fortunate to have Dr. Anne Gorden as an advisor, who has also been patient and understanding, especially when health issues have arisen. I have learned so

much through her mentorship and am incredibly thankful for the creative freedoms she has not just tolerated my indulging in, but supported, and to have been able to develop such a wide skill set in her group. I would also like to acknowledge Dr. John Gorden, who took the time to teach me crystallography, and has been a secondary mentor, and set of eyes and ears. Additionally, I want to thank my committee, Dr. Vince Ortiz, Dr. Chris Goldsmith, Dr. Byron Farnum, and Dr. Xinyu Zhang for helping me complete this journey, and for the knowledge and insights they have imparted to me along the way.

I have been so incredibly fortunate to have gone through this process with a group of people that I am proud to call friends, peers, and colleagues. I want to thank Jessica Krewall, Kara Johnson, Ethan Hiti, and Clay Black not only for helpful academic discussions, but for coffee breaks, fries, baked goods and board game nights, for chicken wings and making sure I never missed a fifty-cent-corndog day, for always being there to lend an ear or a helping hand, and for simply being. I especially want to acknowledge Alex Bredar, who has been an indispensable source of scientific and emotional momentum—I feel privileged to have such a solid friend and conspirator. I also want to thank my undergraduate students, Katherine Hunter and Madeleine Forbes, who have been instrumental in completing projects, and have handled the flux of research exceptionally well. I can only hope they have learned as much from me as I have learned from them.

Much of this research would not have been possible without funding from the Defense Threat Reduction Agency, the Department of Energy, and Auburn University's College of Sciences and Mathematics, and I am grateful for their contributions. I would also like to acknowledge the Graduate School, the Auburn Local Section of the ACS, and the ACS Division of Inorganic Chemistry for their financial support in attending conferences.

Table of Contents

List of Tables

List of Figures and Schemes

List of Abbreviations

ACN	acetonitrile, CH_3CN
Ar	aryl
BIAN	bis(imino)acenaphthene
CAN	ceric ammonium nitrate
CCDC	Cambridge Crystallographic Data Centre
CIF	Crystallographic Information File
CP	coordination polymer
daq	diaminoacenaphthoquinoxaline
DCM	dichloromethane, CH_2Cl_2
DFT	density functional theory
DMF	dimethylformamide, $(CH_3)_2NCHO$
DMSO	dimethylsulfoxide, $(CH_3)_2SO$
en	ethylenediamine
esd	estimated standard deviation
ESI	electrospray ionization
Et_2O	diethyl ether
Et_3N	triethylamine
EtOH	ethanol, CH_3CH_2OH
FT-IR	Fourier Transform Infrared
gbha	glyoxal-bis(hydroxy)anil
HOMO	highest occupied molecular orbital
LUMO	lowest unoccupied molecular obital

MeOH	methanol, CH_3OH
MOF	metal-organic framework
OAc	acetate
RT	room temperature
sal	salicylaldehyde
t-bu	*tert*-butyl
TFA	trifluoroacetic acid
THF	tetrahydrofuran, C_4H_8O
UV	ultraviolet
XRD	X-ray diffraction

Chapter 1

Introduction

The continued development of actinide chemistry, particularly that of uranium, is pertinent to tangible societal and political issues that plague us regarding nuclear waste, such as remediation of environmental contamination[1-2], and the long-term storage or recycling of spent nuclear fuels.[5] Effective management of these waste products is imperative to reaping the benefits of nuclear power, but is unfortunately hindered by the gaps in our fundamental understanding of *f*-element chemistry.[8-9] While the coordination chemistry of much of the *d*-block is considered well-developed and accessible, the same is not true of the 5f-elements, the actinide series. Exploration of the coordination chemistry of uranyl (UO_2^{2+}), which is the most ubiquitous form of uranium encountered in aqueous environments, is vital as it allows for further elucidation of its unique electronic structure and bonding behaviors.[10] In this regard, the strategic design of new ligand systems which bind uranyl and the spectroscopic, structural, and electrochemical properties of the resulting complexes represent a rich and growing field. The work described in this text focuses in large part on the synthesis of redox-non-innocent Schiff base ligands and their implementation as tools for the detailed characterization of the fundamental chemistry of uranyl complexes, as well as investigation of the potential of these frameworks to serve as tunable uranyl sensors. One category of these Schiff bases represents a new class of tetradentate ligands featuring the classically redox-active α-diimine unit, whereas the other category consists of novel derivatives of the well-established and somewhat less electronically-flexible salophen ligand system. Themes addressed across this work include examination of unique interactions of the uranyl oxo moieties in the solid state, evaluation of the impacts of extended ligand conjugation in the equatorial plane on the axial interactions of uranyl, and assessment of how steric and electronic modifications to ligands impact their coordination to uranyl.

Nuclear Energy and Waste

The global energy crisis has been largely accelerated by a long-term dependence on fossil fuels and other non-renewable natural resources. The dwindling supplies of limited these sources and the adverse environmental effects of their extraction demand that increased reliance on cleaner, renewable energy sources be sought. In addition, greater responsibility must be taken for preventing and remediating environmental contamination to limit their impacts. Nuclear power is a controversial energy source—it is arguably one of the most dependable energy sources as it boasts low atmospheric emissions, but as reactors age, rising operational and new-build construction costs impede the continued growth of the industry as a cost-effective fuel source, especially as compared to other renewables.[11-13] Nonetheless, nuclear power still generates more electricity worldwide than wind and solar combined, and the use of nuclear fuels for civilian power generation has contributed significantly to lessening emissions over the last 50 years.[7, 11-14] Accidents are rare, especially in comparison to coal mining, but can be devastating, and highly publicized events such as the 2011 Fukushima-Daiichi meltdown worsen the public perception of nuclear energy.[15-16] Streamlining the safety of storage, transport, and handling of nuclear waste may potentially make nuclear energy a more viable and conventional source; however, to do this, a better understanding of fundamental actinide chemistry, particularly that of uranium, is prerequisite. The current commonly available technology for managing spills is lacking– a Geiger-counter can only detect the presence of radiation, but not distinguish between emission types.[17-18] Existing extraction systems are likewise not 100% successful in distinguishing between actinides or in highly selective extraction.[19] Without an improved understanding of the major actinides, progress in technologies to detect, sense, and remove these elements will not improve sufficiently to streamline the storage and disposal of waste materials. There is a startling dearth of information

regarding the structure and reactivity of actinides, in particular their covalent interactions, though recently researchers have taken more interest in this area, and the field has been developing quickly on this forefront.[20-22]

Nuclear Energy and Waste

Natural uranium consists of ^{238}U (99.275%), ^{235}U (0.720%), and ^{234}U (0.005%), of which ^{235}U is the only fissile isotope,[23] and has nearly four times the radioactivity of ^{238}U.[24] Depleted uranium typically contains 0.20 % ^{235}U (99.80% ^{238}U) , whereas enriched uranium contains up to 4% ^{235}U, and is used as a primary fuel source for nuclear reactors, as it is the only naturally occurring material capable of sustaining a fission chain reaction to produce the necessary energy through the expulsion of neutrons.[23-24] ^{238}U is fertile, and undergoes neutron capture to form ^{239}Pu, another fissile radionuclide— due to the high content of ^{238}U, nearly 60% of the energy in some reactors is derived from this "bred" plutonium.[24] Once these materials have undergone fission, and are no longer usable, the spent fuel rods are removed from the reactors, cooled, and stored. In the United States, nuclear fuel reprocessing is not considered an economically viable option, and nearly all plants keep waste on-site in dry cask storage systems.[25-26] According to the 2019 World Nuclear Industry Status Report, the 415 operational reactors scattered over 36 countries generated 10.2% of the world's electricity in 2018, a share which has been dropping steadily since peaking at 17.5% in 1995 in large part due to the aging reactor fleet (average age 30.3 years).[11] In 2018, nuclear power accounted for approximately 20% of the generated electricity in the United States, and that figure is over 70% for France.[11] One proposed solution for suitable long-term storage of high-level nuclear waste has been actively pursued for decades. The Yucca Mountain facility in southwest Nevada has been proposed as such a site (and billions of dollars have gone into its preparation),

but it has historically been politically controversial and plans to move forward with the project have remained stagnant.[26-28]

Schiff Base Ligands for Actinide Coordination Chemistry and Sensing

Salens (N,N′-bis(salicylidene)ethylenediamines) and salophens (N,N′-bis(salicylidene)-phenylenediamines) are incredibly useful classes of tetradentate Schiff base ligands with O-N-N-O binding pockets. The names are derived from their synthetic precursors as they are prepared from a **sal**icylaldehyde and ethylenediamine (**en**) or **phen**ylenediamine (**Scheme 1.1**).[29] The redox capabilities of these ligands have been exploited for C—C bond formation[30] and the isolation of ligand radical anions,[31] and they have been popular scaffolds for studying the structure and reactivity of uranium species, The mixed aza- and oxo- pocket allows them to bind a wide variety of metal ions, and in cases where the ligand π-system remains fully conjugated, this binding often results in advantageous changes to optical or spectroscopic properties.[32] Though this may make these species suitable for ion sensing applications, their general promiscuity towards Lewis acids is an obstacle to their use as highly-selective sensors. Their synthetic accessibility allows for tuning; however, doing so effectively can be challenging, as both metal identity and small structural changes can have large impacts on coordination, and the synthesis of asymmetric species is quite challenging.[32-33]

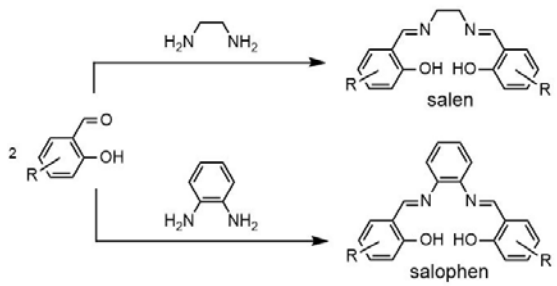

Scheme 1. Synthesis of salens and salophens from salicylaldehydes and diamines.

Previous research in the Gorden group has focused on tuning salqu, a 2-quinoxalinol salen that selectively binds UO_2^{2+}.[34] On complexation, 3,5-di-*tert*-butyl salqu (**Figure 1.1**) was found to distinguish uranyl from many first-row transition metals by UV/Vis and showed promise for use as a chemosensor; however, significant competition was observed for Cu^{2+}, which has a similar charge-to-ionic radius ratio and preferred coordination bite angle.[35] Though the mixed coordination of salqu has been found to be selective for uranyl over lanthanide ions,[35] metal-competition studies and calculated binding constants showed that Cu^{2+} competed considerably with UO_2^{2+} in 20% water/DMF, complicating the use of salqu as an effective UO_2^{2+} sensor in this capacity.[36] Continued investigations into frameworks of this type yielded 'salphenazine', which resulted in greater differentiation of the uranyl UV-Vis signal from transition metal species through extension of the conjugation of the ligand backbone,[37] as well as a non-salen-type Schiff base pentadentate ligand designed for greater selectivity of uranyl by fully occupying its equatorial plane (**Figure 1.1**).[38]

Salen-type ligands have also been shown to provide satisfactory coordination environments for lower-valent actinides, forming 1:1 M:L complexes with solvent or halide ligands occupying the remaining sites,[39] or 1:2 complexes of a variety of geometries.[40-43] The characterization of such

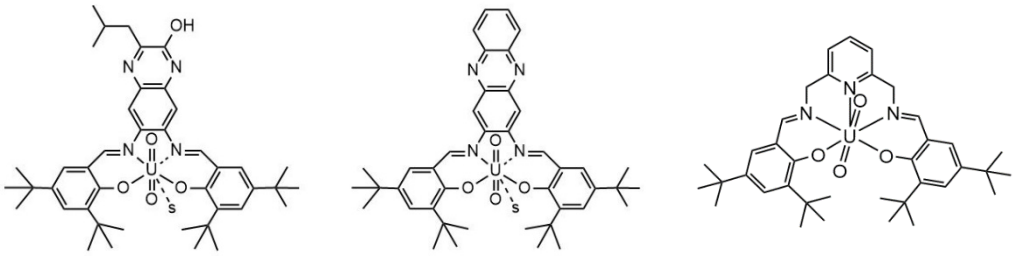

Figure 1. Left to right: Uranyl-salqu complex, uranyl salphenazine complex, pyridine-Schiff base uranyl complex. "**s**" signifies coordinating solvent in the equatorial plane.

complexes has allowed for elucidation of the bonding differences among actinides, as well as among multiple oxidation states of the same actinide.[43-44]

The salophen/Schiff base architecture has also been taken advantage of in larger macrocyclic-type systems. Expanded porphyrin ligands (**Figure 1.2**), which supplement porphyrinoid pyrrole-based pockets with salophen-type diimines, have been shown to be suitable hosts for uranyl and other actinyls (NpO_2^+, PuO_2^+), as they can satisfy the entire equatorial coordination plane of these cations.[7, 45-47] These species have set an important benchmark in regards to sensing: the fixed binding cavities are predisposed in size and geometry for the successful coordination of actinyl cations, and has enabled their use as sensors, but the lack of flexibility in the pocket negatively impacts binding kinetics, and many of these species are synthetically demanding.[45-46] Nonetheless, they have been proven to be useful frameworks for examining fundamental behaviors and bonding interactions of the early-to-mid actinides.[7, 47] Recently, expanded porphyrin complexes of uranyl(VI), U(IV), Th(IV), and Np(IV), which represent the first An(IV) complexes of this type, have been investigated structurally and computationally, showing that covalency of the ligand-metal interaction increases from Th(IV) to Np(IV).[47] Assessment of such properties is vital in the development of chemical systems for the sensing, separation, and extraction of actinides in nuclear waste.

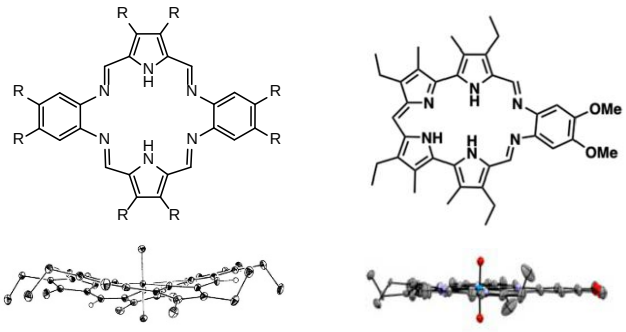

Figure 1.2. Alaskaphyrin[4] (left) and grandephyrin (right),[6-7] and side-on views of uranyl complexes.

Redox-Active Ligands for Uranium

Although salophen-type ligands can coordinate metal cations in multiple oxidation states and do possess enough electronic flexibility to behave in a redox-active fashion, their utilization as redox-active ligands, especially for *f*-elements, is unusual[30, 48-49]. Historically, redox-active, or "redox-non-innocent" ligands of all types have been used extensively for their ability to stabilize transition metals in varied and unusual oxidation states, and to impart catalytic behavior to these systems[50], but their use in actinide complexes is more recent.[2, 51-55] The majority of examples feature the linear uranyl dioxo (UO_2^{2+}) moiety, as this species is incredibly stable. There is a marked deficit of well-characterized lower-oxidation-state uranium complexes, as they are difficult to stabilize.— For example, U(V) readily disproportionates to U(IV) and U(VI), and the strongly reducing character of U(III) is not tolerated by many ligands.[51, 56] The study of these lower-valent species is important with respect to nuclear waste management and understanding their environmental and solution behavior.[57-58] Systems in which the uranyl U(VI)/U(V) redox couple can be studied are of particular interest—for example, the bio-immobilization of the highly water soluble U(VI) by reduction to the insoluble U(IV) is known to proceed through a key pentavalent intermediate, but this process is poorly understood.[2, 59] Complexes which undergo this reduction process or can stabilize U(V) are therefore pertinent to developing a better understanding the reduction of uranyl and the impacts equatorial ligands have on the stability of U(V) (UO_2^{+}) species.[60] Of particular interest is the role that the covalency of equatorial ligands plays in influencing the bonding of the axial oxo ligands of uranyl, and understanding how to manipulate these environments.[61] In this regard, the use of redox-active ligands is a promising tactic for effectively stabilizing and studying low-oxidation state uranium centers, and for the activation and functionalization of the remarkably stable oxo moieties. The inertness of the these oxo ligands

relative to their transition metal counterparts[62] is of interest as it indicates a difference between *d*- and *f*- orbital participation in metal-ligand bonding, particularly in terms of degree of covalent character[63].

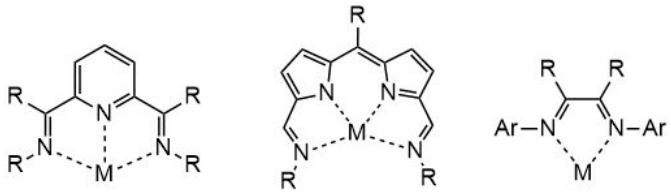

Figure 1.3. General structures of redox-active ligands (left to right: PDI, donor-expanded dipyrrin, α-diimine) and coordination modes. R= H, alkyl, aryl.

Recent work by Bart and coworkers has explored the functionality of the pyridine(diimine) (PDI) ligand framework (**Figure 1.3**) in stabilizing reduced uranium species[55, 64]. Across a series of uranium-$^{Mes}PDI^{Me}$ complexes (Mes= 2,4,6-trimethylphenyl; Me=CH_3), reduction with 1, 2, or 3 equivalents of KC_8 resulted in formally U(IV) complexes bearing di-, tri-[55], and tetraanionic[64] ligands, respectively. Density functional theory (DFT) calculations to characterize the latter revealed that ligand tetraanions were stabilized by dimerization due to π-backbonding interactions of the reduced pyridyl rings with the uranium cations, illustrating the ability of π-acceptor ligands to engage with and support lower-valent uranium centers. [64] This ligand has also been used in the organometallic system Cp*UO_2($^{Mes}PDI^{Me}$) (Cp*= 1,2,3,4,5-pentamethylcyclopentadiene), and its redox activity is implicated in providing a reducing electron towards U-O bond scission upon reductive silylation of the uranyl oxo groups with Me_3SiI[65]. Hayton[66-67] and Arnold[3, 62, 68] have approached oxo-activation and functionalization through reductive silylation and controlled uranyl oxygen-cation interactions, demonstrating the potential of these groups to serve as targets for exploring one of the more fundamental facets of uranium chemistry. Work by the Arnold group has shown that the use of flexible polypyrrolic Schiff base macrocyclic “Pac-man” or “butterfly” ligands allows for sterically forced metal cation-oxo interactions which result in significant

elongation of the *endo* U=O bond, indicating activation (**Figure 1.4**).[3, 10, 69] They have also achieved reduction of uranyl(VI) to U(IV) *via* the oxo groups, assisted by a redox-active donor-expanded dipyrrin ligand (**Figure 1.4**).[2]

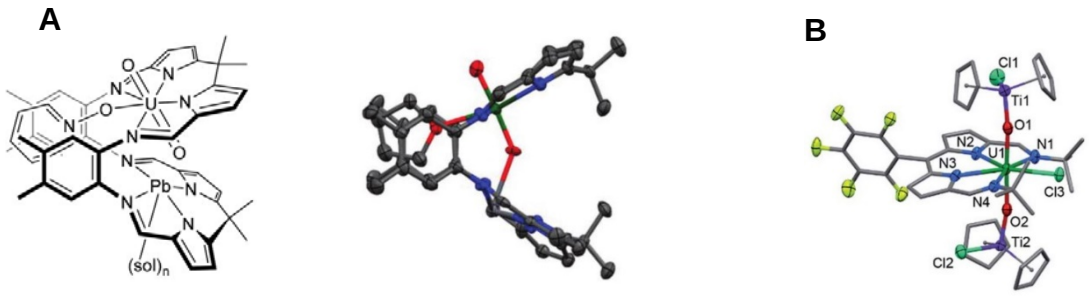

Figure 1.4. (A) Structures of aryl-linked "pac-man" or "butterfly" complexes of uranyl and oxo-cation interaction with the *endo* oxygen[3] and (B) U(IV) dipyrrin complex with Cp_2TiCl-functionalized oxo ligands.[2]

α-Diimine Ligands

The redox-non-innocent α-diimine framework (Figure 3) has been used widely in transition metal chemistry but uranium complexes with redox-active ligands are surprisingly rare[49, 53-54, 70-71], and those that feature the uranyl moiety even more so[2, 72-73]. They have been employed to access

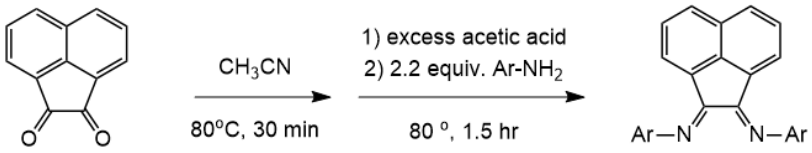

Scheme 1.2. Synthesis of Ar-BIANs such as dpp-BIAN by condensation of acenaphthenequinone with two equivalents of an aniline. In some cases (Ar = mes-, *p*-Cl-, *p*-Me-, and *p*-OMe-), an excess of $ZnCl_2$ or $NiBr_2$ is required, and the resulting complex is then demetallated using K_2CO_3 to yield the free ligand.

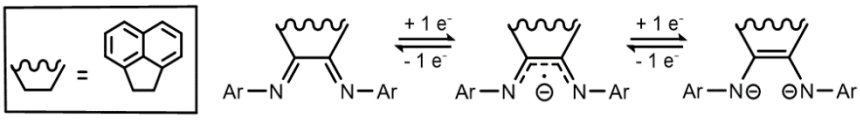

Figure 1.5. Neutral, radical anion, and dianionic ligand oxidation states for Ar-BIAN ligands.

lower-oxidation state uranium centers[53-54], though there are fewer examples than seen for PDI-type ligands. Aryl-BIANs (N,N'-bis[(aryl)imino]acenaphthenes) are redox-non-innocent Schiff base ligands with a general structure consisting of a naphthalene unit fused to an α-diimine system, forming a rigid backbone. These bidentate ligands were first introduced into coordination chemistry in 1991 through the work of Elsevier and coworkers.[74-76] Synthetically, these species are high-yielding and straightforward to prepare, and their steric and electronic properties can be easily tuned through the use of different aryl groups (**Scheme 1.2**).[75] The α-diimine π-orbital system can accept up to two additional electrons upon reduction, forming stable mono- and di-anions[74, 77-78] that can be recognized by their respective C—N and C—C bond lengths in the solid state (**Figure 1.5**).[53, 79] The presence of the radical anion produced by a single-electron reduction can be confirmed by electron paramagnetic resonance (EPR) hyperfine coupling constants, which shows a delocalization of spin density over the N-C-C-N fragment.[74] It is worth noting that while these ligands are predominantly described only as "redox-active," they have also been reported to behave non-innocently[54] in some transition metal complexes due to the similar energies and strong mixing of the metal (dπ) and ligand (pπ) frontier orbitals.[54, 80-81]

Work by Fedushkin and coworkers has shown that the naphthalene π-system can accept an additional two electrons (four total) on reduction of the ligand with sodium metal[77-78]. Sodium complexes of the mono-, di-, tri-, and tetraanions of dipp-BIAN (dpp-BIAN=N,N-bis[(2,6-diisopropylphenyl)imino]acenaphthylene) were isolated, and crystal structures of the latter two showed Na^+ interactions with the naphthalene π-systems, indicating the presence of additional electron density[78]. The EPR signal of the trianion is consistent with coupling of an unpaired electron to 3 distinct pairs of ^1H but no ^{14}N, indicating delocalization over only the naphthalene

unit[77]. Thus, it is presumed that in the course of a four-step reduction, the first two electrons are added into the α-diimine π-system, and the second two to the naphthalene π-system.

The main-group and transition metal chemistry of these complexes has been well-established for some time, but the first examples of *f*-element Ar-BIAN species first appeared in 2007, and since then only a few examples have been reported.[82] These include lanthanide complexes exhibiting 0, 1, and 2-electron transfers as a result of R-group and steric tuning (2007)[83], as well as U(IV)/(III) redox-couples[54]. Kiplinger reported the first actinide α-diimine (Ar-BIAN) complexes in 2010 featuring U(III) and U(IV) centers bearing reduced dpp-BIAN ligands.[54] The complex U(dpp-BIAN)$_2$ maintained tetravalent metal and dianionic ligand oxidation states, however the analogous complex with coordinated tetrahydrofuran (THF) was found to behave as a U(III) center with one dianionic and one monoanionic ligand in the solid state[54]. This work determined that reversible interconversion of the two forms was possible upon solvation and desolvation, and this display of redox-activity is valuable in terms of better understanding 5*f*-orbital participation in bonding interactions; however, this remains the only report featuring Ar-BIAN and uranium. [54]

A Salophen-Like BIAN

Noting these precedents, the observed redox-activity of BIAN species, and previous work from the Gorden group describing the selectivity of salqu and other salen ligands, as well as the under-developed chemistry of low-valent uranium, it was irresistible to consider merging the salen/salophen and BIAN functionalities. Consequently, the new redox-active salen-like Schiff base ligand, “phen-BIAN” (N,N’-bis(iminophenol)acenaphthene) (**Figure 1.6**), was designed and synthesized. This species integrates the redox-active backbone found in Ar-BIAN species with the

trademark tetradentate O-N-N-O salen motif *via* condensation of acenaphthenequinone with a 2-aminophenol. The primary difference of this binding pocket from that of salens is the slightly wider pocket imparted by the different positioning of the imine moieties—phen-BIANs have one fewer carbon atom between the backbone and attached arm. Ar-BIANs were chosen as an inspiration for this work for several reasons: 1) they have well-developed redox non-innocent behavior in transition metal complexes[79] that can serve as a useful benchmark for comparing the unique behaviors exhibited by actinide complexes; 2) the characteristic ligand oxidation states are easily identifiable from C-C and C-N bond lengths in the α-diimine unit, allowing for clear descriptions of metal and ligand oxidation states provided a crystal structure can be obtained;[79] 3) their steric and electronic properties can be easily tuned through by changing the aryl group employed.

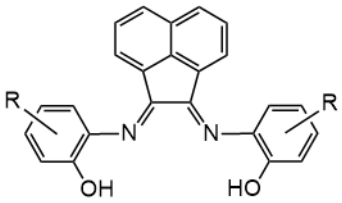

Figure 6. Generic, "open" form of phen-BIAN.

The combination of phen-BIAN's N_2O_2 pocket with the extended conjugation in the backbone distinguishes this ligand framework from many others currently under study. The softer N-donor α-diimine unit functions as a π-acceptor that can engage in π-backbonding, which has been implicated in stabilizing low-valent and reduced metal ions,[64] particularly in conjunction with extended low-lying π-orbitals that allow for electron declocalization.[51] The harder phenolate O-donors can act as π-donors—as it has been proposed that π-donation into the equatorial plane of uranyl complexes can increase the susceptibility of axial oxo ligands to activation, functionalization, and reduction in bond order via competition for the 6*d* orbitals associated with

uranyl-oxo bonding,[84] these interactions are of interest, and can be probed through the tuning of phenolic substituents. The mixed-donor pocket predisposes phen-BIAN ligands to bind readily to a variety of metals and oxidation states, and the extensive capacity for redox activity and tunability makes this system truly unique in its potential to access and stabilize a significant number of actinide oxidation states. The chemistry of non-oxo uranium (VI) species is particularly interesting in this respect, since they are extremely limited in number and are expected to have increased metal-ligand covalency.[85] One of the unique challenges posed by non-oxo U(VI) metal centers is that very few ligand systems, with the exception of alkoxides (OR), can stabilize them.[85] A possible route to access non-oxo uranium (VI) species may exist through the addition of a highly reduced phen-BIAN ligand to U(IV). The characterization of such complexes would be incredibly useful in understanding the bonding interactions that take place between 5*f* and ligand orbitals, as this is still a topic of considerable debate[86], though large U—O—C bond angles in a characterized homoleptic U(VI) complex, $U(O^tBu)_6$ suggest a significant π-interaction is present,[85] and recently evidence for π-backbonding was found between a U(V) ($5f^1$) complex and N_2, which is a significantly poorer π-acceptor ligand than α-diimines.[22]

The work discussed in Chapter 2 details much of the functionality of the phen-BIAN ligand system as well as that of its less-conjugated cousin, the gbha (glyoxal(bis)hydroxyanil) ligand, which lacks the acenaphthene backbone. The uranyl complexes of these shed light on the bonding interactions that take place in these system and show the utility of the more highly conjugated backbone. Chapter 3 also focuses on similar themes but does so for salophen systems which are substantially less electronically flexible, and ventures into related supramolecular actinide complexes. Chapter 4 details the use of macroacyclic pyrrole-based ligands for the molecular recognition of uranyl, showing how investigation of fundamental properties of uranyl can drive

the strategic development of sensors or chelating agents. Though this work is broad and spans a variety of ligand classes, many of the overarching themes are the same, and often results from one project have informed the direction of another—these relationships are tied together in Chapter 5, and the future directions of this research are presented.

References

1. Wu, W.-M.; Carley, J.; Gentry, T.; Ginder-Vogel, M. A.; Fienen, M.; Mehlhorn, T.; Yan, H.; Caroll, S.; Pace, M. N.; Nyman, J.; Luo, J.; Gentile, M. E.; Fields, M. W.; Hickey, R. F.; Gu, B.; Watson, D.; Cirpka, O. A.; Zhou, J.; Fendorf, S.; Kitanidis, P. K.; Jardine, P. M.; Criddle, C. S., Pilot-Scale in Situ Bioremedation of Uranium in a Highly Contaminated Aquifer. 2. Reduction of U(VI) and Geochemical Control of U(VI) Bioavailability. *Environ. Sci. Technol.* **2006,** *40* (12), 3986-3995.

2. Pankhurst, J. R.; Bell, N. L.; Zegke, M.; Platts, L. N.; Lamfsus, C. A.; Maron, L.; Natrajan, L. S.; Sproules, S.; Arnold, P. L.; Love, J. B., Inner-sphere vs. outer-sphere reduction of uranyl supported by a redox-active, donor-expanded dipyrrin. *Chem. Sci.* **2017,** *8* (1), 108-116.

3. Bell, N. L.; Arnold, P. L.; Love, J. B., Controlling uranyl oxo group interactions to group 14 elements using polypyrrolic Schiff-base macrocyclic ligands. *Dalton Trans.* **2016,** *45* (40), 15902-15909.

4. Sessler, J. L.; Vivian, A. E.; Seidel, D.; Burrell, A. K.; Hoehner, M.; Mody, T. D.; Gebauer, A.; Weghorn, S. J.; Lynch, V., Actinide expanded porphyrin complexes. *Coord. Chem. Rev.* **2001,** *216-217*, 411-434.

5. Choppin Gregory, R.; Nash Kenneth, L., Actinide Separation Science. In *Radiochimica Acta*, 1995; Vol. 70-71, p 225.

6. Sessler, J. L.; Gorden, A. E. V.; Seidel, D.; Hannah, S.; Lynch, V.; Gordon, P. L.; Donohoe, R. J.; Drew Tait, C.; Webster Keogh, D., Characterization of the interactions between neptunyl and plutonyl cations and expanded porphyrins. *Inorg. Chim. Acta* **2002,** *341*, 54-70.

7. Brewster, J. T.; Zafar, H.; Root, H. D.; Thiabaud, G. D.; Sessler, J. L., Porphyrinoid f-Element Complexes. *Inorg. Chem.* **2020,** *59* (1), 32-47.

8. Fox, A. R.; Bart, S. C.; Meyer, K.; Cummins, C. C., Towards uranium catalysts. *Nature* **2008,** *455*, 341.

9. Formanuik, A.; Ortu, F.; Liu, J.; Nodaraki, L. E.; Tuna, F.; Kerridge, A.; Mills, D. P., Double Reduction of 4,4′-Bipyridine and Reductive Coupling of Pyridine by Two Thorium(III) Single-Electron Transfers. *Chem. Eur. J.* **2017,** *23* (10), 2290-2293.

10. Arnold, P. L.; Pécharman, A.-F.; Lord, R. M.; Jones, G. M.; Hollis, E.; Nichol, G. S.; Maron, L.; Fang, J.; Davin, T.; Love, J. B., Control of Oxo-Group Functionalization and Reduction of the Uranyl Ion. *Inorg. Chem.* **2015,** *54* (7), 3702-3710.

11. Schneider, M.; Froggatt, A.; Hazemann, J.; von Hirschhausen, C.; Katsuta, T.; Wealer, B.; Lovins, A. B.; Stienne, A.; Ramana, M. V.; Meinass, F.; Ürge-Vorsatz, D. *The World Nuclear Industry Status Report 2019*; Paris, Budapest, Semptember 2019, **2019**.

12. *Nuclear Power in a Clean Energy System*; IEA: Paris, **2019**.

13. *The World Nuclear Performance Report 2019*; 2019/007; August 2019, **2019**.

14. *Annual Energy Outlook 2019*; #AEO2019; January 24, 2019, **2019**.

15. Kormann, C., Is Nuclear Power Worth the Risk? *The New Yorker* December 22, 2019.

16. Willard, R. F. *Lessons learned from the Nuclear Accident at Fukushima Daiichi Nuclear Power Station.*; INPO 11-005 Addendum; Institute of Nuclear Power Operations: August 2012, **2012**.

17. Rutherford, E.; Geiger, H., An electrical method of counting the number of α-particles from radio-active substances. *Proceedings of the Royal Society of London. Series A, Containing Papers of a Mathematical and Physical Character* **1908,** *81* (546), 141-161.

18. Montgomery, C. G.; Montgomery, D. D., The Discharge Mechanism of Geiger-Mueller Counters. *Physical Review* **1940,** *57* (11), 1030-1040.

19. Kauffman, G. B., The Chemistry of the Actinide and Transactinide Elements. 3rd ed., 5 vols. Edited by Lester R. Morss, Norman M. Edelstein, Jean Fuger, and Joseph J. Katz. *Angew. Chem. Int. Ed.* **2007,** *46* (10), 1562-1563.

20. Denning, R. G., Electronic structure and bonding in actinyl ions. In *Complexes, Clusters and Crystal Chemistry*, Springer Berlin Heidelberg: Berlin, Heidelberg, **1992**; pp 215-276.

21. Di Pietro, P.; Kerridge, A., Assessing covalency in equatorial U–N bonds: density based measures of bonding in BTP and isoamethyrin complexes of uranyl. *Physical Chemistry Chemical Physics* **2016,** *18* (25), 16830-16839.

22. Lu, E.; Atkinson, B. E.; Wooles, A. J.; Boronski, J. T.; Doyle, L. R.; Tuna, F.; Cryer, J. D.; Cobb, P. J.; Vitorica-Yrezabal, I. J.; Whitehead, G. F. S.; Kaltsoyannis, N.; Liddle, S. T., Back-bonding between an electron-poor, high-oxidation-state metal and poor π-acceptor ligand in a uranium(V)–dinitrogen complex. *Nat. Chem.* **2019,** *11* (9), 806-811.

23. J. Hála, J. D. N., *Radioactivity, Ionizing Radiation, and Nuclear Energy*. Second ed.; Konvoj, spol. s. r. o. (Ltd.): Czech Republic, **2003**.

24. World Nuclear Association: Uranium and Depleted Uranium.

25. Nikolas Kaltsoyannis, P. S., *The f elements*. Oxford University Press: United States, **1999**.

26. Report and Recommendations of the Nevada Commission on Nuclear Projects. **2017**.

27. H.R. 3053 - Nuclear Waste Policy Amendments Act of 2018. House of Representatives Committee on Energy and Commerce. **2018**.

28. Technical, Schedule, and Cost Uncertainties of the Yucca Mountain Repository Project. G.A.O. **2001**.

29. Gorden, A. E. V.; Wu, X. Preparation of 2-quinoxalinol salen compounds and their use as catalysts in oxidation reactions. US20090286968A1, **2009**.

30. Camp, C.; Toniolo, D.; Andrez, J.; Pecaut, J.; Mazzanti, M., A versatile route to homo- and hetero-bimetallic 5f-5f and 3d-5f complexes supported by a redox active ligand framework. *Dalton Trans.* **2017,** *46* (34), 11145-11148.

31. Herasymchuk, K.; Chiang, L.; Hayes, C. E.; Brown, M. L.; Ovens, J. S.; Patrick, B. O.; Leznoff, D. B.; Storr, T., Synthesis and electronic structure determination of uranium(VI) ligand radical complexes. *Dalton Trans.* **2016,** *45* (31), 12576-12586.

32. Cheng, J.; Ma, X.; Zhang, Y.; Liu, J.; Zhou, X.; Xiang, H., Optical Chemosensors Based on Transmetalation of Salen-Based Schiff Base Complexes. *Inorg. Chem.* **2014,** *53* (6), 3210-3219.

33. Dalla Cort, A.; De Bernardin, P.; Forte, G.; Yafteh Mihan, F., Metal–salophen-based receptors for anions. *Chem. Soc. Rev.* **2010,** *39* (10), 3863.

34. DeVore Ii, M. A.; Kerns, S. A.; Gorden, A. E. V., Characterization of Quinoxolinol Salen Ligands as Selective Ligands for Chemosensors for Uranium: Quinoxolinol Salen Ligands for Chemosensors for Uranium. *Eur. J. Inorg. Chem.* **2015,** *2015* (34), 5708-5714.

35. Wu, X.; Bharara, M. S.; Bray, T. H.; Tate, B. K.; Gorden, A. E. V., Synthesis and characterization of 2-quinoxalinol Schiff-base metal complexes. *Inorg. Chim. Acta.* **2009,** *362* (6), 1847-1854.

36. DeVore II, M. A.; Kerns, S. A.; Gorden, A. E. V., Characterization of Quinoxolinol Salen Ligands as Selective Ligands for Chemosensors for Uranium. *Eur. J. Inorg. Chem.* **2015,** *2015* (34), 5708-5714.

37. Hardy, E. E.; Eddy, M. A.; Maynard, B. A.; Gorden, A. E. V., Solid state π-π stacking and higher order dimensional crystal packing, reactivity, and electrochemical behaviour of salphenazine actinide and transition metal complexes. *Dalton Trans* **2016,** *45* (36), 14243-51.

38. Hardy, E. E.; Wyss, K. M.; Eddy, M. A.; Gorden, A. E. V., An example of unusual pyridine donor Schiff base uranyl (UO_2^{2+}) complexes. *Chem. Comm.* **2017,** *53* (42), 5718-5720.

39. Stobbe, B. C.; Powell, D. R.; Thomson, R. K., Schiff base thorium(iv) and uranium(iv) chloro complexes: synthesis, substitution and oxidation chemistry. *Dalton Trans.* **2017,** *46* (15), 4888-4892.

40. Hardy, E. E.; Wyss, K. M.; Gorden, J. D.; Ariyarathna, I. R.; Miliordos, E.; Gorden, A. E. V., Th(IV) and Ce(IV) napthylsalophen sandwich complexes: characterization of unusual thorium fluorescence in solution and solid-state. *Chem. Comm.* **2017,** *53* (88), 11984-11987.

41. Salmon, L.; Thuéry, P.; Ephritikhine, M., Synthesis and crystal structure of uranium(IV) complexes with compartmental Schiff bases: from mononuclear species to tri- and tetranuclear clusters. *Dalton Trans.* **2004,** (10), 1635-1643.

42. He, F.-F.; Wang, H.-Q.; Wang, X.-F.; Wang, Y.-Y., Crystal structure of bis-[N,N'-bis-(3-allyl salicylidene)-o-phenylene diamine]thorium (IV), $C_{52}H_{44}N_4O_4Th$. In *Zeitschrift für Kristallographie - New Crystal Structures*, 2012; Vol. 227, p 521.

43. Klamm, B. E.; Windorff, C. J.; Celis-Barros, C.; Marsh, M. L.; Meeker, D. S.; Albrecht-Schmitt, T. E., Experimental and Theoretical Comparison of Transition-Metal and Actinide Tetravalent Schiff Base Coordination Complexes. *Inorg. Chem.* **2018,** *57* (24), 15389-15398.

44. Niklas, J. E.; Hardy, E. E.; Gorden, A. E. V., Solid-state structural elucidation and electrochemical analysis of uranyl naphthylsalophen. *Chem. Comm.* **2018,** *54* (83), 11693-11696.

45. Sessler, J. L.; Seidel, D.; Vivian, A. E.; Lynch, V.; Scott, B. L.; Keogh, D. W., Hexaphyrin(1.0.1.0.0.0): An Expanded Porphyrin Ligand for the Actinide Cations Uranyl (UO_2^{2+}) and Neptunyl (NpO_2^{+}). *Angew. Chem. Int. Ed.* **2001,** *40* (3), 591-594.

46. Sessler, J. L.; Melfi, P. J.; Seidel, D.; Gorden, A. E. V.; Ford, D. K.; Palmer, P. D.; Tait, C. D., Hexaphyrin(1.0.1.0.0.0). A new colorimetric actinide sensor. *Tetrahedron* **2004,** *60* (49), 11089-11097.

47. Brewster, J. T., 2nd; Mangel, D. N.; Gaunt, A. J.; Saunders, D. P.; Zafar, H.; Lynch, V. M.; Boreen, M. A.; Garner, M. E.; Goodwin, C. A. P.; Settineri, N. S.; Arnold, J.; Sessler, J. L., In-Plane Thorium(IV), Uranium(IV), and Neptunium(IV) Expanded Porphyrin Complexes. *J Am Chem Soc* **2019,** *141* (44), 17867-17874.

48. Camp, C.; Guidal, V.; Biswas, B.; Pecaut, J.; Dubois, L.; Mazzanti, M., Multielectron redox chemistry of lanthanide Schiff-base complexes. *Chem. Sci.* **2012,** *3* (8), 2433-2448.

49. Camp, C.; Mougel, V.; Horeglad, P.; Pécaut, J.; Mazzanti, M., Multielectron Redox Reactions Involving C−C Coupling and Cleavage in Uranium Schiff Base Complexes. *J. Am. Chem. Soc.* **2010,** *132* (49), 17374-17377.

50. Chirik, P. J.; Wieghardt, K., Radical Ligands Confer Nobility on Base-Metal Catalysts. *Science* **2010,** *327* (5967), 794-795.

51. Korobkov, I.; Gorelsky, S.; Gambarotta, S., Reduced Uranium Complexes: Synthetic and DFT Study of the Role of π Ligation in the Stabilization of Uranium Species in a Formal Low-Valent State. *J. Am. Chem. Soc.* **2009,** *131* (30), 10406-10420.

52. Kiernicki, J. J.; Ferrier, M. G.; Lezama Pacheco, J. S.; La Pierre, H. S.; Stein, B. W.; Zeller, M.; Kozimor, S. A.; Bart, S. C., Examining the Effects of Ligand Variation on the Electronic Structure of Uranium Bis(imido) Species. *J. Am. Chem. Soc.* **2016,** *138* (42), 13941-13951.

53. Kraft, S. J.; Williams, U. J.; Daly, S. R.; J. Schelter, E.; Kozimor, S. A.; Boland, K. S.; Kikkawa, J. M.; Forrest, W. P.; Christensen, C. N.; Schwarz, D. E.; Fanwick, P. E.; Clark, D. L.; Conradson, S. D.; Bart, S. C., Synthesis, Characterization, and Multielectron Reduction Chemistry of Uranium Supported by Redox-Active α-Diimine Ligands. *Inorg. Chem.* **2011,** *50* (20), 9838-9848.

54. Schelter, E. J.; Wu, R.; Scott, B. L.; Thompson, J. D.; Cantat, T.; John, K. D.; Batista, E. R.; Morris, D. E.; Kiplinger, J. L., Actinide Redox-Active Ligand Complexes: Reversible Intramolecular Electron-Transfer in U(dpp-BIAN)$_2$/U(dpp-BIAN)$_2$(THF). *Inorg. Chem.* **2010,** *49* (3), 924-933.

55. Anderson, N. H.; Odoh, S. O.; Yao, Y.; Williams, U. J.; Schaefer, B. A.; Kiernicki, J. J.; Lewis, A. J.; Goshert, M. D.; Fanwick, P. E.; Schelter, E. J.; Walensky, J. R.; Gagliardi, L.; Bart, S. C., Harnessing redox activity for the formation of uranium tris(imido) compounds. *Nat. Chem.* **2014,** *6* (10), 919-926.

56. Arnold, P. L.; Stevens, C. J.; Bell, N. L.; Lord, R. M.; Goldberg, J. M.; Nichol, G. S.; Love, J. B., Multi-electron reduction of sulfur and carbon disulfide using binuclear uranium(III) borohydride complexes. *Chem. Sci.* **2017,** *8* (5), 3609-3617.

57. Gardner, B. M.; Liddle, S. T., Small-Molecule Activation at Uranium(III). *Eur. J. Inorg. Chem.* **2013,** *2013* (22-23), 3753-3770.

58. Ephritikhine, M., The vitality of uranium molecular chemistry at the dawn of the XXIst century. *Dalton Trans.* **2006,** (21), 2501-2516.

59. Renshaw, J. C.; Butchins, L. J. C.; Livens, F. R.; May, I.; Charnock, J. M.; Lloyd, J. R., Bioreduction of Uranium: Environmental Implications of a Pentavalent Intermediate. *Environ. Sci. Technol.* **2005,** *39* (15), 5657-5660.

60. Niklas, J. E.; Hunter, K. M.; Gorden, A. E. V., Bonding Interactions in Uranyl α-Diimine Complexes: A Spectroscopic and Electrochemical Study of the Impacts of Ligand Electronics and Extended Conjugation. *Inorg. Chem.* **2019**.

61. Bell, N. L.; Shaw, B.; Arnold, P. L.; Love, J. B., Uranyl to Uranium(IV) Conversion through Manipulation of Axial and Equatorial Ligands. *J. Am. Chem. Soc.* **2018,** *140* (9), 3378-3384.

62. Arnold, P. L.; Pécharman, A.-F.; Hollis, E.; Yahia, A.; Maron, L.; Parsons, S.; Love, J. B., Uranyl oxo activation and functionalization by metal cation coordination. *Nat. Chem.* **2010,** *2* (12), 1056-1061.

63. Mullane, K. C.; Carroll, P. J.; Schelter, E. J., Synthesis and Reduction of Uranium(V) Imido Complexes with Redox-Active Substituents. *Chem. Eur. J.* **2017,** *23* (24), 5748-5757.

64. Anderson, N. H.; Odoh, S. O.; Williams, U. J.; Lewis, A. J.; Wagner, G. L.; Lezama Pacheco, J.; Kozimor, S. A.; Gagliardi, L.; Schelter, E. J.; Bart, S. C., Investigation of the Electronic Ground States for a Reduced Pyridine(diimine) Uranium Series: Evidence for a Ligand Tetraanion Stabilized by a Uranium Dimer. *J. Am. Chem. Soc.* **2015,** *137* (14), 4690-4700.

65. Kiernicki, J. J.; Cladis, D. P.; Fanwick, P. E.; Zeller, M.; Bart, S. C., Synthesis, Characterization, and Stoichiometric U-O Bond Scission in Uranyl Species Supported by Pyridine(diimine) Ligand Radicals. *J. Am. Chem. Soc.* **2015,** *137* (34), 11115-11125.

66. Brown, J. L.; Wu, G.; Hayton, T. W., Oxo Ligand Silylation in a Uranyl β-Ketoiminate Complex. *J. Am. Chem. Soc.* **2010,** *132* (21), 7248-7249.

67. Pedrick, E. A.; Wu, G.; Hayton, T. W., Oxo Ligand Substitution in a Cationic Uranyl Complex: Synergistic Interaction of an Electrophile and a Reductant. *Inorg. Chem.* **2015,** *54* (14), 7038-7044.

68. Arnold, P. L.; Jones, G. M.; Odoh, S. O.; Schreckenbach, G.; Magnani, N.; Love, J. B., Strongly coupled binuclear uranium–oxo complexes from uranyl oxo rearrangement and reductive silylation. *Nat. Chem.* **2012,** *4* (3), 221-227.

69. Arnold, P. L.; Jones, G. M.; Pan, Q.-J.; Schreckenbach, G.; Love, J. B., Co-linear, double-uranyl coordination by an expanded Schiff-base polypyrrole macrocycle. *Dalton Trans.* **2012,** *41* (22), 6595-6597.

70. Bart, S. C.; Heinemann, F. W.; Anthon, C.; Hauser, C.; Meyer, K., A New Tripodal Ligand System with Steric and Electronic Modularity for Uranium Coordination Chemistry. *Inorg. Chem.* **2009,** *48* (19), 9419-9426.

71. Diaconescu, P. L.; Cummins, C. C., Radical anionic versus neutral 2,2[prime or minute]-bipyridyl coordination in uranium complexes supported by amide and ketimide ligands. *Dalton Trans.* **2015,** *44* (6), 2676-2683.

72. Takao, K.; Tsushima, S.; Ogura, T.; Tsubomura, T.; Ikeda, Y., Experimental and Theoretical Approaches to Redox Innocence of Ligands in Uranyl Complexes: What Is Formal Oxidation State of Uranium in Reductant of Uranyl(VI)? *Inorg. Chem.* **2014,** *53* (11), 5772-5780.

73. Camp, C.; Chatelain, L.; Mougel, V.; Pécaut, J.; Mazzanti, M., Ferrocene-Based Tetradentate Schiff Bases as Supporting Ligands in Uranium Chemistry. *Inorg. Chem.* **2015,** *54* (12), 5774-5783.

74. Hill, N. J.; Vargas-Baca, I.; Cowley, A. H., Recent developments in the coordination chemistry of bis(imino)acenaphthene (BIAN) ligands with s- and p-block elements. *Dalton Trans.* **2009,** (2), 240-253.

75. van Asselt, R.; Elsevier, C. J.; Smeets, W. J. J.; Spek, A. L.; Benedix, R., Synthesis and characterization of rigid bidentate nitrogen ligands and some examples of coordination to divalent palladium. X-ray crystal structures of bis (p-tolylimino) acenaphthene and methylchloro [bis(o,o′-diisopropylphenyl-imino) acenaphthene] palladium (II). *Chem. Ber./Recl.* **1994,** *113* (2), 88-98.

76. van Asselt, R.; Gielens, E. E. C. G.; Rulke, R. E.; Elsevier, C. J., Isolation of alkyl- and acyl-palladium complexes containing rigid bidentate nitrogen ligands by stepwise successive insertion of CO and alkenes. *J. Chem. Sci. Chem. Commun.* **1993,** (15), 1203-1205.

77. Fedushkin, Igor L.; Skatova, Alexandra A.; Chudakova, Valentina A.; Cherkasov, Vladimir K.; Fukin, Georgy K.; Lopatin, Mikhail A., Reduction of 1,2-Bis[(2,6-diisopropylphenyl)imino]acenaphthene (dpp-bian) with Alkali Metals − A Study of the Solution Behaviour of (dpp-bian)n−[M+]n (M = Li, Na; n = 1−4) with UV/Vis, ESR and ^{1}H NMR Spectroscopy. *Eur. J. Inorg. Chem.* **2004,** *2004* (2), 388-393.

78. Fedushkin, I. L.; Skatova, A. A.; Chudakova, V. A.; Fukin, G. K., Four-Step Reduction of dpp-bian with Sodium Metal: Crystal Structures of the Sodium Salts of the Mono-, Di-, Tri- and Tetraanions of dpp-bian. *Angew. Chem. Int. Ed.* **2003,** *42* (28), 3294-3298.

79. Viganò, M.; Ferretti, F.; Caselli, A.; Ragaini, F.; Rossi, M.; Mussini, P.; Macchi, P., Easy Entry into Reduced Ar-BIANH_2 Compounds: A New Class of Quinone/Hydroquinone-Type

Redox-Active Couples with an Easily Tunable Potential. *Chem. Eur. J.* **2014,** *20* (44), 14451-14464.

80. Clark, K. M.; Bendix, J.; Heyduk, A. F.; Ziller, J. W., Synthesis and Characterization of a Neutral Titanium Tris(iminosemiquinone) Complex Featuring Redox-Active Ligands. *Inorg. Chem.* **2012,** *51* (14), 7457-7459.

81. Pierpont, C. G.; Lange, C. W., The Chemistry of Transition Metal Complexes Containing Catechol and Semiquinone Ligands. In *Progress in Inorganic Chemistry*, John Wiley & Sons, Inc.: **2007**; pp 331-442.

82. Schumann, H.; Hummert, M.; Lukoyanov Anton, N.; Chudakova Valentina, A.; Fedushkin Igor, L., Organometallic Compounds of the Lanthanides 182 [1]. Calcium and Neodymium Complexes Containing the dpp-BIAN Ligand System: Synthesis and Molecular Structure of [(dpp-BIAN)CaI(THF)2]$_2$ and [(dpp-BIAN)NdCl(THF)$_2$]$_2$. In *Z. Naturforsch., B: J. Chem. Sci.*, 2007; Vol. 62, p 1107.

83. Vasudevan, K.; Cowley, A. H., Synthesis and structures of 1,2-bis(imino)acenaphthene (BIAN) lanthanide complexes that involve the transfer of zero, one, or two electrons. *Chem. Comm.* **2007,** (33), 3464-3466.

84. Fortier, S.; Hayton, T. W., Oxo ligand functionalization in the uranyl ion (UO_2^{2+}). *Coordination Chemistry Reviews* **2010,** *254* (3), 197-214.

85. Fortier, S.; Wu, G.; Hayton, T. W., Synthesis and Characterization of Three Homoleptic Alkoxides of Uranium: [Li(THF)]$_2$[U^{IV}(OtBu)$_6$], [Li(Et$_2$O)][U^{V}(OtBu)$_6$], and U^{VI}(OtBu)$_6$. *Inorg. Chem.* **2008,** *47* (11), 4752-4761.

86. Bohle, D. S.; Zafar, A.; Goodson, P. A.; Jaeger, D. A., Synthesis and Characterization of Nickel(II) Bis(alkylthio)salen Complexes. *Inorg. Chem.* **2000,** *39* (4), 712-718.

Chapter 2

Redox-Active α-Diimine Ligands and their Uranyl Complexes

Introduction

A thorough understanding of the structural, bonding, and electronic properties of uranium is necessary to develop new technologies for improved remediation of materials that result from the nuclear fuel cycle.[1-2] In order to better comprehend these fundamental properties, the characterization of lower-valent uranium species has become germane.[3-4] Literature describing coordination chemistry of the early actinides consists largely of U(VI) complexes containing the linear uranyl $[O=U=O]^{2+}$ moiety, which is ubiquitous in nature, especially aqueous environments, due to the remarkable stability of its oxo groups.[1, 5-7] The robust nature of uranyl poses a unique challenge with respect to its activation and functionalization. The axial oxo ligands are covalently bound to the uranium center, and mutually reinforce one another via the inverse-*trans*-influence (ITI), which distinguishes the high-valent actinyl species from their transition metal counterparts.[8-10] Recent research efforts have focused on understanding the mechanisms by which this moiety can be reduced through the axial oxo ligands, often with particular interest in perturbation of their bonding character.[11-16] The reduction of uranyl is also of interest in developing our understanding of bioremediation and conversion of UO_2^{2+} (U^{VI}) to the insoluble U^{IV} species through a U^{V} intermediate.[17] U^{V} species are unstable due to disproportionation to the more stable U^{VI} and U^{IV} species, thus characterization of systems in which the $U^{VI/V}$ redox couple can be studied or tuned are valuable, especially where judicious choice of equatorial ligand may assist in the reduction or

stabilization of lower-valent uranium centers. π-bonded ligands, particularly those containing a significant accessible π-system, have been identified as being especially valuable in stabilizing through delocalization formally reduced uranium centers which behave as synthetic equivalents of low-valent species.[18]

As access to stable, well-behaved lower-valent uranium species can be difficult, the employment of redox-active ligands offers a degree of electronic flexibility through which these systems can be prepared and characterized.[19] Redox-active frameworks have long been prevalent in transition metal systems, but have only recently been garnered attention in the characterization of uranium (in particular, uranyl) complexes,[20-22] where participation of the ligand in redox processes and an inherent ability to stabilize atypical metal oxidation states is of interest.[23] Pyridine(diimine) (PDI) ligands are known to assist in U=O bond scission,[13] and have been found to stabilize reduced species through π-backbonding interactions with uranium.[4] The study of systems that can both behave non-innocently and participate in π-backbonding is therefore of interest in evaluating covalent interactions and reduction processes. Such π-backbonding interactions are typically only discussed for more electron-rich actinide centers,[4, 18, 24-25] not closed-shell systems such as UO_2^{2+}; however, Liddle and co-workers recently demonstrated backbonding between an electron-poor U(V) center and dinitrogen, an especially poor π-acceptor.[26] This is attributed to a suitably electron-rich ligand environment capable of providing the necessary electron density for backbonding. The electronic structure and bonding behaviors of actinides are still being explored, so it is worth considering some of these behaviors which may be less obvious or are exhibited in a non-classical way. Towards this end, we have become interested in redox-non-innocent α-diimine ligands, and reported a new system, "phen-BIAN"[27], (2,2'-((1E,1'E)-acenaphthylene-1,2-diylidenebis(azanylylidene))bis(4-(tert-butyl)phenol) or N,N'-bis(imino-

phenol)acenaphthene), that integrates the redox-active backbone and attached naphthalene unit found in N,N'-bis[(aryl)imino]acenaphthenes (Ar-BIAN) species with the characteristic tetradentate mixed-donor O-N-N-O salen binding motif.[28-29] This system was designed to extend the range of available ligand oxidation states past that of either general Ar-BIANs or salen ligands alone (**Figure 2.1**).[27, 30]

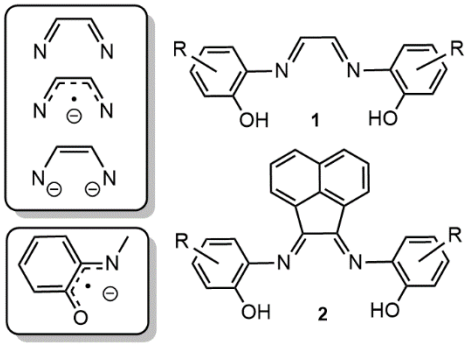

Figure 2.1 Idealized, or "open" α-diimine ligands 1 (glyoxal-bis(2-hydroxyanil) and 2 (phen-BIAN) used in this study (right) and possible redox-states of the O-N-N-O pocket (left).

To accomplish this, we prepared and studied six derivatives of uranyl phen-BIAN complexes as well as a set of the analogous glyoxal-bis(2-hydroxyanil) (gbha) ligand, which lack the acenaphthene backbone of phen-BIANs. Glyoxal-bis(2-hydroxyanils) function as tetradentate diphenolate ligands and have been used in colorimetric Ca^{2+} sensors,[31] as well as reported in work by Wilson from 1962 for use in the detection of trace quantities of metal ions in solution, including uranyl.[32-33] Transition metal complexes of gbhas have not been widely characterized due to their low stability, and the poor solubility of both the free ligands and their complexes, which limits the acquisition of solution-state data and often precludes crystallization.[34-35] There are two reports of structurally characterized uranyl complexes of gbha, showing this complex can exist as a water coordinated monomer ($[UO_2(gbha)(H_2O)]$), or as a μ-phenolato bridged dimer ($[UO_2(gbha)]_2$).[23, 36] As an additional complicating factor, the free, uncomplexed ligands exist primarily in their

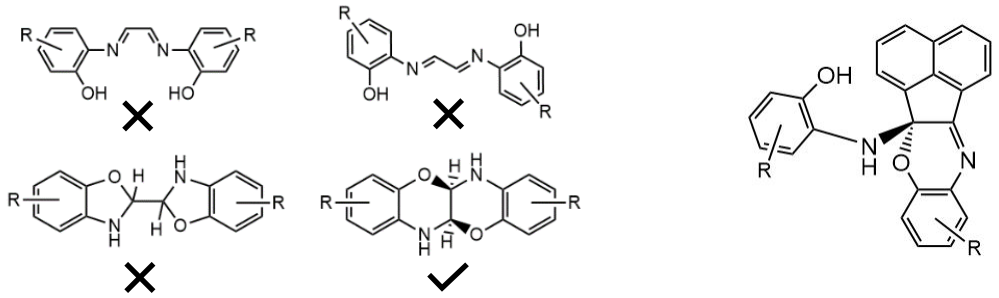

Figure 2.2 (Left) Variety of reported structures for gbha ligands and (right) structure of phen-BIANs.

benzoxazinobenzoxazine forms, which has been frequently misassigned in the literature as a bisbenzoxazoline or as the open *trans* glyoxal-bis(hydroxyanil) form (**Figure 2.2**).[37-39] This behavior is similar to that exhibited by the free ligand (*t*-bu)phen-BIAN, which adopts a singly-cyclized form in both solution and solid-state—the presence of the acenaphthene unit sterically prevents cyclization of both aminophenol arms in contrast to the flexible and unencumbered glyoxal-backbone.[27, 30]

Of the ligands reported here, only the unsubstituted gbha (5a,6,11a,l2-tetrahydro[1,4]benzoxazino[3,2-b][1,4]benzoxazine) has been previously characterized by X-ray diffraction[37]. Presented here are three new gbha ligands (-OMe, -F, and -napthhyl substituted) in addition to the crystal structure of *t*-bu-gbha, and six new uranyl complexes of these ligands (R = OMe, *t*-bu, H, Me, F, 3-naphthyl), four of which have been characterized in the solid-state by single crystal X-ray diffraction. These six complexes are described alongside their phen-BIAN analogues, with special attention to how ligand substituents, especially the presence of accessible π-systems, impact their absorption spectra, ν_3 O=U=O stretching frequencies, electrochemical behaviors, and solid-state structures. Comparisons to the previously characterized uranyl dimer $[UO_2$(*t*-bu)phen-BIAN$]_2$ in solution and solid state are also discussed.

2.1 | Results and Discussion

Synthesis and Characterization of Ligands

The gbha ligands **1a-f (**R = OMe (**a**), *t*-bu (**b**), H (**c**), Me (**d**), F (**e**), and naphthyl (**f**)) were synthesized by means of the condensation of glyoxal and the corresponding aminophenol and isolated in yields ranging from 20-80% as light-colored solids (**Scheme 2.1**). These species exist as cyclic benzoxazinobenzoxazines in solution and solid state as determined by NMR and IR spectroscopy. N—H stretches are apparent at 3,364-3,403 cm^{-1} and imine stretches are absent in the 1,650-1,700 cm^{-1} region, and both C-H and N-H protons can be identified in the ^{1}H NMR spectrum.[30] Additionally, this assignment is confirmed by single-crystal X-ray diffraction analysis for **1b (Figure 2.3)** which to our knowledge is only the second reported crystal structure of a free "gbha" ligand of this type.[37] In protic solvents such as methanol, some of these ligands (most noticeably **1b**) exist in equilibrium with the open gbha form, as evidenced by a blue-purple color of the solution. These species react quickly with uranyl acetate, resulting in very intensely colored green, blue, and purple solutions and pearlescent nearly-black solids. The uranyl complexes were found to form either μ-phenolato bridged dimers or methanol-coordinated monomers.

The phen-BIAN ligand **2b** (R = *t*-bu) was synthesized by condensation of acenaphthenequinone and 4-*tert*-butyl-2-aminophenol in CH_3OH and isolated as a bright yellow solid in 74% yield (**Scheme 2.2**). This is to our knowledge the first such structural characterization of a salen-like BIAN ligand, with the exception of a 1968 paper by Manecke & Gauger wherein the synthesis of an analogous ligand bearing no substituents on the phenolic arms was reported. No evidence or characterization establishing connectivity was provided, though the infrared stretching frequencies reported are in close accord with those observed here.[40] It should be noted that the yellow solid **2b** is unstable to mild heating, and subjecting it to temperatures greater than

35 °C causes a color change to the red-orange hue that is often observed in Ar-BIAN species, suggesting a possible structural change to the idealized open form (**Figure 2.1**). The phen-BIAN ligands **2a,c-f** could not be synthesized and isolated cleanly, so they were instead synthesized in their complexed forms by templation around uranyl (**Scheme 2.1**). Identity of the complexes, and thereby the ligands, was established by NMR and IR spectroscopy in conjunction with elemental analysis.

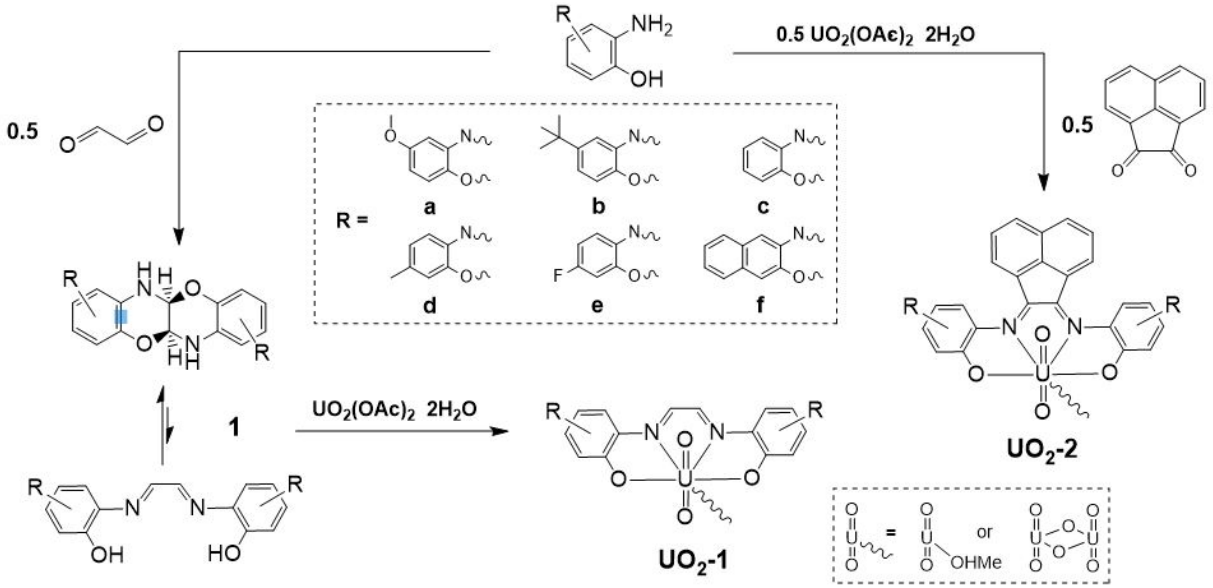

Scheme 2.1 General synthesis of gbha ligands (**1**), and of uranyl complexes **UO_2-1a-f** and **UO_2-2a,c-f**.

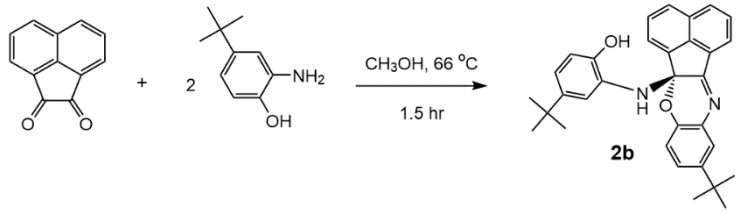

Scheme 2.2 Synthesis of phen-BIAN ligand **2b**.

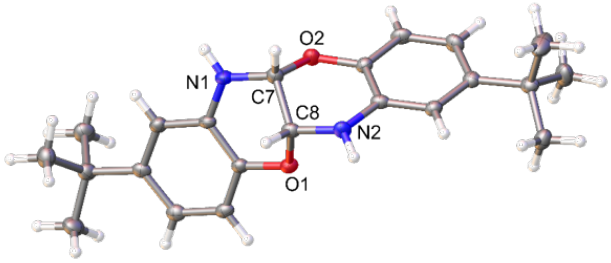

Figure 2.3 Crystal structure of *t*-bu-gbha (**1b**) in bisbenzoxazinobenzoxazine form. Ellipsoids at 50%.

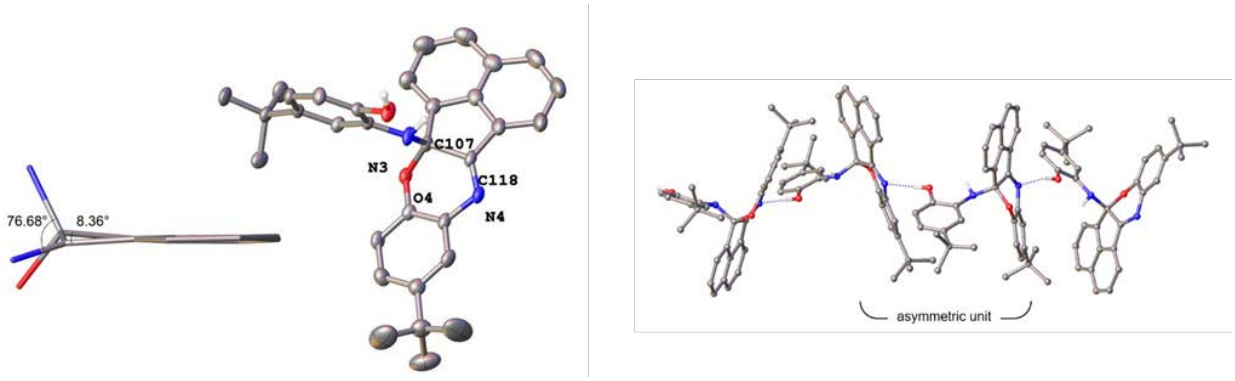

Figure 2.4 Center and right: crystal structure and asymmetric unit of *t*-bu-phen-BIAN (**2b,** R-configuration) showing solid-state hydrogen-bonding interactions (C=N···H(O): 1.928 Å). Far left: abridged side-on view of the N-C-C-N distortion along plane of acenaphthene backbone. All hydrogen atoms except those participating in bonding interactions omitted for clarity. Ellipsoids at 50%.

Large single crystals of **2b** suitable for single crystal X-ray diffraction were grown from CH_2Cl_2/MeOH, allowing analysis of connectivity. Similar to **1b**, the free ligand was found to exist in its cyclized form, though it can only sterically accommodate cyclization of a single arm. It is likely that after the addition of the first arm, the formation of the six-membered ring creates an alternate pathway for the nucleophilic addition of the second arm. The asymmetric unit consists of a racemic mixture of molecules which engage in hydrogen-bonding interactions between the free phenol of one molecule and the imine nitrogen of its adjacent enatiomeric counterpart in a pseudo-

one-dimensional structure. The C107—N3 distance is 1.443 Å, consistent with a single bond, and the imine C118—N4 distance of 1.280 Å is typical for a double bond.[20, 41] In accommodating the single tetrahedral carbon, a distortion of the typically planar N-C-C-N fragment relative to the naphthalene plane occurs—dihedral angles of 7.50° and 76.25° are observed between the two carbon atoms and the two nitrogen atoms, respectively (**Figure 2.4**).

In the solid state, the presence of both O-H and N-H stretches are observed by infrared spectroscopy at 3350 cm^{-1} and 3410 cm^{-1}, respectively, and stretches at1632 cm^{-1} and 1607 cm^{-1} are in range for both typical C=N imine stretching and N-H bending.[27, 40, 42] It is apparent by ^{1}H NMR in THF-d_8,[27] that the solution state structure is consistent with the solid-state structure. Two non-equivalent phenolic arms are apparent by two sets of analogous aromatic resonances between 6.3 and 8.0 ppm, as well as two distinct *tert*-butyl resonances at 1.37 and 1.41 ppm. Sharp singlets are observed at 4.96 and 7.57 ppm that can be assigned to the secondary amine and phenolic protons. ^{13}C NMR data including a resonance at 86.6 ppm consistent with a quaternary hemiaminal carbon[43] also corroborates that the solid-state and solution-state structures are the same; however these observations are exclusive to studies performed in THF-d_8.[27] Attempts to establish connectivity via ^{1}H NMR in $CDCl_3$, DMSO-d_6, DMF-d_7, CD_3CN, CD_3OD, and C_6D_6, even on material from the same batch as the sample studied in THF-d_8, showed multiple sets of resonances suggesting a mixture of ligand forms from which structural determination could not be made.

Synthesis and Characterization of Metal Complexes

The Ni^{2+}, Co^{2+}, and UO_2^{2+} complexes of **2b** were synthesized by reaction of **2b** with metal acetate salts in methanol or ethanol, and the products were isolated as intensely-colored solids (**Scheme 2.3**). Solid state IR data reveals a shift in frequency of the imine vibrations from 1632

cm^{-1} in the free ligand to 1567 cm^{-1}, 1558 cm^{-1}, and 1589 cm^{-1} on complexation to nickel, cobalt and uranyl, respectively. An intense absorption at 921 cm^{-1} for **UO_2-2b** is in good accord with those reported for the O=U(VI)=O asymmetric stretch.[44-45] In all cases, the disappearance of the N-H stretch of **2b** at 3410 cm^{-1} is observed.[27, 30] Complexes of **2b** were characterized by single-crystal X-ray diffraction. Selected bond lengths are summarized in **Table 1**. Crystals of **UO_2-2b** were grown from two solvent mixtures to examine solvent interactions with the uranyl oxo groups and packing effects: **UO_2-2b^1** was grown from CH_2Cl_2 by slow diffusion of MeOH into the saturated solution, and **UO_2-2b^2** was grown from a mixture of CH_2Cl_2 and $CHCl_3$ by slow diffusion of MeOH into the solution. The nickel and cobalt complexes (**Ni-2b** and **Co-2b**) are structurally similar mononuclear species bearing two tridentate (O-N-N) ligands bound meridionally to distorted octahedral metal centers. Surprisingly, the acenaphthene backbones of **Ni-2b** are not orthogonal to one another, and instead adopt a fan-blade configuration (**Figure 2.5**). No significant π-stacking interactions are present. Complex **Co-2b**, on the other hand, retains near-perfect orthogonality of the backbones.

The C—O bond lengths of ~1.35 Å strongly suggest that both free phenolic arms on **Ni-2b** remain protonated— O2—(H2) participates in hydrogen bonding to a series of three MeOH molecules, and the other O4—(H4) hydrogen-bonds intramolecularly to O1. The same singly protonated phenolic arms and MeOH-hydrogen-binding motif is seen for complex **Co-2b**.

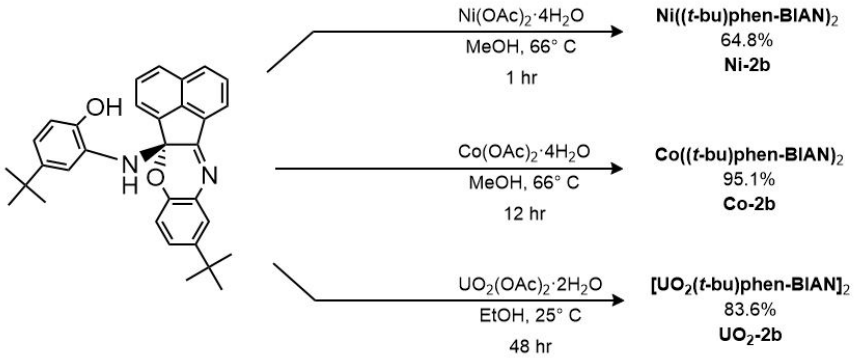

Scheme 2.3 Synthesis of complexes of **2b**.

Table 2.1 Selected average bond lengths (Å) and angles for complexes of **2b**

Complex	α-diimine		M—N	M—O	U=O	U=O···H	O-U-O°
	C=N	C—C					
Ni-2b	1.289 (4)	1.511 (5)	2.089 (3)	2.063 (2)			
Co-2b	1.296 (4)	1.484 (5)	1.920 (3)	1.909 (2)			
UO_2-2b[1]	1.302 (16)	1.496 (18)	2.535 (10)	2.244 (9)	1.756 (6)	2.475	178.05
UO_2-2b[2]	1.293 (10)	1.489 (11)	2.543 (7)	2.232 (5)	1.779 (6)	2.644	178.00

The C—N and C—C bond lengths observed in the α-diimine fragments of **Ni-2b** (C—N_{avg}: 1.289 (4) Å, C—C_{avg}: 1.511 (5) Å) and **Co-2b** (C—N_{avg}: 1.296 (4) Å, C—C_{avg}: 1.484 (5) Å) are consistent with C=N and C—C bonds, and show that each ligand coordinates as a phenolate mono-anion, with the M(II) oxidation states left unchanged. M—O and M—N bond lengths are listed in **Table 2.1**. **Ni-2b** differs from many nickel complexes in its pseudo-octahedral rather than square planar coordination environment. The Ni—N and Ni—O bond lengths are longer than found for square planar complexes, but in good accordance with those found for octahedral Ni(II) salen-type complexes.[46-47] This observed elongation has been previously attributed to the occupation of the

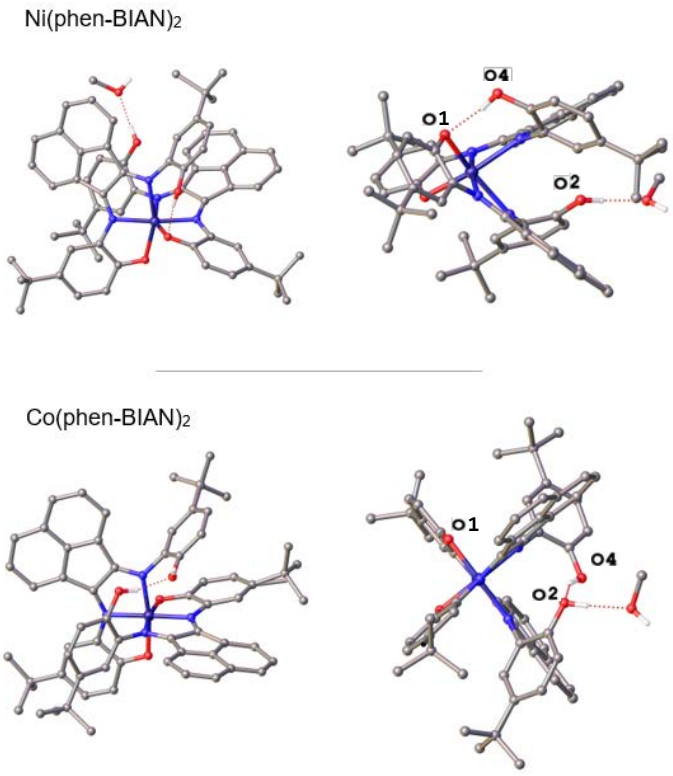

Figure 2.5 Above: molecular structure of **Ni-2b**. Below: molecular structure of **Co-2b**. Hydrogen atoms omitted for clarity.

$d_{x^2-y^2}$ orbital in these systems.[46] The Co—O and Co—N lengths of **Co-2b** are also elongated relative to those found in many similarly-coordinated Co(II) systems, though not to the extent observed for **Ni-2b**. This ~0.1 Å elongation can again be justified by the octahedral environment.

Unlike the ML_2 Co(II) and Ni(II) complexes, the UO_2^{2+} ion binds one tetradentate ligand per metal center, and adopts a dimeric μ-phenolato-bridged structure (M_2L_2), (**Figures 2.6 and 2.7**). As shown in **Figure 2.7**, the two unique crystallized forms, **UO_2-2b[1]** and **UO_2-2b[2]**, feature distinct structural characteristics as a result of the incorporation of either CH_2Cl_2 or $CHCl_3$ into the crystal lattice—the effects of these differences on the long-range order, as seen in the packing insets, are quite striking. In each case, the uranium maintains a pentagonal bipyramidal geometry with linear O=U=O centers (178.0°) and U—U distances of greater than 3.9 Å. The phen-BIAN binds equatorially as a tetradentate dianionic ligand, as evidenced by bond lengths within the α-diimine

fragment (**Table 2.1**). All U=O bond lengths are consistent with the assignment of U(VI) centers in both structures. **UO_2-2b[1]** contains an asymmetric $[UO]_2$ core (**Figure 2.6**) with much larger variations in bond lengths than is observed for similar dimeric salen complexes,[23, 45] though it is worth noting that the repertoire of structurally characterized aryloxide-bridged uranyl dimers is quite limited. The two ligand backbones are tilted downwards from the $[UO]_2$ core, and the phenolic arms upwards—the core is buckled and the uranyl moieties are oblique to one another as a result. U2 sits 0.535 Å below the mean O1-U1-O4 plane.

An intriguing feature of this structure is the position of the associated dichloromethane molecule. While the orientation of the two hydrogen atoms towards the uranyl oxo groups (**Figure**

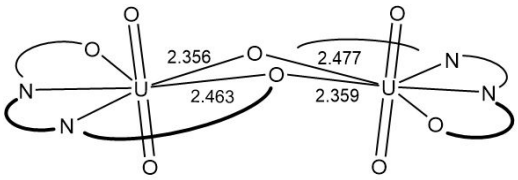

Figure 2.6. $[UO]_2$ core with U—O bond lengths and abrbreviated ligand structure.

2.7) is not surprising sterically or electronically, the U=O···H distances of 2.415 and 2.535 Å place these interactions within the formally defined hydrogen-bonding range of 1.86-2.72 Å (for O···H).[48] A report on solid-state interactions between CH_2Cl_2 or $CHCl_3$ and organic molecules noted the propensity of an interaction to exist between the solvent hydrogen atoms and a doubly bonded oxygen in structures that contained both components[48]. For CH_2Cl_2 and $CHCl_3$, the mean distances of these interactions were 2.41 Å and 2.26 Å, respectively.[48] The mean U=O···H($CHCl_2$) distance of 2.48 Å is in good agreement with being a significant interaction, though the retention of U(VI)=O bond lengths of 1.76 and 1.78 Å in combination with the aprotic nature of these hydrogens precludes true hydrogen-bonding. This does indicate, however, that the

oxo groups in this system are not entirely unreactive. This solvent-yl interaction is quite interesting given that the considerable inertness of these groups in most environments is tied to difficulty removing UO_2^{2+} contamination and that there is a growing interest in activating and functionalizing uranyl oxygen atoms.[6, 49]

To further investigate this interaction, additional crystals of the complex were grown under the same conditions as **UO₂-2b¹**, but using a 50:50 $CHCl_3$:CH_2Cl_2 solution. This resulted in the higher-symmetry structure **UO₂-2b²**, which incorporates two molecules of $CHCl_3$ per asymmetric unit. The two halves of the dimer are symmetry related (S_2), orienting the backbones on opposite sides of the molecule. The $[UO]_2$ core remains perfectly planar (calculated deviation of U2 from mean O1-U1-O1a plane is 0.000 Å), and the difference in its U—O_{br} bond lengths is nearly half that observed for **UO₂-2b¹** (0.60 Å difference vs. 0.11 Å average difference). Both the α-diimine and U=O bond lengths are again diagnostic of U(VI) centers (Table **1**). One of the included $CHCl_3$ molecules engages in a C-H⋯π interaction with one phenolic arm, likely influencing the packing. The H1s⋯centroid distance of 2.649 Å is typical for this type of interaction[50]. The other molecule, as desired, exhibits contacts to the uranyl oxo groups analogous to those in **UO₂-2b¹**. These contacts, on average, are not quite as close (H2s⋯O3: 2.503 Å; H2s⋯O4: 2.784 Å), consistent with their increased steric demand over CH_2Cl_2, but they are present on both sides of the molecule, which is not seen in **UO₂-2b¹**. While the first CH_2Cl_2-oxo interaction was curious given the conditions, the repeatability of this oxo-interaction with aprotic but electropositive solvents suggests that the redox-active phen-BIAN may impart some electronic flexibility to these axial groups through covalent interactions. No additional longer-range ordering is observed.

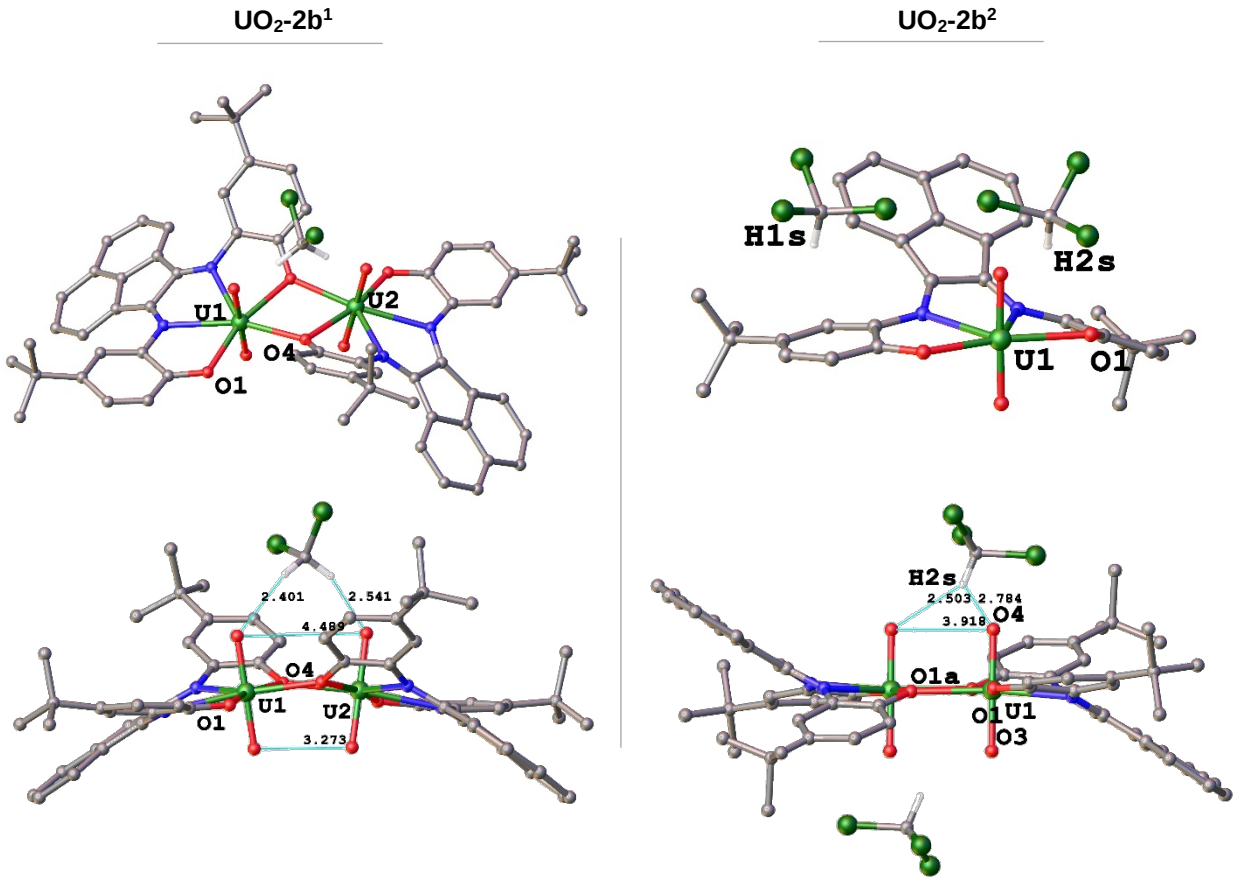

Figure 2.7. Asymmetric unit (top), and side view of dimer (bottom) with oxo-hydrogen distances (Å). Distances indicating interactions between the metal complex and solvent are shown. All non-relevant hydrogen atoms omitted for clarity.

Many similar features are observed for uranyl complexes of the less-conjugated gbha ligands, including the μ-phenolato-bridged dimeric structure and oxo-solvent interactions. The more manageable solubility of the gbha complexes allowed for crystallization of a greater number of derivates (**UO_2-1b-c, e-f**; R = *t*-bu, H, naphthyl, F) which was not attainable for the phen-BIAN complexes. The physicochemical data acquired for **UO_2-1** and **UO_2-2** suggests that the nuclearity of the complexes is solvent-dependent, and in the solid-state, the structure is impacted heavily by crystallization conditions. The analysis by ^{1}H NMR in DMSO consistently indicates a single coordination environment, and only in one case, (**UO_2-2d**) was there indication of coordination by a CH_3OH solvent molecule. Mass spectral analyses of the **UO_2-1** complexes from a 2:1

CH_3CN:THF solution indicate the presence of primarily the dimeric species, though electrochemical characterization attempted in both THF and CH_3CN indicates these complexes behave in an entirely different fashion, not consistent with a dinuclear, bridged complex, but rather as mononuclear species.[30]

The complex **UO_2-1b** crystallizes in $P\bar{1}$ as the μ-phenolato-bridged dimer $[UO_2(t\text{-bu})gbha]_2$ with an interatomic U—U distance of 4.0143 (9) Å (**Figure 2.8**). This is the same bonding motif observed for the analogous complex $[UO_2(t\text{-bu})phen\text{-}BIAN]_2$.[27] The complexes **$UO_2$-1c** and **$UO_2$-1f** are CH_3OH-coordinated monomers in the solid-state, and form pseudo-dimers through hydrogen-bonding between the methanolic proton of one monomer and phenolic O atom of the next. These three complexes all engage in weak, long-range (2.4-2.8 Å) interactions between the uranyl oxo groups and adjacent hydrogen atoms (MeOH, imine H, and interstitial benzene) (**Figures 2.10,12,14-15**) The orientation of the oxo groups into these "proton pockets" is not unusual when taking into account packing and electrostatic forces; however, in the case of **UO_2-1c** (**Figure 2.11-12**), these can be considered a stabilizing force for the elongated U=O bond (1.809(9) Å). The **UO_2-1c** complex is the only structure of this group which features significant uranyl-oxo bond elongation—**UO_2-1b** and **UO_2-1f** have average U=O bond lengths of 1.784 (13) and 1.778 (11) Å, respectively, with only slight asymmetry observed for **UO_2-1f**.

For **UO2-1b** (**Figure 2.8**), the average U—N and U—O distances are 2.547(13) and 2.352(11) Å, respectively, with the latter being asymmetric due to the participation of one phenolate O atom in the bridge. These distances are consistent with those reported for the monomeric U(VI) species $UO_2(gbha)(H_2O)$ and similar dimeric species,[27, 36 23] in that the average U=O bond length of 1.784 (13) Å is consistent with a typical U(VI) center. Of note in this structure is that the aryl rings are not uniform in bond length one might expect, and instead exhibit a quinoid-type distortion,

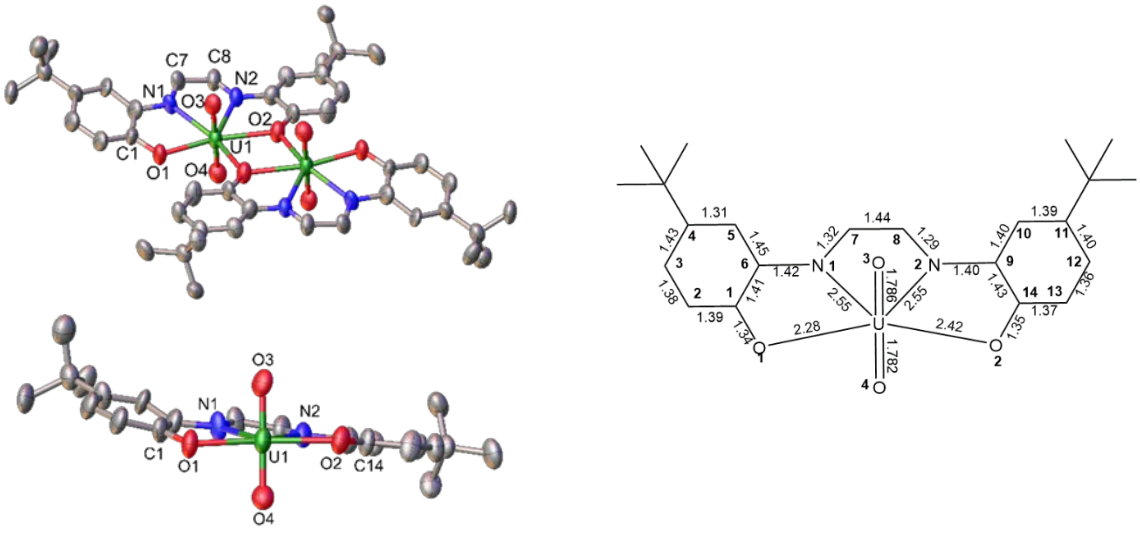

Figure 2.8. Left: Molecular structure and side-on view of asymmetric unit of UO_2-1b. Hydrogen atoms omitted for clarity. Right: Bond lengths for UO_2-1b. Average esd for C—C: (2, two decimal places); average esd for all other bonds (12, three decimal places).

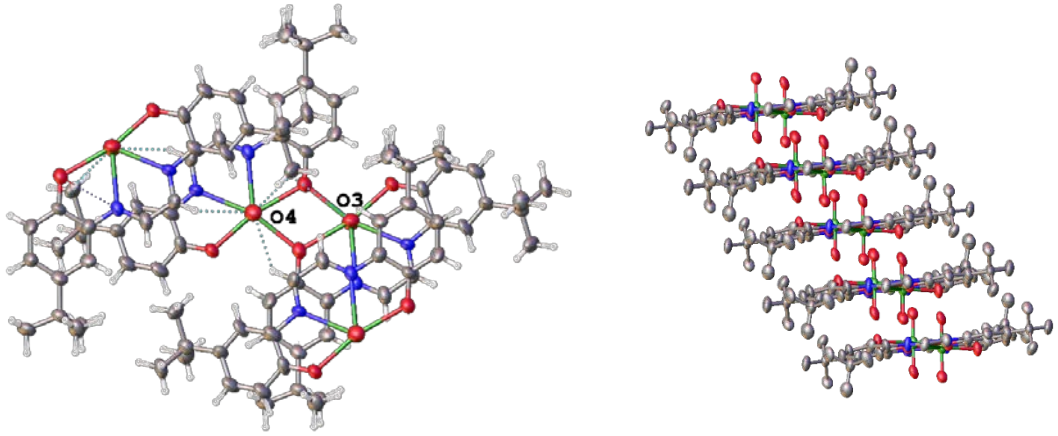

Figure 2.9. View down O=U=O bonds and packing for UO_2-1b.

especially within the C1-6 ring (**Figure 2.8**).[34, 51-52] The C2—C3 and C4—C5 distances average 1.345 (2) Å, whereas the average of the C1—C2, C3—C4, C5—C6, and C6—C1 distances is 1.415 (2) Å. This difference is significant even when the lower precision of C—C bonds in this structure is taken into account. This distortion is also associated with a deviation of the ring (including O1 and N1) 18.13° from the mean plane defined by N2, C9-14, and O2 (**Figure 2.8**).

One of the methyl protons also engages in an interaction of 2.614 Å with uranyl O4 which likely contributes to the plane deviation (**Figure 2.10**).

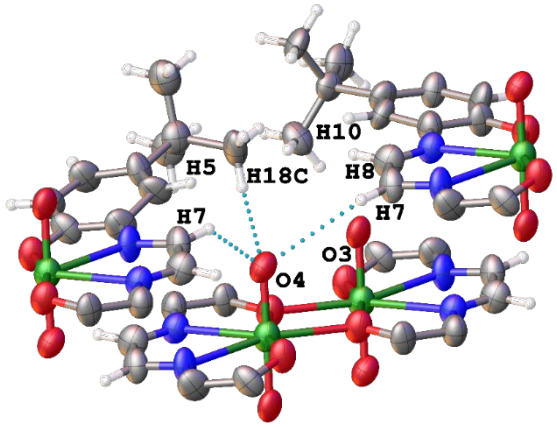

	Distance (Å)
O3—H8	2.845
O3—H10	2.854
O4—H5	2.817
O5—H7	2.877 (3.148*)
O4—H18C	2.614

* Denotes H7 of different molecule

Figure 2.10. Oxo-proton interactions and distances for UO_2-1b.

Additionally, the C—N and C—C distances of glyoxal-derived α-diimine backbones are diagnostic of ligand oxidation state, where neutral diimines have bond lengths of ~1.24 and ~1.49 Å, respectively, and those found for singly reduced radical anions are ~1.32 and ~1.40 Å.[34, 52] Those observed in the structure of **UO_2-1b** are 1.305(10) (C—N_{avg}) and 1.44(2) Å (C—C), which do not fall neatly into either category, suggesting this species has some radical-type character in that there is an unusual distribution of electron density; however it is not a true radical anion. The C—N_{avg} distance in this case is more indicative of such character, though there is no evidence of a radical by EPR spectroscopy. Furthermore, the C1—O1 and C14—O2 distances are 1.342(18) and 1.350(19) Å, which is consistent with phenolate donors and coordination of the ligand as a dianion. The solid-state structure of this species and of **UO_2-1b** is best represented by a U(VI) complex of a gbha ligand for which the *o*-iminobenzosemiquinonate radical anion resonance form contributes significantly.[35]

The monomeric complex **UO_2-1c** features two units of [UO_2(gbha)(MeOH)] which hydrogen-bond with one another *via* the coordinating CH_3OH molecules. The ligand in unit A remains nearly planar, while that in unit B undergoes a significant twist (**Figure 2.11**). Hence, when the mean plane is defined by U-N-C-C-O of one side, the other ring deviates by 15.19° (N102, O102, C109-114) or 11.65° (N101, O101, C101-106). Deviation from planarity is observed for one ring in the water-coordinated complex UO_2(gbha)(H_2O),[36] but this is cited as a repulsive interaction between the ring and a nearby oxo ligand, and this is not observed for our system. Both units (**Figure 5**) have asymmetric and/or elongated uranyl oxo bonds (U1—O3: 1.809(9) Å, U1—O4: 1.776(11) Å; U101—O103: 1.786(10) Å, U101—O104: 1.797(15) Å)—these are notable increases in length (nearly 0.04 Å longer than standard uranyl (VI) oxo bond lengths of ~1.77 Å).[53] The U—O distances for U(V) species are often upwards of 1.88 Å,[14, 54] though they have been cited as low as 1.810 Å.[55-56] For the previously characterized aqua complex, U=O lengths of 1.77(2) and 1.76(2) Å are found; however, the esd's observed are larger by an order of magnitude.[36] We attribute this elongation to the non-innocent character of the gbha ligand, which is most evident from the C1—O1 and C114—O102 bond lengths of 1.29(2) Å. The corresponding bonds in **UO_2-1b** retain their phenolate character with lengths of 1.342(18) and 1.350(19) Å as does the C14—O2 bond of **UO_2-1c**, whereas these shorter bonds are consistent with a higher bond order, as has previously been observed for systems with this type of quinoid distortion, bearing some similarity to radical anion ligands.[34-35, 57] In unit A (**Figure 2.11**), the quinoid-type distortions of the rings can be seen, though they are subtle, especially in comparison to that of **UO_2-1b** and are not significant given the low C—C bond precision of the structure. Additionally, we see differences in the α-diimine fragments of units A and B—most notably, the C107—C108 distance in unit B is shortened to 1.40(2) Å from 1.44(2) Å in unit A and in **UO2-1b**, again consistent with radical-like redistribution of electron

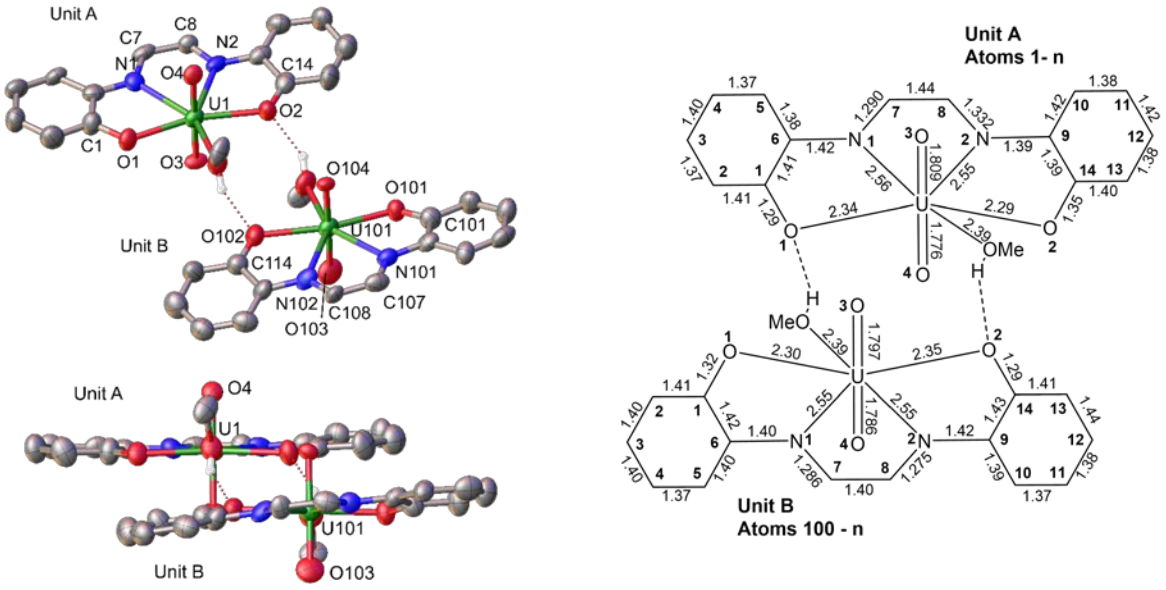

Figure 2.11. Molecular structure and side-on view of asymmetric unit of UO_2-1c (left). Select hydrogen atoms omitted for clarity. Bond lengths of UO_2-1c (right). Average esd for C—C: (2, two decimal places); average esd for all other bonds (13, three decimal places).

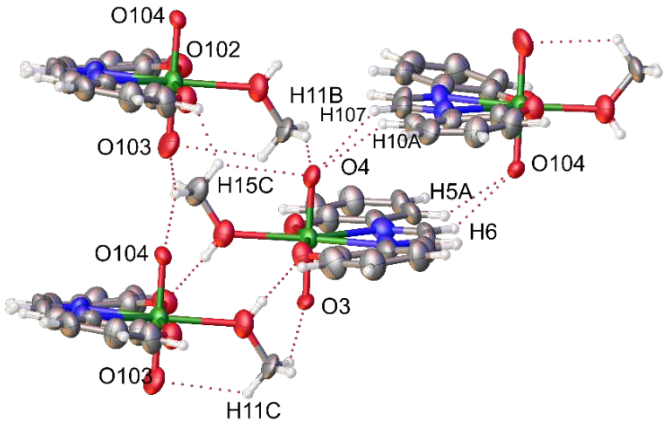

	Distance (Å)
O3—H11B	2.699
O4—H11B	2.617
O4—H15C	2.654
O4—H10A	2.586
O4—H107	2.966
O103—H11C	2.675
O103—H15A	2.725
O104—H15A	2.791
O104—H6	2.736
O104—H5A	2.555

Figure 2.12. Oxo-proton interactions and distances for UO_2-1c.

density. Despite the esd's being large, this difference is still meaningful as it coincides with some elongation of the average C—N distance to 1.281(19) Å, which is intermediate to the approximately 1.32 Å distance diagnostic of the singly reduced radical anion form and the approximately 1.24 Å distance for neutral gbha species.[34, 52] Unit A, which has a very intermediate

C7—C8 distance of 1.44(2) Å, has a longer average C—N distance of 1.311(19) Å, which is much more consistent with a reduced bond order than with a typical double bond. The equatorial U—N and U—O bond lengths of 2.558(12) and 2.319(10) are consistent with the assignment of a U(VI) species[58-59] and suggest the nitrogen is still donating as a neutral atom, not an anionic one, which would be reflected by U—N distances approximately 0.20 Å shorter than those observed.[4] In solution, this species shows no indication of persistent radicals, as the NMR spectra appear typical for diamagnetic complexes, and is EPR silent. We therefore favor assignment of this species as a gbha U(VI) complex which exclusively in the crystalline state has some characteristics of a U(VI) gbha-radical. These findings clearly illustrate the non-innocent character of the gbha ligand and its impact on structural features of uranyl complexes.

We also examined the structures of complexes **UO_2-1e** and **f**, which crystallize as H_2O- and CH_3OH-coordinated monomers, respectively (**Figure 2.13**). While there is some deviation from planarity of the ligand in both cases, it is much less significant (7.40° (**e**), 7.33° (**f**)) than that in **UO_2-1b** and **UO_2-1c**. **UO_2-1e** has average U—N and U—O bond lengths of 2.558(4) and 2.312(4) Å, and those of **UO_2-1f** are 2.546(13) and 2.267(11) Å. These values are consistent with the other species and with the assignment of U(VI) centers. In both cases, the α-diimine fragments bear some radical-type character (C—C: 1.452 (7), C—N: 1.283 (7) for **UO_2-1e**; C—C: 1.44(2), C—N: 1.293(8) for **UO_2-1f**), but this is not reflected elsewhere in the complexes, perhaps due to the electronegativity of the fluorine, and greater degree of delocalization possible for the naphthyl system. The uranyl U=O bond lengths for both of these species only show very small variations—for **UO2-1e**, 1.779(5) (U1—O3) and 1.791(5) (U1—O4), and for **UO_2-1f**, 1.770(11) (U1—O3)

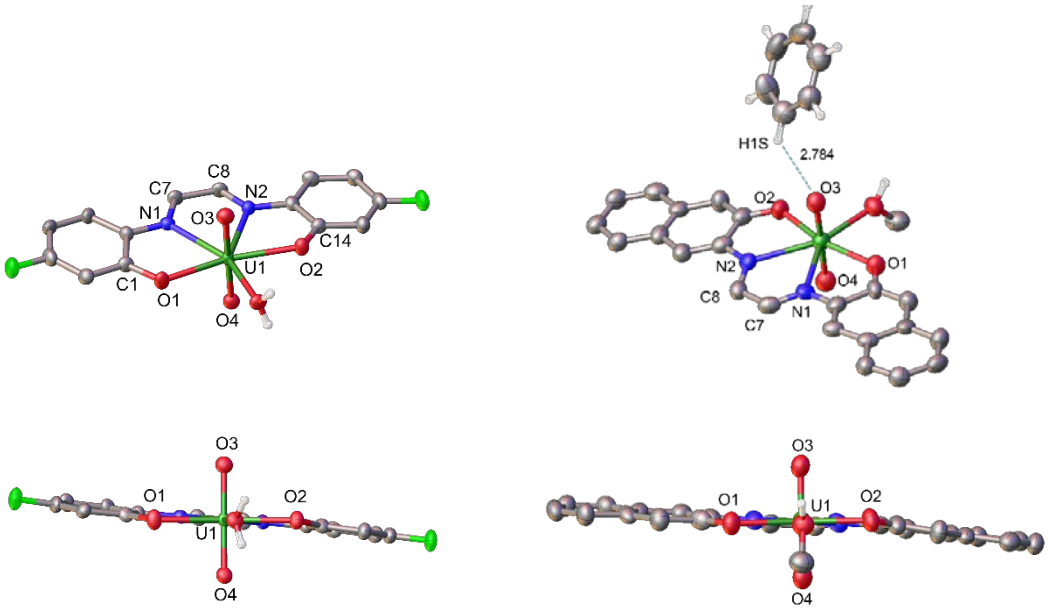

Figure 2.13. Left: Molecular structure and side-on view of asymmetric unit of UO_2-1e. Right: Molecular structure and side-on view of asymmetric unit of UO_2-1f. Select hydrogen atoms omitted for clarity.

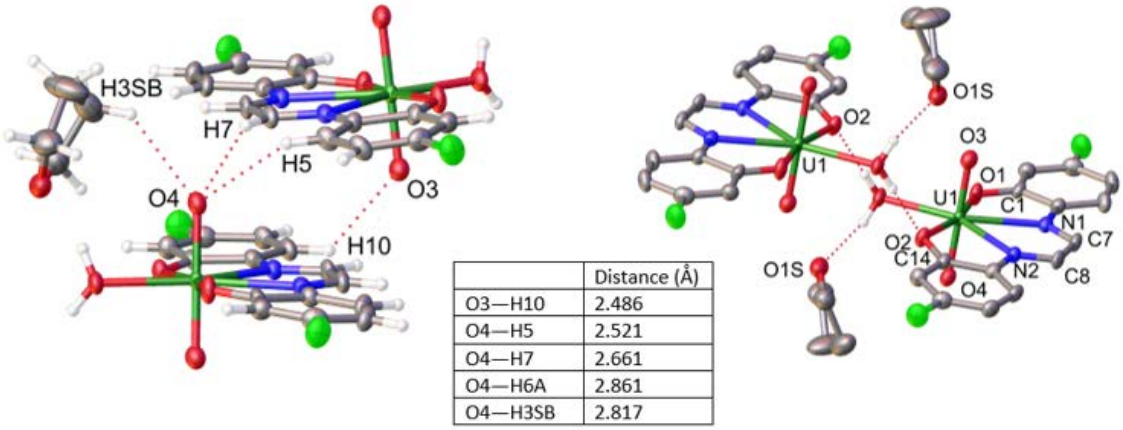

	Distance (Å)
O3—H10	2.486
O4—H5	2.521
O4—H7	2.661
O4—H6A	2.861
O4—H3SB	2.817

Figure 2.14. Oxo-proton interactions (left) and H-bonding interactions (right) in UO_2-1e.

and 1.785(11) (U1—O4). Although this lengthening of the U1—O4 for the naphthyl complex (**UO_2-1e**) is rather small and is in fact *statistically* insignificant, it is of interest as O3 engages in several long-range, weak contacts to H-atoms in a "proton pocket", including to the interstitial benzene H1S shown in **Figures 2.13** and **2.15** (2.784 Å). Generally, an increase in bond length

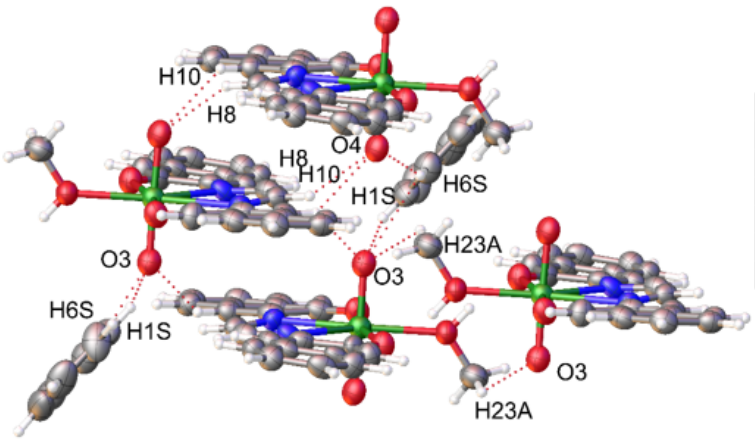

	Distance (Å)
O3—H23A	2.623
O3—H6S	2.931
O3—H1S	2.784
O4—H6S	3.114
O4—H8	2.560
O4—H10	2.592

Figure 2.15. Oxo-proton interactions and distances for UO_2-1f.

would be expected for the oxo ligand engaging in contacts with electropositive species[5], not the oxo ligand *trans* to it; however, we have observed this slight "asymmetry" previously in cases where uranyl-solvent interactions are present.[60] The latter, more predictable behavior is observed for **UO_2-1e**, where O4 engages in a greater number of weak H-atom interactions.

Infrared Spectroscopy

To gain better insight into how the equatorial ligand electronics impact the uranyl moieties across the gbha and phen-BIAN complexes, the vibrational properties of complexes **UO_2-1a-f** and **UO_2-2a-f** were characterized using infrared spectroscopy. The symmetric (ν_1, Raman active) and asymmetric (ν_3, IR active) vibrational modes are characteristic of the uranyl moiety,[61-63] making vibrational spectroscopy a useful probe to evaluate ligand influence on axial interactions. It has been well-established that uranyl stretching frequencies are strongly indicative of the binding strength of the equatorial ligands and can therefore serve as a measure of covalency[64-66]. The large assembly of compounds presented herein represents a unique opportunity to examine the impacts

of both R-group substitution and degree of ligand conjugation on the axial -yl interactions. The IR spectra featuring the ν_3 stretches of the two sets of uranyl complexes (gbha and phen-BIAN) are shown in **Figure 2.16**. While no trends are obvious at first glance other than the *t*-bu-substituted complex having the highest frequency in both cases, on closer inspection several features become apparent. First, as the phen-BIAN complexes show a greater variation in their ν_3 values and are overall lower in energy by an average of 8.4 cm^{-1} than those of the gbha complexes, it is notable that for most cases, the values are closely matched. The exceptions here are the fluoro- (901 cm^{-1})

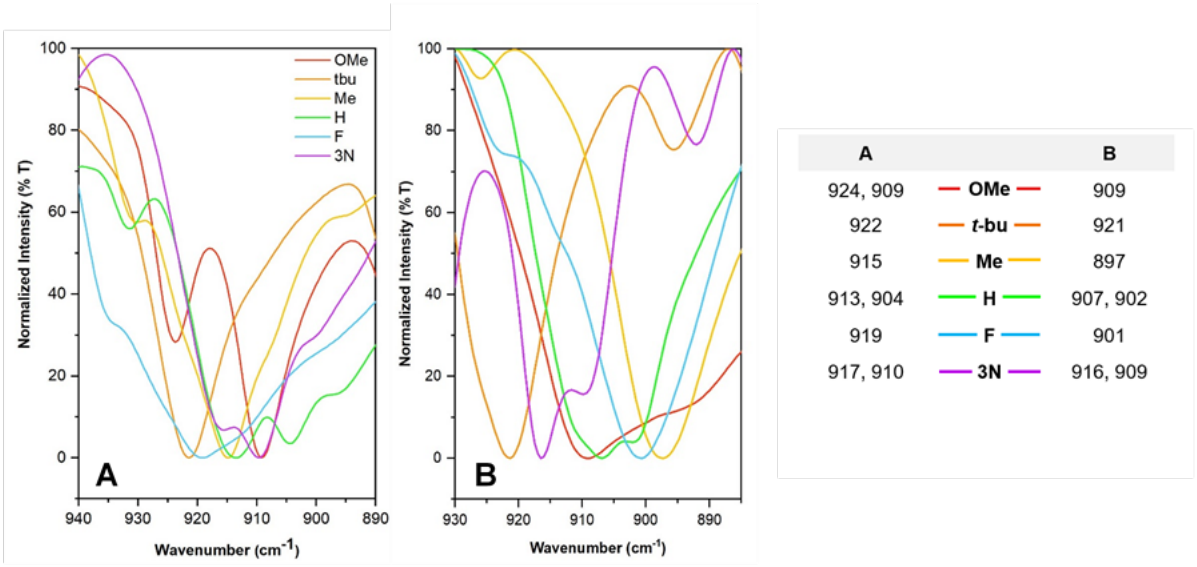

A		B
924, 909	OMe	909
922	*t*-bu	921
915	Me	897
913, 904	H	907, 902
919	F	901
917, 910	3N	916, 909

Figure 2.16. Uranyl U=O asymmetric (ν3) stretches for gbha complexes (A) and phen-BIAN complexes (B) and table of vibrational frequencies (cm^{-1}).

and methyl-substituted phen-BIAN (897 cm^{-1}) complexes (**Figure 2.16**), indicating that the presence of electron-donating groups *para* to the imine N in conjunction with the extended π-system offered by the acenaphthene backbone affords a unique ligand environment that is more strongly donating and thus possessing of somewhat greater covalent character than its gbha counterparts[64]. The electron-donating effects of these substituents can also be observed in the N—

H stretching frequencies of the gbha ligands as benzoxazinobenzoxazines.[30] Second, the presence of an electron-donating substituent *para* to the phenolic donor does not have the same effect on the ν_3 O=U=O stretch. In fact, these complexes (OMe, *t*-bu) generally have the highest stretching frequencies. While these substituents should increase the electron density of the phenolic donor, this behavior is not necessarily reflected in the IR data, rather the concomitant decrease of electron density at the imine N may be reflected here. In the case of the phen-BIAN complexes, these data implicate a greater covalent contribution from the imine N-atoms than the phenolic oxygens. This is curious, given the π-accepting nature of the α-diimine fragment, and the unambiguous retention of the electron-deficient U(VI) oxidation state.

For those species that exhibit two ν_3 stretching frequencies, this splitting may be attributed to the asymmetry of the U=O bonds. For the unsubstituted gbha complex **UO_2-1c**, the presence of two stretching frequencies at 913 and 904 cm^{-1} is consistent with its solid-state structure, where the latter corresponds to the elongated U=O bond (1.809(9) Å). **UO_2-1f** also exhibits elongation of one of the U=O bonds to a lesser extent, but this asymmetry is still reflected by the IR data. No new crystal structures of the phen-BIAN complexes could be obtained due in large part to their poor solubility, but these data indicate that both **UO_2-2c** (-H) and **UO_2-2f** (-3N) may also show perturbations of the oxo bonds.

Electronic Spectroscopy

UV-Vis studies of the gbha (**1**) and phen-BIAN (**2**) ligands and their complexes were conducted. To compare the uranyl and transition metal complexes of (*t*-bu)phen-BIAN (**2b**), spectra were recorded in CH_2Cl_2, and to compare derivatives of the gbha and phen-BIAN uranyl complexes, spectra were recorded in THF. Additional studies were conducted on the zinc complex

of the gbha ligand **1b** to establish the identity of the UV-Vis features, as the free ligands **1b** and **2b** were noted to have solvent-dependent hues. It is clear that the primary CT bands for these complexes are ligand-based—when the white solid **1b** is dissolved in most solvents, the solution is colorless or extremely pale yellow, but in CH_3OH is lavender-blue, and the bright yellow solid **2b** is yellow in most solvents but purple in CH_3OH. For **1b** in CH_3OH, in addition to the primary absorption at 296 nm, the solution exhibits two bands at 365 nm (379 M^{-1} cm^{-1}) and 584 nm (530 M^{-1} cm^{-1}) and a shoulder at ~480 nm (**Figure 2.17**). Other ligand derivatives were not investigated for this behavior, as only the *t*-bu derivative has the requisite solubility in room-temperature CH_3OH solutions. This suggested the UV-Vis features were of intraligand charge transfer (ILCT) type– as ILCT processes typically exhibit solvent-polarity dependence,[67] we sought a route to further confirm this assignment. The closed-shell Zn^{2+} complex of **1b** was synthesized and studied by UV-Vis in several solvents (**Figure 2.18**). This complex is solvatochromic and exhibits the same general absorption profile as the free ligand (CH_3OH) and the uranyl gbha complexes (**Figure 2.20**). The λ_{max} values of the longest-wavelength ILCT band are labeled below (**Figure 2.18**). The complexes are intensely colored in solution, with the exception of EtOAc (pale pink). The complex is somewhat soluble in CH_3OH and CH_2Cl_2 (blue-purple and purple solutions, respectively) at this concentration but is less soluble in ethyl acetate—hence the weaker CT bands. These λ_{max} values do not correlate exactly with the polarity of solvents CH_3OH > EtOAc > CH_2Cl_2), but the collection of additional data is hampered by the insolubility of the complex. Dependence of the CT energy on solvent is nonetheless observed. Based on this data, these CT bands can unambiguously be assigned to ligand-based ILCT processes.

In CH_2Cl_2, the λ_{max} of **2b** appears at 356 nm (**Figure 2.19**). **Ni-2b** and **Co-2b** display small hypsochromic (blue) shifts of λ_{max} to 341 nm (Ni) and 342 nm (Co). A shoulder at 411 nm is

observed for **Ni-2b** as well as a charge transfer (CT) band at 551 nm, which is accompanied by shouldering at approximately 630 nm. On sitting unperturbed over the course of 30 minutes, this

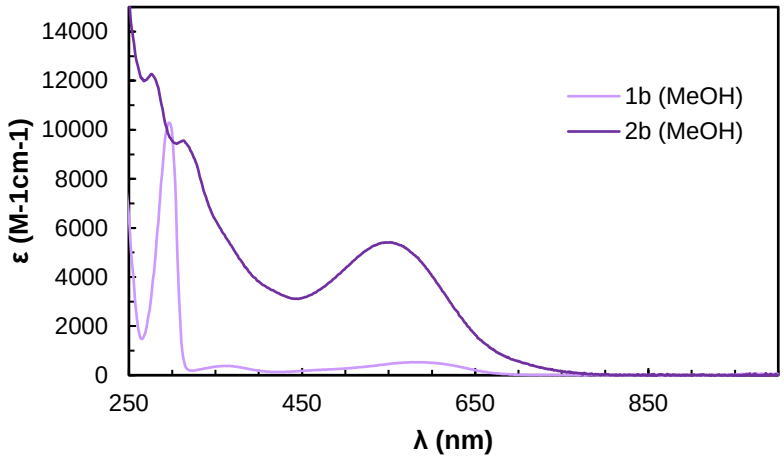

Figure 2.17. UV-Vis spectra of the free ligands **1b** (*t*-bu-gbha, 100 μM) and **2b** (*t*-bu-phen-BIAN, 40 μM) in methanol.

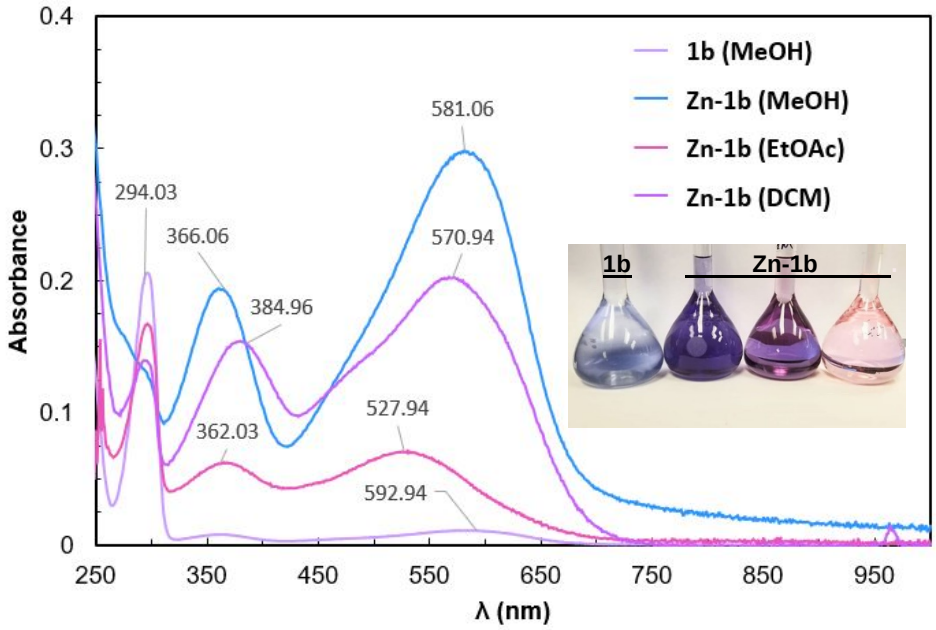

Figure 2.18. UV-Vis spectra of the free ligand **1b** and the complex **Zn-1b** in methanol, ethyl acetate, and dichloromethane. Samples of **Zn-1b** were measured immediately after preparation and are of equal concentration (~20μM) and **1b** (100 μM) has been scaled by 0.20 to approximate a 20 μM solution for reference. Inset photo is of solutions measured.

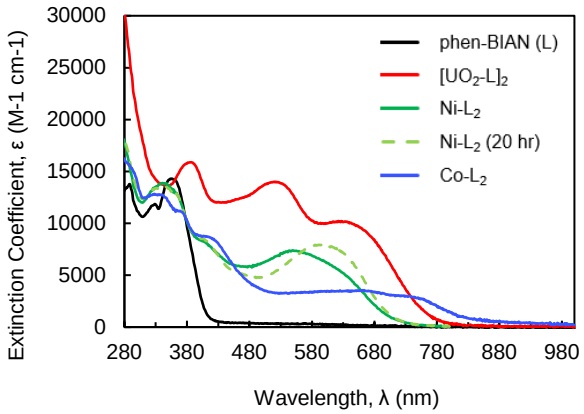

Figure 2.19. UV/Vis absorption spectra of (*t*-bu)phen-BIAN (2b, black), Ni-2b (green), Ni-2b after 20 hours in solution (green dashed), Co-2b (blue), and UO_2-2b (red) as 20 μM solutions in CH_2Cl_2.

solution (CH_2Cl_2) turned from a deep purple color to a medium green-blue. After 20 hours, no additional color change was observed, and UV/Vis data was recollected, showing a bathochromic (red) shift of the main CT band to 598 nm. This suggests a change in coordination geometry[68], particularly considering the presence of the two available phenolic donors. The spectrum of **Co-2b** displays two small shoulders at 363 nm and 415 nm, and a broad absorption feature from 550-780 nm that is significantly weaker than the CT bands observed for either of the other complexes. **UO_2-2b** exhibits a bathochromic shift of λ_{max} to 387 nm, and two CT bands are observed at 522 nm and 622 nm. This is also the only complex associated with an increase in the extinction coefficient. The UV-Vis data collected for the larger array of compounds in THF as well as computational studies of the gbha ligands were particularly useful in understanding the electronic environments afforded by these unique α-diimine frameworks. The absorption spectra of the UO_2-gbha complexes is shown in **Figure 2.20**. These spectra generally feature two primary intense absorption bands at 578-712 nm (9,400-13,500 M^{-1} cm^{-1}) and 366 – 388 nm (~5,400-9,600 M^{-1} cm^{-1}), which can be attributed to $\pi \rightarrow \pi^*$ transitions between the phenolic donors and the α-diimine moiety (ILCT type), and the formation of phenoxyl radicals, respectively.[34, 69] The lower-energy

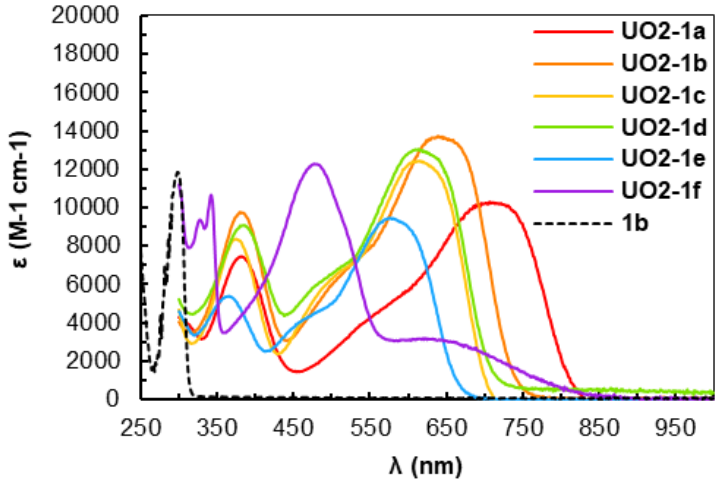

Figure 2.20. UV-Vis data for uranyl-gbha complexes (UO_2-1a-f), 20 μM in THF. Representative free ligand trace shown for comparison as dashed line ((*t*-bu)-gbha (1b), 40 μM in THF). The UO_2-1f complex includes some free ligand component.

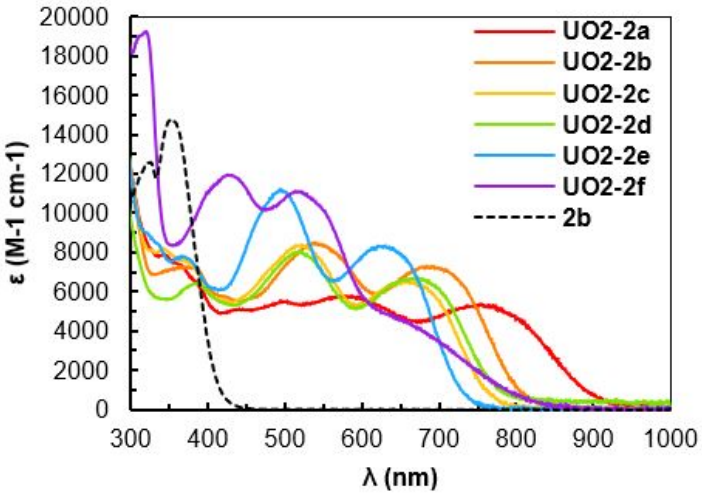

Figure 2.21. UV-Vis data for uranyl-phen-BIAN complexes (UO_2-2a-f), 20 μM in THF. Representative free ligand trace shown for comparison as dashed line (tbu-phenBIAN, 40 μM in THF)

transitions are of intraligand charge transfer (ILCT) type and arise due to the presence of phenolic donors and a π-acceptor unit within the same framework.[67] The uranyl naphthyl-gbha complex (**UO_2-1f**) behaves similarly, but this is somewhat of an exception—the higher-energy π → π* transition occurs at 481 nm (12,300 M^{-1} cm^{-1}), and the lower-energy band at 620 nm is much broader and less intense (3,200 $M^{-1}cm^{-1}$). We can attribute this at least in part to some included

free ligand in solution as the ligand and complex components were inseparable, and therefore we do not assign much weight to this data, despite it approximately matching the behavior of **UO_2-2f**. Shoulders at ~450-520 nm are also observed in the spectra of each of the uranyl complexes. These high-intensity ligand features unfortunately preclude any observation of the weak oxo → U(VI) LMCT.

Characterization of the UO_2-phen-BIAN complexes using UV-Vis spectroscopy (**Figure 2.21**) revealed similar features to those of the gbha complexes with several key distinctions. First, the energies of λ_{max}^1 are lower in energy by an average of 0.14 eV (+45 nm), as are those of λ_{max}^2 (by ~0.06 eV, +~20 nm) which can be attributed to the presence of the extended π-system of the acenaphthene unit. Second, the more significant energy-lowering of the λ_{max}^1 CT band relative to that of λ_{max}^2 allows for better resolution of the second CT process. Rather than appearing as shoulders in the gbha complexes, these peaks are distinct, and as in the case of the gbha complexes, can be assigned to ILCT-type transitions. The high-energy bands (λ_{max}^3) are again characteristic of the formation of phenoxyl radicals.[34, 69] Interestingly, the molar absorptivities of these complexes are overall significantly lower than those of the gbha complexes, particularly in the visible region. This is surprising given that these species are more highly conjugated—though a significant difference can be seen between the naphthyl derivative and the others in this respect (**Figure 2.21**), especially at lower wavelengths. **UO_2-2e** also has higher molar absorptivities for both CT bands, in contrast to the **UO_2-1e** complex, which has the lowest overall values for ε, indicating that different interactions with the ligand backbone are taking place for these two ligand sets. Additionally, the presence of the BIAN backbone allows for better "tuning" of the longest-wavelength ILCT energy, as these peaks occur over a wider range of energies with greater variance among them.

For both the uranyl gbha and uranyl phen-BIAN complexes, a notable trend emerges that those bearing more strongly electron-donating groups have lower-energy absorptions, with the methoxy (**1a, 2a**) derivative being the most strongly donating to the *para* position (in this case the phenolic donor) and having by far the highest $\lambda_{max}{}^{1}$ value. The $\lambda_{max}{}^{1}$ values of the -*t*-bu, -Me, and -H (unsubstituted) complexes are intermediate, and the -F derivative is lowest. This behavior is consistent with the relative donor strengths of the substituents and their positions relative to the phenolic donor. In both cases, the naphthyl-substituted complex features a broad, less-intense $\lambda_{max}{}^{1}$ absorption that may result from greater delocalization of charge. These data are summarized in **Tables 2.1-2.2.**

Table 2.2. λ_{max} values and extinction coefficients of uranyl gbha complexes **UO_2-1a-f**.

UO_2 -1	**$\lambda_{max}{}^{1}$ (nm)**	**$\lambda_{max}{}^{2}$ (nm)**	**$\lambda_{max}{}^{3}$ (nm)**
OMe	709 *(10,300)*	~550[a]	382 *(7,500)*
t-bu	648 *(13,600)*	~525 [a]	380 *(9,800)*
Me	614 *(13,000)*	~510 [a]	388 *(9,000)*
H	613 *(12,400)*	~500 [a]	375 *(8,400)*
F	575 *(9,500)*	~470 [a]	366 *(5,400)*
3N	620 *(3,100)*	-- [b]	481 *(12,300)*

Italicized values are extinction coefficients (M^{-1} cm^{-1}). [a] Shoulder- estimated λ_{max}, 3,500-7,000 M^{-1} cm^{-1}. [b] Obscured.

Table 1.3. λ_{max} values and extinction coefficients of uranyl phen-BIAN complexes **UO_2-2a-f.**

UO_2-2	**$\lambda_{max}{}^{1}$**	**$\lambda_{max}{}^{2}$ (nm)**	**$\lambda_{max}{}^{3}$ (nm)**
OMe	753	578	
t-bu	693	540	381 *(7,200)*
Me	674	519	386 *(6,400)*
H	660	519	370 *(7,600)*
F	629	495	370 *(7,800)*
3N	~640[a]	514	426

Italicized values are extinction coefficients (M^{-1} cm^{-1}). [a] Extinction coefficient ~4,600-4,900 M^{-1} cm^{-1}.

To further elucidate the electronic structure of these ligand systems and corroborate the trend observed experimentally, a series of qualitative calculations were performed on **1a-f**. Because the free ligands exist as cyclic benzoxazinobenzoxazines that lack the α-diimine unit, the open, or "bound" configurations of the of the ligands as diphenolate Schiff bases were modeled (**Figure 2.22**). Calculated energies of the longest wavelength ILCT for **1a-e** are on average 0.191 eV higher (57.4 nm lower) than those determined experimentally for their complexes (**Table 3**), which is nonetheless a good fit despite excluding the uranyl center from the calculations. The calculated ILCT energies for $\lambda_{max}{}^{1}$ match very well with the observed trend for these species, in which complexes of ligands bearing more electron-donating substituents have lower-energy ILCTs. A similar, yet less consistent trend is observed for the $\lambda_{max}{}^{2}$ values, and these processes can also be assigned as ILCT-type transitions (HOMO-1 → LUMO).

Though the predicted ILCT energies ($\lambda_{max}{}^{1}$) support the experimental data for **UO_2-1a-e,** that of the naphthyl-gbha ligand (**1f**), is 0.193 eV lower (66 nm higher) than the experimentally observed value ($\lambda_{max}{}^{1,\ calc}$ = 686 nm; $\lambda_{max}{}^{1,\ obs}$ =620 nm) for the complex, which deviates substantially from the trend exhibited by the rest of the data. The presence of some free ligand in solution may be a complicating factor. It is unsurprising that the predicted energy of this ILCT is lower than those for the other ligands given the presence of the extended π-system; however, the discrepancy between this and the experimentally determined ILCT energy warrants further examination. While the greater degree of delocalization is most likely implicated here, this deviation could also indicate the presence of more complicated metal-ligand interactions that may increase the energy required to transfer additional charge to the diimine LUMO. There are other possible sources for this behavior. The solid-state structure of this species does show a slight twist of the ligand, and in solution, two distinct peaks are observed by ^{1}H NMR that can be assigned to

two imine protons in different environments. These protons are not observed with the free ligand. If the naphthyl rings are distorted significantly out of plane in solution, this CT process would likely be higher in energy, and this would account for the low intensity of the band. Similar spectroscopic behavior is observed for **UO_2-2f**, which also features extended conjugation. Especially considering recent work highlighting backbonding interactions between an electron-poor uranium center and a poor π-acceptor in the presence of suitable ancillary ligands[26], we do entertain the idea that ligand environments such as those of **1f** and **2f** which provide large, accessible π-systems may be sufficiently π-accepting to participate in similar bonding interactions, even with U(VI). Given that the electron density necessary for metal back-donation to the diimine unit could be supplied by the phenolic donors, as has been observed previously in d^0 transition metal complexes,[70] this is worth investigating in further studies.

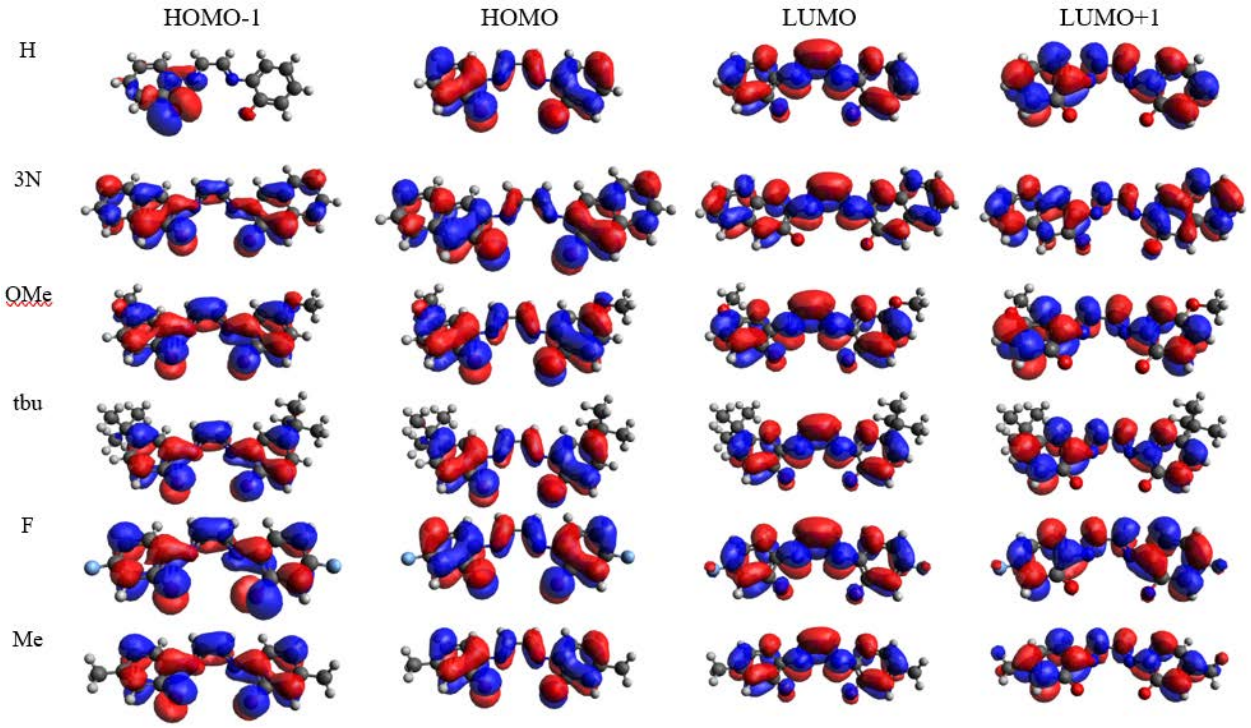

Figure 2.22. Molecular orbitals of 1a-f.

Table 2.4. Calculated and experimental values for lowest-energy ILCT processes (gbha ligands).

gbha	Calculated	Experimental	difference	
			nm	eV
OMe (a)	621	709	-88	-0.248
t-bu (b)	575	648	-73	-0.245
Me (d)	563	614	-51	-0.182
H (c)	570	613	-43	-0.152
F (e)	543	575	-32	-0.128
3N (f)	686	620	+66	+0.193

Electrochemical Studies

Cyclic voltammetry (CV) and differential pulse voltammetry (DPC) were employed to study the redox chemistry of the α-diimine ligands and their complexes (particularly those of uranyl). All reported values are referenced to the $Fc^{+/0}$ couple. The gbha ligands, which exist in the bisbenzoxazinobezoxaine form, were electrochemically unremarkable as there is no α-diimine or single imine moiety; however, the electrochemistry of the (*t*-bu)phen-BIAN ligand **2b** bears many similarities to that established for Ar-BIAN species[41]. The CV of **2b** (**Figure 2.23**) features a prominent reduction at E_{pc} = -1.92 V that is in good agreement with a two-electron reduction of the α-diimine unit (**2b**$^{2-}$)[41]. Unlike Ar-BIAN systems, this peak is preceded by a shoulder at -1.74 V, and shows poor reversibility, likely due to the presence of the cyclized form. This initial process may correspond to the formation of an unstable radical during the de-cyclization of **2b** to the open form. Through a series of stepwise scans, it was determined that the oxidation at E_{pa} = -0.93 V, which appears to be a one-electron process, is linked to these reductions. This ΔE of nearly 1.0 V and the disruption of clean reduction and oxidation events implicates an associated slow process such as a structural rearrangement. A second reversible reduction occurs at $E_{1/2}$= -2.42 V (ΔE_p = 77 mV) which is in good agreement with the formation of a radical anion within the α-diimine unit

(**2b**$^{\bullet 3-}$)[41]. Further reduction of the acenaphthene backbone would be expected at potentials of approximately -3.0 V[41], however, the electrochemical window of CH_3CN did not allow quality scans to be performed past -2.75 V (v. Fc^+/Fc), so these processes unfortunately could not be observed.

The oxidation at E_{pa} = 0.41 V can be assigned to the formation of a phenoxyl radical, and though this process is typically considered irreversible due to O—H bond dissociation, the reduction at E_{pc} = -0.05 V appears to be the other half of this couple (ΔE_p = 460 mV), which can be supported in that transfer of the proton to the imine nitrogen is possible, and that the *para-tert*-butyl group is known to stabilize the phenoxyl radical[71-73], thereby contributing to the reversibility of this process. These features are noticeably absent for Ar-BIAN species[41]. It should also be noted that the shape of the peak at 0.41 V is similar to that observed at -1.92 V—these shoulders may be attributable to an equilibrium between two species (the cyclized and open forms). The oxidation peak observed at E_{pa} = 1.00 V is comparable to those seen for Ar-BIAN species—Viganò et al.

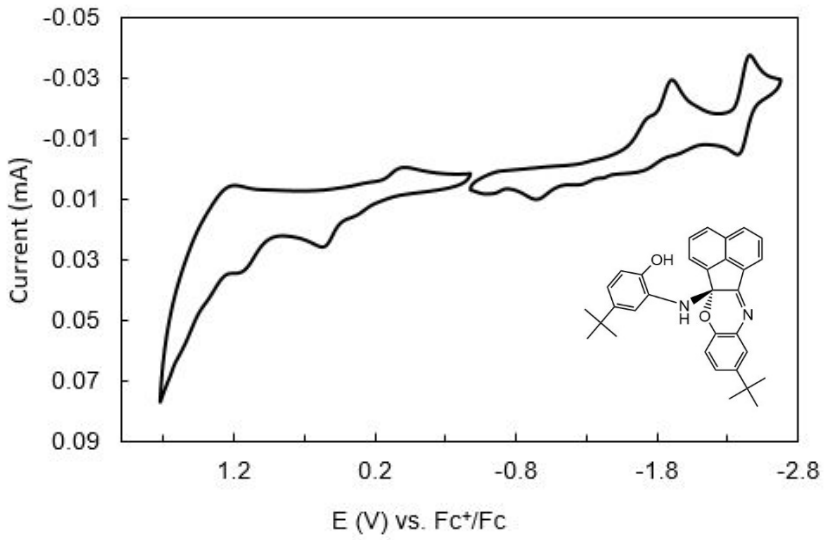

Figure 2.23. CV features of 1 (0.001 M in MeCN + 0.1M $TBAClO_4$).

suggests such a peak is attributable to the formation of a radical cation within the aryl substituent[41]. The final irreversible oxidation at E_{pa} = 1.31 V is only observed in scans that reach a cathodic potential of at least -0.975 V, and can be attributed to the oxidation of the acenaphthene backbone[74].

The redox behavior of the phen-BIAN complexes **Ni-2b**, **Co-2b**, and **UO_2-2b** was also probed using CV and DPV techniques. Summaries of ligand-based and metal-based redox processes are presented in **Tables 2.5** and **2.6**. The CV of **Ni-2b** features two reversible redox events at $E_{1/2}$ = -1.21 V (ΔE = 346 mV) and $E_{1/2}$ = -1.61 V (ΔE = 60 mV) that correspond to the Ni(II/I) and Ni(I/0) couples, respectively[75-77], indicating a clear stepwise reduction of the complex (**Figure 2.24**). The somewhat large ΔE_p of the Ni(II/I) couple is in range of those reported for Ni(II) Schiff base complexes[75-76], though the possibility for an octahedral distortion upon reduction to a d^9 metal center could account for this. These events are followed by an irreversible reduction at E_{pc} = -2.05 V, consistent with the two-electron reduction of the α-diimine unit. This feature is also shifted to a slightly more negative potential than observed previously for the free ligand. Two very weak irreversible features are observed at 0.31 V and 0.76 V that likely correspond to the oxidation of an unbound phenol to a phenoxyl radical and aryl radical cation formation, respectively.

The CV of **Co-2b** (Figure **8**) reveals three main reductive events. The first, at E_{pc}= -0.65 V, is linked to a much weaker return oxidation feature at E_{pa} = -0.33 V. Given that 1) no typical Co(III/II) couple is observed at a positive potential as expected, and 2) this feature does not align with any ligand redox processes, it is conceivable that the Co(III/II) couple has been shifted. Precedent for this couple occurring at -0.40 V has been established[78]. The two following irreversible reductions at E_{pc}= -1.36 V and -1.73 V can then be assigned to the Co(II/I) couple and the two-electron reduction of the ligand α-diimine unit, respectively. The oxidation observed at E_{pa} = -0.89 V appears to be linked to the reduction of the α-diimine reduction, as seen for **2b,** and the irreversible

oxidations at 0.29 V and 0.79 V are in good agreement with those observed for **Ni-2b** (phenoxyl radical and aryl radical cation).

In contrast to the CV data obtained for the transition metal complexes, the cathodic portion of the CV for **UO_2-2b** is considerably more complex, and distinguishing the ligand and metal redox processes from one another with certainty is much more challenging, particularly given the presence of two metal centers. As the reductive chemistry of the uranyl complex is of greater interest, the features of the anodic portion of the CV for **UO_2-2b** are not of major concern; however, the reversible feature at $E_{1/2}$ = 0.00 V is unique to the dimer and resulted in

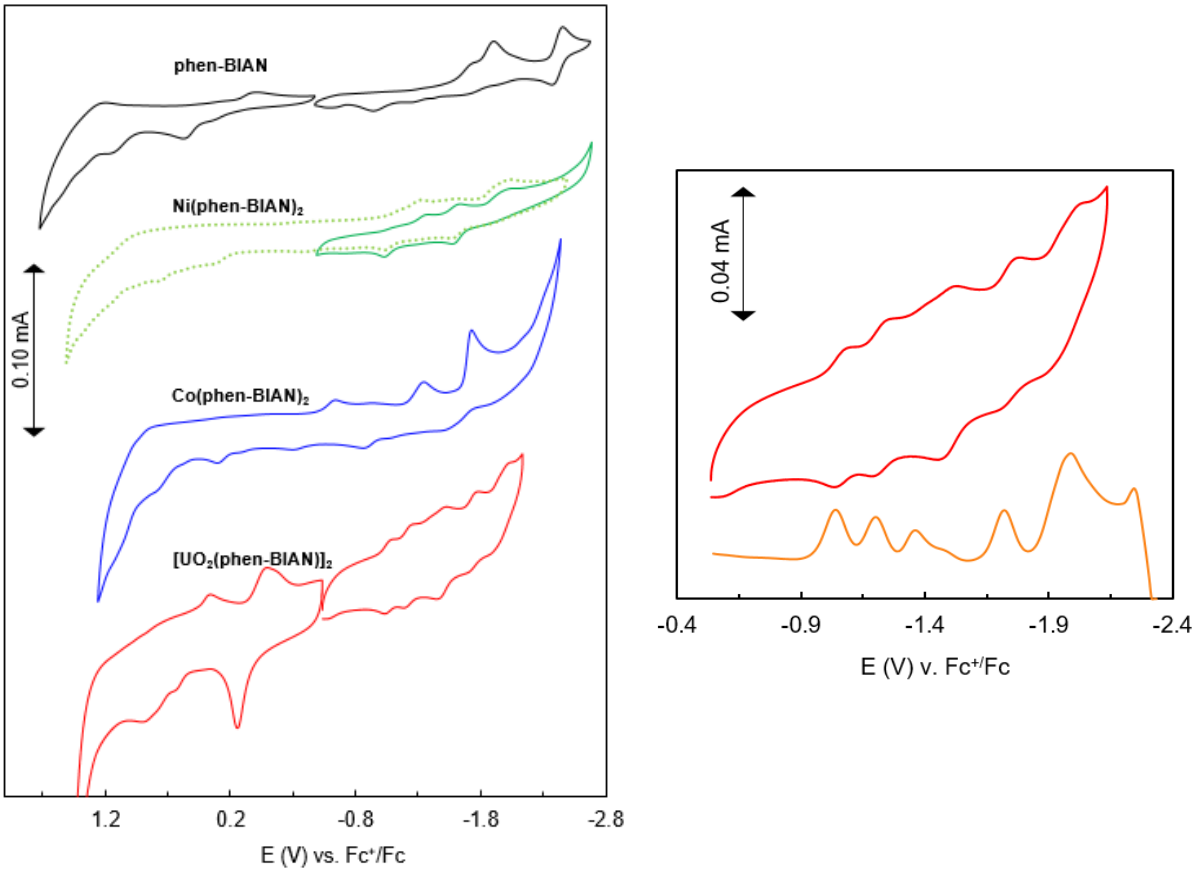

Figure 2.24. Left: 2b 0.001 M in MeCN + 0.1 M $TBAClO_4$; Ni-2b, Co-2b: 0.0003 M in MeCN + 0.1 M $TBAClO_4$; UO_2-2b: 0.0001 M in anhydrous CH_2Cl_2 + 0.1 M $TBAClO_4$. Data normalized to that of 2b based on ligand concentration. Right: Enlargement of cathodic potion of CV of UO_2-2b (red) and DPV of UO_2-2b (gold).

electrodeposition at the electrode surface (**Figure 2.25**). Given the potential at which it occurs, it is likely a phenoxy-based process. The cathodic scan of **UO_2-2b** shows a clustered series of five uniform features that all appear either reversible or quasireversible (**Figure 2.24**). DPV was employed to better resolve these features, and this revealed six well-defined reductions (**Table 2.6**) with one additional shoulder.

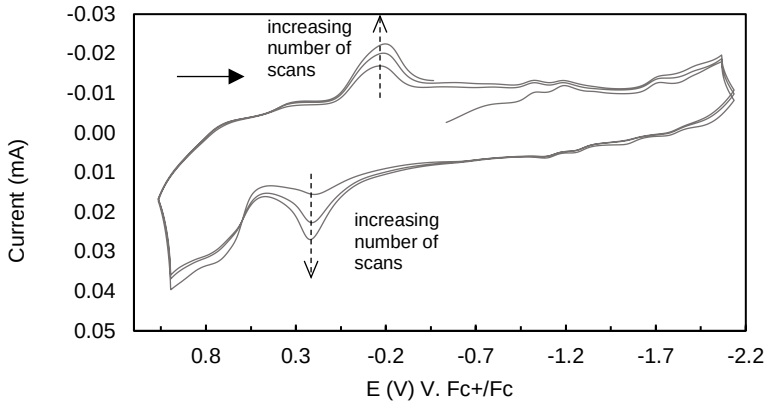

Figure 2.25. Cyclic voltammograms of UO_2-2b. ($[UO_2$(phen-BIAN)$]_2$) 0.001 M in CH_2Cl_2 + 0.1 M TBAP, 500 mV/s.

Given the tendency of uranium complexes to undergo single-electron processes, and the markedly larger peak area at -1.99 V (DPV), this event can be confidently assigned to the two-electron reduction of the α-diimine unit, as it occurs at a very similar potential to that seen in **Ni-2b**, and to values reported for the known uranium Ar-BIAN species[79]. A considerable number of reduction processes can be assigned based on very close agreement with previously reported values for mixed-valent uranium complexes[80-81]. The first redox process at -1.04 V ($E_{1/2}$ = -1.07 V from CV) is consistent with the one-electron reduction of the [U(VI)-U(VI)] system to a mixed-valent [U(VI)-U(V)] system[80]. The event observed at -1.38 V by DPV can be attributed to the [U(VI)-U(V)] → [U(V)-(V)] couple[80]. With the added resolution of the DPV scan, the feature at -1.38 V is more pronounced than its shoulder at -1.49 V; however, in the CV, the latter dominates ($E_{1/2}$ of

this process is -1.50 V). As the [U(V)-U(V)] → [U(V)-U(IV)] couple has been reported at $E_{1/2}$ = -1.55 V[81], it can be surmised that these two reductions happen concomitantly, possibly favoring the mixed-valent species. The following reduction at -1.72 V ($E_{1/2}$ = -1.76 V) is on the upper end of ranges reported for the U(V/IV) couple in monomeric complexes (-1.25 V to -1.81 V), and thus, this process likely involves the reduction of a [U(V)-U(IV)] mixed-valent complex to a [U(IV)-U(IV)] system[81]. Though these assignments do not account for the reduction observed at -1.20 V ($E_{1/2}$ = -1.23 V), we believe that the initial reduction to the [U(VI)-U(V)] system may induce sufficient structural changes to the μ-O_{Ar} bridge system for it to undergo a reduction at this potential. The last reduction observed by DPV at -2.23 V is very likely a ligand reduction that has shifted to a more positive potential on coordination, though this is not seen for **Ni-2b** or **Co-2b**. As there have been U(IV/III) couples reported in the range -1.94 V to -2.5 V,[82-85] this would be of interest in future work for comparative analyses.

Table 2.5. Electrochemical data for ligand-based redox processes for complexes of **2b.**

	α-diimine (E_{pc}, V)	
	$1/1^{2-}$	$1^{2-}/1^{3-\bullet}$
2b	*-1.74*, -1.92	-
Ni-2b	-2.05	-
Co-2b	-1.73	-
UO_2-2b	-1.99	-2.23*

Values given versus Fc^+/Fc. Italics denote shoulder. *Tentative peak assignment.

Table 2.6. Electrochemical data for metal-based redox couples.

Process	$E_{1/2}$ (V)
Ni(II/I)	-1.21
Ni(I/0)	-1.61
Co(III/II)	-0.48
Co(II/I)	-1.36
[U(VI)-U(VI)] → [U(VI)-U(V)]	-1.04
[U(VI)-U(V)] → [U(V)-U(V)]	-1.38
[U(V)-U(V)] → [U(V)-U(IV)]	-1.49
[U(V)-U(IV)] → [U(IV)-U(IV)]	-1.72

Values given versus Fc^+/Fc. All uranium values are E_{pc}'s from the DPV experiment.

Electrochemical studies of the uranyl gbha complexes were carried out to characterize the electronic effects of ligand substitution on the uranyl center. Due to poor solubility of many of the complexes, quality electrochemical data could not be obtained for all derivatives. The electrochemical behavior of these species is also highly solvent-dependent (**Figure 2.26**). For **UO_2-1b** and **c**, a fairly complex electrochemical profile is observed (**Figure 2.28**), featuring multiple metal-centered redox events and indicating that these species exist as dimers in solution. **UO_2-1d-e** (-Me and -F derivatives); however, each exhibits only one distinct peak that can be attributed to a metal-centered process (**Figure 2.27**), suggesting that these complexes are most likely monomeric in solution. These three species all bear substituents that are *ortho*/*para*-directors and remove electron density from the phenolic carbon (Me, F), or delocalize electron density over the entire arm (3N), which should disfavor the μ-phenolato bridged dimers observed for *t*-tbu and -H substituted complexes in the solution state.

UO_2-1b and **UO_2-1c** feature multiple sequential redox events, with those of **UO_2-1b** occurring at potentials 40-50 mV more negative than those of **UO_2-1c**, which is expected based on the presence of the electron-donating *t*-bu group. Processes 1, 2, and 3 occur at -1.11 V (ΔE = 68 mV), -1.32 V (ΔE = 75 mV), and -1.48 V (ΔE = 102 mV) for **UO_2-1b**, and -1.06 V (ΔE = 64 mV), -1.27

V (ΔE = 84 mV), and -1.44 V (ΔE = 104 mV) for **UO_2-1c**, respectively. In both cases, processes 1 and 2 are reversible (or nearly reversible), and process 3 is quasireversible. This behavior is similar to that previously observed for [UO_2(*t*-bu)phen-BIAN]$_2$ (**UO_2-2b**), which was determined to

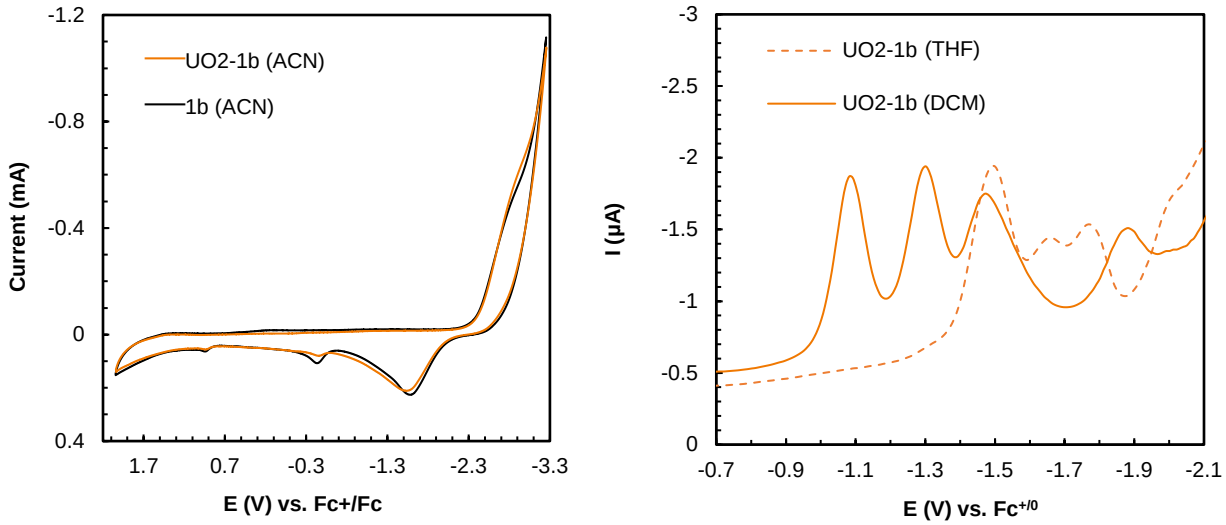

Figure 2.26. Solvent-dependence of electrochemical behavior, using UO_2-1b as an example. Left: CV of complex and ligand in ACN, 100 µM, 0.1 M $TBAPF_6$, 0.1 V/s. Right: DPVs of complex in DCM vs THF (100 µM, 0.1 M $TBAPF_6$). In ACN, DCM, RE: Ag/AgCl sat. KCl/H_2O, WE: glassy carbon, CE: Pt wire. In THF, RE: Ag/Ag^+ wire (non-aq.) in ACN, 0.01 M $AgNO_3$), WE: glassy carbon, CE: Pt wire.

undergo reduction from [U^{VI}-U^{VI}] to [U^{IV}-U^{IV}] through a series of mixed-valent states.[27] The $UO_2^{2+/+}$ ($U^{VI/V}$) redox couple is highly dependent on the nature of the equatorial ligand, and can range from -1.1 V to -1.8 V (vs. $Fc^{+/0}$).[12, 55] While the values for processes 1-3 are consistent with one-electron reductions of dimeric uranyl species as previously observed, the formation of ligand-centered radicals and retention of the U^{VI} center or formation of U^{VI}-U^{V} ligand radicals is also probable, as these ligands are non-innocent and we have determined from the solid-state structures of **UO_2-1b** and **UO_2-1c** that the (*t*-bu)gbha and gbha ligands already possess some radical-anion-like characteristics.[58] As the electrochemical behavior is strongly solvent-dependent, and

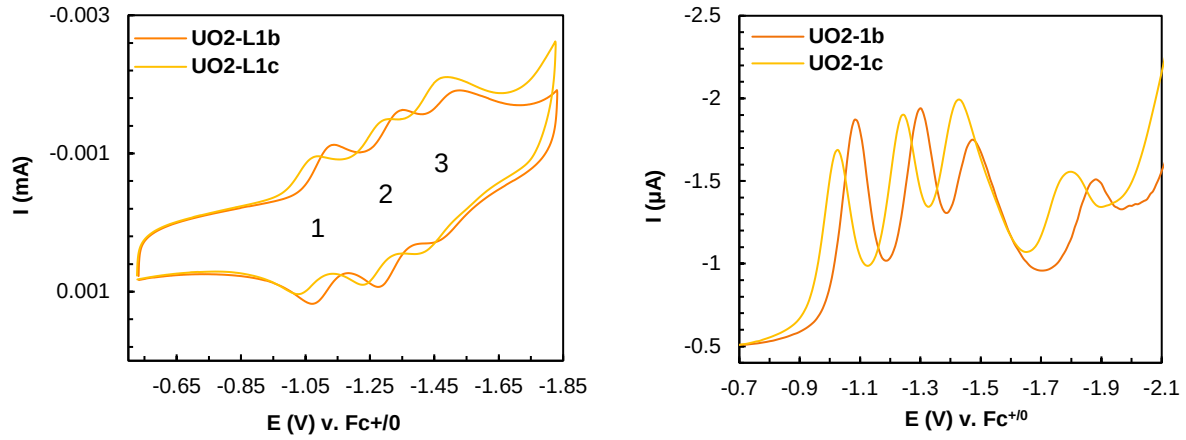

Figure 2.28. CV (left) and DPV (right) of uranyl complexes, 100 µM in CH_2Cl_2. WE: glassy carbon; CE: Pt wire; WE: Ag/AgCl, sat'd. KCl/H_2O. CV: 0.1 V/s.

reductions at -1.80 V (**UO_2-1c**) and -1.87 V (**UO_2-1b**) consistent with reduction of the diimine[41, 86-87] are observed in the DPVs of the complexes, the former assignment is most likely. This feature is mostly obscured in a large increase in current in CV experiments, and once this reduction occurs, the reductive behavior between -1.0 and -1.7 V is drastically altered in repeated scans (**Figure 2.29**). Regardless of the nature of these processes, it is clear that the non-innocence of these α-

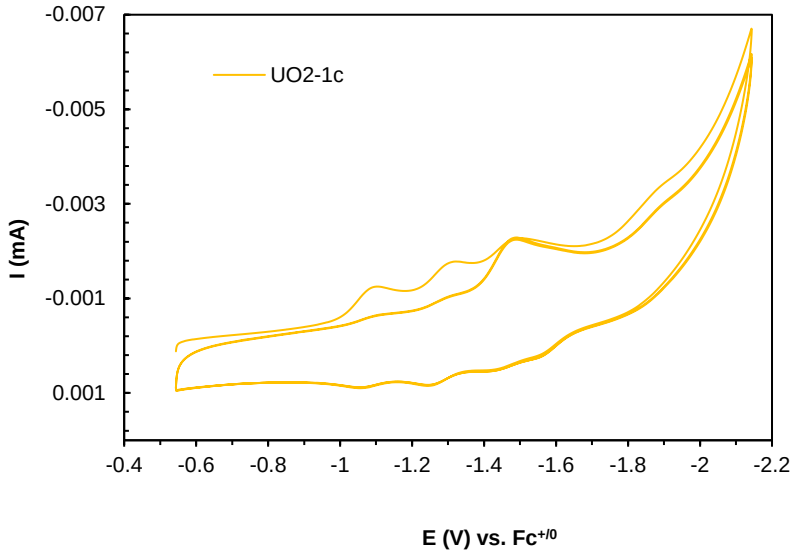

Figure 2.29. CV of UO_2-1c showing change after first scan once ligand reduction (~ -1.9 V) is reached. 100 µM in CH_2Cl_2, 0.1 M $TBAPF_6$, 0.1 V/s. RE: Ag/AgCl sat. KCl/H_2O, WE: glassy carbon, CE: Pt wire.

diimine frameworks affords access to reduced metal oxidation states or their radical anion equivalents. The redox features presented here in context with similar literature indicate the presence of a wealth of intricacies concerning the interaction of uranyl with non-innocent ligands that have yet to be completely resolved. [12, 23, 41, 58]

Table 2.7. Reduction potentials (V vs $Fc^{+/0}$) from DPV.

Process	UO_2-1b (V)	UO_2-2b (V)
1	-1.08	-1.04
2	-1.26	-1.20
3	-1.42	-1.38, -1.49
4		-1.72
5	-1.87	-1.99

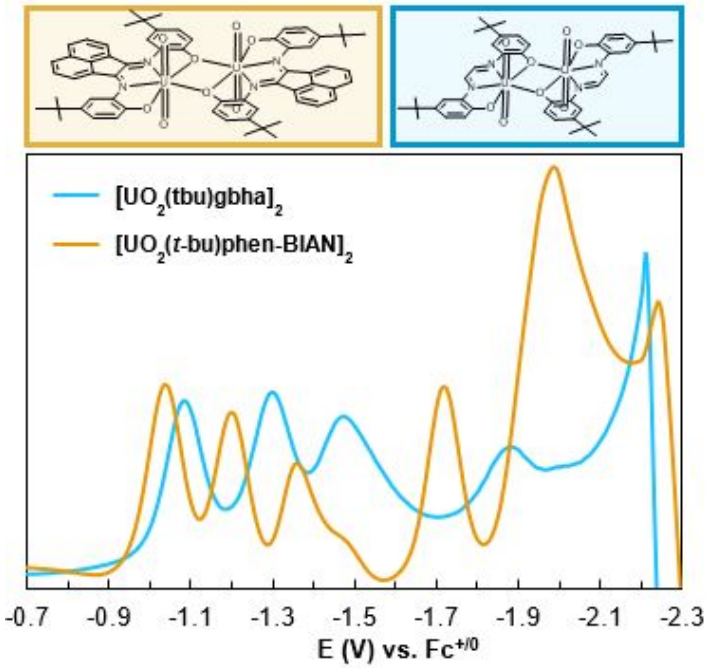

Figure 2.30. DPVs of uranyl α-diimine complexes.

Of note in our evaluation of the impacts of ligand conjugation is the difference in reduction potentials of the *t*-bu-derivatives, **UO_2-1b** and **UO_2-2b**. For the first three processes, those of **UO_2-**

2b are consistently 40 mV less negative than those of **UO_2-1b** (**Table 2.7**). Also, for **UO_2-2b**, an additional shoulder and distinct reduction are observed. From this, it is clear that the large accessible π-system offered by the phen-BIAN framework effectively lowers the reduction potentials as well as provides additional opportunity for reduction of the entire complex by acting as reservoir that electrons can be easily shuttled in to and out of. This demonstrated significant utility over its gbha counterpart with respect to the possibility of stabilizing lower formal oxidation state uranium centers.

Conclusions

A small library of tetradentate redox-active Schiff base ligands has been assembled, including both derivatives of the highly-conjugated phen-BIAN system as well as derivatives of the less-conjugated glyoxal-(bis)hydroxyanil (gbha) framework. Initially, the phen-BIAN ligand **2b** and its complexes of Ni^{2+}, Co^{2+}, and UO_2^{2+} were characterized in the solution and solid state *via* NMR, FT-IR, UV-Vis, and crystallographic studies—the divalent transition metal species were used as references for how this novel system behaved in complexes of 3*d* and 5*f* elements, and were found to adopt unexpected pseudo-octahedral geometries upon coordination of two tridentate **2b** ligands. The behavior of the uranyl species was distinct in this regard, forming a 1:1 (2:2) μ-phenolato-bridged dimer with two pentagonal bipyramidal uranyl centers in which **2b** coordinated as a planar tetradentate ligand. Two distinct solid-state structures are observed for **UO_2-2b**, showing interactions of the uranyl oxo groups with CH_2Cl_2 or $CHCl_3$ that demonstrate they are not inert, likely due to the incorporation of a redox non-innocent ligand. To examine the effect of the conjugated acenaphthene backbone on the behavior of uranyl complexes, additional studies were conducted on uranyl complexes of derivatized gbha ligands, and the phen-BIAN ligand family was

expanded to include the analogous derivatives so that both the electronic effects of an extended π-system in the backbone and of the aryl arm substitution could be accounted for. All of these ligands contain the π-accepting α-diimine fragment and donor phenolic groups that result in the absorption spectra of their complexes being dominated by intense intraligand charge transfer (ILCT) processes. DFT calculations for the gbha ligands support this assignment and agree with the experimentally observed trend in energies as they depend on the electron-donating ability of the aryl substituent, though a deviation in this trend is observed for **UO_2-1f**. Despite the poor solubility of some of these complexes which complicated their characterization, we were able to obtain crystal structures for **UO_2-1b**, **UO_2-1c**, and **UO_2-1f**, showing that these species can form μ-phenolato-bridged dimers as we have previously observed for **UO_2-2b**,[27] or CH_3OH-coordinated monomers. The nuclearity and solvent coordination are solvent-dependent, and therefore highly dependent on solubility and crystallization conditions, thus, the solution-state and solid-state structures are not necessarily constant. These α-diimine ligands behave non-innocently when coordinated to uranyl, as observed for **UO_2-1c**, though we do not observe this species behaving as a U(V) equivalent.

Electrochemically, the non-innocence of these systems manifests as multiple redox-processes and allows significant reduction of the complexes. It is not clear if these are strictly ligand-based processes, or if the metal centers are primarily involved, rather, these reductions likely correspond to significant delocalization of charge throughout the entire species. The reductive profile of **UO_2-2b** fits that of multiple single-electron reductions *via* a series of formally U(VI)/U(V) and U(V)/U(IV) mixed-valence complexes. The unusual behavior of these complexes suggests a wealth of redox-activity and accessible oxidation states for this framework. The inclusion of the conjugated BIAN backbone appears to be advantageous as it lowers the overall reduction

potentials and allows for a greater number of reductions as observed in our comparison of **UO_2-1b** and **UO_2-2b**. FT-IR analysis of these species also shows slightly lower ν_3 O=U=O stretching frequencies overall for the **UO_2-2** complexes (phen-BIAN), indicating some contribution of the more highly conjugated ligand in impacting this axial feature. **UO_2-2d** and **UO_2-2e**, which bear methyl and fluoro substituents *para* to the imine nitrogen, also have significantly lower stretching frequencies (18 cm^{-1}) than their gbha counterparts (**UO_2-1d-e**). This not only demonstrates that the combination of an electron-donating group in this position and the BIAN backbone creates a unique electronic environment that more drastically impacts the covalent character of the oxo ligands, but also implicates the nitrogen donors as greater contributors to this environment than the phenolic oxygen atoms.

2.2 | Synthesis of Compounds and Methods

General Considerations

Caution! The uranium metal salt – $UO_2(OAc)_2 \cdot 2H_2O$ – used in this study contained depleted uranium. Standard precautions for handling radioactive materials or heavy metals such as uranyl nitrate and lead sulfate were followed. Organic solvents (EtOH, Pharmco-Aaper; MeOH, anhydrous THF (DriSolv), EMD Millipore; CH_2Cl_2, $CHCl_3$, acetone, THF, EtOAc, heptane, BDH Chemicals; benzene, Fisher Scientific; n-pentane, Acros Organics) were used as received without additional purification. Acenaphthenequinone, 2-amino-4-tert-butylphenol, 3-amino-2-naphthol, 2-amino-4-methoxyphenol, anhydrous $ZnCl_2$ (Alfa Aesar), *o*-aminophenol, chlorotrimethylsilane (Acros Organics), 2-amino-5-methylphenol, 2-amino-5-fluorophenol (Ark Pharm), and Et_3N (BDH Chemicals), were used as received. $TBAPF_6$ (Beantown Chemical) and $TBAClO_4$

(electrochemical grade, Sigma-Aldrich) were recrystallized from anhydrous EtOH, and uranyl acetate (Polysciences) was recrystallized from CH_3OH prior to use.

Identity and purity of compounds has been established *via* NMR, mass spectrometry (TOF MS, ESI+), and elemental analysis. ^{1}H and ^{13}C NMR were recorded on a Bruker AV 400 or 600 MHz spectrometer using DMSO-d_6, DMF-d_7, $CDCl_3$, or THF-d_8 (Cambridge Isotope Laboratories). Chemical shifts are reported in parts per million (δ) and referenced against TMS or residual internal solvent signals. Elemental analyses were performed by Atlantic Microlab, Inc.. UV/Vis data was collected on a Varian Cary 50 WinUV spectrophotometer.

Infrared spectra were obtained in the solid state using an attenuated total reflectance (ATR) method on a Thermo Scientific Nicolet iS50 FT-IR, and normalization of spectra [0, 100] was performed using OriginPro.

X-ray Crystallography

1b, UO_2-1b, UO_2-1c, UO_2-1e, UO_2-1f:

Crystals suitable for single crystal X-ray diffraction were selected and mounted on a 50-micron MiTeGen loop using Paratone-n oil and data set collection was completed on a Bruker D8 VENTURE κ-geometry diffractometer using Cu Kα radiation (Incoatec IμS DIAMOND microfocus sealed tube (λ = 1.54178 Å). Crystals were kept at 100 K (150 K for **UO_2-1e**) during unit cell and data collection. Determination of the unit cell and collection of data were performed using the APEX III software, and determination of integrated intensities and global cell refinement were performed with the Bruker SAINT software package. A multi-scan absorption correction (SADABS) was applied. Structures were solved using Intrinsic Phasing/Direct Methods[88] (ShelXT) and least-squares refinement was performed using ShelXL in APEX III. Olex2.1.[89] was

used to mask solvent molecules (**UO_2-1c**) in order to achieve convergence. Restraints and constraints such as FLAT, SIMU, ISOR, and EADP were employed for atoms that would otherwise be split and could not be modeled over two positions due to unresolved twinning, or for atoms that could not be refined anisotropcially without resulting in non-positive definites. Projections were created on Olex2.1.

2b, Ni-2b, Co-2b, UO_2-2b:

Single-crystal x-ray diffraction measurements were carried out on a Bruker SMART APEX CCD diffractometer at 182 K using Mo Kα radiation. Crystals were mounted on glass fibers with Paratone-N oil. Projections were generated using the Olex2-1.2.8 graphics program[89]. Determination of integrated intensities and global cell refinement were performed with the Bruker SAINT software package. Structures were solved with the SHELXL (v 5.1) program using direct methods[88], and refined with the olex2.refine refinement package using Gauss-Newton minimization[90]. Non-H atoms on disordered *t*-butyl groups were held isotropic for **1**, **3**, and **4b** to avoid NPD values and allow convergence, except in the case of **1**, which did not reach convergence due to a particularly disordered *t*-butyl group. The crystal of **4a** was of poor quality, and attempts to constrain O1 resulted in NPD values and non-convergence.

Computational Methods

All electronic structure calculations were performed in the Gaussian 16 suite[91] using the B3LYP functional and 6-31G(d) basis set. Atom coordinates were adapted from the asymmetric unit of **UO_2-1b** after removing the central UO_2^{2+} fragment and adding aryl substituents in Avogadro v1.2.0.[92] The binding pocket atoms (O-C-C-N-C-C-N-C-C-O) were held rigid and all remaining atoms geometry optimized. Molecular orbitals were visualized in Avogadro.

Electrochemical Measurements.

Electrochemical measurements were carried out using a CH Instruments 660 E potentiostat in HPLC-grade CH_2Cl_2, CH_3CN (BDH Chemicals), or anhydrous THF (DriSolv, EMD Millipore) with tetrabutylammonium hexafluorophosphate ($TBAPF_6$) or tetrabutylammonium perchlorate ($TBAClO_4$) supporting electrolyte (0.1 M). $TBAPF_6$ was recrystallized from EtOH and dried overnight in vacuo at 60 °C immediately before use. Solutions were purged for 30 minutes with N_2 using a pre-purge solution. Potentials were scanned using a three-electrode cell consisting of a glassy carbon disc working electrode, Pt wire counter electrode, and Ag/AgCl/satd. KCl/H_2O reference electrode. For measurements in THF, a non-aqueous reference electrode (Ag/Ag^+ wire in ACN, 0.01 M $AgNO_3$) was used. Data were corrected to versus ferrocene based on values for $E_{1/2}(Fc^{+/0})$ collected using the same three-electrode cell before and after measurements. DPV conditions: Increment= 0.01 V; amplitude= 0.05 V; pulse width= 0.05 s; sample width= 0.0167 s; pulse period= 0.5 s.

Synthesis of Compounds

Synthesis of OMe-gbha (1a). A solution of glyoxal (40% w/w aq., 0.11 mL, 1.0 mmol) in methanol (5 mL) was heated to 65 °C in a 250-mL round-bottom flask while stirring. 2-Amino-4-methoxyphenol (0.278 g, 2.0 mmol) was dissolved in methanol (5 mL) and added to the solution. Then one drop of glacial acetic acid was added. A precipitate formed within several minutes and the solution was heated and stirred at reflux temperature for 3 hr. After allowing to cool to room temperature, a mustard-yellow product was collected by filtration and rinsed with methanol. Yield:

0.153 g, 55.0 %. ^{1}H NMR (400 MHz, DMSO-d_6): δ 7.27 (s, 2H), 6.56 (d, 2H, J = 8.55), 6.26 (s, 2H), 6.18 (d, 2H, J = 8.53), 5.13 (s, 2H), 3.64 (s, 6H). ^{13}C NMR (600 MHz, DMSO-d_6): δ 154.25, 135.11, 130.90, 116.28, 103.34, 99.86, 75.16, 55.15. FT-IR (ATR): 3,374 cm^{-1} (N—H). λ_{max}: 305 nm (10,400 M^{-1} cm^{-1}). HRMS (ESI+) *m/z* [M+1] Calc'd 301.1188, found 301.1187.

Synthesis of tbu-gbha (1b). A solution of glyoxal (40% w/w aq., 0.58 mL, 5 mmol) in methanol (5 mL) with one drop of glacial acetic acid added was heated to 65 ˚C in a 250-mL round-bottom flask with stirring. To this solution, 2 equivalents of 2-amino-4-*tert*-butylphenol (1.65 g, 10 mmol) in hot methanol (45 mL) was added, and the resulting brown solution was heated and stirred at reflux temperature for 1 hour. The resulting white precipitate was collected via vacuum filtration and rinsed with methanol. The filtrate was concentrated by rotary evaporator and placed in the freezer overnight, yielding additional product. Yield: 1.25g, 71%. Single crystals suitable for X-ray diffraction were grown from a concentrated solution of $CDCl_3$. ^{1}H NMR (400 MHz, $CDCl_3$): δ 6.79 (dd, 2H, J = 8.48, 2.08), 6.74 (d, 2H, J = 8.40), 6.71 (d, 2H, J = 1.72), 5.29 (d, 2H, J = 3.6 Hz), 4.85 (d, 2H, J = 3.6 Hz), 1.27 (s, 18H). ^{13}C NMR (400 MHz, $CDCl_3$): 145.14, 139.12, 127.73, 117.56, 116.55, 112.17, 76.12, 34.19, 31.49. FT-IR(ATR): 3,372 cm^{-1} (N—H). λ_{max}: 298 nm (11,800 M^{-1} cm^{-1}). HRMS (ESI+) *m/z* [M+1] Calc'd 353.2229, found 353.2222.

Synthesis of gbha (1c). A solution of glyoxal (40% w/w aq., 0.58 mL, 5 mmol) in methanol (5 mL) with one drop of glacial acetic acid added was heated to 65 °C in a 250-mL round-bottom flask with stirring. To this solution, 2 equivalents of *o*-aminophenol (1.09 g, 10 mmol) in hot MeOH (45 mL) was added and the resulting brown solution was heated and stirred at reflux temperature for 1 hour. A pale purple crystalline precipitate formed and was collected by vacuum

filtration and rinsed with MeOH. The filtrate was concentrated by rotary evaporator and placed in the freezer to yield additional product. Yield: 01.20 g, 50%. ^{1}H NMR (400 MHz, DMF-d_7): δ 7.34 (d, 2H, J = 3.88), 6.80 (m, 4H), 6.68 (m, 4H), 5.38 (d, 2H, J = 4.12). ^{13}C NMR (400 MHz, DMF-d_7): δ 142.94, 131.60, 122.44, 119.86, 117.26, 115.44, 77.02. FT-IR(ATR): 3,370, 3,379 cm^{-1} (N—H). λ_{max}: 286 nm (8,100 M^{-1} cm^{-1}). HRMS (ESI+) *m/z* [M+1] Calc'd 241.0977, found 241.0977.

Synthesis of Me-gbha (1d). A solution of glyoxal (40% w/w aq., 0.58 mL, 5.0 mmol) in methanol (5 mL) with one drop of glacial acetic acid was heated to 65 °C in a 250-mL round-bottom flask with stirring. To this solution, 2-amino-5-methylphenol (1.23 g, 10 mmol) in hot methanol (45 mL) was added and the resulting brown solution was heated and stirred at reflux temperature for 1.5 hour. The resulting white precipitate was collected via vacuum filtration and rinsed with methanol. Yield: 1.04 g, 77.0%. ^{1}H NMR (400 MHz, DMSO-d_6): δ 7.11 (d, 2H, J = 4.01), 6.55 (m, 4H), 6.46 (s, 2H), 5.20 (d, 2H, J = 3.98), 2.12 (s, 6H). ^{13}C NMR (600 MHz, DMSO-d_6): δ 141.31, 127.53, 127.49, 121.66, 116.49, 114.07, 75.48, 20.28. FT-IR (ATR): 3,371 cm^{-1} (N—H). λ_{max}: 301 (12,400 M^{-1} cm^{-1}). HRMS (ESI+) *m/z* [M+Na^{+}] Calc'd 277.0793, found 291.1109.

Synthesis of F-gbha (1e). A solution of glyoxal (40% w/w aq., 0.11 mL, 2.0 mmol) in methanol (5 mL) was heated to 65 °C in a 100-mL round-bottom flask while stirring. To this solution, 2-amino-5-fluorophenol (0.278 g, 2 mmol) dissolved in methanol (10 mL) was added, then one drop of glacial acetic acid was added. A precipitate formed within several minutes and the solution was heated and stirred at reflux temperature for 6 hours. After cooling to room temperature, a brown crystalline solid was collected by filtration and rinsed with methanol. The filtrate was concentrated by rotary evaporator and placed in the freezer for several weeks, yielding

a small amount of additional product. Yield: 0.047 g, 17.1%. ^{1}H NMR (400 MHz, DMSO-d_6) δ 7.31 (s, 2H), 6.66 (m, 2H), 6.58 (m, 4H), 5.33 (s, 2H). ^{13}C NMR (600 MHz, DMSO-d_6): δ 156.42, 154.87, 142.01 (d), 126.43 (d), 114.30 (d), 107.40 (d), 103.55 (d), 75.426. FT-IR (ATR): 3,364 cm^{-1} (N—H). λ_{max}: 302 nm (10,200 M^{-1} cm^{-1}). HRMS (ESI+) *m/z* [M+1] Calc'd 277.0789, found 277.0793.

Synthesis of 3N-gbha (1f). A solution of 3-amino-2-naphthol (0.160 g, 1.00 mmol) in methanol (25 mL) was heated to reflux temperature 65 °C in a 100-mL round bottom flask until completely dissolved. Glyoxal (40% w/w aq., 0.11 mL, 1.00 mmol) was diluted to ~5 mL in deionized water and 4 drops glacial acetic acid were added. The glyoxal solution was added dropwise to the 3-amino-2-naphthol solution over 7 minutes, during which time a light precipitate formed. The mixture was stirred and heated for an additional five minutes then cooled to room temperature, and the pearlescent tan solid produced was collected by vacuum filtration and rinsed with MeOH. Yield: 0.085 g, 25.0%. ^{1}H NMR (400 MHz, DMSO-d_6): δ 7.93 (s, 2H), 7.59 (t, 4H, J = 9.28), 7.22 (m, 4H), 7.07 (s, 2H), 5.49 (s, 2H). ^{13}C NMR (600 MHz, DMSO-d_6): δ 143.31, 130.95, 129.88, 128.09, 126.17, 125.34, 123.90, 122.62, 111.18, 108.07, 75.49. FT-IR(ATR): 3,403 cm^{-1} (N—H). λ_{max}: 342 nm (22,600 M^{-1} cm^{-1}). HRMS (ESI+) *m/z* [M+1] Calc'd 341.1283, found 341.1290.

Synthesis of gbha complexes: For the R-gbha (R- H, Me, *t*-bu, OMe), the complexes were synthesized by direct addition of the gbha ligand to the metal salt. The fluoro- and 3N- complexes were synthesized by templation due to the low yield (F-) and poor solubility (3N-) of the free ligands.

Synthesis of UO_2-1a. A methanolic solution (20 mL) of OMe-gbha (0.061 g, 0.20 mmol) was heated to 65 °C in a 100-mL round bottom flask and stirred until dissolved. $UO_2(OAc)_2 \cdot 2H_2O$ (0.084 g, 0.20 mmol) was dissolved in a minimum amount of methanol and added to the ligand solution, which turned dark green. The reaction mixture was stirred and heated for 4.5 hours, then cooled to room temperature and stored in the freezer overnight. A dark solid was collected by filtration. Yield: 0.065 g, 57.2%. ^{1}H NMR (400 MHz, DMSO-d_6): δ 7.43 (s, 2H), 7.15 (d, 2H, J = 9.08), 6.76 (d, 2H, J = 8.95), 3.83 (s, 2H). ^{13}C NMR (600 MHz, DMSO-d_6): δ 168.51, 151.74, 150.74, 138.24, 123.14, 121.51, 91.72, 55.90. FT-IR (ATR): 924, 909 cm^{-1} (O=U=O, ν_3). $\lambda_{max}{}^1$: 709 nm (10,300 M^{-1} cm^{-1}). HRMS (ESI+) *m/z* [M+Na] Calc'd 1159.2617, found 1159.2583.

Synthesis of UO_2-1b. A methanolic solution (45 mL) of tbu-gbha (0.141 g, 0.4 mmol) was heated to 65 °C in a 250-mL round bottom flask and stirred until dissolved. $UO_2(OAc)_2 \cdot 2H_2O$ (0.170 g, 0.4 mmol) was dissolved in a minimum amount of hot methanol and added to the solution. The resulting blue-green solution was stirred at reflux temperature for 4 hours, yielding a dark precipitate. The solution was cooled to room temperature then stored in the freezer overnight. A dark bronze precipitate was collected via vacuum filtration (yield: 0.215 g, 72%). Red-purple crystals suitable for X-ray diffraction were grown from a concentrated acetone solution in a small test tube inside a sealed vial containing pentane. ^{1}H NMR (400 MHz, DMSO-d_6): δ 9.43 (s, 2H), 7.83 (d, 2H, J = 2.28), 7.55 (dd, 2H, J = 8.92, 2.28), 6.76 (d, 2H, J = 8.76), 1.36 (s, 18H). ^{13}C NMR (600 MHz, DMSO-d$_6$): δ 171.05, 151.33, 139.97, 137.82, 131.55, 120.35, 113.29, 34.17, 31.42. FT-IR (ATR): 921 cm^{-1} (O=U=O, ν_3). $\lambda_{max}{}^1$: 648 nm (12,600 M^{-1} cm^{-1}). HRMS (ESI+) *m/z* [M+1] Calc'd 1241.4879, found 1241.4877.

Synthesis of UO_2-1c. A methanolic solution of gbha (0.057 g, 0.23 mmol) was heated to 65 °C in a 100-mL round bottom flask and stirred until dissolved. $UO_2(OAc)_2 \cdot 2H_2O$ (0.100 g, 0.23 mmol) was dissolved in a minimum amount of hot methanol and added to the solution. The resulting dark blue solution was stirred at reflux temperature for 3 hours, yielding a dark precipitate. The solution was cooled to room temperature, and a dark green solid collected by filtration. Yield: 0.068 g, 58.2%. Single crystals suitable for X-ray diffraction were grown by vapor diffusion in a CH_2Cl_2 solution inside a vial of methanol. ^{1}H NMR (400 MHz, DMSO-d_6): δ 9.41 (s, 2H), 7.93 (d, 2H, J = 9.60), 7.46 (t, 2H, J=4.46), 6.81 (m, 4H). ^{13}C NMR (600 MHz, DMSO-d_6): δ 173.44, 152.76, 139.17, 134.43, 121.53, 118.00, 117.75. FT-IR (ATR): 913, 904 cm^{-1} (O=U=O, ν_3). λ_{max}[1]: 660 nm (6,500 M^{-1} cm^{-1}). HRMS (ESI+) *m/z* [M+1] Calc'd 509.1227, found 509.1226.

Synthesis of UO2-1d. A methanolic solution (40 mL) of Me-gbha (0.187 g, 0.700 mmol) was heated to 65 °C in a 250-mL round bottom flask and stirred until dissolved. $UO_2(OAc)_2 \cdot 2H_2O$ (0.297 g, 0.7 mmol) was dissolved in a minimum amount of hot methanol and added to the solution, which turned dark blue. The reaction mixture was stirred at reflux temperature for two hours, producing a dark precipitate, then was cooled to room temperature. A dark green solid was collected by filtration. Yield: 0.362 g, 96.0%. ^{1}H NMR (400 MHz, DMSO-d_6): δ 9.30 (s, 2H), 7.78, d, 2H, J = 8.36), 6.62 (m, 4H), 2.35 (s, 6H). ^{13}C NMR (600 MHz, DMSO-d_6): δ 150.78, 144.30, 136.79, 121.00, 118.73, 116.99, 21.65. FT-IR (ATR): 915 cm^{-1} (O=U=O, ν_3). λ_{max}[1]: 613 nm (13,100 M^{-1} cm^{-1}). HRMS (ESI+) *m/z* [M+1] Calc'd 537.1540, found 537.1531.

Synthesis of UO_2-1e. A solution of glyoxal (40% w/w aq., 0.06 mL, 0.5 mmol) in methanol (5 mL) was heated to 65 °C with stirring. $UO_2(OAc)_2 \cdot 2H_2O$ (0.212 g, 0.5 mmol) was dissolved in a minimum amount of hot methanol and added to the solution. 2-Amino-5-fluorophenol (0.127 g, 1.00 mmol) was dissolved in ~20 mL hot methanol and added to the reaction mixture, resulting in a dark purple solution and formation of a dark precipitate. The solution was heated and stirred for 5 hours, then cooled to room temperature, and the dark solid collected by filtration. Yield: 0.164 g, 60.2%. Single crystals suitable for X-ray diffraction were grown by vapor diffusion in a THF solution inside a vial of pentane. ^{1}H NMR: δ 8.40 (s, 2H), 7.99 (t, 2H, J = 7,42), 6.67 (m, 2H) ^{13}C NMR (600 MHz, DMSO-d_6): δ 174.15 (d), 167.78, 166.12, 152.72, 136.05, 118.77, 106.77, 104.95. FT-IR (ATR): 919 cm^{-1} (O=U=O, ν_3). λ_{max}[1]: 575 nm (9,500 M^{-1} cm^{-1}). HRMS (ESI+) *m/z* [M+Na] Calc'd 1111.1818, found 1111.1838.

Attempted synthesis of UO_2-1f. Several methods of synthesizing **UO_2-1f** were employed to acquire pure product, however the poor solubilites of both the ligand (and stability of the cyclic form) and the complex precludes their separation. Reaction of the ligand with uranyl acetate in hot methanol either with or without base, in an 80:20 THF:methanol mixture with base, and by templation in methanol with and without base each yielded a dark brown product which, by NMR, contains a 50:50 mixture of the metal complex and ligand. Attempts to separate the ligand from the complex with a variety of solvent systems (including THF, THF/methanol mixtures, hexanes, and dichloromethane) were unsuccessful. After these attempts, a reduction in the ligand peaks was not observed by NMR, hence, the complex may be unstable in solution. A single crystal of the product by crystallization from a benzene/methanol mixture and pentane was obtained to confirm

its identity. FT-IR (ATR): 917, 910 (O=U=O, ν_3). λ_{max}[1]: ~640 nm (~4,600-4,900 M^{-1} cm^{-1}). HRMS (ESI+) *m/z* [M+1] Calc'd 609.1540, found 609.1540

Synthesis of Zn-1b. **1b** (0.100 g, 0.28 mmol) was dissolved in 20 mL acetonitrile and heated to 80 °C. An excess of $ZnCl_2$ (0.049 g, 0.36 mmol) was dissolved in 5 mL MeOH and added to the solution of **1b**. Et_3N (0.04 mL, 0.03 mmol) was added to the reaction mixture, causing a change from colorless to dark blue over ~10 minutes. After 3 hours, the mixture was cooled, and solvent removed by rotary evaporator and the solids redissolved in methanol. This solution was stirred overnight at 68 °C, during which time it turned deep purple, producing a dichroic red-purple solid. The precipitate was collected by filtration and dried in a vac oven at 60 °C for 24 hours. Yield: 0.095 g, ~82%. Due to insolubility of the complex and its instability in solution, structural confirmation could not be achieved through NMR. Elemental analysis suggests the formula Zn(1b)(OH_2): Anal. Calc'd for $C_{22}H_{28}N_2O_3Zn$, C: 60.91, H:6.51, N:6.46; Found C: 61.06, H: 6.41, N: 6.46.

Synthesis of N,N'-bis(4-*tert*-butyl-2-iminophenol)acenaphthene ((*t*-bu)phen-BIAN) (2b). Acenaphthenequinone (0.455 g, 2.50 mmol) and 2-amino-4-*tert*-butylphenol (1.24 g, 5.00 mmol) were added to a 100-mL round bottom Schlenk flask containing a stir bar. These solids were subsequently dissolved in 30 mL of anhydrous MeOH. The solution was partially evacuated and charged with Ar three times, and the solution heated to reflux temperature (65 °C) for 1.5 hr. The red-orange solution was allowed to cool to room temperature on the bench, and then frozen overnight (12 hours). On warming to room temperature, a bright yellow crystalline solid precipitated, and this was collected by filtration. Yield: 74.0%, 0.881 g. Yellow crystals suitable

for X-ray diffraction were grown by slow diffusion of MeOH into a saturated CH_2Cl_2 solution. ^{1}H NMR (400 MHz THF-d_8): δ 8.05 (d, *J* = 7.0 Hz, 1H), 7.97 (d, *J* = 8.1 Hz, 1H), 7.85 (d, *J* = 2.3 Hz, 1H), 7.83 (d, *J* = 8.3 Hz, 1H), 7.73 (t, *J* = 7.6 Hz, 1H), 7.63 (d, *J* = 2.3 Hz, 1H), 7.60 (d, *J* = 6.9 Hz, 1H), 7.57 (s, 1H), 7.44 (dd, *J* = 8.4, 7.1 Hz, 1H), 7.29 (dd, *J* = 8.4, 2.4 Hz, 1H), 7.15, (d, *J* = 8.4 Hz, 1H), 6.70 (dd, *J* = 8.2, 2.4 Hz, 1H), 6.39 (d, *J* = 8.2 Hz, 1H), 4.96 (s, 1H), 1.41 (s, 9H), 1.37 (s, 9H). ^{13}C NMR (600 MHz THF-d_8): δ 163.1, 146.3, 146.2, 142.5, 139.7, 138.6, 136.1, 133.8, 132.2, 131.9, 129.28, 129.25, 128.7, 126.5, 126.1, 125.3, 121.1, 120.8, 118.7, 118.6, 117.6, 114.3, 86.6, 35.0, 34.8, 32.2, 31.9. FT-IR (ATR): 3350 cm^{-1} (m), 3410 cm^{-1} (w) 1632 cm^{-1} (w), 1607 cm^{-1} (w), 1268 cm^{-1} (w). Anal. Calc'd. for $C_{32}H_{30}N_2O_2$: C, 80.64; H, 6.77; N, 5.88. Found: C, 80.27; H, 6.66; N, 5.79.

Synthesis of Ni(phen-BIAN)$_2$ (Ni-2b). A MeOH solution (40 mL) of **1** (0.190 g, 0.399 mmol) was heated to reflux temperature in a 100-mL round-bottom flask charged with a stir bar. Subsequently, a hot solution of $Ni(OAc)_2{\cdot}4H_2O$ (0.105 g, 0.399 mmol) in ~ 5 mL MeOH was added slowly by pipette. The resulting dark indigo solution was stirred at 65 °C for 1 hour, then cooled in an ice bath for 30 minutes. A dark blue-black solid was collected by vacuum filtration and dried in vacuo at 60 °C for 12 hours. Single crystals suitable for X-ray diffraction were obtained by precipitations from a saturated MeOH solution after several days. Yield: 70.9%, 0.143 g. FT-IR (ATR): 1567 cm^{-1} (m), 1260 cm^{-1} (νC_{Ar}—O, s), 532 cm^{-1} (νNi—N, m), 447 cm^{-1} (νNi—O, w). For the purpose of acquiring additional material for elemental analysis, the 2:1 reaction was performed as described above using 0.190g (0.399 mmol) of **1** and 0.0496 g (0.199 mmol) of $Ni(OAc)_2{\cdot}4H_2O$. Yield: 64.8%, 0.130 g. Anal. Calc'd for $C_{64}H_{62}N_4NiO_4{\cdot}5H_2O$: C, 69.88; H, 6.60; N, 5.09. Found: C, 70.15; H, 6.24; N, 4.92.

Synthesis of Co(phen-BIAN)$_2$ (Co-2b). A MeOH solution (40 mL) containing **1** (0.190 g, 0.399 mmol) was heated to reflux temperature in a 100-mL round-bottom flask containing a stir bar. Subsequently, a hot solution of $Co(OAc)_2 \cdot 4H_2O$ (0.104 g, .399 mmol) in ~5 mL MeOH was added slowly by pipette. The resulting dark red solution was stirred overnight at 65 °C, after which time it had turned green. It was then allowed to cool to room temperature, and the dark green solid was collected by vacuum filtration. The volume of the mother liquor was reduced by half using a rotary evaporator, and the additional solid filtered off. This product was dried in vacuo at 60 °C for 4 hours. Crystals suitable for X-ray diffraction were grown by slow diffusion of MeOH into a saturated CH_2Cl_2 solution. Yield: 95.1%, 0.192 g. FT-IR (ATR): 3380 cm^{-1} (νO_{Ar}—H, w, br), 1558 cm^{-1} (νC=N, m), 1260 cm^{-1} (νC_{Ar}—O, s), 541 cm^{-1} (νCo—N, m), 444 cm^{-1} (νCo—O, w). Anal. Calc'd. for $C_{65}H_{67}CoN_4O_6$: C, 73.71; H, 6.38; N, 5.29. Found: C, 74.01; H, 6.07; N, 5.32.

Synthesis of UO$_2$-2a. Acenaphthenequinone (0.091g, 0.50 mmol) was added to a 100-mL round bottom flask charged with a stir bar and heated to 68 °C in methanol (40 mL) with stirring until completely dissolved. 2-amino-4-methoxyphenol (0.139 g, 1.0 mmol) and $UO_2(OAc)_2 \cdot 2H_2O$ (0.212 g, 0.5 mmol) were added as solids. and the flask was rinsed with an additional 5 mL of methanol. The solution turned black within 10 minutes and was heated and stirred for 24 hours, producing a black precipitate. After cooling the solution to room temperature, a small quantity of fine, black powder was collected by filtration and rinsed with copious amounts of methanol. Attempts to isolate additional product by concentrating the filtrate and storing it in the freezer were unsuccessful. Yield: 0.064 g, 18.5%. ^{1}H NMR: δ 8.81 (d, 2H, J = 7.28), 8.32 (d, 2H, J = 8.28), 7.93 (t, 2H, J = 7.85), 7.59 (d, 2H, J = 2.59), 7.17 (dd, 2H, J = 8.98, 2.75), 6.83 (d, 2H, J = 9.80), 3.82 (s, 6H). FT-IR (ATR): 909 cm^{-1} (O=U=O, ν_3). $\lambda_{max}{}^1$: 753 nm (5,400 M^{-1} cm^{-1}). Anal. Calc'd for $C_{78}H_{54}N_6O_{18}U_3 \cdot H_2O$: C, 44.71; H, 2.69; N, 4.01. Found: C, 44.71; H, 2.84; N, 4.09.

Synthesis of [UO_2(phen-BIAN)]$_2$ (UO_2-2b). An EtOH solution (50 mL) of **1** (0.250 g, 0.525 mmol) in a 100-mL round-bottom flask containing a stir bar was heated to reflux temperature, a hot solution of $UO_2(OAc)_2 \cdot 2H_2O$ (0.245 g, 0.578 mmol) in ~10 mL EtOH was added slowly by pipette. The resulting dark purple solution was stirred at room temperature for 2 days, then filtered and rinsed with ice-cold EtOH. The purple-brown product was dried in vacuo at 60 °C overnight. Yield: 83.6% (0.327 g). Single crystals suitable for X-ray diffraction were grown by slow diffusion of MeOH into saturated CH_2Cl_2 (**4a**) and 50:50 CH_2Cl_2/$CHCl_3$ (**4b**) solutions. ^{1}H NMR (400 MHz $(CD_3)_2SO$): δ 8.75 (d, 2H, *J* = 7.4 Hz), 8.35 (d, 2H, *J* = 8.3 Hz), 8.07 (d, 2H, *J* = 1.8 Hz), 7.91 (t, 2H, *J* = 7.8 Hz), 7.58 (dd, 2H, *J* = 8.6, 1.9 Hz), 6.82 (d, 2H, *J* = 8.7 Hz), 1.39 (s, 18H). ^{13}C NMR (600 MHz $(CD_3)_2SO$): δ 168.8, 160.3, 143.1, 138.5, 136.5, 131.3, 130.2, 127.9, 127.2, 122.9, 119.8, 117.3, 34.1, 31.4. FT-IR (ATR): 1589 cm^{-1} (*ν*C=N, w), 1267 cm-1 (*ν*CAr—O, s), 921 cm^{-1} (ν_3O=U=O, s), 546-485 cm^{-1} (*ν*U—N, m), 450-417 cm^{-1} (*ν*U—O, m). Anal. Calc'd. for $C_{64}H_{60}N_4O_8U_2$: C, 52.62; H, 4.06; N, 3.76. Found: C, 51.51; H, 4.12; N, 3.67.

Synthesis of UO_2-2c. The synthesis of *o*-trimethylsilyl-2-aminophenol was adapted from published procedure.[93] In a 50-mL round-bottom flask, *o*-aminophenol (0.437 g, 4.0 mmol) was stirred at room temperature in dichloromethane (5 mL). Chlorotrimethylsilane (0.51 mL, 4.0 mmol) and triethylamine (0.56 mL, 4.0 mmol) were added and the mixture was stirred for 18 hours, and the solvent removed by rotary evaporator. The product was extracted into pentane and filtered over a short pad of Celite to remove the triethylamine salt, then dried to an orange oil which crystallized below room temperature. Yield: 0.583 g, 80.5%. ^{1}H NMR (400 MHz, $CDCl_3$): δ 6.83-6.74 (m, 3H), 6.65 (td, 1H, J = 7.56, 1.60), 0.32 (s, 9H). ^{13}C NMR (400 MHz, $CDCl_3$): 142.92, 138.35, 122.13, 118.69, 118.57, 115.81, 0.60.

Acenaphthenequinone (0.091 g, 0.50 mmol) was added to a 250-mL round bottom flask charged with a stir bar and heated to 78 °C in ethanol (30 mL) with stirring until completely dissolved. *O*-trimethylsilyl-2-aminophenol (0.181 g, 1.0 mmol) and $UO_2(OAc)_2 \cdot 2H_2O$ (0.212 g, 0.5 mmol) were added, and the flask was rinsed with an additional 5 mL of ethanol. The reaction mixture turned golden-brown and was heated and stirred for 18 hours during which time it turned black. After cooling the solution to room temperature, a fine, black powder was collected by filtration. Yield: 0.211 g, 67.0%. ^{1}H NMR (400 MHz, DMSO-d_6): δ 7.52 (d, 2H, J = 7.42), 7.17 (d, 2H, J = 8.20), 6.98 (d, 2H, 7.08), 6.81 (t, 2H, J = 7.84), 6.50 (t, 2H, J = 8.28), 6.01 (m, 4H). FT-IR (ATR): 907, 902 cm^{-1} (O=U=O, ν_3). λ_{max}[1]: 753 nm (5,400 M^{-1} cm^{-1}). Anal. Calc'd for $C_{24}H_{14}N_2O_4U \cdot Cl$: C, 43.16; H, 2.11; N, 4.19. Found: C, 43.10; H, 2.23; N, 4.10.

Synthesis of UO_2-2d. Acenaphthenequinone (0.091g, 0.50 mmol) was added to a 250-mL round bottom flask charged with a stir bar and heated to 68 °C in methanol (40 mL) with stirring until completely dissolved. 2-amino-5-methylphenol (0.123 g, 1.0 mmol) and $UO_2(OAc)_2 \cdot 2H_2O$ (0.212 g, 0.5 mmol) were added as solids. and the flask was rinsed with an additional 5 mL of methanol. The solution turned dark immediately and was heated and stirred 1 hour, producing purple precipitate. After cooling the solution to room temperature, the purple-black solid was collected by filtration. Yield: 0.184 g, 55.7%. ^{1}H NMR (400 MHz, DMSO-d_6): δ 8.78 (d, 2H, J = 7.37), 8.32 (d, 2H, J = 8.19), 7.98 (d, 2H, J = 8.68), 7.87 (t, 2H, J = 7.82), 6.70 (m, 4H), 4.11 (4, 2H, J = 5.25, MeOH), 3.17 (d, 6H, J = 5.25, MeOH), 2.39 (s, 6H). ^{13}C NMR (600 MHz, DMSO-d_6): δ 171.07, 160.22, 156.51, 143.20, 135.37, 131.34, 131.23, 128.33, 127.17, 123.20, 120.94, 120.60, 117.40, 21.76. FT-IR (ATR): 897 cm^{-1} (O=U=O, ν_3). λ_{max}[1]: 674 nm (6,600 M^{-1} cm^{-1}). Anal. Calc'd for $C_{52}H_{36}N_4O_8U_2 \cdot 4(H_2O)$: C, 44.84; H, 3.18; N, 4.02. Found: C, 44.86; H, 3.18; N, 4.00.

Synthesis of UO_2-2e. Acenaphthenequinone (0.063 g, 0.35 mmol) was added to a 100-mL round bottom flask charged with a stir bar and heated to 68 °C in methanol (40 mL) with stirring until completely dissolved. 2-Amino-5-fluorophenol (0.102 g, 0.8 mmol) and $UO_2(OAc)_2 \cdot 2H_2O$ (0.170 g, 0.40 mmol) were added as solids and the flask was rinsed with an additional 5 mL of ethanol. The reaction mixture heated and stirred for 18 hours, producing a black precipitate. After cooling the solution to room temperature, a fine, black powder was collected by filtration. Yield: 0.180 g, 77.0%. ^{1}H NMR: δ 8.75 (d, 2H, J = 7.66), 8.36 (d, 2H, J = 8.35), 8.14 (t, 2H, J = 7.98), 7.90 (t, 2H, J = 7.38), 6.72 (d, 4H, J = 9.59). FT-IR (ATR): 901 cm^{-1} (O=U=O, ν_3). λ_{max}[1]: 629 nm (8,300 M^{-1} cm^{-1}). Anal Calc'd for $C_{48}H_{24}F_4N_4O_8U_2$: C, 43.13; H, 1.81; N, 4.19. Found: C, 43.18; H, 1.79; N, 4.20.

Synthesis of UO_2-2f. The synthesis of 2-trimethylsiloxy-3-aminonaphthalene was adapted from the published procedure for the synthesis of *o*-trimethylsilyl-2-aminophenol[93]. In a 50-mL round-bottom flask, 3-amino-2-naphthol (0.159 g, 1.00 mmol) was stirred at room temperature in dichloromethane (5 mL). Chlorotrimethylsilane (0.13 mL, 1.00 mmol) and triethylamine (0.14 mL, 41.0 mmol) were added and the mixture was stirred for 18 hours, and the solvent removed by rotary evaporator. The product was extracted into heptane and filtered over a short pad of Celite to remove the triethylamine salt, then dried to a red-orange oil which crystallized below room temperature. Yield: 0.220 g, 95.1%. ^{1}H NMR (400 MHz, $CDCl_3$): δ 7.58 (dd, 2H, J = 8.2, 2.8), 7.30-7.20 (m, 2H), 7.11 (s, 1H), 7.04 (s, 1H), 4.02 (bs, 2H), 0.39 (s, 9H). ^{13}C NMR (600 MHz, DMSO-d_6): δ 146.12, 138.52, 129.52, 127.38, 125.40, 124.53, 122.66, 121.17, 107.96, 106.65, 2.04, 1.84.

Acenaphthenequinone (0.073 g, 0.400 mmol) was added to a 250-mL round bottom flask and heated to 78 °C in ethanol (40 mL) with stirring until completely dissolved. 2-trimethylsiloxy-3-aminonaphthalene (0.185 g, 0.8 mmol) and $UO_2(OAc)_2 \cdot 2H_2O$ (0.170 g, 0.400 mmol) were added, and the flask was rinsed with an additional 5 mL of ethanol. The reaction mixture was heated and stirred for 48 hours. After cooling the solution to room temperature, a black solid was collected by filtration. Yield: 0.244 g, 83.3%. ^{1}H NMR: δ 8.90 (d, 2H, J = 7.52), 8.68 (s, 2H), 8.44 (d, 2H, J = 8.18), 7.93 (m, 4H), 7.72 (d, 2H, J = 8.16), 7.45 (t, 2H, J = 7.55), 7.23 (t, 2H, 7.21), 7.13 (s, 2H). FT-IR(ATR): 916, 909 cm^{-1} (O=U=O, ν_3). λ_{max}[1]: ~640 nm (~4,600-4900 M^{-1} cm^{-1}). Anal Calc'd for $C_{64}H_{36}N_4O_8U_2 \cdot H_2O$ C: 51.83 H: 2.58 N: 3.78; Found: C: 52.11, H: 2.61, N 3.78.

References

1. Anderson, N. H.; Xie, J.; Ray, D.; Zeller, M.; Gagliardi, L.; Bart, S. C., Elucidating bonding preferences in tetrakis(imido)uranate(VI) dianions. *Nat. Chem.* **2017,** *9* (9), 850-855.

2. Arnold, P. L.; Dutkiewicz, M. S.; Zegke, M.; Walter, O.; Apostolidis, C.; Hollis, E.; Pécharman, A.-F.; Magnani, N.; Griveau, J.-C.; Colineau, E.; Caciuffo, R.; Zhang, X.; Schreckenbach, G.; Love, J. B., Subtle Interactions and Electron Transfer between U(III), Np(III), or Pu(III) and Uranyl Mediated by the Oxo Group. *Angew. Chem.* **2016,** *128* (41), 12989-12993.

3. Gardner, B. M.; Liddle, S. T., Small-Molecule Activation at Uranium(III). *Eur. J. Inorg. Chem.* **2013,** *2013* (22-23), 3753-3770.

4. Anderson, N. H.; Odoh, S. O.; Williams, U. J.; Lewis, A. J.; Wagner, G. L.; Lezama Pacheco, J.; Kozimor, S. A.; Gagliardi, L.; Schelter, E. J.; Bart, S. C., Investigation of the

Electronic Ground States for a Reduced Pyridine(diimine) Uranium Series: Evidence for a Ligand Tetraanion Stabilized by a Uranium Dimer. *J. Am. Chem. Soc.* **2015,** *137* (14), 4690-4700.

5. Arnold, P. L.; Pécharman, A.-F.; Hollis, E.; Yahia, A.; Maron, L.; Parsons, S.; Love, J. B., Uranyl oxo activation and functionalization by metal cation coordination. *Nat. Chem.* **2010,** *2* (12), 1056-1061.

6. Brown, J. L.; Wu, G.; Hayton, T. W., Oxo Ligand Silylation in a Uranyl β-Ketoiminate Complex. *J. Am. Chem. Soc.* **2010,** *132* (21), 7248-7249.

7. Kiernicki, J. J.; Zeller, M.; Bart, S. C., Facile Reductive Silylation of UO_2^{2+} to Uranium(IV) Chloride. *Angew. Chem.* **2017,** *129* (4), 1117-1120.

8. Denning, R. G.; Snellgrove, T. R.; Woodwark, D. R., The electronic structure of the uranyl ion. *Molecular Physics* **1979,** *37* (4), 1109-1143.

9. Gregson, M.; Lu, E.; Mills, D. P.; Tuna, F.; McInnes, E. J. L.; Hennig, C.; Scheinost, A. C.; McMaster, J.; Lewis, W.; Blake, A. J.; Kerridge, A.; Liddle, S. T., The inverse-*trans*-influence in tetravalent lanthanide and actinide bis(carbene) complexes. *Nature Communications* **2017,** *8*, 14137.

10. Tatsumi, K.; Hoffmann, R., Bent *cis* d^0 MoO_2^{2+} vs. linear *trans* d^0f^0 UO_2^{2+}: a significant role for nonvalence 6p orbitals in uranyl. *Inorg. Chem.* **1980,** *19* (9), 2656-2658.

11. Cowie, B. E.; Nichol, G. S.; Love, J. B.; Arnold, P. L., Double uranium oxo cations derived from uranyl by borane or silane reduction. *Chem. Comm.* **2018,** *54* (31), 3839-3842.

12. Bell, N. L.; Shaw, B.; Arnold, P. L.; Love, J. B., Uranyl to Uranium(IV) Conversion through Manipulation of Axial and Equatorial Ligands. *J. Am. Chem. Soc.* **2018,** *140* (9), 3378-3384.

13. Kiernicki, J. J.; Cladis, D. P.; Fanwick, P. E.; Zeller, M.; Bart, S. C., Synthesis, Characterization, and Stoichiometric U-O Bond Scission in Uranyl Species Supported by Pyridine(diimine) Ligand Radicals. *J. Am. Chem. Soc.* **2015,** *137* (34), 11115-11125.

14. Arnold, P. L.; Pécharman, A.-F.; Lord, R. M.; Jones, G. M.; Hollis, E.; Nichol, G. S.; Maron, L.; Fang, J.; Davin, T.; Love, J. B., Control of Oxo-Group Functionalization and Reduction of the Uranyl Ion. *Inorg. Chem.* **2015,** *54* (7), 3702-3710.

15. Pedrick, E. A.; Schultz, J. W.; Wu, G.; Mirica, L. M.; Hayton, T. W., Perturbation of the O–U–O Angle in Uranyl by Coordination to a 12-Membered Macrocycle. *Inorg. Chem.* **2016,** *55* (11), 5693-5701.

16. Pedrick, E. A.; Wu, G.; Hayton, T. W., Oxo Ligand Substitution in a Cationic Uranyl Complex: Synergistic Interaction of an Electrophile and a Reductant. *Inorg. Chem.* **2015,** *54* (14), 7038-7044.

17. Renshaw, J. C.; Butchins, L. J. C.; Livens, F. R.; May, I.; Charnock, J. M.; Lloyd, J. R., Bioreduction of Uranium: Environmental Implications of a Pentavalent Intermediate. *Environ. Sci. Technol.* **2005,** *39* (15), 5657-5660.

18. Korobkov, I.; Gorelsky, S.; Gambarotta, S., Reduced Uranium Complexes: Synthetic and DFT Study of the Role of π Ligation in the Stabilization of Uranium Species in a Formal Low-Valent State. *J. Am. Chem. Soc.* **2009,** *131* (30), 10406-10420.

19. Bart, S. C.; Heinemann, F. W.; Anthon, C.; Hauser, C.; Meyer, K., A New Tripodal Ligand System with Steric and Electronic Modularity for Uranium Coordination Chemistry. *Inorg. Chem.* **2009,** *48* (19), 9419-9426.

20. Kraft, S. J.; Williams, U. J.; Daly, S. R.; J. Schelter, E.; Kozimor, S. A.; Boland, K. S.; Kikkawa, J. M.; Forrest, W. P.; Christensen, C. N.; Schwarz, D. E.; Fanwick, P. E.; Clark, D. L.;

Conradson, S. D.; Bart, S. C., Synthesis, Characterization, and Multielectron Reduction Chemistry of Uranium Supported by Redox-Active α-Diimine Ligands. *Inorg. Chem.* **2011,** *50* (20), 9838-9848.

21. Pattenaude, S. A.; Mullane, K. C.; Schelter, E. J.; Ferrier, M. G.; Stein, B. W.; Bone, S. E.; Lezama Pacheco, J. S.; Kozimor, S. A.; Fanwick, P. E.; Zeller, M.; Bart, S. C., Redox-Active vs Redox-Innocent: A Comparison of Uranium Complexes Containing Diamine Ligands. *Inorg. Chem.* **2018,** *57* (11), 6530-6539.

22. Li Manni, G.; Walensky, J. R.; Kraft, S. J.; Forrest, W. P.; Pérez, L. M.; Hall, M. B.; Gagliardi, L.; Bart, S. C., Computational Insights into Uranium Complexes Supported by Redox-Active α-Diimine Ligands. *Inorg. Chem.* **2012,** *51* (4), 2058-2064.

23. Takao, K.; Tsushima, S.; Ogura, T.; Tsubomura, T.; Ikeda, Y., Experimental and Theoretical Approaches to Redox Innocence of Ligands in Uranyl Complexes: What Is Formal Oxidation State of Uranium in Reductant of Uranyl(VI)? *Inorg. Chem.* **2014,** *53* (11), 5772-5780.

24. Lukens, W. W.; Speldrich, M.; Yang, P.; Duignan, T. J.; Autschbach, J.; Kögerler, P., The roles of 4f- and 5f-orbitals in bonding: a magnetochemical, crystal field, density functional theory, and multi-reference wavefunction study. *Dalton Trans.* **2016,** *45* (28), 11508-11521.

25. Fortier, S.; Walensky, J. R.; Wu, G.; Hayton, T. W., High-Valent Uranium Alkyls: Evidence for the Formation of $U^{VI}(CH_2SiMe_3)_6$. *J. Am. Chem. Soc.* **2011,** *133* (30), 11732-11743.

26. Lu, E.; Atkinson, B. E.; Wooles, A. J.; Boronski, J. T.; Doyle, L. R.; Tuna, F.; Cryer, J. D.; Cobb, P. J.; Vitorica-Yrezabal, I. J.; Whitehead, G. F. S.; Kaltsoyannis, N.; Liddle, S. T., Back-bonding between an electron-poor, high-oxidation-state metal and poor π-acceptor ligand in a uranium(V)–dinitrogen complex. *Nat. Chem.* **2019,** *11* (9), 806-811.

27. Niklas, J. E.; Farnum, B. H.; Gorden, J. D.; Gorden, A. E. V., Structural Characterization and Redox Activity of a Uranyl Dimer and Transition-Metal Complexes of a Tetradentate BIAN Ligand. *Organometallics* **2017,** *36* (23), 4626-4634.

28. Fedushkin, I. L.; Skatova, A. A.; Chudakova, V. A.; Fukin, G. K., Four-Step Reduction of dpp-bian with Sodium Metal: Crystal Structures of the Sodium Salts of the Mono-, Di-, Tri- and Tetraanions of dpp-bian. *Angew. Chem. Int. Ed.* **2003,** *42* (28), 3294-3298.

29. Fedushkin, Igor L.; Skatova, Alexandra A.; Chudakova, Valentina A.; Cherkasov, Vladimir K.; Fukin, Georgy K.; Lopatin, Mikhail A., Reduction of 1,2-Bis[(2,6-diisopropylphenyl)imino]acenaphthene (dpp-bian) with Alkali Metals − A Study of the Solution Behaviour of $(dpp\text{-}bian)_n{-}[M+]_n$ (M = Li, Na; n = 1−4) with UV/Vis, ESR and ^{1}H NMR Spectroscopy. *Eur. J. Inorg. Chem.* **2004,** *2004* (2), 388-393.

30. Niklas, J. E.; Hunter, K. M.; Gorden, A. E. V., Bonding Interactions in Uranyl α-Diimine Complexes: A Spectroscopic and Electrochemical Study of the Impacts of Ligand Electronics and Extended Conjugation. *Inorg. Chem.* **2019**.

31. Milligan, C. W.; Lindstrom, F., Colorimetric determination of calcium using reagents of the glyoxal bis(2-hydroxyanil) class. *Anal. Chem.* **1972,** *44* (11), 1822-1829.

32. Wilson, A. D., The use of glyoxal bis-(2-hydroxyanil) in determining microgram amounts of uranium. *Analyst* **1962,** *87* (1038), 703-706.

33. Bayer, E., Synthese Makromolekularer Komplexbildner aus Aminophenolen und Glyoxal. *Chem. Ber.* **1957,** *90* (12), 2785-2791.

34. Roy, A. S.; Muresan, N.; Tuononen, H. M.; Rath, S. P.; Ghosh, P., Electronic structure of the glyoxalbis(2-hydroxyanil) (gha) ligand in $[Co^{III}(gha)(PPh_3)_2]$+: radical vs. non-radical states. *Dalton Trans.* **2008,** (26), 3438-3446.

35. Min, K. S.; Weyhermüller, T.; Bothe, E.; Wieghardt, K., Tetradentate Bis(o-iminobenzosemiquinonate(1−)) π Radical Ligands and Their o-Aminophenolate(1−) Derivatives in Complexes of Nickel(II), Palladium(II), and Copper(II). *Inorg. Chem.* **2004,** *43* (9), 2922-2931.

36. Bandoli, G.; Clemente, D. A., Preparation and crystal structure of aqua[bis(2-hydroxyphenylimino)-ethanato-OO′NN′-]dioxouranium. *Journal of the Chemical Society, Dalton Transactions* **1975,** (7), 612-615.

37. Tauer, E.; Grellmann, K.-H.; Kaufmann, E.; Noltemeyer, M., The condensation product of 2-aminophenol and glyoxal. Structure and photochemistry. *Chem. Ber.* **1986,** *119* (11), 3316-3325.

38. Malek, A.; Fresco, J. M., Formation of New Tetradentate Schiff Base Metal Chelates. *Canadian Journal of Chemistry* **1973,** *51* (12), 1981-1989.

39. Xiong, D.; Fu, Z.; Zhong, S.; Jiang, X.; Yin, D., Novel homogeneous Salen Mn(III) catalysts synthesized from dialdehyde or diketone with o-aminophenol for catalyzing epoxidation of alkenes. *Catal. Letters* **2007,** *113* (3), 155-159.

40. Manecke, G.; Gauger, J., Notiz über chelatbildende Kondensationsprodukte aus cyclischen 1.2-Dionen und 2-Amino-phenol. *Chem. Ber.* **1968,** *101* (9), 3326-3328.

41. Viganò, M.; Ferretti, F.; Caselli, A.; Ragaini, F.; Rossi, M.; Mussini, P.; Macchi, P., Easy Entry into Reduced Ar-BIANH_2 Compounds: A New Class of Quinone/Hydroquinone-Type Redox-Active Couples with an Easily Tunable Potential. *Chem. Eur. J.* **2014,** *20* (44), 14451-14464.

42. Meermann, C.; Törnroos, K. W.; Anwander, R., Scandium SALEN Complexes Bearing Chloro, Aryloxo, and Hydroxo Ligands. *Inorg. Chem.* **2009,** *48* (6), 2561-2570.

43. Patel, K.; Deshmukh, S. S.; Bodkhe, D.; Mane, M.; Vanka, K.; Shinde, D.; Rajamohanan, P. R.; Nandi, S.; Vaidhyanathan, R.; Chikkali, S. H., Secondary Interactions Arrest the

Hemiaminal Intermediate To Invert the Modus Operandi of Schiff Base Reaction: A Route to Benzoxazinones. *J. Org. Chem.* **2017,** *82* (8), 4342-4351.

44. Bell, N. L.; Arnold, P. L.; Love, J. B., Controlling uranyl oxo group interactions to group 14 elements using polypyrrolic Schiff-base macrocyclic ligands. *Dalton Trans.* **2016,** *45* (40), 15902-15909.

45. Takao, K.; Ikeda, Y., Structural Characterization and Reactivity of UO_2(salophen)L and [UO_2(salophen)]$_2$: Dimerization of UO_2(salophen) Fragments in Noncoordinating Solvents (salophen = N,N‘-Disalicylidene-o-phenylenediaminate, L = N,N-Dimethylformamide, Dimethyl Sulfoxide). *Inorg. Chem.* **2007,** *46* (5), 1550-1562.

46. Bohle, D. S.; Zafar, A.; Goodson, P. A.; Jaeger, D. A., Synthesis and Characterization of Nickel(II) Bis(alkylthio)salen Complexes. *Inorg. Chem.* **2000,** *39* (4), 712-718.

47. Mukherjee, P.; Biswas, C.; Drew, M. G. B.; Ghosh, A., Structural variations in Ni(II) complexes of salen type di-Schiff base ligands. *Polyhedron* **2007,** *26* (13), 3121-3128.

48. Allen, F. H.; Wood, P. A.; Galek, P. T. A., Role of chloroform and dichloromethane solvent molecules in crystal packing: an interaction propensity study. *Acta Crystallogr., Sect. B: Struct. Sci.* **2013,** *69* (4), 379-388.

49. Arnold, P. L.; Jones, G. M.; Odoh, S. O.; Schreckenbach, G.; Magnani, N.; Love, J. B., Strongly coupled binuclear uranium–oxo complexes from uranyl oxo rearrangement and reductive silylation. *Nat. Chem.* **2012,** *4* (3), 221-227.

50. Karthikeyan, S.; Ramanathan, V.; Mishra, B. K., Influence of the Substituents on the CH...π Interaction: Benzene–Methane Complex. *J. Phys. Chem.* **2013,** *117* (30), 6687-6694.

51. Ghosh, P.; Bill, E.; Weyhermüller, T.; Neese, F.; Wieghardt, K., Noninnocence of the Ligand Glyoxal-bis(2-mercaptoanil). The Electronic Structures of [Fe(gma)]$_2$, [Fe(gma)(py)]·py,

[Fe(gma)(CN)]$^{1-/0}$, [Fe(gma)I], and [Fe(gma)(PR_3)$_n$] (n = 1, 2). Experimental and Theoretical Evidence for “Excited State” Coordination. *J. Am. Chem. Soc.* **2003,** *125* (5), 1293-1308.

52. Gardiner, M. G.; Hanson, G. R.; Henderson, M. J.; Lee, F. C.; Raston, C. L., Paramagnetic Bis(1,4-di-tert-butyl-1,4-diazabutadiene) Adducts of Lithium, Magnesium, and Zinc. *Inorg. Chem.* **1994,** *33* (11), 2456-2461.

53. Fortier, S.; Hayton, T. W., Oxo ligand functionalization in the uranyl ion (UO_2^{2+}). *Coord. Chem. Rev.* **2010,** *254* (3), 197-214.

54. Arnold, P. L.; Hollis, E.; Nichol, G. S.; Love, J. B.; Griveau, J.-C.; Caciuffo, R.; Magnani, N.; Maron, L.; Castro, L.; Yahia, A.; Odoh, S. O.; Schreckenbach, G., Oxo-Functionalization and Reduction of the Uranyl Ion through Lanthanide-Element Bond Homolysis: Synthetic, Structural, and Bonding Analysis of a Series of Singly Reduced Uranyl–Rare Earth 5f1-4fn Complexes. *J. Am. Chem. Soc.* **2013,** *135* (10), 3841-3854.

55. Hayton, T. W.; Wu, G., Synthesis, Characterization, and Reactivity of a Uranyl β-Diketiminate Complex. *J. Am. Chem. Soc.* **2008,** *130* (6), 2005-2014.

56. Denning, R. G., Electronic Structure and Bonding in Actinyl Ions and their Analogs. *J. Phys. Chem.* **2007,** *111* (20), 4125-4143.

57. Lu, C. C.; Bill, E.; Weyhermüller, T.; Bothe, E.; Wieghardt, K., The Monoanionic π-Radical Redox State of α-Iminoketones in Bis(ligand)metal Complexes of Nickel and Cobalt. *Inorg. Chem.* **2007,** *46* (19), 7880-7889.

58. Pankhurst, J. R.; Bell, N. L.; Zegke, M.; Platts, L. N.; Lamfsus, C. A.; Maron, L.; Natrajan, L. S.; Sproules, S.; Arnold, P. L.; Love, J. B., Inner-sphere vs. outer-sphere reduction of uranyl supported by a redox-active, donor-expanded dipyrrin. *Chem. Sci.* **2017,** *8* (1), 108-116.

59. Hardy, E. E.; Wyss, K. M.; Eddy, M. A.; Gorden, A. E. V., An example of unusual pyridine donor Schiff base uranyl (UO_2^{2+}) complexes. *Chem. Comm.* **2017,** *53* (42), 5718-5720.

60. Niklas, J. E.; Hardy, E. E.; Gorden, A. E. V., Solid-state structural elucidation and electrochemical analysis of uranyl naphthylsalophen. *Chem. Comm.* **2018,** *54* (83), 11693-11696.

61. Jones, L. H., Systematics in the vibrational spectra of uranyl complexes. *Spectrochimica Acta* **1958,** *10* (4), 395-403.

62. Jones, L. H.; Penneman, R. A., Infrared Spectra and Structure of Uranyl and Transuranium (V) and (VI) Ions in Aqueous Perchloric Acid Solution. *J. Chem. Phys.* **1953,** *21* (3), 542-544.

63. Kalaj, M.; Carter, K. P.; Cahill, C. L., Isolating Equatorial and Oxo Based Influences on Uranyl Vibrational Spectroscopy in a Family of Hybrid Materials Featuring Halogen Bonding Interactions with Uranyl Oxo Atoms. *Eur. J. Inorg. Chem.* **2017,** *2017* (40), 4702-4713.

64. Di Pietro, P.; Kerridge, A., U–Oyl Stretching Vibrations as a Quantitative Measure of the Equatorial Bond Covalency in Uranyl Complexes: A Quantum-Chemical Investigation. *Inorg. Chem.* **2016,** *55* (2), 573-583.

65. Di Pietro, P.; Kerridge, A., Assessing covalency in equatorial U–N bonds: density based measures of bonding in BTP and isoamethyrin complexes of uranyl. *Phys. Chem. Chem. Phys.* **2016,** *18* (25), 16830-16839.

66. Syt'ko, V. V.; Kabaeva, E. N., Special Features of the Correlation between the Uranium–Oxygen Interatomic Distances and the Frequencies of the Valence Vibrations of the UO22+ Group in Complex Compounds of Uranyl. *J. Appl. Spectrosc.* **2002,** *69* (4), 566-570.

67. Benedix, R.; Dietz, F.; Hennig, H., Spectroscopic and theoretical investigations of Schiff base metal complexes with intraligand charge-transfer behavior. *Inorg. Chim. Acta.* **1988,** *147* (2), 179-183.

68. Dommaschk, M.; Thoms, V.; Schütt, C.; Näther, C.; Puttreddy, R.; Rissanen, K.; Herges, R., Coordination-Induced Spin-State Switching with Nickel Chlorin and Nickel Isobacteriochlorin. *Inorg. Chem.* **2015,** *54* (19), 9390-9392.

69. Altwicker, E. R., The Chemistry of Stable Phenoxy Radicals. *Chem. Rev.* **1967,** *67* (5), 475-531.

70. Lynn, M. A.; Bursten, B. E., An analysis of the bonding in some 'nonclassical' d0 and d10 metal carbonyl complexes. *Inorg. Chim. Acta.* **1995,** *229* (1), 437-443.

71. Maki, T.; Araki, Y.; Ishida, Y.; Onomura, O.; Matsumura, Y., Construction of Persistent Phenoxyl Radical with Intramolecular Hydrogen Bonding. *J. Am. Chem. Soc.* **2001,** *123* (14), 3371-3372.

72. Thomas, F., Ligand-centred oxidative chemistry in sterically hindered salen complexes: an interesting case with nickel. *Dalton Trans.* **2016,** *45* (27), 10866-10877.

73. Butsch, K.; Günther, T.; Klein, A.; Stirnat, K.; Berkessel, A.; Neudörfl, J., Redox chemistry of copper complexes with various salen type ligands. *Inorg. Chim. Acta.* **2013,** *394*, 237-246.

74. Sakamoto, M.; Cai, X.; Hara, M.; Fujitsuka, M.; Majima, T., Intermolecular Electron Transfer from Naphthalene Derivatives in the Higher Triplet Excited States. *J. Am. Chem. Soc.* **2004,** *126* (31), 9709-9714.

75. Chai, L.-Q.; Zhang, H.-S.; Huang, J.-J.; Zhang, Y.-L., An unexpected Schiff base-type Ni(II) complex: Synthesis, crystal structures, fluorescence, electrochemical property and SOD-like activities. *Spectrochim. Acta, Part A* **2015,** *137*, 661-669.

76. Martin, D. J.; McCarthy, B. D.; Donley, C. L.; Dempsey, J. L., Electrochemical hydrogenation of a homogeneous nickel complex to form a surface adsorbed hydrogen-evolving species. *Chem. Comm.* **2015,** *51* (25), 5290-5293.

77. Downard, A. J.; Hanton, L. R.; McMorran, D. A.; Paul, R. L., Electrochemical Studies of Nickel(II) Complexes with Tri- and Bidentate Arsine Ligands. A Stereochemically and Electronically Accommodating Donor Set. *Inorg. Chem.* **1993,** *32* (26), 6028-6033.

78. Lacy, D. C.; McCrory, C. C. L.; Peters, J. C., Studies of Cobalt-Mediated Electrocatalytic CO_2 Reduction Using a Redox-Active Ligand. *Inorg. Chem.* **2014,** *53* (10), 4980-4988.

79. Schelter, E. J.; Wu, R.; Scott, B. L.; Thompson, J. D.; Cantat, T.; John, K. D.; Batista, E. R.; Morris, D. E.; Kiplinger, J. L., Actinide Redox-Active Ligand Complexes: Reversible Intramolecular Electron-Transfer in U(dpp-BIAN)$_2$/U(dpp-BIAN)$_2$(THF). *Inorg. Chem.* **2010,** *49* (3), 924-933.

80. Zheng, X.-J.; Bell, N. L.; Stevens, C. J.; Zhong, Y.-X.; Schreckenbach, G.; Arnold, P. L.; Love, J. B.; Pan, Q.-J., Relativistic DFT and experimental studies of mono- and bis-actinyl complexes of an expanded Schiff-base polypyrrole macrocycle. *Dalton Trans.* **2016,** *45* (40), 15910-15921.

81. Schmidt, A.-C.; Heinemann, F. W.; Lukens, W. W.; Meyer, K., Molecular and Electronic Structure of Dinuclear Uranium Bis-μ-Oxo Complexes with Diamond Core Structural Motifs. *J. Am. Chem. Soc.* **2014,** *136* (34), 11980-11993.

82. Camp, C.; Andrez, J.; Pécaut, J.; Mazzanti, M., Synthesis of Electron-Rich Uranium(IV) Complexes Supported by Tridentate Schiff Base Ligands and Their Multi-Electron Redox Chemistry. *Inorg. Chem.* **2013,** *52* (12), 7078-7086.

83. Sonnenberger, D. C.; Gaudiello, J. G., Cyclic Voltammetric Study of Organoactinide Compounds of Uranium(IV) and Neptunium(IV). Ligand Effects on the M(IV)/M(III) Couple. *Inorg. Chem.* **1988,** *27* (15), 2747-2748.

84. Morris, D. E.; Da Re, R. E.; Jantunen, K. C.; Castro-Rodriguez, I.; Kiplinger, J. L., Trends in Electronic Structure and Redox Energetics for Early-Actinide Pentamethylcyclopentadienyl Complexes. *Organometallics* **2004,** *23* (22), 5142-5153.

85. Schelter, E. J.; Yang, P.; Scott, B. L.; Thompson, J. D.; Martin, R. L.; Hay, P. J.; Morris, D. E.; Kiplinger, J. L., Systematic Studies of Early Actinide Complexes: Uranium(IV) Fluoroketimides. *Inorg. Chem.* **2007,** *46* (18), 7477-7488.

86. Sondermann, C.; Ringenberg, M. R., Tuning the overpotential of electrocatalytically active cyclopentadienylnickel complexes containing 1,4-diaza-1,3-butadienes (DAB) for proton reduction. *Dalton Trans.* **2017,** *46* (16), 5143-5146.

87. Hasan, K.; Zysman-Colman, E., Synthesis, UV–Vis and CV properties of a structurally related series of bis(Arylimino)acenaphthenes (Ar-BIANs). *J. Phys. Org. Chem.* **2013,** *26* (3), 274-279.

88. Sheldrick, G. M., Crystal structure refinement with SHELXL. *Acta Crystallographica. Section C, Structural Chemistry* **2015,** *71* (Pt 1), 3-8.

89. Dolomanov, O. V.; Bourhis, L. J.; Gildea, R. J.; Howard, J. A. K.; Puschmann, H., OLEX^2: a complete structure solution, refinement and analysis program. *J. Appl. Crystallogr.* **2009,** *42* (2), 339-341.

90. Bourhis, L. J.; Dolomanov, O. V.; Gildea, R. J.; Howard, J. A. K.; Puschmann, H., The anatomy of a comprehensive constrained, restrained refinement program for the modern computing environment – Olex2 dissected. *Acta Crystallographica. Section A, Foundations and Advances* **2015,** *71* (Pt 1), 59-75.

91. Frisch, M. J.; Trucks, G. W.; Schlegel, H. B.; Scuseria, G. E.; Robb, M. A.; Cheeseman, J. R.; Scalmani, G.; Barone, V.; Petersson, G. A.; Nakatsuji, H.; Li, X.; Caricato, M.; Marenich, A.

V.; Bloino, J.; Janesko, B. G.; Gomperts, R.; Mennucci, B.; Hratchian, H. P.; Ortiz, J. V.; Izmaylov, A. F.; Sonnenberg, J. L.; Williams; Ding, F.; Lipparini, F.; Egidi, F.; Goings, J.; Peng, B.; Petrone, A.; Henderson, T.; Ranasinghe, D.; Zakrzewski, V. G.; Gao, J.; Rega, N.; Zheng, G.; Liang, W.; Hada, M.; Ehara, M.; Toyota, K.; Fukuda, R.; Hasegawa, J.; Ishida, M.; Nakajima, T.; Honda, Y.; Kitao, O.; Nakai, H.; Vreven, T.; Throssell, K.; Montgomery Jr., J. A.; Peralta, J. E.; Ogliaro, F.; Bearpark, M. J.; Heyd, J. J.; Brothers, E. N.; Kudin, K. N.; Staroverov, V. N.; Keith, T. A.; Kobayashi, R.; Normand, J.; Raghavachari, K.; Rendell, A. P.; Burant, J. C.; Iyengar, S. S.; Tomasi, J.; Cossi, M.; Millam, J. M.; Klene, M.; Adamo, C.; Cammi, R.; Ochterski, J. W.; Martin, R. L.; Morokuma, K.; Farkas, O.; Foresman, J. B.; Fox, D. J. *Gaussian 16 Rev. B.01*, Wallingford, CT, **2016**.

92. Avogadro: an open-source molecular builder and visualization tool. Version 1.2.0. http://avogadro.cc/.

93. Suttil, J. A.; Wasserscheid, P.; McGuinness, D. S.; Gardiner, M. G.; Evans, S. J., A survey of pendant donor-functionalised (N,O) phosphine ligands for Cr-catalysed ethylene tri- and tetramerisation. *Catalysis Science & Technology* **2014,** *4* (8), 2574-2588.

Chapter 3

Actinide Salophen and Bis-Salophen Complexes

Portions of this chapter are reproduced from Niklas, J. E.; Hardy, E. E.; Gorden, A. E. V., Chem. Comm. 2018, 54 (83), 11693-11696 by permission of The Royal Society of Chemistry

Introduction

Salophen ligands (N,N′-bis(salicylidene)-phenylenediamines), which feature N2O2 pockets, have been popular frameworks for studying a multitude of coordination complexes due their ease of synthesis and tunability. The commercial availability of a range of substituted o-phenylenediamines and salicylaldehydes allows for extensive libraries of these ligands to be assembled, and their mixed-donor pockets predispose them to bind a large variety of metal ions upon deprotonation of the two phenolic donors. Though the inclusion of the phenylene backbone renders these ligands fairly rigid, particularly in comparison to their salen counterparts, they retain a considerable degree of flexibility which can result in an assortment of unexpected conformations and structural features, depending on the size and preferred coordination geometry of the metal ion as well as ligand substituents. Previous work in the Gorden lab has investigated salophen derivatives such as “salqu”, “salphenazine”, and “naphthylsalophen”, and the use of these species as selective chemosensors for uranyl, and for their unique structural and electronic properties. Complexes of naphthylsalophen exhibit unusual electronic communication aided by extended π-conjugation, including an emissive thorium species. Lanthanide naphthylsalophen complexes adopt a triple-decker sandwich (M2L3) configuration for Ln^{3+} ions, and ML2 structures for Ce^{4+} and Th^{4+} (**Figure 3.1**), and phenylene-derivatized naphthylsalophen Ln2L3 complexes are currently being investigated for their ability to undergo two-photon upconversion. Salophens are redox-active;; however, they do not exhibit nearly the range of redox behavior as BIAN-type

ligands, which are known for their redox-non-innocence. Nonetheless, the unique properties of naphthylsalophen ligands and their electronic flexibility has prompted us to pursue salophens for their potential to yield unusual and fundamentally interesting f-element complexes.

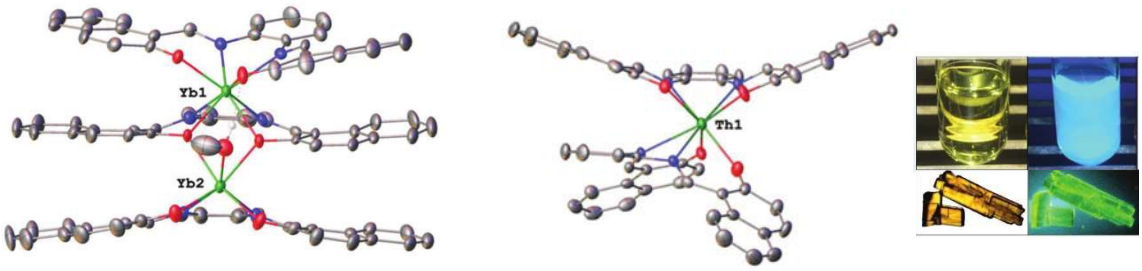

Figure 3.1. Naphthylsalophen complexes of M_2L_3 and ML_2 type, and solution-state and solid-state fluorescence of thorium naphthylsalophen. [4,8]

The first section of this chapter details the synthesis and characterization of the ligand, "naphthylsalophen" and its uranyl complex which exhibits some noteworthy features in both the solution and solid-state. The extended conjugation of the napthhthyl arms sets this ligand apart from traditional salophens, and as observed in the α-diimine complexes, this extension of the ligand π-system allows for unique behaviors.

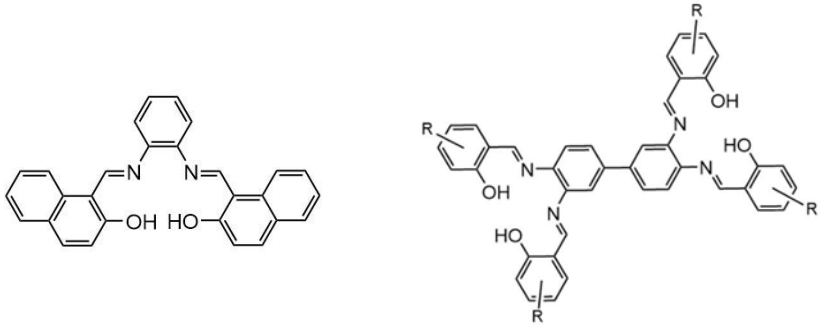

Figure 3.2. Structures of naphthylsalophen and bis-salophens discussed in this chapter.

The second section of this chapter describes preliminary investigations into the synthesis of larger bis-salophen ligands and their actinide complexes. These systems feature two N_2O_2 pockets linked to one another, allowing for the coordination of more than one metal center, and for the formation of supramolecular complexes. The field of supramolecular actinide chemistry is dominated by examples of clusters and inorganic-organic hybrid materials such as metal-organic frameworks (MOFs) or coordination polymers, with examples of molecular complexes being mostly limited to macrocyclic species, with fewer examples of higher-nuclearity complexes ($n \geq 3$) and metallamacrocycles, complexes held together by cation-cation interactions (CCIs), and only a small number of polynuclear helicates. The use of these linked bis-salophens has allowed for isolation of a di-uranyl complex as well as the first circular thorium helicate.

3.1 | Uranyl Naphthylsalophen

The coordination chemistry of uranium is dominated by uranyl(VI) complexes as a result of the stability of the linear [O=U=O]2+ moiety, especially in aqueous systems; however, the study of lower-valent uranium complexes and multielectron processes has garnered wide interest for applications in catalysis and nuclear waste remediation. For example, the bio-immobilization of the highly water soluble U(VI) by reduction to the insoluble U(IV) is known to proceed through a key pentavalent intermediate, but this process is poorly understood. U(V) species are generally unstable with respect to disproportionation, which complicates their study and often precludes their isolation. Systems in which the U(VI)/U(V) redox couple can be studied are therefore pertinent to developing a better understanding the reduction of uranyl and the impacts equatorial

ligands have on the stability of U(V) (UO2+) species. Efforts to more thoroughly describe the unique bonding and electronic properties of uranium have increased of late, with significant focus on oxo- functionalization of uranyl complexes, as this both displays the reactivity of the terminal oxo moieties, which were long considered to be inert, and allows for more facile reduction of the metal center. Recently, pairing strongly donating equatorial ligands with Lewis acid acceptors has proven a useful route to oxo-functionalization and consequent reduction to UO_2^+. Using a dipyrrin derivative, the Arnold group demonstrated tunability of the nonaqueous U(VI)/U(V) and U(V)/U(IV) redox couples to ranges that are accessible to mild reducing agents. These features speak to the importance of equatorial ligand interactions with the metal center, and illustrate the profound impacts that subtle differences in the coordination sphere can have on the reactivity of uranium species.

Salophen ligands, which differ from popular salen ligands through the incorporation of a phenylene backbone, thereby extending conjugation, coordinate to the equatorial plane of uranyl through two phenolate and two neutral imine donors. This framework has been popular for studying the structure and reactivity of uranium species, and its redox capabilities have been exploited for C—C bond formation and the isolation of ligand radical anions. Using naphthylsalophen, we were able to take advantage of the features offered by this ligand system to examine the electronic properties of an unusual uranyl complex. The ligand, **H_2L**, was prepared from the reaction of two equivalents of 2-hydroxynaphthaldehyde with 1,2-diaminobenzene in methanol (**Scheme 3.1**). A precipitate formed after heating the solution to 70 °C for four hours and was isolated as a bright orange solid via vacuum filtration. The product identity was confirmed by ^{1}H NMR, HRMS and single crystal X-ray diffraction. The metal complex **UO_2L** was synthesized by addition of $UO_2(NO_3)_2$•$6H_2O$ to a solution of **UO_2L** and triethylamine dissolved in 1:1

methanol/dichloromethane and subsequent heating (**Scheme 3.2**). The resulting dark red solid was isolated by means of vacuum filtration and characterized using NMR, HRMS, and single crystal X-ray diffraction.

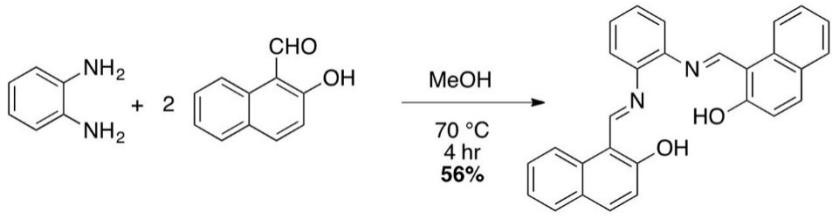

Scheme 3.1. Synthesis of **H_2L** or "naphthylsalophen" from 2-hydroxynaphthaldehyde and 1,2-diaminobenzene. Isolated as a bright orange solid.

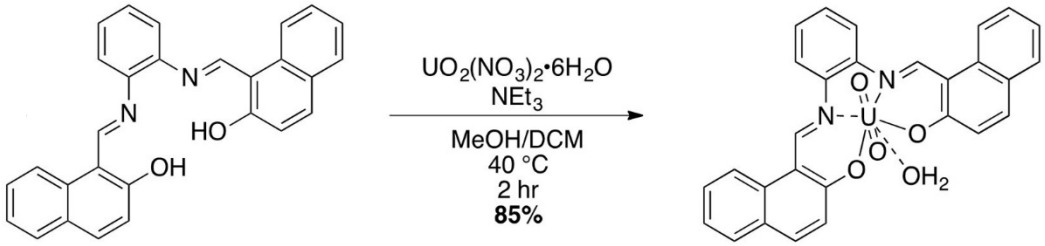

Scheme 3.2. Synthesis of **UO_2L**. Isolated as a dark red solid.

Single crystals of **H_2L** suitable for X-ray diffraction were grown by slow evaporation of a saturated 1:1 dichloromethane/methanol solution. The ligand crystallizes in the orthorhombic space group $P2_12_12_1$ with an interstitial CH_2Cl_2 molecule in the asymmetric unit (**Figure 3.2**). The tautomerization of the ligand (**Scheme 3.3**) can be observed in the solid-state—two converged, suitable structure solutions can be found which differ only in the placement of a hydrogen atom on either O1 or N1, representing the "enolimine" and "ketoamine" forms, respectively. It is clear from examination of the bond lengths in these two solutions (**Table 3.1**) that the "ketoamine" tautomer is more stable than the "enolimine" tautomer in the solid-state, as both solutions have two distinct C—O bond lengths reflective of different bond orders, regardless of the mathematical placement of the proton. The longer C_{imine}—N1 distance of 1.319(3) Å in comparison to C_{imine}—

N2 of 1.302(2) Å also confirms this assignment, although not as clearly. This tautomerization has been observed and explained before for this system in solution using ^{1}H NMR and IR, as well as crystallographically.

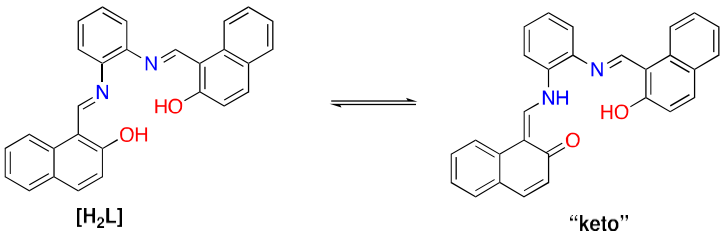

Scheme 3.3. Projection of the "enolimine" and "ketoamine" tautomers of **H_2L**. The solution phase data and metal complexes suggest the equilibrium lies on the "enolimine" form, but the solid-state data favors the "ketoamine" form.

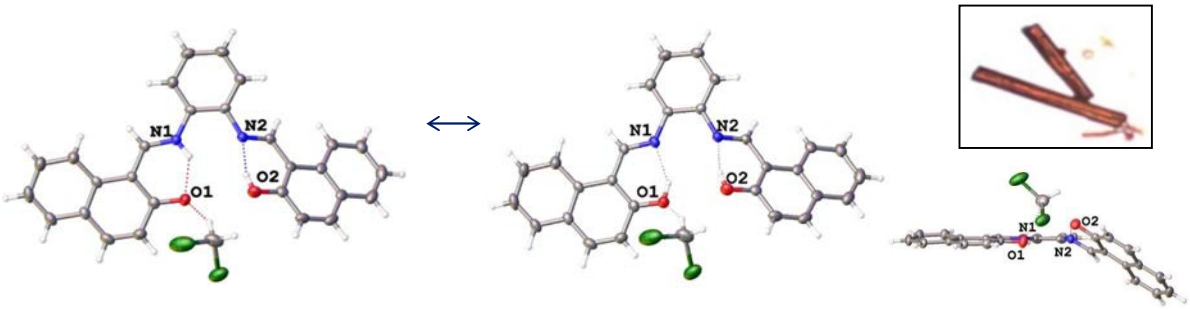

Figure 3.2. Projection of **H_2L** and interstitial CH_2Cl_2 solvent molecule. Inset image of crystals.

Table 3.1. Bond lengths for "enolimine" (A) and "ketoamine" (B) tautomers of **H_2L**.

	A	**B**
C—O1	1.276(3)	1.271(3)
C—O2	1.338(3)	1.339(3)
C_{im}—N1	1.319(3)	1.329(3)
C_{im}—N2	1.298(3)	1.292(3)
N1—H	0.88	-
O1—H	-	0.84
R1	0.0556	0.0570

Single crystals of **UO_2L** were grown by slow diffusion of hexanes into a saturated solution of **UO_2L** in CH_2Cl_2. **UO_2L** crystallizes in the $P2_1/n$ space group with four interstitial dichloromethane molecules, and two distinct **UO_2L** units per asymmetric unit (**Figure 3.3).** The average U—N_{imine} bond lengths of 2.515(6) Å, U—O_{H_2O} bond lengths of 2.450(5) Å, and the U—O_{phenol} bond lengths of 2.286(5) Å are within normal ranges for U(VI) species. Of note is the coordinated water molecule, which participates in hydrogen bonding with one of the phenolic oxygens, resulting in a lengthened U—O_{phenol} distance of 2.311(5) Å, as well as interacts with the

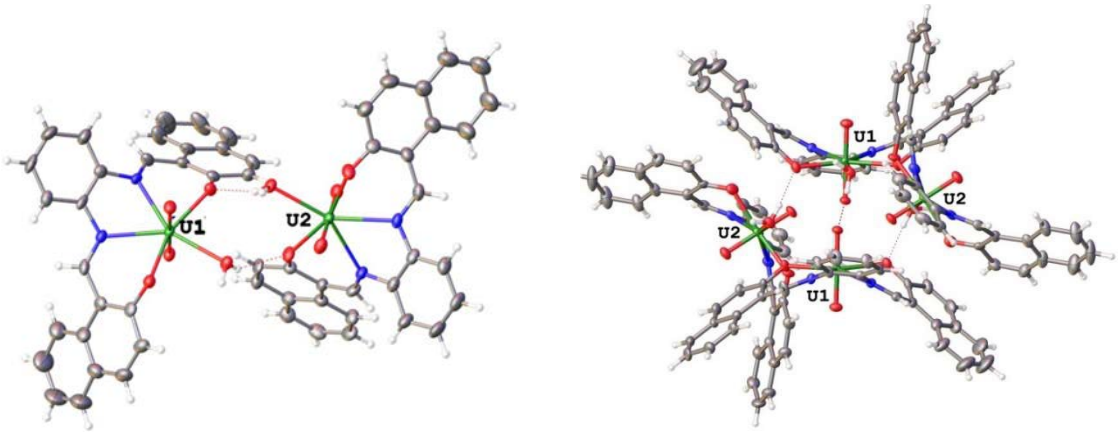

Figure 3.3 Projection of the asymmetric unit of **UO_2L** (left) and packing highlighting the hydrogen bonded tetramers (right). Interstitial CH_2Cl_2 solvent molecules have been removed for clarity.

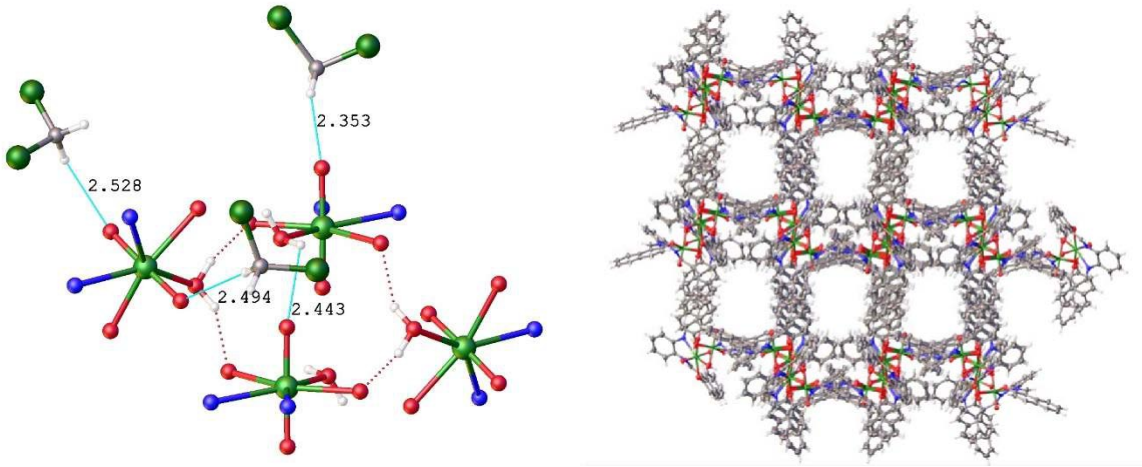

Figure 3.4 Left: Coordination spheres and -yl oxo distances to hydrogen atoms on coordinated H_2O and interstitial CH_2Cl_2. All ligand carbon and hydrogen atoms omitted for clarity. Right: Extended packing of **UO_2L** showing channels (CH_2Cl_2 molecules occupy these channels but are removed for clarity).

-yl oxygen of the neighboring complex. These two distinct **UO_2L** molecules in the asymmetric unit are symmetry- related to two other molecules, resulting in a tetrad of **UO_2L** complexes held together through hydrogen bonding interactions (**Figure 3.3**). The coordinated water molecule has H—O_{phenol} distances of 1.923 and 2.032 Å, and an H⋯O_{yl} distance of 2.443 Å. The longer-range H⋯Oyl interaction does not qualify as a true hydrogen bond, as the U—Oyl distances of 1.795(5) Å and 1.769(5) Å are typical for U(VI)—O_{yl} bonds, however the former does show a slight lengthening. Recent work by Arnold has examined Lewis acid interactions with the -yl oxygen, and in these cases, the reduction of uranyl(VI) to uranyl(V) is confirmed by U—Oyl bond lengths upwards of 1.88 Å, but such changes are not observed for our system. Additionally, hydrogen atoms on three of the four interstitial CH_2Cl_2 molecules are 2.353 Å, 2.495 Å and 2.528 Å away from the -yl oxygen, the latter two of which interact with opposite ends of the same uranyl unit (**Figure 3.4**). We previously observed similar interactions of CH_2Cl_2 with the uranyl oxo moiety in the presence of a redox-active equatorial ligand, however no perturbations of U—Oyl bond lengths were observed. The H⋯Oyl distance in this case, which is 0.062 Å shorter, does correspond to the slightly elongated U—Oyl bond, indicating the oxo moieties are not entirely inert.

Table 3.2. Bond distances for **UO_2L** and interactions with solvent.

Bond	Distance (Å)
U1=O_{yl}	1.795(5)
	1.771 (5)
U2=O_{yl}	1.769 (5)
	1.771 (5)
O_{yl} ⋯ H(OH)	2.443
O_{yl} ⋯ H($CHCl_2$)	2.353
	2.494
	2.528

The hydrogen bonding interactions observed in the complex **UO_2L**, paired with π-π stacking of the naphthalene rings of 4.304 Å, affords an interesting long-range supramolecular stacking structure with channels that are occupied by interstitial CH_2Cl_2 in the solid-state (**Figure 3.4**), similar to those observed in metal organic frameworks (MOFs). These stacking interactions are off-set, which is common in structures such as these, but is a consequence of the packing rather than an interaction that would allow this structure to maintain these tetramers in solution and therefore limits their application.

The free base **H_2L** has three electronic absorption features at 316 nm ($\varepsilon = 9.57 \times 10^3$ cm^{-1} M^{-1}), 391 nm (ε = 9.50 x 103 cm^{-1} M^{-1}), and 456 nm (ε = 8.02 x 103 cm^{-1} M^{-1}), with a shoulder at 477 nm (ε = 7.08 x 103 cm^{-1} M^{-1}). The lowest-energy feature is consistent with proton transfer *via* deprotonation/tautomerism of the naphthol arms. The loss of this feature is observed upon coordination to UO_2^{2+}. Additionally, coordination to uranyl results in a bathochromic shift in λ_{max} to 340 nm ($\varepsilon = 1.21 \times 10^4$ cm^{-1} M^{-1}) and a moderate increase in extinction coefficient, as well as a bathochromic shift and broadening of the second ligand feature. The change in the UV-Vis signature with the addition of a uranyl nitrate solution by serial titration of **H_2L** (**Figure 3.5**) was followed, and appears consistent with overall 1:1 binding, as levelling-off of the traces is observed at the 1:1 point; however, additional changes to the spectrum are observed past this point. The source of these changes has not been identified, but they may be attributable to the continued addition of water– given that **UO_2L** has been found to form water-coordinated monomers which hydrogen-bond to one another in the solid-state, these changes, especially the continued increase in extinction coefficient at 340 nm, may reflect the coordination of water and subsequent aggregation effects.

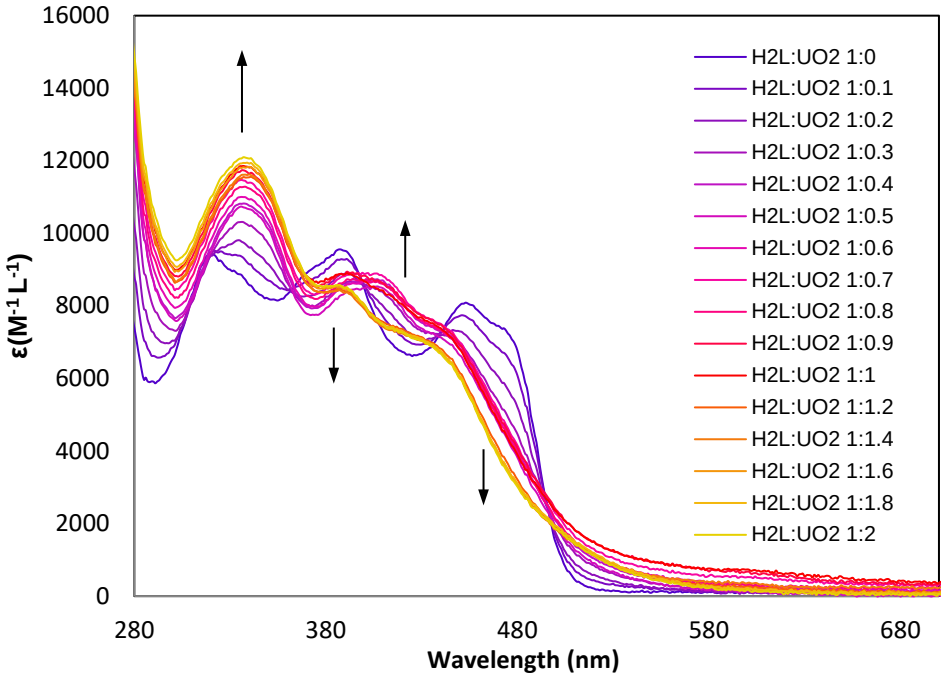

Figure 3.5. Serial titration of 20 μM solution of **H_2L** in MeOH with increasing ratios of $UO_2(NO_3)_2$•$6H_2O$ dissolved in water. Change in the UV spectrum plateaued after a 1:1 addition of metal salt. Minimal water was added through this titration (~100 μL).

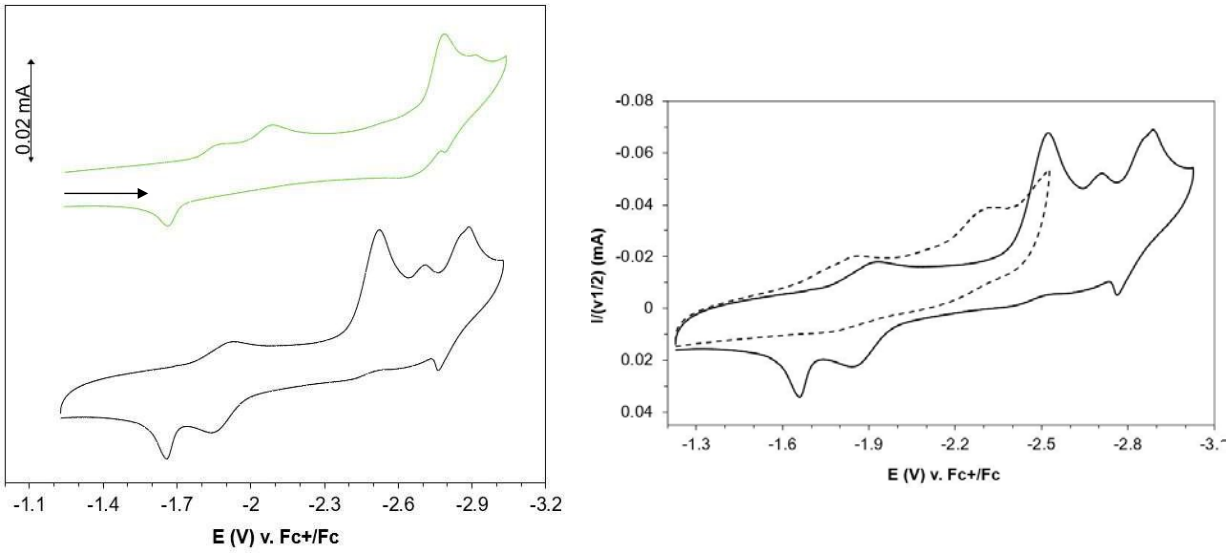

Figure 3.6. Cyclic voltammograms of **H_2L** (top, green) and **UO_2L** (bottom, black) (0.25 mM in CH_3CN; 0.1 M $TBAClO_4$, ν = 0.2 V/s). Right: Scan-rate normalized cyclic voltammograms of **UO_2L** between -1.2 and -3.0 V (solid, original scan rate 0.2 V/s), and -1.2 and -2.5 V (dashed, original scan rate 0.1 V/s). ((1000)*(I/ν1/2); I= current (A), ν= scan rate (V/s).

Cyclic voltammetry experiments were conducted in acetonitrile (0.1 M TBAClO4 supporting electrolyte), and all values are reported versus the Fc^{+}/Fc couple. For the free ligand, **H_2L**, multiple reductive events were observed (**Figure 3.6**). The irreversible reduction at Epc= -2.79 V can be assigned to the $2e^-$ reduction of **H_2L** to **L^{2-}**, which is shifted anodically by 100 mV relative to that of salophen, and can be attributed to the extension of the π-conjugated system. The quasireversible reduction at E_{pc}= -2.90 V (E_{pa}= -2.80 V) corresponds to the formation of the naphthyl radical anion and is associated with the oxidation at -1.67 V, which is not observed unless the scan is conducted to potentials more negative than -2.6 V. The positions and intensities of the peaks at -1.87, and -2.1 V are scan-rate-dependent (**Figure 3.7**), and could not be assigned definitively, though we posit that while these events are in range for the reduction of **H_2L** to **$H_2L^{\bullet-}$**, they may result from the intermolecular H-bonding of the phenolic protons to the imine nitrogen atoms or tautomerism of the species in solution, as they are not observed in the voltammogram of the uranyl complex. This behavior is distinct from that of salophen, which undergoes reduction (assigned to the formation of **$H_2L^{\bullet-}$**) at similar potentials, but does not exhibit the same scan-rate dependence.

In the cathodic scan of **UO_2L**, four peaks are observed at E_{pc}= -1.93 V, -2.53 V, -2.71 V, and -2.89 V. Irreversible reduction of the ligand occurs at -2.53 V (an anodic shift of 260 mV relative to the free ligand), and the quasireversible reduction of the naphthyl substituents is again seen at -2.89 V (**Figure 3.6**). Additionally, the oxidation event at E_{pa} = -1.66 V is ligand-based and only occurs when the scan is conducted to appreciably cathodic potentials, as observed for the free ligand. The reduction at -1.93 V is quasireversible (though nearly reversible) and associated with the return oxidation event at E_{pa}= -1.84 V ($E_{1/2}$= -1.89 V, ΔE = 86 mV) and can be assigned to

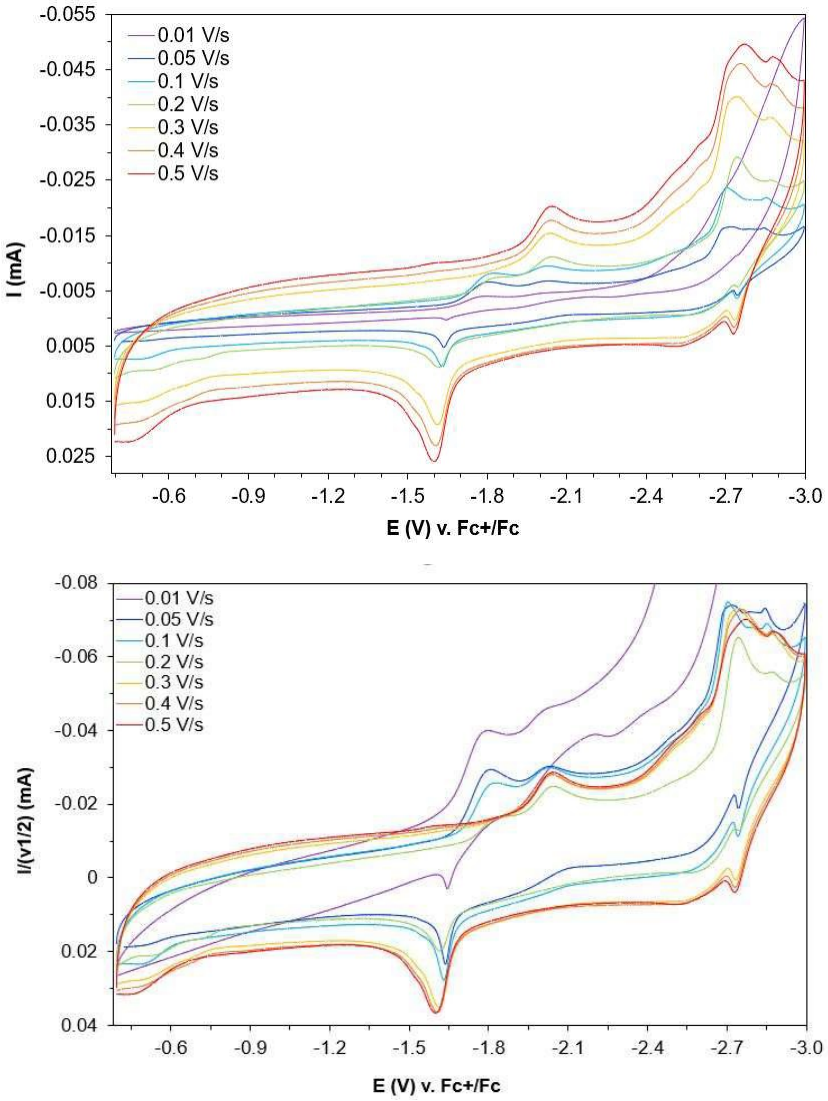

Figure 3.7. Top: Cyclic voltammograms of **H_2L** (0.25 mM in CH_3CN, 0.1M $TBAClO_4$) at scan rates of 0.01 V/s – 0.5 V/s. Bottom: Scan rate normalized cyclic voltammograms of **H_2L** (0.25 mM in CH_3CN, 0.1M $TBAClO_4$) at scan rates of 0.01 V/s – 0.5 V/s. ((1000)*($I/v^{1/2}$); I= current (A), ν= scan rate (V/s)

the U(VI)/U(V) ($UO_2^{2+/}UO2^+$) couple. This value agrees with those previously reported for uranyl salen-type complexes, though it is more negative than those reported for [UO_2(salophen)] complexes (*ca*. -1.65 V) and associated with a much smaller ΔE. The irreversible reduction at -2.71 V warrants further investigation as it is in range for the formation of a $L^{\bullet 2-}$–U(IV) species. This reduction peak overlaps with the reduction of the free ligand to L^{2-}, for which a small shoulder is observed at scan rates greater than 0.3 V/s, precluding any clear assignment of this process.

It is worth noting that the definition of the U(VI)/U(V) couple appears to be dependent on scanning to more negative potentials and may be associated with the ligand-based reduction at -2.89 V. When the sweep range is limited to more positive potentials, a couple can still be seen but is poorly defined, anodically shifted (E_{pc}= -1.85 V, E_{pa}= -1.76 V), and includes a shoulder at -1.73 V which is likely associated with a ligand reduction process (**Figure 3.6**). Additionally, a peak at -2.3 V is observed that may correspond to a more drastic anodic shift of the L/L^{2-} reduction potential. These sweep-range-dependent events indicate a significant degree of electronic communication exists between the ligand and the metal center in solution.

In conclusion, the tetradentate Schiff base ligand, naphthylsalophen, and its hexavalent uranyl complex, have been synthesized and characterized in solution and in the solid-state. Interactions of coordinated water and solvent protons with the uranyl oxo moiety result in a slight elongation of the U—Oyl bond in the solid state. The fairly complex electrochemical profile and observed 260 mV shift in the ligand reduction potential is evidence that this derivative of the thoroughly studied uranyl salophen system shows interesting redox behavior that is usually observed only with more specialized redox-active ligands, and is a candidate for further investigation with respect to any oxo reactivity it may exhibit. These findings speak to the intricacies of 5f metal-ligand interactions and highlight the need to of the fundamental behaviors of the actinides.

3.2 | Bis-Salophen Complexes

The utility of salophens has led to the development of a wide array of substituted ligands, including those which feature more than one binding pocket. Such ligand frameworks can have a range of flexibilities and binding pocket configurations (**Figure 3.8**), and allow for the synthesis of asymmetrically substituted and hetero- or homo-bimetallic species, as well as give rise to extended supramolecular structures, catalytic behavior, tunable magnetic properties, and fluorescence. The use of these ligands in f-element coordination chemistry appears to be restricted to only two examples—a dinuclear uranyl complex of type B (**Figure 3.10**), and Ln^{3+} complexes of type A (Ln^{3+} = Dy^{3+}, Tb^{3+}, Ho^{3+}, Gd^{3+}, Y^{3+}). The studies in this section focus on symmetric bis-salophen ligands of type A which feature a biphenyl linker and are prepared by condensation of 3,3'-diaminobenzidine (or 3,3'-diaminobenzidine tetrahydrochloride in the presence of 4 equivalents of triethylamine) and a salicylaldehyde (**Scheme 3.4**). Given the ability of bis-salophens to coordinate more than one metal center, we were particularly interested in their use as supporting ligands for multiple actinide centers and the potential for forming supramolecular

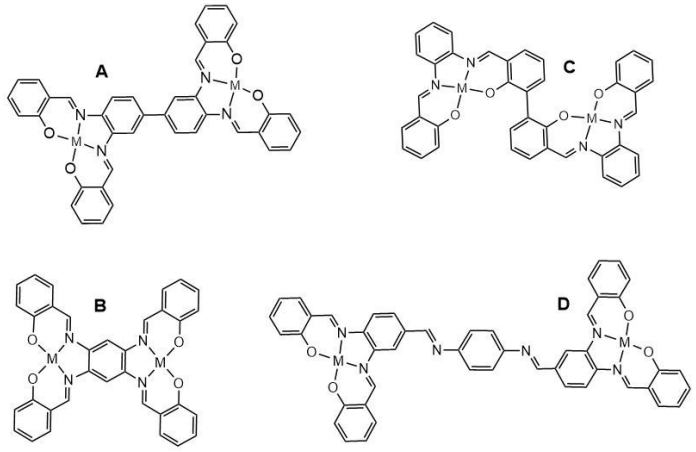

Figure 3.8. Types of "bis-salophen" ligands.

actinide complexes. Considerable efforts were also made to coordinate both U(VI) and Th(IV) within a discrete complex, as there are only four structurally characterized complexes which contain both atoms, and only one of these is a discrete complex rather than a MOF, network, or ion pair, but these efforts have so far not yielded such a species. To date, a dinuclear uranyl complex of “bis-naphthylsalophen” has been isolated, as has a trinuclear thorium helicate of “bis-diethylaminosalophen”, which is the first complex of its kind.

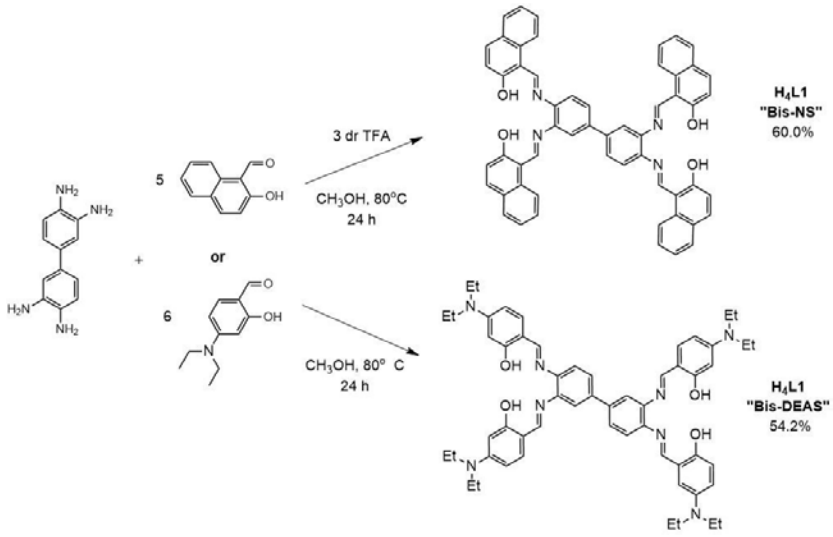

Scheme 3.4. Synthesis of bis-salophen ligands **H₄L1** and **H₄L2**

The ligand **H₄L1**, “bis-naphthylsalophen”, was synthesized through the acid-catalyzed condensation of excess 2-hydroxynapthhaldehyde with 3,3’-diaminobenzidine and is isolated as a bright orange-red solid. The poor solubility of the ligand unfortunately prevented quality NMR spectra from being obtained, and though this compound has been reported before, the reliability of this report and the compound identity is questionable, as the elemental analysis data presented does not reflect the calculated elemental composition of this species. We have yet to characterize **H₄L1** by elemental analysis. Through extensive screening of reaction conditions, and qualitative analysis of solid-state FT-IR spectra as well as mass spectrometry, the synthesis was optimized for

the formation of the tetraamine product, rather than formation of diimine or triamine species. For **H_4L1**, identity has so far been established through the absence of free amine (NH_2) stretching in the 3500-3200 cm^{-1} region, HRMS (ESI+) where the primary peak is found at *m/z* [M+H]+ 831.2968, as well as through crystallographic characterization of its uranyl complex.

The reaction of **H_4L1** with two equivalents of uranyl acetate in methanol resulted in formation of the dinuclear uranyl complex, **$(UO_2)_2$L1** (**Figure 3.9**). The connectivity of this species was confirmed through single-crystal X-ray diffraction, but unfortunately a high-quality structural solution could not be obtained due to near-instantaneous desolvation of the crystals. The presence

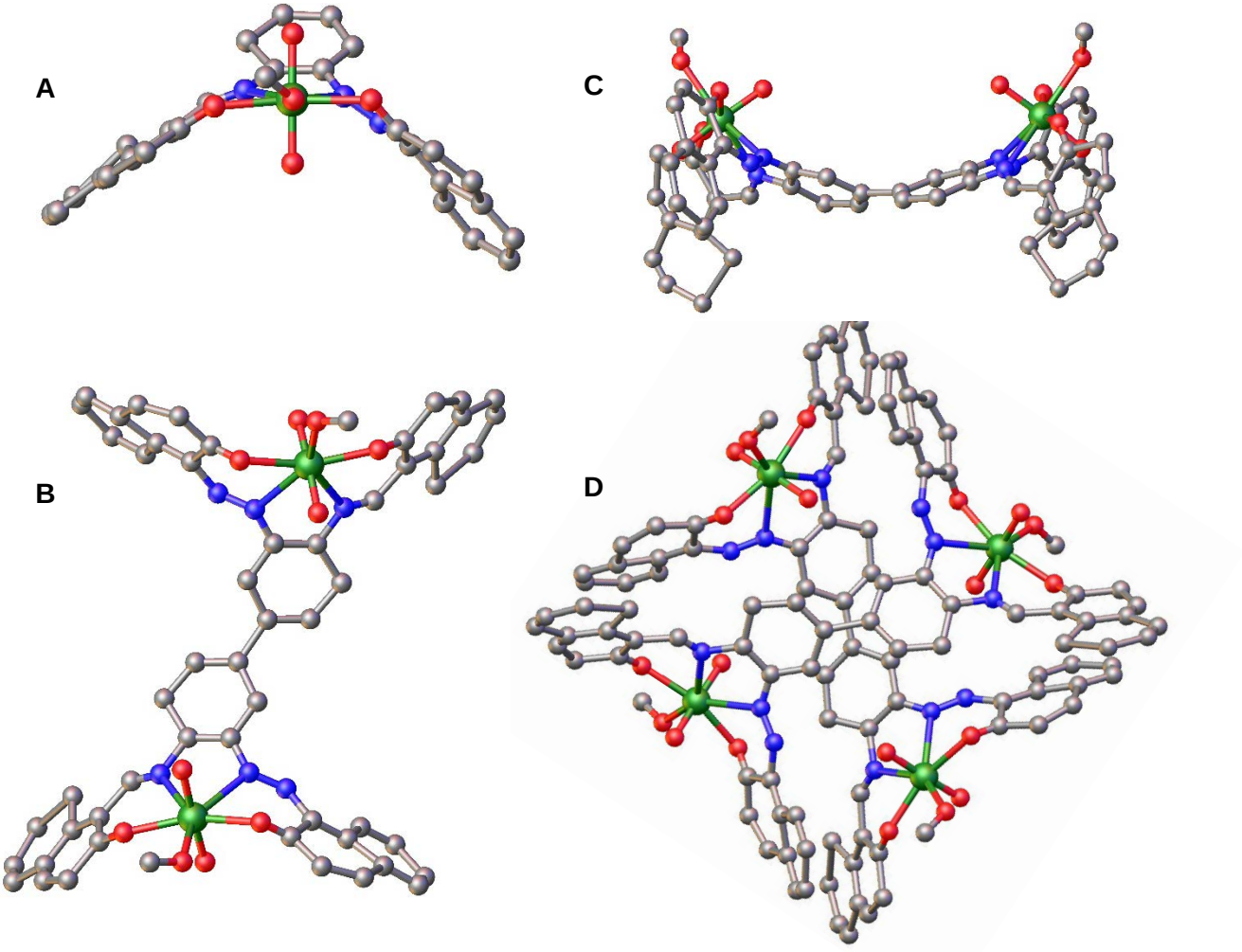

Figure 3.9. Ball-and-stick projection of the dinuclear uranyl complex **$(UO_2)_2$L1**. (A) Asymmetric unit. (B) Full molecular structure. (C) Side-on view of complex. (D) Packing arrangement.

of multiple twin domains requires additional efforts in the refinement process as well. The unit cell is tetragonal, and the solution which is pictured is in the space group $I4_1/a$, where the asymmetric unit is one-half of the complex. The fifth equatorial site of each uranyl center is observed is occupied by methanol in the solid-state; however, in solution, ^{1}H NMR in DMSO indicates the presence of only one THF molecule. The asymmetric unit of this species contains two molecular units which bend around one another via distortion of the biphenyl linker (**Figure 3.9**). These two units pack into square-shaped assemblies which feature a total of four uranyl centers. This bears some similarities to the behavior exhibited in the solid-state by uranyl naphthylsalophen **(UO_2L),** namely the formation of hydrogen-bonded pseudo-tetramers; however, the dinuclear complex **$(UO_2)_2$L1** does not feature any hydrogen bonding, and the units are held together exclusively by electrostatic interactions.

To further compare the behavior of uranyl naphthylsalophen and the di-uranyl bis-naphthylsalophen complex, preliminary electrochemical studies were conducted for **$(UO_2)_2$L1** (**Figure 3.10**). Due to the poor solubility of the complex in acetonitrile, the experiments were performed in anhydrous THF using a non-aqueous reference electrode, so the results are not directly comparable to those of uranyl naphthylsalophen. Differential pulse voltammetry was employed to better resolve the reductive features of this complex. Two features are observed in the CV, both of which are better resolved by the DPV experiment. The first is quasireversible with an $E_{1/2}$ of -1.49 V vs. $Fc^{+/0}$ (E_{pc} = -1.55 V, E_{pa} = -1.43 V; ΔE = 0.120 V), and can be assigned to the U(VI)/U(V) (UO_2^{2+}/UO2$^+$) couple, which often occurs near -1.65 V vs. $Fc^{+/0}$ in uranyl-salophen systems. The corresponding features in the DPVs occur at -1.49 V (E_{pc}) and -1.50 V (E_{pa}). These values are somewhat more positive than those of typical uranyl-salophen complexes, and significantly more positive than the redox couple of uranyl naphthylsalophen (-1.89 V). While

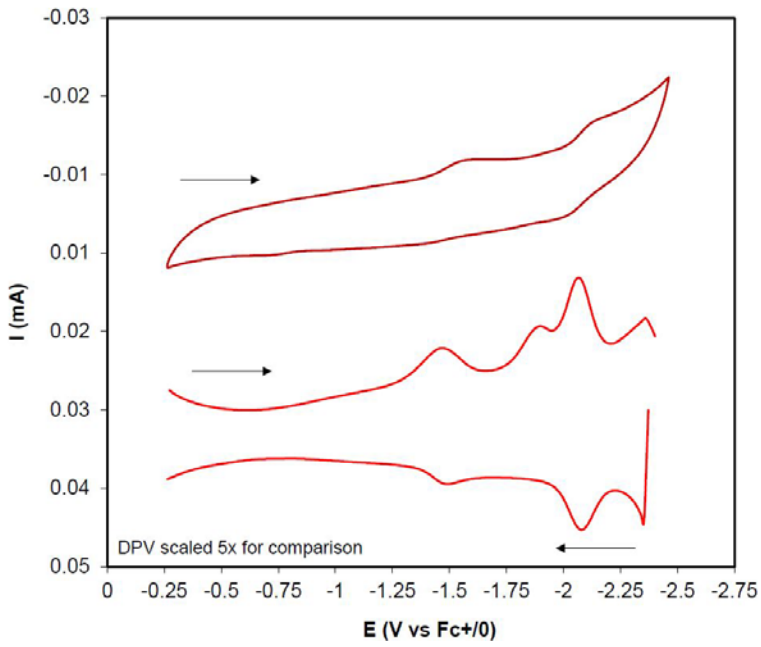

Figure 3.10. CV (dark red) and DPVs (red) of **$(UO_2)_2$L1**; 0.15 mM in THF; 0.1 M $TBAClO_4$, ν 0.1 V/s; RE: Ag/Ag^+ wire in CH_3CN, 0.1 M $AgNO_3$; WE: glassy carbon; CE: Pt wire.

it is reasonable that the larger conjugated ligand framework should shift reduction potentials to more positive values, and this is likely much of the reason for this difference, the change of both solvent and reference electrode cannot be ruled out as a contributing factor without repeating the experiments for uranyl naphthylsalophen under non-aqueous conditions. The second feature seen in the CV of **$(UO_2)_2$L1** is a quasireversible couple with $E_{1/2}$ = -2.10 V (E_{pc} = -2.13 V, E_{pa} = -2.06 V; ΔE = 0.070 V). In the DPV scan, this resolves as two reductive peaks (E_{pc} = -1.87 V, -2.06 V), the latter of which is associated with the return oxidation at -2.08 V. As the ligand reduction at -2.53 V for **UO_2L** (uranyl naphthylsalophen) is irreversible, this suggests the irreversible feature at -1.87 V for **$(UO_2)_2$L1** is associated with ligand reduction; however, the presence of a second uranyl moiety precludes clear assignment without further studies, as this is still within range for the U(VI)/U(V) couple.

Infrared spectroscopy was conducted for **$(UO_2)_2$L1** to further probe the impacts of the

extended bis-naphthylsalophen framework on the uranyl coordination sphere. As has been previously discussed, the frequency of $O=U=O^{2+}$ stretching is a reliable indicator of equatorial covalency, and we have found lower uranyl ν3 stretching frequencies associated with complexes bearing more highly conjugated ligands, indicating greater equatorial covalency. For **$(UO_2)_2$L1** the asymmetric uranyl stretch is observed as a strong band at 885 cm^{-1} with a shoulder at 897 cm^{-1}, whereas that of the mononuclear complex **UO_2L** is observed exclusively at 898 cm^{-1}. This indicates greater covalent contributions in the equatorial plane of at least one uranyl center for **$(UO_2)_2$L1**, supporting the use of highly-conjugated ligands as suitable tools for not only studying covalent bonding interactions of actinides, but also in providing favorable environments for supporting axial actinyl chemistry such as oxo reduction, activation, and/or functionalization.

In addition to studies of the bis-naphthylsalophen ligand and its uranyl complex, another bis-salophen derivative and its thorium complex were investigated. **H_4L2,** "bis-diethylaminosalophen", was synthesized by condensation of 3,3'-diaminobenzidine with 4-diethylaminosalicylaldehyde. The ligand is isolated as an orange-yellow solid with yellow fluorescence under UV light. Product identity was established by 1H NMR, FT-IR, and single-crystal X-ray diffraction. The crystal structure is of high enough quality to confirm connectivity and to analyze conformational features and long-range packing (**Figure 3.11**) but suffers from a significant amount of unresolved electron density and disorder due to twinning. Surprisingly, in the solid-state, the two binding units are positioned in a *cis* conformation about the biphenyl linker rather than a *trans* conformation, which should be sterically favored. The asymmetric unit contains two ligand molecules which are interlocked through alignment of the diethylaminosalicylidene arms, which have an average centroid-centroid distance of 5.09 Å (**Figure 3.11**).

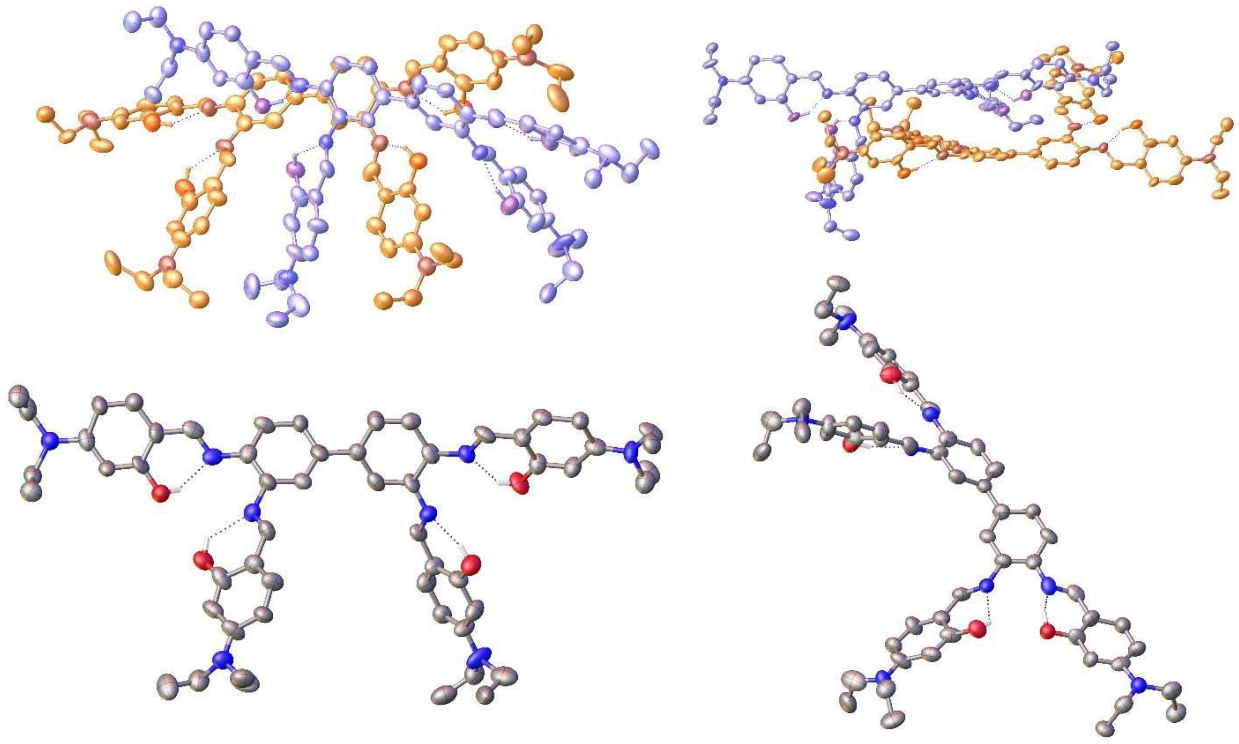

Figure 3.11. Crystal structure of **H_4L2.** Top: Asymmetric unit containing two ligand molecules. Bottom: Single molecule of **H_2L4**. Hydrogen atoms not involved in hydrogen-bonding removed for clarity. Thermal ellipsoids at 30% probability.

Reaction of **H_4L2** with thorium nitrate in a THF/CH_3OH mixture and subsequent crystallization of the product from CH_3CN/CH_3OH yielded the trimeric complex **[ThL2]$_3$** which crystallizes in the hexagonal space group $P\bar{3}c1$. This species is a discrete supramolecular thorium helicate in which the asymmetric unit consists of one thorium atom and one half of a ligand (**Figure 3.12)**. Very few supramolecular actinide complexes have been characterized, and many of these are macrocyclic species or extended networks. A small number of actinide helicates have been reported, but these complexes are either triple- or quadruple-stranded helicates—this thorium complex is to our knowledge the first circular actinide helicate of any nuclearity. **[ThL2]$_3$** contains three Th(IV) centers with Th—Th distances of 11.868 Å, and average Th—N and Th— O bond lengths of 2.637(4) Å and 2.294(3) Å, respectively, which are distances typical of similar thorium

sandwich complexes. The ligand biphenyl linker unit twists to accommodate the left- handed helical structure (**Figure 3.12-13**). The interior pocket contains one disordered water molecule which was masked from the structure solution—this suggests the pocket size is appropriate for small neutral molecules or ions such as NO_3^-, and this species may be worth investigating as a colorimetric or fluorometric sensor.

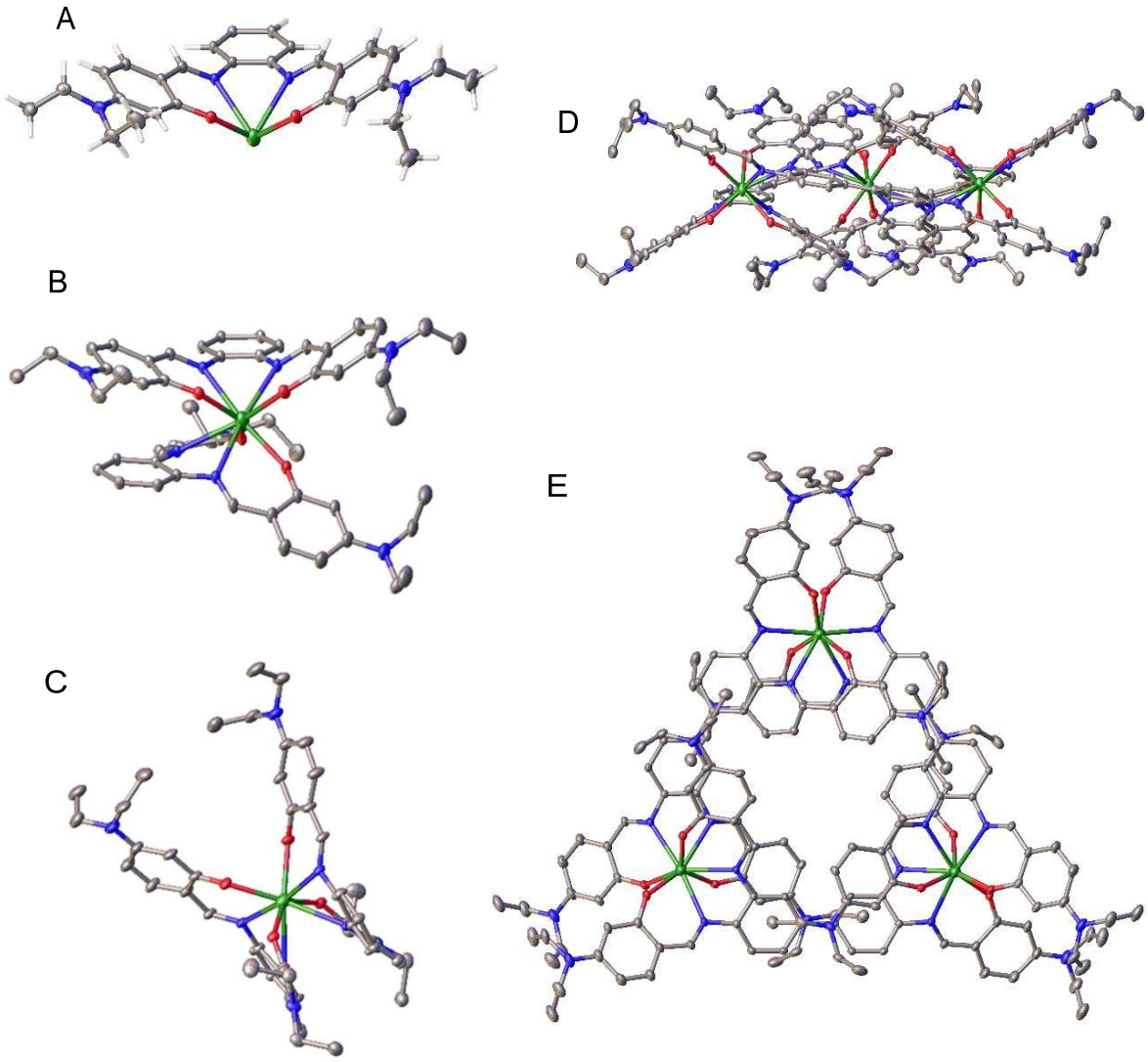

Figure 3.12. Crystal structure of **[ThL2]$_3$.** (A) Asymmetric unit of complex. (B/C) Coordination sphere of each Th center. (D) Side-on view of complex. € Top-down view of complex. Hydrogen atoms removed for clarity. Thermal ellipsoids at 50% probability.

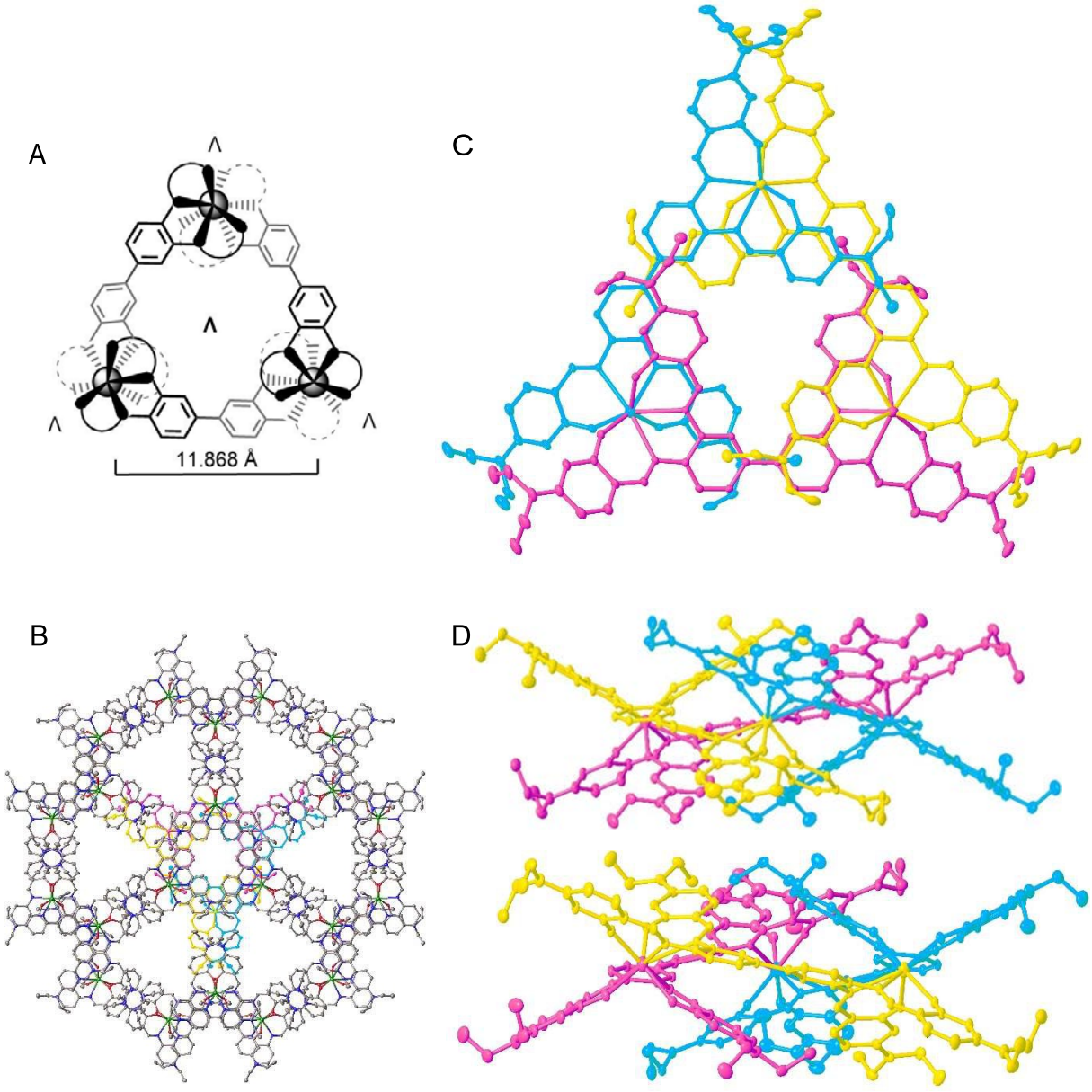

Figure 3.13. Structure of **[ThL2]**$_3$. (A) Abridged representation of complex. (B) Long-range order of complex viewed down the *c*-axis highlighting the hexagonal lattice. One color-coded molecule shown in center. (C) View down the *c*-axis of complex with color-coded strands to emphasize circular helical structure. (D) Side-on views of complex down *a* and *b* axes (120° rotation about *c*-axis). Hydrogen atoms removed for clarity. Thermal ellipsoids at 50% probability.

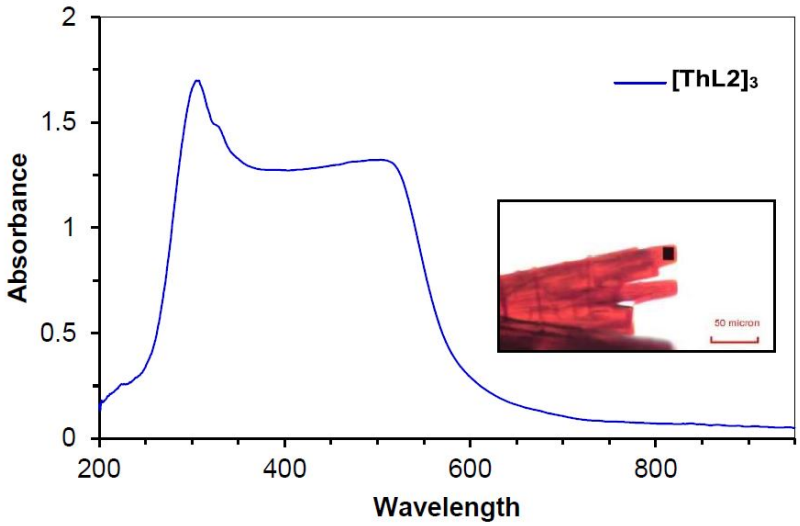

Figure 3.14. Solid-state absorbance spectra of a single crystal of **[ThL2]$_3$** and photo of crystalline sample.

The solid-state absorbance of single crystals of **[ThL2]$_3$** was also examined. A broad, precipitous absorbance from ~300 nm to ~550 nm is observed, with a sharp λ_{max} at 307 nm which is likely attributed to $\pi \rightarrow \pi^*$ transitions along one axis of **L2**. The broad, slightly less intense band from approximately 375-550 nm can be assigned to LMCT processes. The previously-characterized thorium naphthylsalophen sandwich complex also features a broad, but significantly more gaussian-shaped absorption from 475-575 nm. Current efforts are being made towards producing similar thorium helicates of other bis-salophen ligand derivatives, as well as the analogous U(IV) complexes, as this would provide a useful comparison of some of the properties of tetravalent actinides, and allows for the unique opportunity to study complexes containing multiple actinide centers.

3.3 | Synthesis of Compounds and Methods

General Considerations

Caution! The uranium metal salt – $UO_2(OAc)_2 \cdot 2H_2O$ – used in this study contained depleted uranium. Standard precautions for handling radioactive materials or heavy metals such as uranyl nitrate and lead sulfate were followed. Any solvents not specifically identified were ACS grade, purchased from EMD, and used as received without further purification. The reagents acetonitrile (99.9%, HPLC grade, BDH), 1,2-diaminobenzene (99.5%, Aldrich), 2-hydroxynaphthaldehyde (98%, Alfa Aesar), 4-diethylaminosalicylaldehyde (99%, Alfa Aesar), 3,3'-diaminobenzidine (98%, Aldrich), and Th(NO3)4•5H5O (99%, Fluka) were used as received without further purification. UO2(NO3)2•6H2O (98%, J. T. Baker) was recrystallized from a 50% nitric acid solution and stored under hexanes until use. UO2(OAc)2•2H2O was (Fischer) was recrystallized from methanol before use. Anhydrous dichloromethane (BDH) was purchased, stored under argon, and dispensed from a solvent purification system. Triethylamine (99%, Alfa Aesar) was distilled and stored under argon until use. (CD3)2SO and CDCl3 were purchased from Cambridge Isotope Laboratories and stored in a desiccator.

1H NMR spectra were recorded with a Bruker spectrometer at 600 MHz. 13C NMR spectra were recorded with a Bruker spectrometer at 151 MHz. NMR spectroscopic data were collected using deuterated chloroform (CDCl3) or deuterated DMSO (D6-DMSO). Chemical shifts are reported in parts per million (δ) and are referenced against TMS or residual internal solvent signals Infrared spectra were obtained in the solid state using an attenuated total reflectance (ATR) method on a Thermo Scientific Nicolet iS50 FT-IR. Solid-state UV-Vis spectra were recorded on a CRAIC microspectrophotometer using a quartz slide with the crystal suspended in Paratone-n oil.

X-ray Crystallography

H_2L and UO_2L:

Crystals suitable for single crystal X-ray diffraction were selected and mounted on a glass fiber using Paratone-N oil and data set collection was completed on a 'Bruker APEX CCD' diffractometer using Mo Kα radiation. The crystal was kept at 180 K during unit cell and data collection. SMART (v. 5.624) was used for preliminary determination of cell constants and data collection control. Determination of integrated intensities and global cell refinement were performed with the Bruker SAINT software package, and empirical absorption correction (SADABS) was applied. The structures were solved with the ShelXS structure solution program using Direct Methods and refined with the olex2.refine refinement package using Gauss-Newton minimization. Projections were created on Olex2.1.

$(UO_2)_2L1$, H_4L_2, and $[ThL2]_3$:

Crystals suitable for single crystal X-ray diffraction were selected and mounted on a 50-micron MiTeGen loop using Paratone-N oil and data set collection was completed on a Bruker D8 VENTURE κ-geometry diffractometer using Cu Kα radiation (Incoatec IμS DIAMOND microfocus sealed tube (λ = 1.54178 Å). Crystals were kept at 100 K during unit cell and data collection. Determination of the unit cell and collection of data were performed using the APEX III software, and determination of integrated intensities and global cell refinement were performed with the Bruker SAINT software package. An absorption correction (SADABS) was applied. Structures were solved using Intrinsic Phasing/Direct Methods (ShelXT) and least-squares refinement was performed using ShelXL in APEX III. Olex2.1 was used to mask solvent molecules [ThL2]3. Restraints and constraints such as FLAT, SIMU, ISOR, and EADP were

employed for atoms that would otherwise be split and could not be modeled over two positions due to unresolved twinning, or for atoms that could not be refined anisotropcially without resulting in non-positive definites. Projections were created on Olex2.1.

Electrochemical Measurements

Electrochemical measurements were carried out using a CH Instruments 660 E potentiostat in HPLC-grade CH_2Cl_2, CH_3CN (BDH Chemicals), or anhydrous THF (DriSolv, EMD Millipore) with tetrabutylammonium hexafluorophosphate ($TBAPF_6$) supporting electrolyte (0.1 M). $TBAPF_6$ was recrystallized from EtOH and dried overnight in vacuo at 60 °C immediately before use. Solutions were purged for 30 minutes with N_2 using a pre-purge solution. Potentials were scanned using a three-electrode cell consisting of a glassy carbon disc working electrode, Pt wire counter electrode, and Ag/AgCl/satd. KCl/H_2O reference electrode. For measurements in THF, a non-aqueous reference electrode (Ag/Ag^+ wire in ACN, 0.01 M $AgNO_3$) was used._Data was corrected to versus ferrocene based on values for $E_{1/2}(Fc^{+/0})$ collected using the same three-electrode cell before and after measurements. All data were recorded using an initial cathodic sweep and anodic return sweep. DPV conditions: Increment= 0.01 V; amplitude= 0.05 V; pulse width= 0.05 s; sample width= 0.0167 s; pulse period= 0.5 s.

Absorbance Spectroscopy

All solution phase absorbance spectra were collected on a VARIAN Cary 50 WinUV Spectrometer with a xenon lamp with absorbance spectra from 200 nm to 900 nm with a 1 cm path length quartz cuvette. Serial titrations were completed by introducing a known amount of the metal salt (uranyl nitrate in H_2O) to a solution of the free base ligand H_2L in MeOH. A solution of uranyl

nitrate hydrate was prepared by dissolving 3.0 mg of recrystallized uranyl nitrate in water, and then bringing this to volume in a 25.0 mL volumetric flask. Titrations were completed in MeOH by serial additions of 20 μL of the (0.24 mM) uranyl nitrate aqueous solution, maintaining less than 1% water in MeOH. The solutions were agitated for 5 seconds, the cuvette replaced in the spectrometer, and the absorbance spectrum collected. This procedure was repeated until a large excess of metal salt was present. A control series to observe any absorption change upon of water addition was also conducted, and no significant change was observed. The absorbance was adjusted for concentration by this serial dilution method by the reporting the data as extinction coefficient.

Synthesis of Compounds

Synthesis of H_2L: 1,2-diaminobenzene (0.433 g, 7.23 mmol) and 2-hydroxynaphthaldehyde (1.32 g, 15.0 mmol) were added to 150 mL of MeOH, and stirred for 6 hours at reflux temperature (65 °C), during which time the color changed from yellow to dark orange and a precipitate formed. The solution was allowed to cool to room temperature, and the solid was filtered and washed with hexanes to yield a bright orange powder (2.54 g, 84%). ^{1}H NMR (600 MHz, $CDCl_3$) δ 7.18 (d, 2H, J = 9.2 Hz), 7.34 (t, 2H, J = 7.4 Hz), 7.44-7.39 (m, 4H), 7.51 (t, 2H, J = 8.2 Hz), 7.73 (d, 2H, J = 7.9 Hz), 7.82 (d, 2H, J = 9.2 Hz), 8.14 (d, 2H, J = 8.5 Hz), 9.46 (d, 2H, J = 3.6 Hz), 15.08 (s, 2OH); 13C NMR (151 MHz, $CDCl_3$) δ 109.40, 119.03, 119.15, 122.09, 123.63, 127.42, 127.51, 128.08, 129.41, 133.21, 136.67, 139.73, 156.17, 169.08; TOF MS (ESI) m/z (M+ + 1) Calcd 417.1525, Found 417.1550. CCDC: 1523762.

Synthesis of UO_2L: The naphthylsalophen ligand **H_2L** (970. mg, 2.33 mmol) and NEt_3 (1 mL)

were added to 40 mL of DCM and 20 mL of MeOH in a 100 mL round bottom flask. The mixture was stirred until all the solids were dissolved. Uranyl nitrate hexahydrate (963 mg, 2.27 mmol) was then added to the flask. The reaction was heated to 40 °C and heated with stirring for 2 hours. The solution volume was reduced by half by rotary evaporation, and subsequently put in ice for 30 minutes. A red solid precipitated and was filtered off and rinsed with hexanes (132 mg, 83%). Crystals suitable for x-ray diffraction were grown in 3 days from layering a saturated DCM solution of UO2[L] with hexanes. The ^{1}H NMR (600 MHz, d_6-DMSO) δ 7.31 (t, 2H, J = 7.4 Hz), 7.38 (d, 2H, J = 9.1 Hz), 7.53-7.55 (m, 4H), 7.85-7.88 (m, 4H), 8.20 (d, 2H, J = 8.1 Hz), 8.36 (d, 2H, J = 8.5 Hz), 10.20 (s, 2H) ppm; ^{13}C NMR (151 MHz, d_6-DMSO) δ 114.72, 120.33, 121.36, 122.92, 124.20, 127.03, 127.91, 128.49, 128.75, 134.49, 137.12, 147.38, 160.09, 171.33 ppm; TOF MS (ESI+) m/z $[M + H]^+$ Calcd 685.1774, Found 685.1777, $[M(H2O) + H]^+$ Calcd 703.1880, Found 703.1902. FT-IR (ATR): 897.6 cm^{-1} (ν3, O=U=O). CCDC: 1827293.

Synthesis of H_4L1 (Bis-NS). Method 1: To a 50-mL round-bottom flask containing a stir bar, 3,3’-diaminobenzidine (0.050 g, 0.233 mmol) and 2-hydroxynaphthaldehyde (0.200 g, 1.668 mmol) were added. 15 mL of methanol was added, and the mixture was stirred and heated to 80 °C. Two drops of trifluoroacetic acid were added, resulting in immediate formation of a deep red precipitate, and the reaction was stirred and heated for 24 h. The precipitate was collected by vacuum filtration, rinsed with methanol and hexanes, and dried as a bright red-orange solid. Yield: 60.0%. Method 2: To a 50-mL round bottom flask containing a stir bar, 3,3’-diaminobenzidine tetrahydrochloride (0.050 g, 0.233 138 mmol) and 10 mL methanol were added, and the solution was heated to 60 °C with stirring until the solid was completely dissolved. 2-Hydroxynaphthaldehye (0.120 g, 0.694 mmol) was dissolved completely in 10 mL hot methanol

then added to the flask containing the diaminobenzidine solution, at which point the mixture became dark and a precipitate began to form. The reaction was heated to 75 °C and stirred for 18 h, then triethylamine (77 μL, 0.554 mmol) was added using a micropipette, causing the solution and precipitate in the flask to immediately turn bright red. The product was collected by vacuum filtration, rinsed with methanol and hexanes, and dried as a bright red-orange solid. Yield: 56.1%. HRMS (ESI+) *m/z* [M+H]+ Calcd 831.2971, Found 831.2968. FT-IR (ATR): 1620-1540 cm-1 (νC=N).

Synthesis of H_4L2 (Bis-DEAS). To a 50-mL round-bottom flask containing a stir bar, 3,3'-diaminobenzidine (0.050 g, 0.233 mmol) and 10 mL methanol were added, and the mixture was warmed to 60 °C with stirring. 4-Diethylaminosalicylaldehyde (0.271 g, 1.400 mmol) was dissolved completely in 10 mL hot methanol and then added to the flask containing the diaminobenzidine suspension. The resulting brown solution was heated to 80 °C and stirred for 24 h, during which time an orange precipitate formed. The solid was collected by vacuum filtration, rinsed with methanol and hexanes, and dried as a bright orange-yellow precipitate with yellow fluorescence. Yield: 54.3%. ^{1}H NMR (600 MHz, DMSO-d_6) δ 13.59 (brs, 4H), 8.78 (s, 2H), 8.69 (s, 2H), 7.73 (s, 2H), 7.66 (d, 2H, J = 7.43 Hz), 7.44 (d, 2H, J = 7.90 Hz), 7.34 (d, 4H, J = 9.28 Hz), 6.31 (d, 4H, J = 7.79 Hz), 6.06 (s, 4H), 3.40 (d, 12H, J = 6.14 Hz), 1.12 (t, 24H, J = 6.24 Hz). FT-IR (ATR) 2950 cm^{-1} (νCH, Et), 1620-1540 cm^{-1} (νC=N).

Synthesis of $(UO_2)_2$L1. To a 50-mL round bottom flask containing a stir bar, H_4L1 (0.050 g, 0.060 mmol) and 10 mL THF were added, and the mixture was heated to 60 °C with stirring. Triethylamine (32.4 μL, 0.246 mmol) was added to the mixture. $UO_2(OAc)_2$•$2H_2O$ (0.025 g, 0.246 mmol) was dissolved in 10 mL hot methanol, then added to the ligand solution. The reaction was

heated to 75 °C, then stirred for 18 h, during which time it slowly turned dark orange-red and produced a red precipitate. The solution concentrated using a rotary evaporator then placed in the freezer overnight. A dark red solid was collected by filtration and rinsed with cold methanol and hexanes. Yield: ~30%. ^{1}H NMR (600 MHz, DMSO-d_6) δ 10.40 (s, 2H), 10.27 (s, 2H), 8.46 (s, 2H), 3.38 (t, 4H, J = 8.03 Hz), 8.21-8.14 (m, 6H), 8.02 (d, 2H, J = 8.29 Hz), 7.85 (dd, 4H, J = 23.4 Hz, 7.83 Hz), 7.56 (t, 2H, J = 7.56 Hz), 7.44 (t, 2H, J = 7.54 Hz), 7.38 (d, 2H, J = 9.41 Hz), 7.36 (d, 2H, J = 9.07 Hz), 7.32 (t, 2H, 7.34 Hz), 7.26 (t, 2H, J = 7.32 Hz), 3.59 (THF) (t, 4H, J = 6.24 Hz), 1.76 (THF) (q,5, 4H, J = 3.16). FT-IR (ATR): 896.7, 884.9 cm^{-1} (ν3, O=U=O).

Synthesis of [ThL2]$_3$. In a 50-mL round-bottom flask containing a stir bar, H_4L2 (0.050 g, 0.0546 mmol) and 10 mL THF were added, and heated to 60 °C with stirring until dissolved, and triethylamine (31.1 μL, 0.225 mmol) was added using a micropipette. Th(NO3)4•5H2O (0.032 g, 0.0546 mmol) was dissolved in 10 mL hot methanol, then added to the ligand solution, causing a color change from orange-yellow to dark orange-red. The mixture was heated and stirred at 75 °C for 24 h. After cooling to room temperature, a small amount of dark precipitate was filtered off, and the filtrate was dried using a rotary evaporator, then redissolved in a minimum amount of acetonitrile (3-5 mL). To this concentrated solution, 10-15 mL of methanol were added, and the flask was sealed and stored in the freezer for one week, during which time needle-like orange-red crystals formed. Several crystals suitable for single crystal X-ray diffraction were isolated from the solution, and the rest were collected by vacuum filtration and rinsed with methanol and hexanes. Yield: 24.2%. HRMS (ESI+) m/z (z=2) [M+2H]2+ 1715.4966. CCDC 1964435.

References

1. Leoni, L.; Dalla Cort, A., The Supramolecular Attitude of Metal–Salophen and Metal–Salen Complexes. *Inorganics* **2018,** *6* (2), 42.

2. Dalla Cort, A.; De Bernardin, P.; Forte, G.; Yafteh Mihan, F., Metal–salophen-based receptors for anions. *Chem. Soc. Rev.* **2010,** *39* (10), 3863.

3. Ebrahimipour, S. Y.; Mohamadi, M.; Torkzadeh Mahani, M.; Simpson, J.; Mague, J. T.; Sheikhshoaei, I., Synthesis and structure elucidation of novel salophen-based dioxo-uranium(VI) complexes: In-vitro and in-silico studies of their DNA/BSA-binding properties and anticancer activity. *Eur. J. Med. Chem.* **2017,** *140*, 172-186.

4. Hardy, E. E.; Wyss, K. M.; Keller, R. J.; Gorden, J. D.; Gorden, A. E. V., Tunable ligand emission of napthylsalophen triple-decker dinuclear lanthanide(III) sandwich complexes. *Dalton Trans.* **2018,** *47* (4), 1337-1346.

5. Klamm, B. E.; Windorff, C. J.; Celis-Barros, C.; Marsh, M. L.; Meeker, D. S.; Albrecht-Schmitt, T. E., Experimental and Theoretical Comparison of Transition-Metal and Actinide Tetravalent Schiff Base Coordination Complexes. *Inorg. Chem.* **2018,** *57* (24), 15389-15398.

6. DeVore II, M. A.; Kerns, S. A.; Gorden, A. E. V., Characterization of Quinoxolinol Salen Ligands as Selective Ligands for Chemosensors for Uranium. *Eur. J. Inorg. Chem.* **2015,** *2015* (34), 5708-5714.

7. Hardy, E. E.; Eddy, M. A.; Maynard, B. A.; Gorden, A. E. V., Solid state π-π stacking and higher order dimensional crystal packing, reactivity, and electrochemical behaviour of salphenazine actinide and transition metal complexes. *Dalton Trans.* **2016,** *45* (36), 14243-51.

8. Hardy, E. E.; Wyss, K. M.; Gorden, J. D.; Ariyarathna, I. R.; Miliordos, E.; Gorden, A. E.

V., Th(IV) and Ce(IV) napthylsalophen sandwich complexes: characterization of unusual thorium fluorescence in solution and solid-state. *Chem. Comm.* **2017,** *53* (88), 11984-11987.

9. Niklas, J. E.; Hardy, E. E.; Gorden, A. E. V., Solid-state structural elucidation and electrochemical analysis of uranyl naphthylsalophen. *Chem. Comm.* **2018,** *54* (83), 11693-11696.

10. Camp, C.; Toniolo, D.; Andrez, J.; Pecaut, J.; Mazzanti, M., A versatile route to homo- and hetero-bimetallic 5f-5f and 3d-5f complexes supported by a redox active ligand framework. *Dalton Trans.* **2017,** *46* (34), 11145-11148.

11. Isse, A. A.; Gennaro, A.; Vianello, E., Electrochemical reduction of Schiff base ligands H_2salen and H_2salophen. *Electrochimica Acta* **1997,** *42* (13), 2065-2071.

12. Viganò, M.; Ferretti, F.; Caselli, A.; Ragaini, F.; Rossi, M.; Mussini, P.; Macchi, P., Easy Entry into Reduced Ar-BIANH_2 Compounds: A New Class of Quinone/Hydroquinone-Type Redox-Active Couples with an Easily Tunable Potential. *Chem. Eur. J.* **2014,** *20* (44), 14451-14464.

13. McKinven, J.; Nichol, G. S.; Arnold, P. L., Arene-ligated heteroleptic terphenolate complexes of thorium. *Dalton Trans.* **2014,** *43* (46), 17416-17421.

14. Carter, K. P.; Surbella III, R. G.; Kalaj, M.; Cahill, C. L., Restricted Speciation and Supramolecular Assembly in the 5f Block. *Chem. Eur. J.* **2018,** *24* (49), 12747-12756.

15. Mei, L.; Wang, L.; Liu, C.-m.; Zhao, Y.-l.; Chai , Z.-f.; Shi, W.-q., Tetranuclear Uranyl Polyrotaxanes: Preferred Selectivity toward Uranyl Tetramer for Stabilizing a Flexible Polyrotaxane Chain Exhibiting Weakened Supramolecular Inclusion. *Chem. Eur. J.* **2015,** *21* (28), 10226-10235.

16. Frisch, M.; Cahill, C. L., Thorium(IV) Coordination Polymers in the Pyridine and Pyrazinedicarboxylic Acid Systems. *Cryst. Growth Des.* **2008,** *8* (8), 2921-2928.

17. Baker, R. J., New Reactivity of the Uranyl(VI) Ion. *Chem. Eur. J.* **2012,** *18* (51), 16258-16271.

18. Andrews, M. B.; Cahill, C. L., Uranyl Bearing Hybrid Materials: Synthesis, Speciation, and Solid-State Structures. *Chem. Rev.* **2013,** *113* (2), 1121-1136.

19. Alexander, V., Design and Synthesis of Macrocyclic Ligands and Their Complexes of Lanthanides and Actinides. *Chem. Rev.* **1995,** *95* (2), 273-342.

20. Ward, A. L.; Buckley, H. L.; Lukens, W. W.; Arnold, J., Synthesis and Characterization of Thorium(IV) and Uranium(IV) Corrole Complexes. *J. Am. Chem. Soc.* **2013,** *135* (37), 13965-13971.

21. Arnold, P. L.; Potter, N. A.; Carmichael, C. D.; Slawin, A. M. Z.; Roussel, P.; Love, J. B., Constructing cerium supramolecular wheels and encapsulating uranium with a Schiff-base calixpyrrole ligand. *Chem. Comm.* **2010,** *46* (11), 1833-1835.

22. Rounaghi, G. H.; Nazari, E.; Ghaemi, A.; Mohajeri, M., Complexing ability of a macrocyclic ligand, dibenzo-24-crown-8, with UO_2^{2+} in some binary mixed non-aqueous solvents. *J. Coord. Chem.* **2010,** *63* (13), 2349-2359.

23. Brewster, J. T., 2nd; Mangel, D. N.; Gaunt, A. J.; Saunders, D. P.; Zafar, H.; Lynch, V. M.; Boreen, M. A.; Garner, M. E.; Goodwin, C. A. P.; Settineri, N. S.; Arnold, J.; Sessler, J. L., In-Plane Thorium(IV), Uranium(IV), and Neptunium(IV) Expanded Porphyrin Complexes. *J Am Chem Soc* **2019,** *141* (44), 17867-17874.

24. Brewster, J. T.; Zafar, H.; Root, H. D.; Thiabaud, G. D.; Sessler, J. L., Porphyrinoid f-Element Complexes. *Inorg. Chem.* **2020,** *59* (1), 32-47.

25. Shen, X.; Liao, L.; Chen, L.; He, Y.; Xu, C.; Xiao, X.; Lin, Y.; Nie, C., Spectroscopic study on the reactions of bis-salophen with uranyl and then with fructose 1,6-bisphosphate and the

analytical application. *Spectrochim. Acta, Part A* **2014,** *123*, 110-116.

26. Thuéry, P.; Villiers, C.; Jaud, J.; Ephritikhine, M.; Masci, B., Uranyl-Based Metallamacrocycles: Tri- and Tetranuclear Complexes with (2R,3R,4S,5S)-Tetrahydrofurantetracarboxylic Acid. *J. Am. Chem. Soc.* **2004,** *126* (22), 6838-6839.

27. Arnold, P. L., Uranyl steps in the ring. *Nat. Chem.* **2012,** *4* (12), 967-969.

28. Bénaud, O.; Berthet, J.-C.; Thuéry, P.; Ephritikhine, M., The Bis Metallacyclic Anion $[U(N\{SiMe_3\}_2)(CH_2SiMe_2N\{SiMe_3\})_2]^-$. *Inorg. Chem.* **2010,** *49* (17), 8117-8130.

29. Salmon, L.; Thuéry, P.; Ephritikhine, M., Synthesis and crystal structure of uranium(IV) complexes with compartmental Schiff bases: from mononuclear species to tri- and tetranuclear clusters. *Dalton Trans.* **2004,** (10), 1635-1643.

30. Kadish, K. M.; Liu, Y. H.; Anderson, J. E.; Charpin, P.; Chevrier, G.; Lance, M.; Nierlich, M.; Vigner, D.; Dormond, A.; et al., First example of a trimeric metalloporphyrin. Synthesis, electrochemical, and spectroelectrochemical studies of [(P)Th(OH)2]3 where P is the dianion of octaethyl- or tetraphenylporphyrin. Crystal structure of a dihydrated trinuclear complex of dihydroxy(5,10,15,20-tetraphenylporphinato)thorium(IV) heptane solvate. *J. Am. Chem. Soc.* **1988,** *110* (19), 6455-6462.

31. Bjorklund, J. L.; Pyrch, M. M.; Basile, M. C.; Mason, S. E.; Forbes, T. Z., Actinyl-cation interactions: experimental and theoretical assessment of $[Np(VI)O_2Cl_4]_2^-$ and $[U(VI)O_2Cl_4]_2^-$ systems. *Dalton Trans.* **2019,** *48* (24), 8861-8871.

32. Nazarenko, O. M.; Rusanova, J. A.; Krautscheid, H.; Domasevitch, K. V., catena-Poly[thorium(IV)-tetrakis(μ2-3-carboxyadamantane-1-carboxylato)]: a quadruple helical strand driven by a synergy of coordination and hydrogen bonding. *Acta Crystallogr., Sect. C* **2010,** *66* (10), m276-m279.

33. Xu, J.; Raymond, K. N., Structurally Characterized Quadruple-Stranded Bisbidentate Helicates. *Angew. Chem. Int. Ed.* **2006,** *45* (39), 6480-6485.

34. An, S.-w.; Mei, L.; Wang, C.-z.; Xia, C.-q.; Chai, Z.-f.; Shi, W.-q., The first case of actinide triple helices: pH-dependent structural evolution and kinetically-controlled transformation of two supramolecular conformational isomers. *Chem. Comm.* **2015,** *51* (43), 8978-8981.

35. Fox, A. R.; Bart, S. C.; Meyer, K.; Cummins, C. C., Towards uranium catalysts. *Nature* **2008,** *455*, 341.

36. Halter, D. P.; Heinemann, F. W.; Bachmann, J.; Meyer, K., Uranium-mediated electrocatalytic dihydrogen production from water. *Nature* **2016,** *530*, 317.

37. Renshaw, J. C.; Butchins, L. J. C.; Livens, F. R.; May, I.; Charnock, J. M.; Lloyd, J. R., Bioreduction of Uranium: Environmental Implications of a Pentavalent Intermediate. *Environ. Sci. Technol.* **2005,** *39* (15), 5657-5660.

38. Seaman, L. A.; Pedrick, E. A.; Wu, G.; Hayton, T. W., Promoting oxo functionalization in the uranyl ion by ligation to ketimides. *Journal of Organometallic Chemistry* **2018,** *857*, 34-37.

39. Cowie, B. E.; Nichol, G. S.; Love, J. B.; Arnold, P. L., Double uranium oxo cations derived from uranyl by borane or silane reduction. *Chem. Comm.* **2018,** *54* (31), 3839-3842.

40. Hayton, T. W.; Wu, G., Exploring the Effects of Reduction or Lewis Acid Coordination on the U═O Bond of the Uranyl Moiety. *Inorg. Chem.* **2009,** *48* (7), 3065-3072.

41. Arnold, P. L.; Hollis, E.; Nichol, G. S.; Love, J. B.; Griveau, J.-C.; Caciuffo, R.; Magnani, N.; Maron, L.; Castro, L.; Yahia, A.; Odoh, S. O.; Schreckenbach, G., Oxo-Functionalization and Reduction of the Uranyl Ion through Lanthanide-Element Bond Homolysis: Synthetic, Structural, and Bonding Analysis of a Series of Singly Reduced Uranyl–Rare Earth 5f1-4fn Complexes. *J. Am. Chem. Soc.* **2013,** *135* (10), 3841-3854.

42. Arnold, P. L.; Pécharman, A.-F.; Lord, R. M.; Jones, G. M.; Hollis, E.; Nichol, G. S.; Maron, L.; Fang, J.; Davin, T.; Love, J. B., Control of Oxo-Group Functionalization and Reduction of the Uranyl Ion. *Inorg. Chem.* **2015,** *54* (7), 3702-3710.

43. Bell, N. L.; Shaw, B.; Arnold, P. L.; Love, J. B., Uranyl to Uranium(IV) Conversion through Manipulation of Axial and Equatorial Ligands. *J. Am. Chem. Soc.* **2018,** *140* (9), 3378-3384.

44. Herasymchuk, K.; Chiang, L.; Hayes, C. E.; Brown, M. L.; Ovens, J. S.; Patrick, B. O.; Leznoff, D. B.; Storr, T., Synthesis and electronic structure determination of uranium(VI) ligand radical complexes. *Dalton Trans.* **2016,** *45* (31), 12576-12586.

45. Popović, Z.; Roje, V.; Pavlović, G.; Matković-Čalogović, D.; Giester, G., The first example of coexistence of the ketoamino–enolimino forms of diamine Schiff base naphthaldimine parts: the crystal and molecular structure of N,N′-bis(1-naphthaldimine)-o-phenylenediamine chloroform (1/1) solvate at 200 K. *J. Mol. Struct.* **2001,** *597* (1), 39-47.

46. Mota, V. Z.; de Carvalho, G. S. G.; Corbi, P. P.; Bergamini, F. R. G.; Formiga, A. L. B.; Diniz, R.; Freitas, M. C. R.; da Silva, A. D.; Cuin, A., Crystal structure and theoretical studies of the keto-enol isomerism of N,N′-bis(salicylidene)-o-phenylenediamine (salophen). *Spectrochim. Acta, Part A* **2012,** *99*, 110-115.

47. Niklas, J. E.; Farnum, B. H.; Gorden, J. D.; Gorden, A. E. V., Structural Characterization and Redox Activity of a Uranyl Dimer and Transition-Metal Complexes of a Tetradentate BIAN Ligand. *Organometallics* **2017,** *36* (23), 4626-4634.

48. Hao, Z.; Song, X.; Zhu, M.; Meng, X.; Zhao, S.; Su, S.; Yang, W.; Song, S.; Zhang, H., One-dimensional channel-structured Eu-MOF for sensing small organic molecules and Cu^{2+} ion. *J. Mat. Chem.* **2013,** *1* (36), 11043-11050.

49. Wang, Y.; Liu, Z.; Li, Y.; Bai, Z.; Liu, W.; Wang, Y.; Xu, X.; Xiao, C.; Sheng, D.; Diwu, J.; Su, J.; Chai, Z.; Albrecht-Schmitt, T. E.; Wang, S., Umbellate Distortions of the Uranyl Coordination Environment Result in a Stable and Porous Polycatenated Framework That Can Effectively Remove Cesium from Aqueous Solutions. *J. Am. Chem. Soc.* **2015,** *137* (19), 6144-6147.

50. Manolova, Y.; Kurteva, V.; Antonov, L.; Marciniak, H.; Lochbrunner, S.; Crochet, A.; Fromm, K. M.; Kamounah, F. S.; Hansen, P. E., 4-Hydroxy-1-naphthaldehydes: proton transfer or deprotonation. *Phys. Chem. Chem. Phys.* **2015,** *17* (15), 10238-10249.

51. Camp, C.; Guidal, V.; Biswas, B.; Pecaut, J.; Dubois, L.; Mazzanti, M., Multielectron redox chemistry of lanthanide Schiff-base complexes. *Chem. Sci.* **2012,** *3* (8), 2433-2448.

52. Vasilieva, N. V.; Irtegova, I. G.; Vaganova, T. A.; Shteingarts, V. D., Electrochemical, ESR and quantum chemical study of 1-substituted naphthalenes and their radical anions. *J. Phys. Org. Chem.* **2008,** *21* (1), 73-78.

53. Kim, S.-Y.; Tomiyasu, H.; Ikeda, Y., Electrochemical Studies on $[UO_2(DMF)_5](ClO_4)_2$, $UO_2(acac)_2DMF$, and UO_2(salen)DMF (DMF=N, N-dimethylformamide, acac=acetylacetonate, salen=N, N′-disalicylideneethylenediaminate) Complexes in DMF. *J. Nucl. Sci. Technol.* **2002,** *39* (2), 160-165.

54. Nocton, G.; Horeglad, P.; Vetere, V.; Pécaut, J.; Dubois, L.; Maldivi, P.; Edelstein, N. M.; Mazzanti, M., Synthesis, Structure, and Bonding of Stable Complexes of Pentavalent Uranyl. *J. Am. Chem. Soc.* **2010,** *132* (2), 495-508.

55. Arnold, P. L.; Jones, G. M.; Pan, Q.-J.; Schreckenbach, G.; Love, J. B., Co-linear, double-uranyl coordination by an expanded Schiff-base polypyrrole macrocycle. *Dalton Trans.* **2012,** *41* (22), 6595-6597.

56. Mizuoka, K.; Kim, S.-Y.; Hasegawa, M.; Hoshi, T.; Uchiyama, G.; Ikeda, Y., Electrochemical and Spectroelectrochemical Studies on UO2(saloph)L (saloph = N,N‘-Disalicylidene-o-phenylenediaminate, L = Dimethyl Sulfoxide or N,N-Dimethylformamide). *Inorg. Chem.* **2003,** *42* (4), 1031-1038.

57. Pankhurst, J. R.; Bell, N. L.; Zegke, M.; Platts, L. N.; Lamfsus, C. A.; Maron, L.; Natrajan, L. S.; Sproules, S.; Arnold, P. L.; Love, J. B., Inner-sphere vs. outer-sphere reduction of uranyl supported by a redox-active, donor-expanded dipyrrin. *Chem. Sci.* **2017,** *8* (1), 108-116.

58. Pyrlin, S. V.; Hine, N. D. M.; Kleij, A. W.; Ramos, M. M. D., Self-assembly of bis-salphen compounds: from semiflexible chains to webs of nanorings. *Soft Matter* **2018,** *14* (7), 1181-1194.

59. Escudero-Adán, E. C.; Belmonte, M. M.; Martin, E.; Salassa, G.; Benet-Buchholz, J.; Kleij, A. W., A Short Desymmetrization Protocol for the Coordination Environment in Bis-salphen Scaffolds. *J. Org. Chem.* **2011,** *76* (13), 5404-5412.

60. Piccinno, M.; Angulo-Pachón, C. A.; Ballester, P.; Escuder, B.; Cort, A. D., Rational design of a supramolecular gel based on a Zn(II)–salophen bis-dipeptide derivative. *RSC Advances* **2016,** *6* (62), 57306-57309.

61. Sardarian, A. R.; Kazemnejadi, M.; Esmaeilpour, M., Bis-salophen palladium complex immobilized on Fe3O4@SiO2 nanoparticles as a highly active and durable phosphine-free catalyst for Heck and copper-free Sonogashira coupling reactions. *Dalton Trans.* **2019,** *48* (9), 3132-3145.

62. Gao, F.; Yang, F.-L.; Zhu, G.-Z.; Zhao, Y., Syntheses, structures, and magnetic properties of homodinuclear lanthanide complexes based on dinucleating Schiff base ligands. *Dalton Trans.* **2015,** *44* (46), 20232-20241.

63. Changai, D.; Chao, P.; Shaohua, Y., Determination of Trace zinc by Fluorescence Spectrophotometry with Bis-sulfosalophen. *IOP Conf. Ser.: Earth Environ. Sci* **2019,** *267*.

64. Schnorr, R.; Handke, M.; Kersting, B., Synthesis, characterization and molecular structure of a dinuclear uranyl complex supported by N,N′,N″,N‴-tetra-(3,5-di-tert-butylsalicylidene)-1,2,4,5-phenylenetetraamine. In *Z. Naturforsch., B: J. Chem. Sci.*, 2015; Vol. 70, p 757.

65. Rebizant, J.; Apostolidis, C.; Spirlet, M. R.; Kanellakopulos, B., Crystal and molecular structure of a novel Organoactinide Complex: $[U(C_5H_5)_3(NCCH_3)_2]^+$ $[Th(C_5H_5)Cl_4(NCCH_3)]^-$. *Inorg. Chim. Acta.* **1987,** *139* (1), 209-210.

66. Dolgopolova, E. A.; Ejegbavwo, O. A.; Martin, C. R.; Smith, M. D.; Setyawan, W.; Karakalos, S. G.; Henager, C. H.; zur Loye, H.-C.; Shustova, N. B., Multifaceted Modularity: A Key for Stepwise Building of Hierarchical Complexity in Actinide Metal–Organic Frameworks. *J. Am. Chem. Soc.* **2017,** *139* (46), 16852-16861.

67. Nelson, A.-G. D.; Bray, T. H.; Stanley, F. A.; Albrecht-Schmitt, T. E., Periodic Trends in Actinide Phosphonates: Divergence and Convergence between Thorium, Uranium, Neptunium, and Plutonium Systems. *Inorg. Chem.* **2009,** *48* (10), 4530-4535.

68. Schelter, E. J.; Wu, R.; Scott, B. L.; Thompson, J. D.; Morris, D. E.; Kiplinger, J. L., Mixed Valency in a Uranium Multimetallic Complex. *Angew. Chem. Int. Ed.* **2008,** *47* (16), 2993-2996.

69. Venkatachalam, G.; Raja, N.; Pandiarajan, D.; Ramesh, R., Binuclear ruthenium(III) Schiff base complexes bearing N_4O_4 donors and their catalytic oxidation of alcohols. *Spectrochim. Acta, Part A* **2008,** *71* (3), 884-891.

70. Niklas, J. E.; Hunter, K. M.; Gorden, A. E. V., Bonding Interactions in Uranyl α-Diimine Complexes: A Spectroscopic and Electrochemical Study of the Impacts of Ligand Electronics and Extended Conjugation. *Inorg. Chem.* **2019**.

71. Bullock, J. I., Raman and infrared spectroscopic studies of the uranyl ion: the symmetric stretching frequency, force constants, and bond lengths. *Journal of the Chemical Society A:*

Inorganic, Physical, Theoretical **1969,** (0), 781-784.

72. Syt'ko, V. V.; Kabaeva, E. N.; Proleskovskij, Y. A., Correlation of uranium-oxygen interatomic distances with stretching frequencies in the uranyl ion. *Zhurnal Neorganicheskoj Khimii* **2001,** *46* (6), 962-965.

73. Syt'ko, V. V.; Kabaeva, E. N., Special Features of the Correlation between the Uranium–Oxygen Interatomic Distances and the Frequencies of the Valence Vibrations of the UO22+ Group in Complex Compounds of Uranyl. *J. Appl. Spectrosc.* **2002,** *69* (4), 566-570.

74. Kalaj, M.; Carter, K. P.; Cahill, C. L., Isolating Equatorial and Oxo Based Influences on Uranyl Vibrational Spectroscopy in a Family of Hybrid Materials Featuring Halogen Bonding Interactions with Uranyl Oxo Atoms. *Eur. J. Inorg. Chem.* **2017,** *2017* (40), 4702-4713.

75. Di Pietro, P.; Kerridge, A., U–Oyl Stretching Vibrations as a Quantitative Measure of the Equatorial Bond Covalency in Uranyl Complexes: A Quantum-Chemical Investigation. *Inorg. Chem.* **2016,** *55* (2), 573-583.

76. Di Pietro, P.; Kerridge, A., Assessing covalency in equatorial U–N bonds: density based measures of bonding in BTP and isoamethyrin complexes of uranyl. *Phys. Chem. Chem. Phys.* **2016,** *18* (25), 16830-16839.

77. Sheldrick, G. M., Crystal structure refinement with SHELXL. *Acta Crystallogr., Sect. C: Struct. Chem.* **2015,** *71* (Pt 1), 3-8.

78. Dolomanov, O. V.; Bourhis, L. J.; Gildea, R. J.; Howard, J. A. K.; Puschmann, H., OLEX^2: a complete structure solution, refinement and analysis program. *J. Appl. Crystallogr.* **2009,** *42* (2), 339-341.

79. Bourhis, L. J.; Dolomanov, O. V.; Gildea, R. J.; Howard, J. A. K.; Puschmann, H., The anatomy of a comprehensive constrained, restrained refinement program for the modern

computing environment – Olex2 dissected. *Acta Crystallographica. Section A, Foundations and Advances* **2015,** *71* (Pt 1), 59-75.

80. Dormond, A.; El Bouadili, A.; Aaliti, A.; Moise, C., Insertion of carbonyl compounds into actinide—carbon σ bonds: Reactivity of [(Me3Si)2)2N]2M□Ch2Si(Me)2NSiMe3. *Journal of Organometallic Chemistry* **1985,** *288* (1), C1-C5.

Chapter 4

Pyrrophen: a Hexadentate Macroacyclic Framework for Uranyl

Portions of this chapter are reprinted from Mayhugh, J. T., Niklas, J. E., Forbes, M. G., Gorden, J. D., Gorden, A. E. V., which has been submitted to *Inorganic Chemistry*. The American Chemical Society gives permissions for the reuse of submitted material.

Introduction

In *f*-element coordination chemistry, the linear uranyl cation (UO_2^{2+}) is generally characterized as a hard acceptor based on Pearson's HSAB (hard-soft acid-base) principle, owing to its highly Lewis acidic and oxophilic nature.[1-3] Current research topics of interest include novel ligands that contain hard donor heteroatoms for sensing or extraction of uranyl (UO_2^{2+}) from aqueous environments; however, many of these systems are indiscriminate towards other cations [4-5] or would not be industrially-viable in environmental systems.[6-7] Though some simple mixed-donor systems, such as salens, have been investigated,[8] those featuring primarily or exclusively soft-donors are largely unexplored as a viable alternative in uranyl-coordinating complexes because of their more covalent-like coordination character. One exception is expanded-porphyrin macrocycles, which have been shown to be suitable hosts for uranyl and other actinyl cations, though they suffer from unfavorable kinetics and can be synthetically challenging to prepare.[9-13]

The synthetic accessibility and modularity of salen-type Schiff base ligands have made them attractive targets for potential use in separations applications; however, their affinity for a panoply of cations often precludes them from use when selective coordination is desired.[14-15] Recently, a new class of ligands has been reported which utilizes a similar synthetic methodology, but replaces the salicylaldehyde with a pyrrol-2-yl analogue.[16] These species are of interest for understanding self-assembly and molecular recognition.[17-20] Previous reports focus on changes in the system's architecture which result from altering the enediamine spacer unit or the pyrrolic arms. Most

notably, these ligands self-assemble with Cu^{2+} and Zn^{2+} to form M_2L_2 helicate structures through the coordination of the N-donor atoms exclusively.[16, 21] Both the Cu^{2+} and Zn^{2+} cations have ionic radii and charge-to-radius ratios similar to that of uranyl (UO_2^{2+}),[22-23] but the affinity of the ligand towards uranyl, to the best of our knowledge, has not been investigated. Given the presence of six suitable donor atoms in this pyrrolic salen-type system (akin to expanded-porphyrin analogs), its utilization in uranyl coordination was of interest. As this system is macroacyclic, it presents one opportunity to explore the bridging of the salen-type and extended porphyrin-type systems to form a new class of ligand that effectively coordinates the uranyl cation while utilizing a softer donor to increase its relative discrimination. The ability to tune the ligand by altering the substitution presents opportunites for improved coordination kinetics over those of macrocyclic species, and for improved binding with uranyl versus other metals. Here, we present two bench-stable benzyl ester derivatives of a previously reported ethyl ester bis(pyrrole)phenylenediamine ligand system[16] which we have nicknamed 'pyrrophen', new uranyl and transition metal complexes, and describe the features that make this framework particularly suitable for uranyl coordination.

4.1 | Pyrrophen Ligands and Complexes

The pyrrophen ligands $\mathbf{H_2L^1}$ and $\mathbf{H_2L^2}$ were prepared through the condensation of the respective o-phenylenediamines with benzyl 4-ethyl-5-formyl-3-methyl-1H-pyrrole-2-carboxylate (**3**) (**Scheme 4.1)** in methanol at room temperature. The resulting products were found to precipitate from solution as bright yellow solids. The synthesis of compound **3** is achieved with the regiospecific oxidation of a 5-methyl pyrrole using cerium (IV) ammonium nitrate.[24-25] Single crystals of $\mathbf{H_2L^1}$ and $\mathbf{H_2L^2}$ suitable for X-ray diffraction were grown by slow diffusion

(CH_2Cl_2/CH_3OH). In the solid-state, both the **H_2L^1** and **H_2L^2** free ligands were found to adopt slightly cupped conformations and form adducts with neutral solvent molecules (methanol) (**Figure 4.1**) through pyrrolic hydrogen-bonding. Such interactions have been observed previously in macrocyclic calix[4]pyrrole species[26-27] as well as for Schiff base expanded porphyrins.[11] Both ligands were found to have donor-acceptor distances that compare well with those of their macrocyclic cousins, though they more strongly resemble that of the Schiff base expanded porphyrins (**Table 4.1**). The diffuse nature of the N_{pyr}—H bond that predisposes it to these

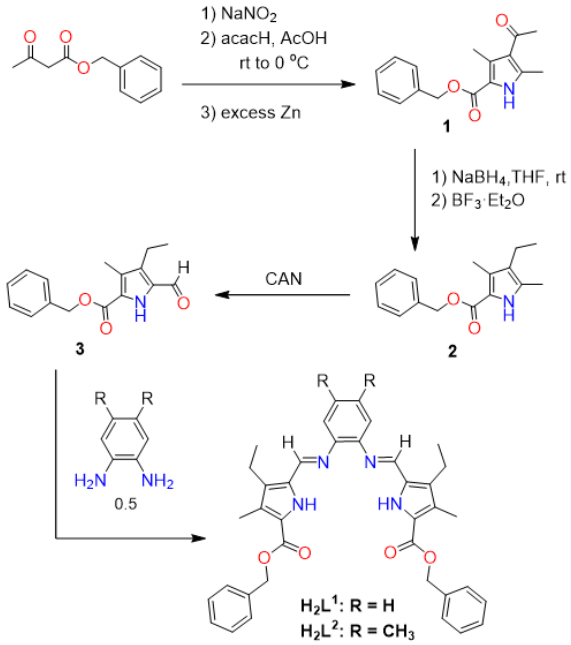

Scheme 4.1. Synthesis of benzyl 4-ethyl-5-formyl-3-methyl-1H-pyrrole-2-carboxylate and pyrrophen ligands.

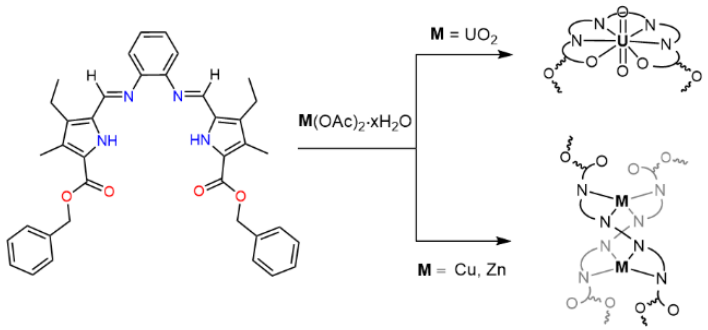

Scheme 4.2. Coordination modes of pyrrophen.

interactions is also apparent in the solution state by ^{1}H NMR—the pyrrole H-atoms are observed downfield at 9.70 ppm (**H_2L^1**) and 10.25 ppm (**H_2L^2**) as broad resonances, indicating considerable hydrogen delocalization.[28] These similarities to macrocyclic species are of note for not only their

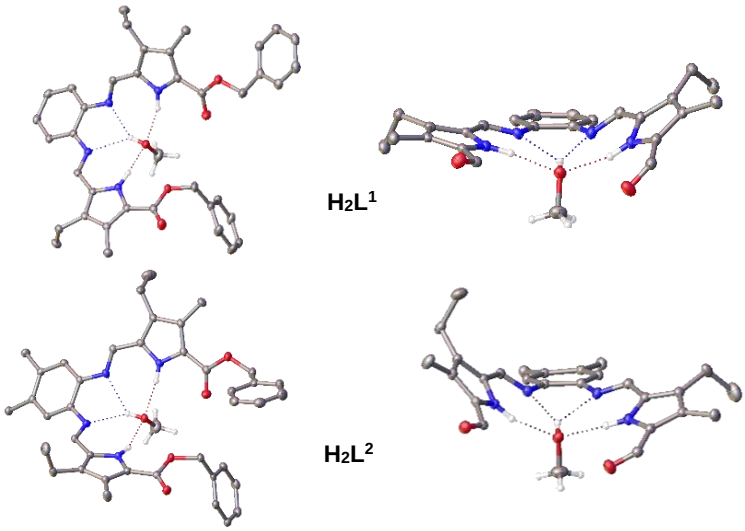

Figure 4.1. Left: structures of $H_2L^1{\cdot}CH_3OH$ (top) and $H_2L^2{\cdot}CH_3OH$ (bottom), grown from CH_2Cl_2/CH_3OH and CH_3OH, respectively. Right: side-on views of $H_2L^1{\cdot}CH_3OH$ and $H_2L^2{\cdot}CH_3OH$ along coordination plane (right) showing solvent interactions. H atoms and substituents (right) partially removed for clarity. Ellipsoids at 50%.

reported correlation in anion binding,[29] but give the pyrrophen framework a prospective amphoteric coordination module for insight into self-assembly and molecular recognition of other species.

Table 4.1. Average bond lengths (Å) for hydrogen bonds and methanol for pyrrophen ligands and adducts from references 11 & 27.

Bond	**H_2L^1**	**H_2L^2**	**Ref 11**	**Ref 27**
H**O**$\cdots$$N_{im}$	2.935	2.899	2.891	-
O**H**$\cdots$$N_{im}$	(2.22)	(2.19)	(2.09)	-
O—H	*0.85(2)*	*0.852(2)*	*0.95(4)*	*nr*
N$\cdots\cdots$**O**H	2.844	2.825	2.853	3.155
N**H**$\cdots$**O**H	(1.95)	(1.96)	(1.97)	(2.33)
N—H	*0.919(19)*	*0.884(16)*	*0.89(3)*	*0.90*
H_3**C—O**H	1.4251(19)	1.4094(15)	1.409(3)	1.286(13)

Complexes were prepared by adding 1.2 eq of $M(OAc)_2$ (M = Cu, Zn, UO_2) into a THF/MeOH (20:1, v/v) solution of $\mathbf{H_2L^1}$ or $\mathbf{H_2L^2}$. Upon addition of the metal acetate, each solution featured a distinct colour change from yellow to brown, orange, or deep red for the copper, zinc, and uranyl complexes, respectively. Intensely-colored solids were isolated by filtration after concentrating the solution under reduced pressure and cooling to 0° C. Single crystals of the copper, zinc, and uranyl complexes of $\mathbf{H_2L^1}$ and the uranyl complex of $\mathbf{H_2L^2}$ were grown from CH_2Cl_2/CH_3OH and characterized by X-ray diffraction. Unsurprisingly, the copper and zinc pyrrophen complexes form M_2L_2 helicate ensembles (**Figure 4.2**) comparable to those previously reported by Wu and Yang[16, 21], whereas the uranyl complexes adopt the hexagonal bipyramidal geometry (**Figure 4.3**) seen in

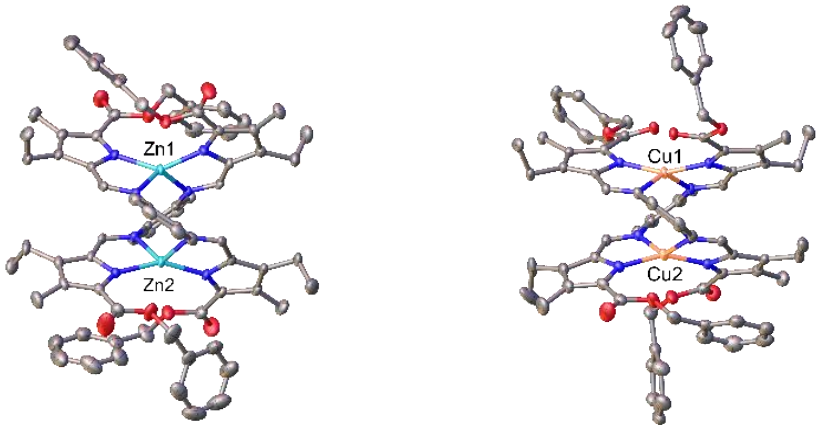

Figure 4.2. Structures of $\mathbf{Zn_2(L^1)_2}$ (left) and $\mathbf{Cu_2(L^1)_2}$ (right) viewed along planes of phenyl spacers. Ellispsoids at 50%. Hydrogen atoms removed for clarity.

porphyrin-type macrocyclic complexes.[30] To date, there is only one other reported structure in which the equatorial plane of uranyl is satisfied completely by a single, soft, non-macrocyclic ligand—a bipodal aroylthiourea-substituted bipyridine ligand (N_4S_2).[31] Recently, chelation of uranyl by a harder, catecholamine-based ligand was also reported, but no structures were presented.[32] $\mathbf{UO_2L^1}$ and $\mathbf{UO_2L^2}$ represent unique complexes in this regard, and highlight the potential the pyrrophen system shows for molecular recognition of uranyl by completely

occupying the equatorial plane. Selected bond lengths for all complexes as well as the free ligands are summarized in **Table 4.2**.

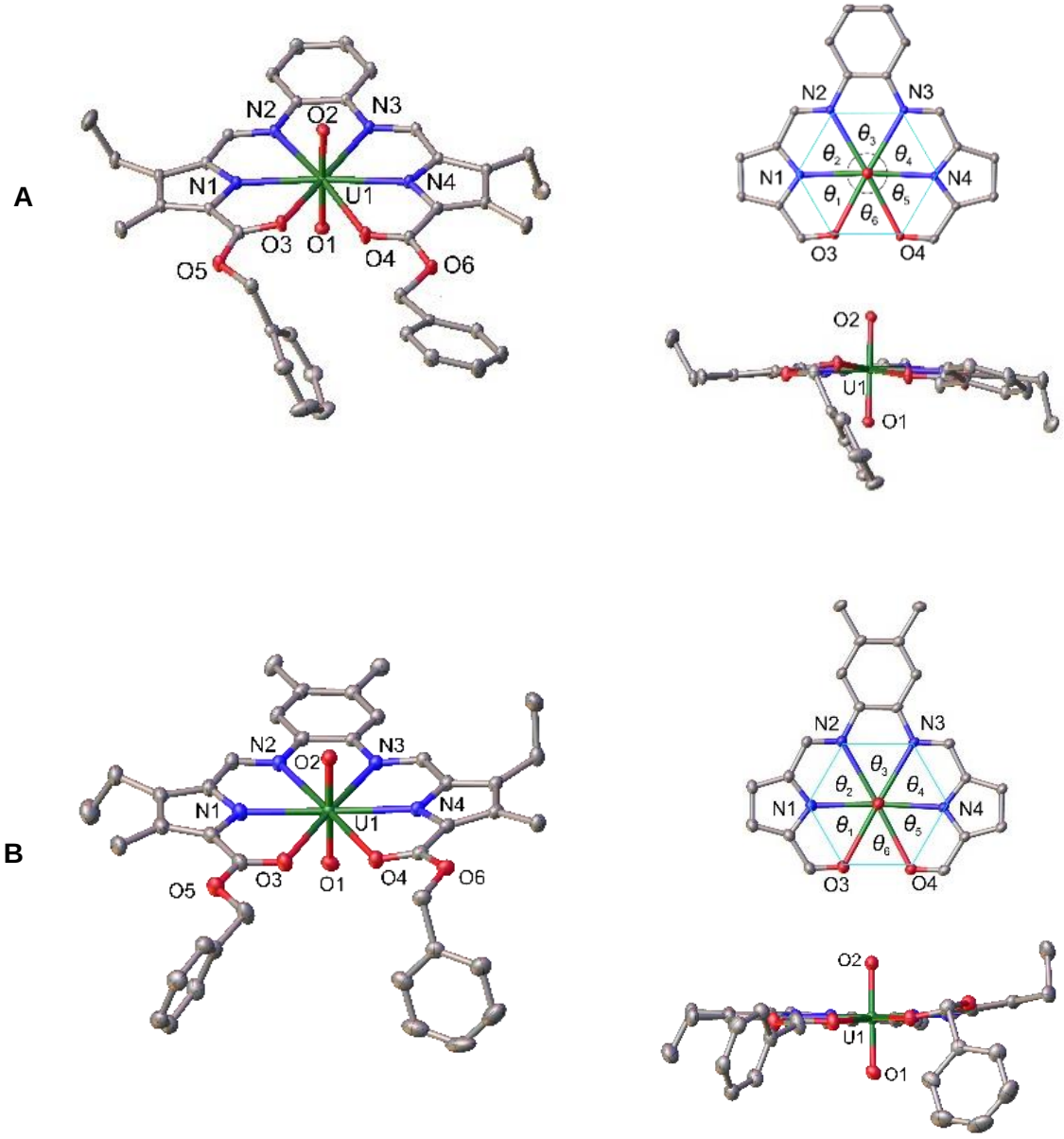

Figure 4.3. Structures of UO_2L^1 (**a**) and UO_2L^2 (**b**) showing full structure, views down the O=U=O units, and the equatorial planes. Hydrogen atoms and/or substituents removed for clarity. Ellipsoids at 50%. (**a**) θ_1: 60.93(5)°; θ_2 61.45(5)°; θ_3: 60.64(4)°; θ_4: 61.87(5)°; θ_5: 60.10(5)°; θ_6: 55.90(4)°; θ_{avg}: 60.15(5)°; $\Sigma\theta$ = 360.13°. (**b**) 60.23(7)°; θ_2 61.36(7)°; θ_3: 60.25(7)°; θ_4: 62.05(7)°; θ_5: 60.06(7)°; θ_6: 56.17(7)°; θ_{avg}: 60.02(7)°; $\Sigma\theta$ = 360.12°.

Notably, the formation of the double-stranded dinuclear copper and zinc complexes indicates that the binding pocket of the pyrrophen system cannot satisfy the coordination sphere of these

late transition metals in a 1:1 binding motif, and instead the ligand twists about the phenyl spacer to form a ditopic system in the observed 2:2 fashion. The zinc and copper centers adopt distorted tetrahedral geometries with average Cu—N_{pyr}, Cu—N_{im}, Zn—N_{pyr}, and Zn—N_{im} bond lengths of 1.993(2) Å, 2.048(2) Å, 1.9592(9) Å, and 2.0793(9) Å, respectively. The metal centres lie 3.300 Å (Cu) and 3.667 Å (Zn) apart. The formation of this helicate can also be observed for the zinc complex in solution *via* ^{1}H NMR as the ligand's methylene protons (δ 5.29) split into two distinct diasteriotopic peaks (δ 5.20, d; 4.27, d), signifying axial chirality.[16, 28]

While Zn^{2+} and Cu^{2+} undergo self-assembly into 2:2 helicate complexes in the presence of $\mathbf{H_2L^1}$, the distinct steric demands of the uranyl ion render complexes with a 1:1 configuration in which $\mathbf{L^1}$ and $\mathbf{L^2}$ fully occupy the equatorial plane as hexadentate ligands. This is evident in both solution and the solid state. ^{1}H NMR of the uranyl complexes shows single enantiotopic signals for the benzylic methylene protons (*ca.* 5.8 ppm).[28] The hexagonal bipyramidal uranyl complexes are undoubtably U(VI) species, evidenced by average U=O_{yl} bond lengths of 1.7722(16) Å ($\mathbf{UO_2L^1}$) and 1.774(2) Å ($\mathbf{UO_2L^2}$).[33] Notably, the average C=O distances of 1.236(3) Å unambiguously represent a coordinative interaction of the carbonyl oxygen with uranium in both cases. The corresponding average C=O distance in the "free" ester carbonyls for $\mathbf{Cu_2(L^1)_2}$ and $\mathbf{Zn_2(L^1)_2}$ is 1.209(3) Å, and 1.2084(14). The average U—N_{im} lengths of both complexes (**Table 4.2**) are approximately 0.15 Å longer than those usually found for U(VI) salophen species,[34] and are on par with U—N_{im} lengths reported for expanded porphyrin complexes, as are the average U—N_{pyr} lengths,[9] though these distances do differ somewhat from those of a comparable macrocyclic uranyl grandephyrin complex[11] which features a slightly larger pocket— the U—N_{im} and U—$_{Npyr}$ lengths of the pyrrophen species are nearly 0.20 Å and 0.10 Å shorter, respectively. It is noted for the grandephryin complex that the uranyl cation is shifted off-center away from the imine N

atoms— the uranium center lies 2.536 Å from the midpoint of the vector defined by the imine N atoms and 2.265 Å from the vector defined by the meso-bridged pyrrole N atoms,[11] whereas the pyrrophen complexes are significantly more centered with the uranium atom lying an average of 2.299 Å from the imine midpoint and 2.318 Å from the midpoint of the vector defined by the carbonyl O atoms. The near linearity of the pyrrole donors for **UO_2L^1** and **UO_2L^2** (N_1—U—N_4 = 175.61(6)^o and 174.99(9)°, respectively) as well as the average angle between donors and Σθ values (60.15(6)^o, 360.91°, and 60.02(8)°, 360.14°, respectively) also reflect that the uranyl resides almost perfectly in the center of the ligand's pocket, similar to some macrocyclic systems, as well as highlights the planarity of these complexes, a feature which is uncommon among the typically ruffled macrocyclic complexes[11-13] (**Figure 4.3**). This illustrates the ability of uranyl to engage favorably in primarily covalent interactions, as the deprotonated pyrrole N atoms possess low ionic character, especially when part of a large π-conjugated system.

Table 4.2. Selected bond lengths (Å) for pyrrophen ligands and their complexes.

	H_2L^1	**H_2L^2**	**$Zn_2L^1{}_2$**	**$Cu_2L^1{}_2$**	**UO_2L^1**	**UO_2L^2**
C=N_{im}	1.2839(19)	1.2816(14)	1.3075(13)	1.299(3)	1.302(2)	1.302(4)
C=O_{ester}	1.2134(19)	1.2132(13)	1.2085(14)	1.209(3)	1.237(2)	1.235(4)
M—N_{im}	-	-	2.0793(9)	2.048(2)	2.6597(17)	2.664(2)
M—N_{pyr}	-	-	1.9592(9)	1.933(2)	2.4374(16)	2.441(3)
M—O	-	-	-		2.5789(14)	2.673(2)
U=O_{yl}	-	-	-		1.7722(16)	1.774(2)

While these species are interesting for their unique and gratifying solid-state structures, the solution state behavior of pyrrophen is also worth investigation, as the structural features of the uranyl complexes suggest that the pyrrophen system is particularly well-suited for forming stable uranyl complexes. Given the spontaneous assembly of each metal complex at room temperature

and without the addition of base, as well as the marked colour differences among them, there is the potential of this system to be exploited in further studies for molecular recognition of UO_2^{2+}. Initial screening of a wide array of metal acetates (Mg^{2+}, Ca^{2+}, VO^{2+}, Mn^{2+}, Fe^{2+} Fe^{3+}, Co^{2+}, Ni^{2+}, Cu^{2+}, Zn^{2+}, Ce^{3+}, Ce^{4+}, Dy^{3+}, Th^{4+}, and UO_2^{2+}) was conducted to determine the range of coordinating cations for **H_2L^1**. As determined by UV-Vis spectroscopy, only Co^{2+}, Ni^{2+}, Cu^{2+}, Zn^{2+}, and UO_2^{2+} were found to form metal complexes under ambient conditions. No other ions were observed to induce a visible change to pyrrophen. The ligand (**H_2L^1**) features an intense $\pi\rightarrow\pi^*$ band (Soret-like) at 328 nm (ε = 42,800 M^{-1} cm^{-1}) with a shoulder at 375 nm ($\varepsilon \approx$ 22,000 M^{-1} cm^{-1}) indicative of charge-transfer from a coordinating solvent molecule (as seen in the solid-state). Similar features are observed for **H_2L^2** (λ_{max} = 319 nm, ε = 49, 100 M^{-1} cm^{-1}) (**Figure 4.4).** Coordination of to Co^{2+}, Ni^{2+}, Cu^{2+}, Zn^{2+}, or UO_2^{2+} results in a substantial bathochromic shift of the $\pi\rightarrow\pi^*$ band. Only coordination to UO_2^{2+} results in retention of approximately the same ε, or an increase in ε (41,600 M^{-1} cm^{-1} for **UO_2L^1**; 55,000 for **UO_2L^2**) as the free ligand (**Figure 4.11**), indicating the uranyl complexes are planar in solution whereas the transition metal complexes are not. This behavior is also distinct from expanded porphyrin analogues, which either show a marked

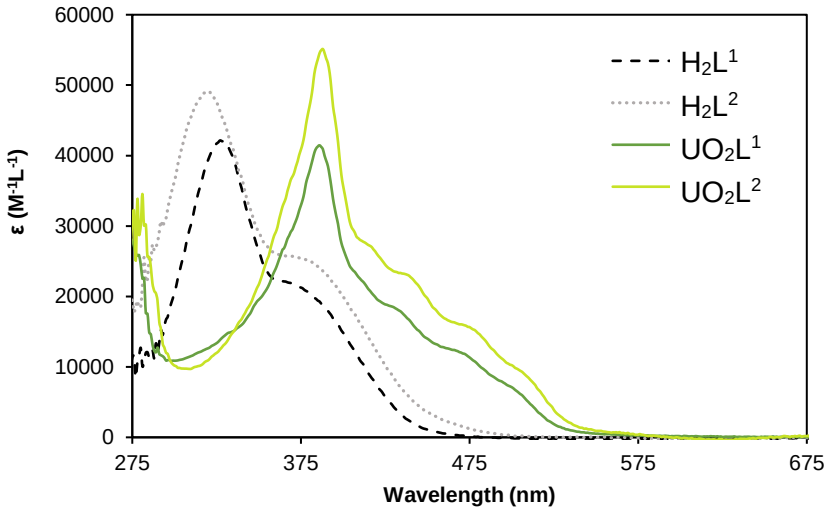

Figure 4.4 UV-Vis of **H_2L^1**, **H_2L^2**, **UO_2L^1** and **UO_2L^2** (20 μM) in 9:1 THF:MeOH.

increase or decrease in ε due to ruffling or bowing of the ligand on complexation.[6, 12] UV-Vis titrations of metal acetates into a solutions of pyrrophen (**H_2L^1**) show clear isosbestic points, and confirm 1:1 binding ratios for all complexes (1:1 or 2:2), but the presence of multiple isosbestic points in the nickel titration data, and the smaller bathochromic shift of the π→π* band suggest structural features distinct from that of the other transition metal species (**Figure 4.6**).

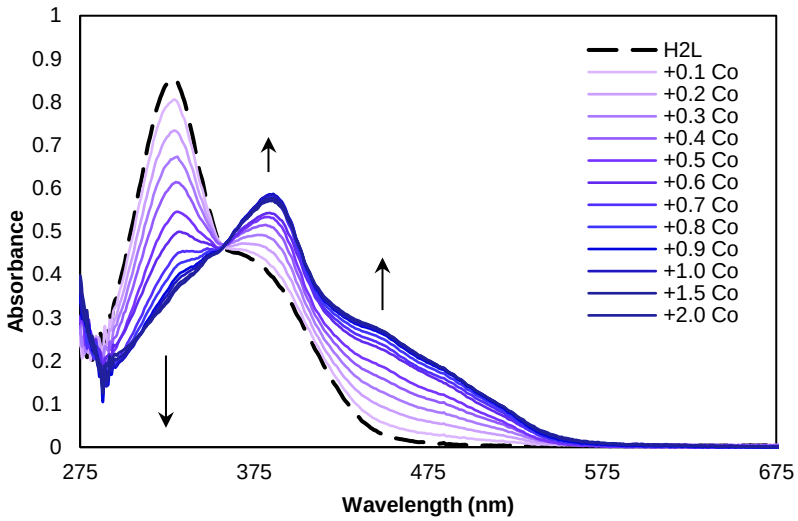

Figure 4.5 UV-Vis titration of 20 μM H_2L in 9:1 THF:MeOH with 1000 μM $Co(OAc)_2•4H_2O$ in MeOH (0.1 equiv. aliquots).

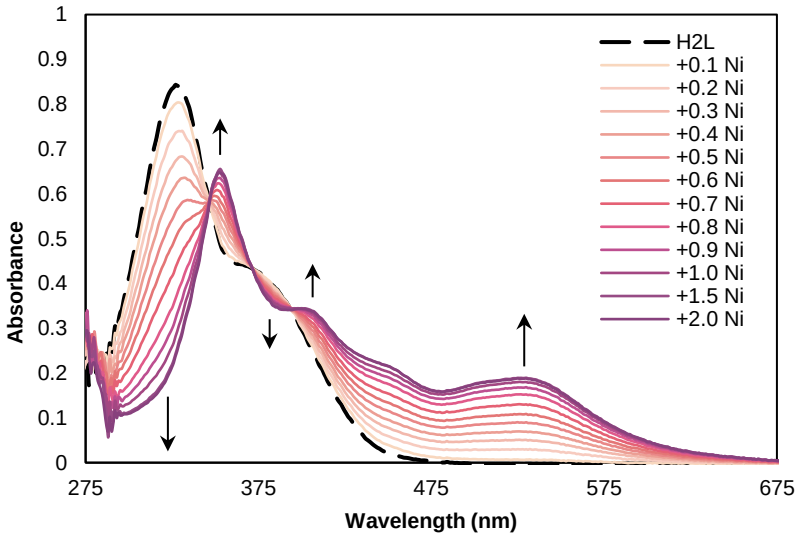

Figure 4.6 UV-Vis titration of 20 μM H_2L in 9:1 THF:MeOH with 1000 μM $Ni(OAc)_2•4H_2O$ in MeOH (0.1 equiv. aliquots).

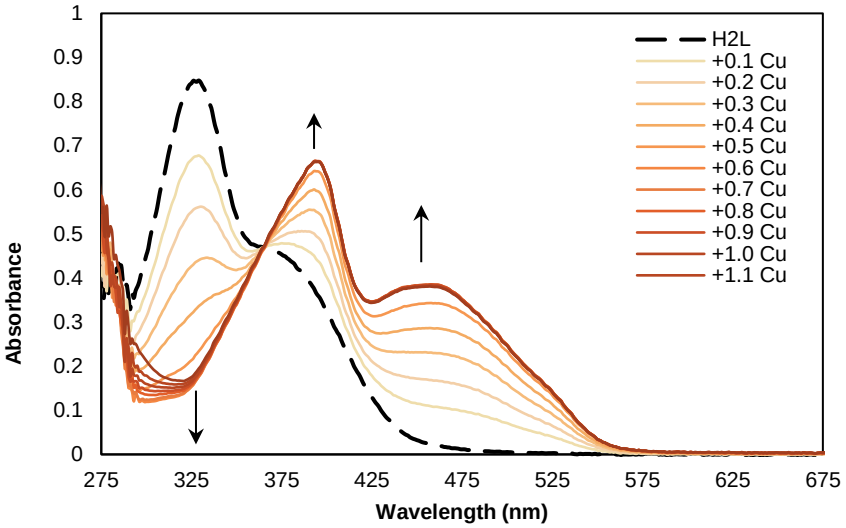

Figure 4.7 UV-Vis titration of 20 μM H_2L in 9:1 THF:MeOH with 1000 μM $Cu(OAc)_2 \cdot H_2O$ in MeOH (0.1 equiv. aliquots).

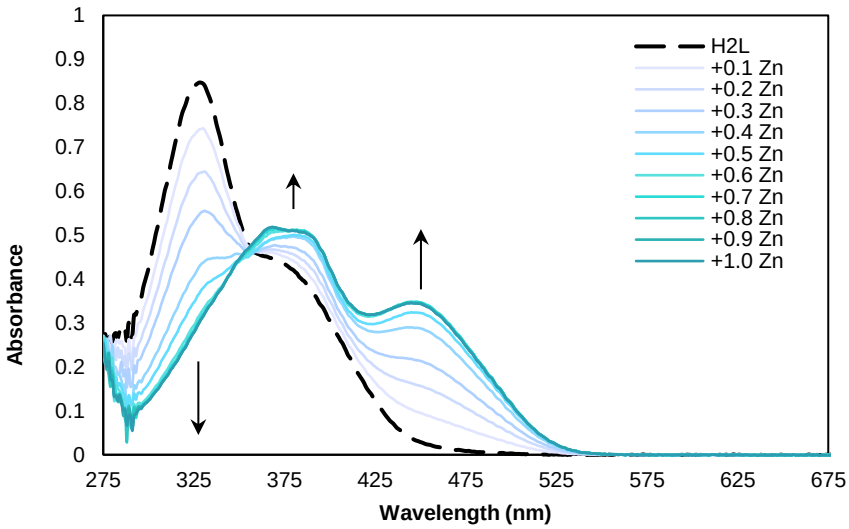

Figure 4.8 UV-Vis titration of 20 μM H_2L in 9:1 THF:MeOH with 1000 μM $Zn(OAc)_2 \cdot 2H_2O$ in MeOH (0.1 equiv. aliquots).

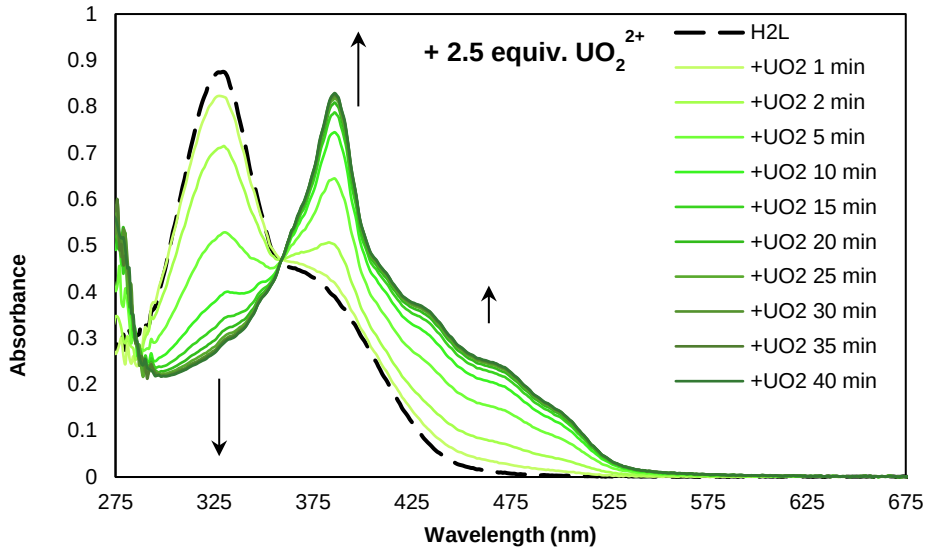

Figure 4.9. Addition of 150 µL 1000 µM $UO_2(OAc)_2$•$2H_20$ (2.5 equivalents) to 3 mL 20 µM H_2L in 9:1 THF:MeOH.

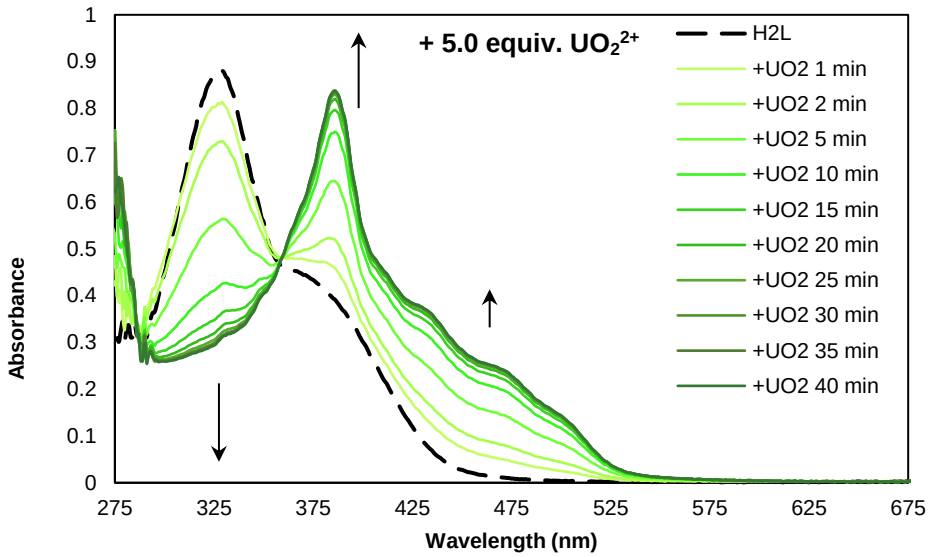

Figure 4.10. Addition of 150 µL 2000 µM $UO_2(OAc)_2$•$2H_20$ (5.0 equivalents) to 3 mL 20 µM H_2L in 9:1 THF:MeOH.

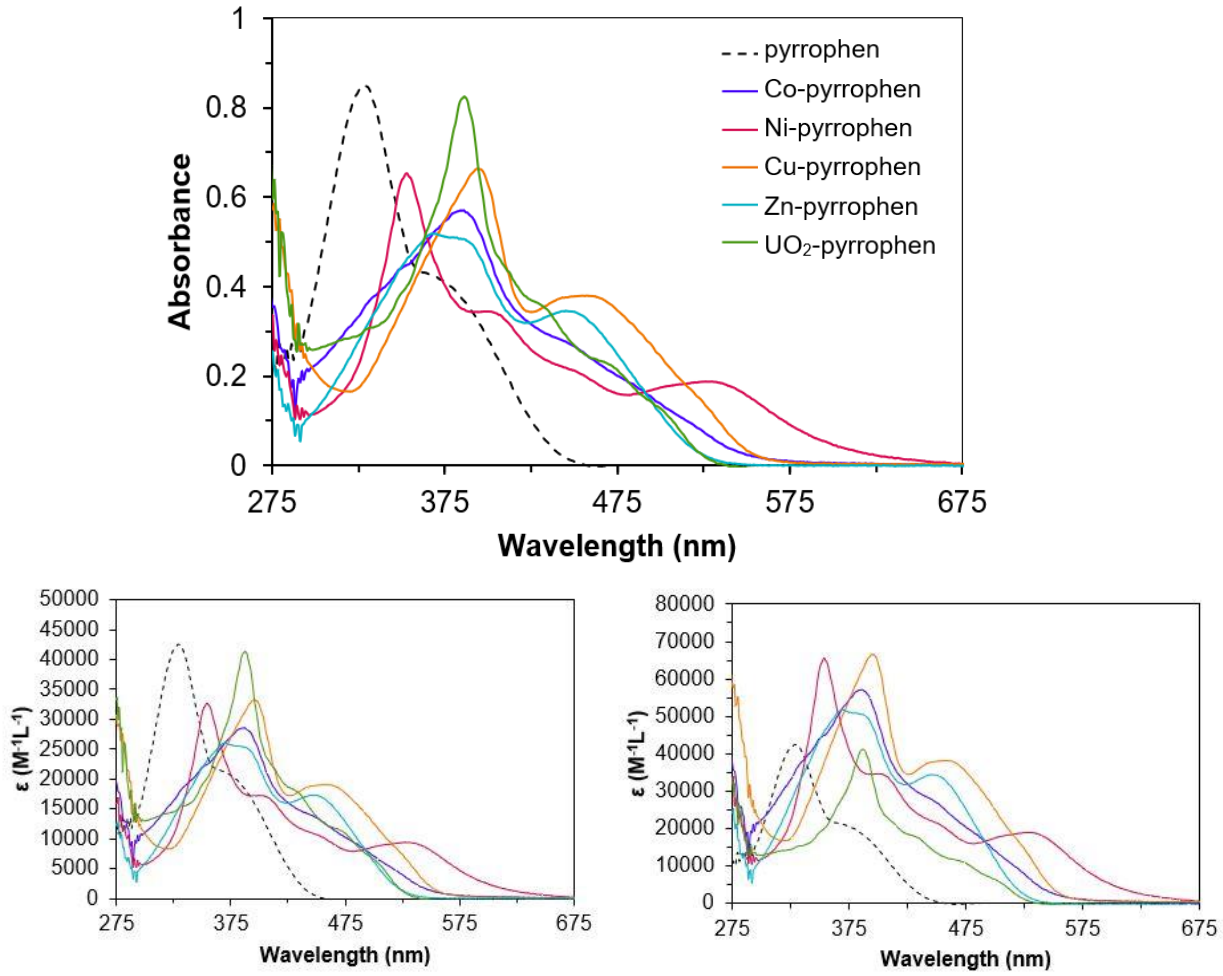

Figure 4.11 Top: UV-Vis spectra of $\mathbf{H_2L^1}$ and complexes in 9:1 THF:MeOH (v/v). Bottom: UV-Vis spectra of complexes in 9:1 THF:MeOH, where molar extinction coefficient is calculated per metal center (or per "1:1" unit of M:L) (left) and where molar extinction coefficient is calculated per complex, assuming a 1:1 stoichiometry for UO_2L and M_2L_2 for transition metal species (right). Data shown are final traces of the titration of 20 μM H_2L with M^{2+} to form 1:1 or 2:2 complexes.

Table 4.3. Comparison of molar absorptivity (per complex and per metal center or 1:1 unit) for pyrrophen and metal-pyrrophen complexes and λ_{max} values

Species	ε (M^{-1}·cm^{-1})	ε (M^{-1}·cm^{-1})/metal	λ_{max} (nm)	$\Delta\lambda_{max}$ (nm)
H_2L^1	42,800	-	328	-
H_2L^2	49,000	-	319	-
Co-L^1	56,700	28,300	385	57
$Cu_2(L^1)_2$	66,200	33,100	394	66
Ni-L	65,400	32,700	352	24
UO_2L^1	41,600	41,600	386	58
UO_2L^2	55,000	55,000	388	69
$Zn_2(L^1)_2$	51,700	25,800	367	29

Figure 4.12 (a) 500 μM (upper vials) and 50 μM (lower vials) colorimetric series of $\mathbf{H_2L^1}$ and complexes in 9:1 THF:MeOH (v/v); (b) top-down views of $\mathbf{UO_2L^1}$ (right) and $\mathbf{Zn_2(L^1)_2}$ (left) solutions, 500 μM in CH_3CN.

Titrations of $\mathbf{H_2L}$ with acetic acid resulted in no observable spectroscopic changes, affirming complex formation is not hindered by ligand-acetate interactions. Most of the transition metal complexes feature a λ_{max} in a similar range (approx. 370-390 nm) as that of the uranyl complex, except for nickel (λ_{max} = 352), but their lower-energy absorptions are more intense, leading to visible color differences in solution (**Figure 4.11, 4.12**). The uranyl and zinc complexes are the most similar in color when viewed side-on; however, when viewed from above, the $\mathbf{UO_2L^1}$ solution is distinctly red-orange in color (**Figure 4.12b**). Given the combination of visible color differences, and unique spectroscopic profiles, it is possible to identify the uranyl complex among the transition metal species. Though these features are promising in terms of molecular recognition of uranyl, they do not speak to the ability of this ligand to selectively bind uranyl from a mixture. Thus, further qualitative studies to determine the binding preferences of pyrrophen were conducted in which the ability of UO_2^{2+} to displace zinc or copper from the M_2L_2 complexes was investigated.

Replacement of cobalt and nickel was not pursued, as the cobalt complex is observed by UV-Vis to dissociate rather quickly after formation, even in an excess of Co^{2+}, and both the cobalt and nickel complexes are colorimetrically distinct from the uranyl complex in solution (**Figure 4.12**). On addition of UO_2^{2+} to solutions of $\mathbf{Zn_2(L^1)_2}$, displacement of Zn^{2+} was observed using UV-Vis spectroscopy *via* the immediate growth of the characteristic $\mathbf{UO_2L^1}$ absorption features (**Figure**

4.13). Even when 0.5 per-metal equivalents UO_2^{2+} was introduced, this replacement was observed within minutes. The same experiments were conducted using **$Cu_2(L^1)_2$**, but formation of the uranyl complex was not observed, indicating the copper helicate is more stable in solution. From these studies, we have determined that the stability of the monomeric **UO_2L^1** complex is intermediate to that of the ditopic **$Cu_2(L^1)_2$** and **$Zn_2(L^1)_2$** helicates, though this may not necessarily reflect the preference of formation of 1:1 species.

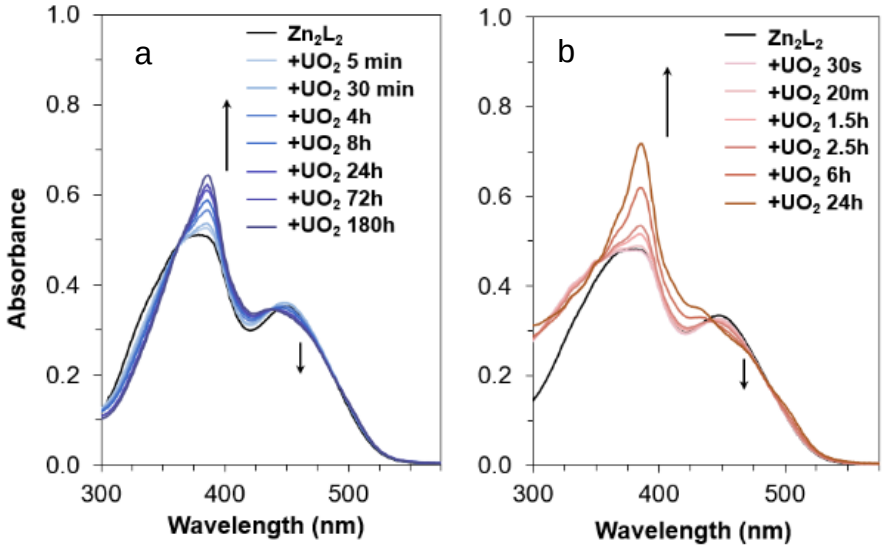

Figure 4.13 Addition of 0.5 (a) and 1.0 (b) equivalent UO_2^{2+} (per Zn^{2+}) to **$Zn_2(L^1)_2$**, 10 μM in 9:1 THF:MeOH).

In an attempt to characterize this quantitatively, formation constants were calculated for complexes of **H_2L^1** (**Table 4.3**) using UV-Vis titration data, [35-37] though it must be acknowledged that the methods used are based on the assumption that 1:1 complexes are being formed, not the 2:2 complexes which are known to self-assemble in the presence of Zn^{2+} or Cu^{2+}.[16, 21] Where higher order supramolecular self-assembly is concerned, such studies are non-trivial and require a clear mechanism of formation and independent treatment of intra- and inter-molecular constants.[36, 38] Approximations of the binding constants for 1:1 complexes in 9:1 THF:MeOH are a reasonable benchmark for comparing the *relative* binding affinity of **H_2L^1** for transition metal ions,[35, 37] and

should always be secondary to more detailed qualitative studies. These approximated $\log\beta_{11}$ values (Co^{2+}, 6.11 ± 0.71; Ni^{2+}, 7.31 ± 0.53; Cu^{2+}, 6.02 ± 1.33; Zn^{2+}, 5.27 ± 0.09, UO_2^{2+}, 6.74 ± 0.80) suggest that the copper complex should be more stable than the zinc complex. This is consistent with what is observed experimentally for the prepared 2:2 complexes with respect to replacement by uranyl; however, this is difficult to conclude given the non-traditional solvent system. The cobalt complex is observed to fall apart after formation, yet the calculated $\log\beta_{11}$ is higher than other stable complexes, and the $\log\beta_{11}$ for **UO_2L^1** is calculated to be higher than that of the 1:1 copper complex. Additionally, formation of the uranyl complex at concentrations appropriate for UV-Vis spectroscopy is significantly slower than that of the transition metal species (**Figure 4.14**), which further complicates analysis—this is likely tied to the coordination of methanol by the

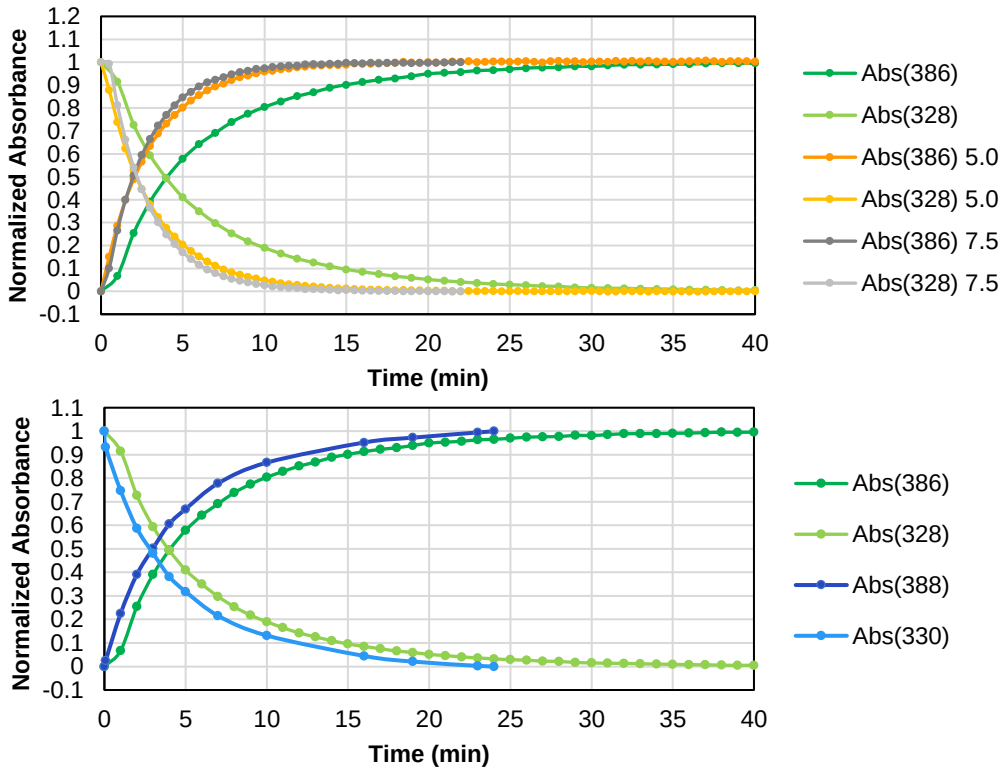

Figure 4.14 Top: Normalized absorbance of for **H_2L^1/UO_2L^1** at 328 nm and 386 nm vs time after addition of 150 µL 1000, 2000, or 3000 µM $UO_2(OAc)_2$•$2H_20$ (2.5, 5.0, or 7.5 equivalents) to 3 mL 20 µM H_2L in 9:1 THF:MeOH. Bottom: Normalized absorbance at 328 nm and 386 nm (for **H_2L^1/UO_2L^1** green) and at 330 nm and 388 nm (for **H_2L^2/UO_2L^2**, blue) vs time after addition of 150 µL1000µM $UO_2(OAc)_2$•$2H_20$ (2.5 equivalents) to 3 mL 20 µM H_2L in 9:1 THF:MeOH.

ligand under these conditions, and may also be impacted by the steric bulk of the benzyl ester groups and the need for "side-on" coordination of the linear cation (which is not necessary for the spherical transition metal cations. The presence of methyl groups on the backbone of $\mathbf{H_2L^2}$ appears to improve the kinetics considerably- complete binding takes ~25 minutes, as compared to nearly 40 minutes for $\mathbf{H_2L^1}$**.** The formation constant for $\mathbf{UO_2L^1}$ cannot be reasonably compared to those of other reported aqueous-soluble systems[32, 39], but is greater than those reported for macrocyclic systems in mixed organic solvents, reflecting the value of a well-sized and flexible binding pocket.[40-41] Further commentary on binding constants is provided in the Methods section.

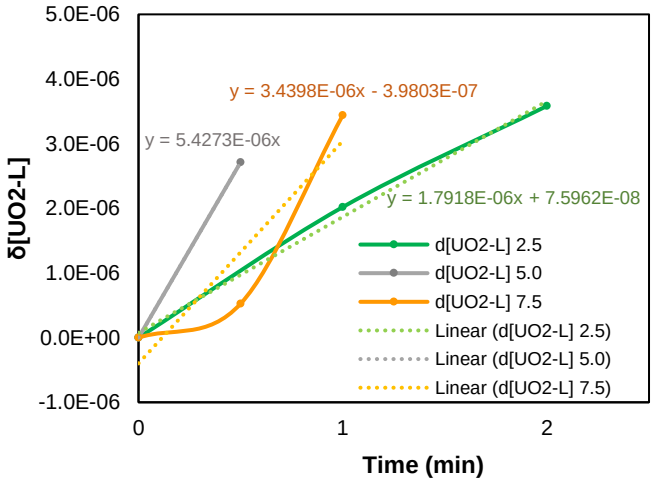

Figure 4.15 Calculated changes in concentration of $\mathbf{UO_2L^1}$ over time (initial rates of formation) from normalized absorbance at 328 nm and 386 nm based on addition of 150 µL 1000, 2000, or 3000 µM $UO_2(OAc)_2$•$2H_20$ (2.5, 5.0, or 7.5 equivalents) to 3 mL 20 µM H_2L in 9:1 THF:MeOH.

Table 4.4. Estimated formation constants of pyrrophen complexes

Complex	**logβ_{11}**
Co^{2+}	6.11 ± 0.71 [a]
Ni^{2+}	7.31 ± 0.53 [a]
Cu^{2+}	6.02 ± 1.33 [a]
Zn^{2+}	5.27 ± 0.09 [a]
UO_2^{2+}	7.61 ± 1.32 (8.87 ± 0.80 [b], 6.74 ± 0.80 [a])

Data collected in 9:1 THF:MeOH and fit using Bindfit v0.5 (supramolecular.org)[a] Calculated from UV-Vis serial or batch titration data. [b] Calculated from time-dependent UV-vis data in presence of excess UO_2^{2+}.

In conclusion, pyrrophen, a sal-porphyrin analogue, as well as its dimethyl derivative have been prepared and characterized in the solution and solid state *via* NMR and UV-Vis spectroscopy, and with single crystal X-ray diffraction, as have the complexes $\mathbf{Cu_2(L^1)_2}$, $\mathbf{Zn_2(L^1)_2}$, $\mathbf{UO_2L^1}$, and $\mathbf{UO_2L^2}$. Of particular note is the coordination of the free ligands to methanol, thereby showing the inherent lack of electronegativity on the pyrrole moieties and preferred pseudo-planar orientation, as observed in calix[4]pyrrole systems.[29] Structural analyses of the UO_2^{2+} complexes suggest this ligand framework is especially well-suited for uranyl coordination and help to further elucidate the covalent-type coordination behavior of the uranyl cation. Remarkably, uranyl displaces the only other metal which gives the most similarly-colored complex (Zn), indicating that the combination of binding preference and colorimetric or spectroscopic response allows for identification of UO_2^{2+} in solution. This ligand and its complexes give insight into the potential of soft donor macroacyclic systems as suitable candidates for selective uranyl recognition or extraction by taking advantage of uranyl's proposed covalent f-orbitals.[42-43] With uranyl forming the only planar complex of the cations and given the synthetic modularity of the ligand, it is feasible to prepare a pyrrophen derivative that sterically disfavors the formation of transition metal helicate complexes—this is a potential route by which to more clearly study the solution phase thermodynamics without needing to consider the self-assembly of higher order complexes as a complicating factor. Future work will also include the preparation of water-soluble derivatives as such data are most relevant in aqueous systems and would be best for comparison with other systems. Despite the limitations encountered in quantitatively describing the binding preferences of this system, it is encouraging that the narrow range of cations which pyrrophen can coordinate, as our preliminary investigations demonstrate it has no affinity for Ln^{3+} ions or Th^{4+} under ambient conditions—exclusion of these species is valuable with respect to applications for environmental clean-up or nuclear waste remediation.

Studies on the selective coordination of uranyl are ongoing, with modifications to improve binding kinetics, sensitivity and colorimetric response being pursued. This (along with the work from Abram et al[31]) warrants further investigation into selective actinyl recognition with the use of this highly modular and chromatic framework.

4.2| Synthesis of Compounds and Methods

General Considerations

Caution! The uranium metal salt – $UO_2(OAc)_2 \cdot 2H_2O$ – used in this study contained depleted uranium. Standard precautions for handling radioactive materials or heavy metals such as uranyl nitrate and lead sulfate were followed.

All ^{1}H NMR spectra were recorded on a Bruker AV 400 MHz or Bruker AV 600 MHz spectrometer, reported in parts per million (δ, ppm) and referenced to residual protio-solvent ($CDCl_3$, δ 7.27) or tetramethylsilane (TMS, δ 0.00). Deuterated chloroform ($CDCl_3$) was obtained from Cambridge Isotopes Laboratories, Inc., Andover, MA, and used without further purification. High-resolution mass spectrometry (HRMS) was performed using a quadrupole time-of-flight spectrometer (Q- TOF Premier, Waters) with electrospray ionization (ESI). All chemicals and solvents were used as received from commercial sources, unless otherwise stated. All solution-phase absorbance spectra were collected from 1000 nm to 200 nm on a VARIAN Cary 50 WinUV Spectrometer with a xenon lamp using a 1 cm path length quartz cuvette. Titration studies were performed using capped cuvettes to minimize evaporation of volatile solvent during the course of the experiment. Binding constants were calculated using Bindfit from supramolecular.org[35]

UV-Vis titrations

A 20 μM stock solution of H_2L in 9:1 THF/MeOH (v/v) was prepared, and 3 mL were added to a quartz cuvette. Transition metal acetate salts (1000 μM in MeOH) were added in 6 μL aliquots (0.1 equiv)—during each addition, the solution in the cuvette was gently agitated with the pipette, and the trace immediately recorded. Several additional traces at each aliquot were collected until absorbance values were static. Experiments were performed in triplicate.

For UO_2^{2+} titrations used in binding constant calculation, a 20 μM stock solution of H_2L in 9:1 THF/MeOH (v/v) was prepared, and 6 mL aliquots were added to cone-cap scintillation vials with flea stir bars. $UO_2(OAc)_2 \cdot 2H_2O$ (1000 μM in MeOH) was added in 0.1-molar-equivalent aliquots (0.7-1.2), and the vials were capped tightly, then heated to 45 °C with synchronous stirring for 36 hours. Binding progress was tracked by UV-Vis measurements at 2, 6, 12, 24, and 36 hours until absorbance values at 328 and 386 were static. Data points from the final set of measurements (36 h) were used to calculate the binding constant. Experiments were performed in triplicate.

Calculation of Binding Constants and Limitations

While transition metal species appear to coordinate instantaneously (consistent with the tendency of these complexes to self-assemble), formation of the uranyl complex is slower, roughly obeying 1st-order kinetics (with respect to uranyl). The time taken to coordinate to the transition metal ions appears to be fairly independed of the concentration of the metal under these conditions. At low concentrations, such as those at which appropriate spectrophotometric data for the calculation of binding constants can be collected, formation of UO_2-L is non-linear with respect to the number of added molar equivalents of UO_2^{2+}, and misleadingly indicates 1:1.5 (L:M) binding. This is likely an artifact of aggregation, as this is a known complication for supramolecular-type interactions.[36, 44] All other data collected in the solution and solid state indicates the 1:1 complex

UO_2-L, as does an analysis of UV-Vis data collected in the presence of excess UO_2^{2+}. Formation of higher-order complexes is not geometrically or sterically reasonable. Attempts to extract formation constants from numerous data sets from batch titrations resulted in a wide array of fits to 1:1, 1:2, and 2:1 L:M complexes with values of K (or K_{11}) ranging from 10^2-10^{20}.

To better estimate the formation constant for UO_2L, we examined UV-vis data from experiments with various excesses of uranyl and calculated the ratios of "host" (pyrrophen) and "guest" (uranyl) at each timepoint throughout the experiment based on extinction coefficients and normalized values. In doing so, we assumed the following: 1) the product of uranyl and pyrrophen is the 1:1 complex "UO_2L", 2) the concentration of the guest species can be approximated as the apparent concentration of UO_2L, and 3) the reaction proceeds to completion and the absorbance is essentially constant at any guest concentration greater than one molar equivalent. Formation constants were calculated from experiments in which 2.5 equivalents, 5.0 equivalents, and 7.5 equivalents of uranyl were added, and averaged. We note that this value ($\log\beta_{11} = 8.87 \pm 0.80$) is greater than that calculated from abridged batch titration data ($\log\beta_{11} = 6.74 \pm 0.80$), which was poorly behaved, and that both values suggest a greater stability of the uranyl complex over the copper complex, but replacement of Cu^{2+} by UO_2^{2+} is not achieved within 24 hours under ambient conditions. Additionally, there are large errors associated with the copper complex formation constant, and removal of the outlier data gives essentially the same $\log\beta$ value as for the Zn complex. The values listed in Table S2 are not likely an accurate representation of the true stabilities of these complexes, which are not necessarily comparable to that of the uranyl complex given their different stoichiometries and potential mechanisms of formation, and more in-depth calculations would be required which take such information into consideration.

Synthesis of Compounds

Synthesis of Benzyl 4-acetyl-3,5-dimethyl-1H-pyrrole-2-carboxylate (1). Compound **1** was synthesized using modifications of a known procedure.[1] A cold solution of sodium nitrite (8.7 g, 0.13 mol) in water (12 mL) was added dropwise to a stirring solution of benzyl acetoacetate (22.5 mL, 0.13 mol) in acetic acid (28 mL) at 0 ºC. Once added, the solution was allowed to warm to room temperature and stirred overnight. Acetylacetone (13.0 mL, 0.13 mol) and additional acetic acid (48 mL) were added to the solution and the flask was cooled in an ice bath while zinc powder (33 g, 0.50 mol) was added slowly. The reaction flask was then equipped with a condenser and heated to 100 ºC for 1 h in an oil bath. The still-hot solution was poured over ice-water to end the reaction. The resulting precipitate was collected via vacuum filtration and washed with additional DI water. The solid was dissolved in hot ethanol, then filtered while hot to remove any remaining zinc. Crystallization from ethanol gave compound **1** as a white solid (25.2 g, 71 %). ^{1}H NMR (400 MHz, $CDCl_3$) δ 2.45 (s, 3H). 2.51 (s, 3H), 2.62 (s, 3H), 5.33 (s, 2H), 7.45-7.33 (m, 5H), 9.04 (brs, 1H).

Synthesis of Benzyl 4-ethyl-3,5-dimethyl-1H-pyrrole-2-carboxylate (2). Compound **2** was synthesized using modifications of a known procedure.[1] A reaction flask was charged with a magnetic stir bar, **1** (24.4 g, 0.09 mol), sodium borohydride (8.0 g, 0.21 mol) and THF (240 mL) and stirred at room temperature. The flask was then equipped with a dropping funnel containing boron trifluoride diethyl etherate (53 mL, 0.43 mol) and the entire system was kept under a constant stream of nitrogen. $BF_3 \cdot OEt_2$ was added dropwise over the course of one hour. After the addition was

completed, the mixture was stirred for an additional hour. The reaction was then quenched with the slow addition of 10 % HCl in water (until neutral) and extracted three times with chloroform. The organic layers were collected and evaporated to dryness under reduced pressure. The crude solid was then dissolved in 400 mL of 80 % ethanol in water and stored in a refrigerator overnight. Compound **2** is collected as a white, needle-like crystalline precipitate from this solution (18.9 g, 82 %). ^{1}H NMR (400 MHz, $CDCl_3$) δ 1.05 (t, *J* = 7.6 Hz, 3H), 2.20 (s, 3H), 2.30 (s, 3H), 2.38 (q, *J* = 7.5 Hz, 2H), 5.30 (s, 2H), 7.45-7.31 (m, 5H), 8.52 (brs, 1H).

Synthesis of Benzyl 4-ethyl-5-formyl-3-methyl-1H-pyrrole-2-carboxylate (3). Compound **3** was synthesized using modifications of a known procedure.[2] Compound **2** (3.0 g, 12 mmol) was dissolved in a mixture of THF (125 mL), acetic acid (32 mL) and water (32 mL) and vigorously stirred at room temperature. To this mixture, cerium (IV) ammonium nitrate (28.2 g, 51 mmol) was added in a single portion. The reaction allowed to stir for 20 min before being poured into water (250 mL) and extracted three times with chloroform. The organic layers were combined, washed with saturated sodium bicarbonate and passed through a pad of silica gel. The solution was then concentrated via rotary evaporator and triturated with hexanes to give **3** as an off-white powder which was collected by filtration (2.6 g, 83 %). ^{1}H NMR (400 MHz, $CDCl_3$) δ 1.20 (t, *J* = 7.6 Hz, 3H), 2.31 (s, 3H), 2.75 (q, *J* = 7.6 Hz, 2H), 5.34 (s, 2H), 7.45-7.35 (m, 5H), 9.44 (brs, 1H), 9.77 (s, 1H).

Synthesis of (Dibenzyl 5,5'-((1E,1'E) -(1,2-phenylenebis(azanylylidene)) bis(methanylylidene)) bis(4-ethyl-3- methyl-1H-pyrrole-2-carboxylate)) (Pyrrophen, H_2L^1). Pyrrophen was synthesized using a modification from a known procedure.[3] To a solution containing compound **3** (1.1 g, 4.1 mmol) dissolved in a minimum amount of methanol, *o*-

phenylenediamine (0.22 g, 2 mmol) was added as a solid. The flask was loosely capped, and the mixture stirred at room temperature. After two hours, the ligand precipitated as a yellow powder; however, the reaction was allowed to stir overnight to go to completion. The product was collected by vacuum filtration (1.00 g, 82%), washed with methanol and ethanol, and used directly for metal complexation without further purification. ^{1}H NMR (400 MHz, $CDCl_3$) δ 1.08 (t, J = 7.5 Hz, 6H), 2.32 (s, 6H), 2.59 (q, J = 7.6 Hz, 4H), 5.31 (s, 4H), 7.12-7.06 (m, 2H), 7.26-7.21 (m, 2H), 7.43-7.28 (m, 10H), 8.30 (s, 2H), 9.71 (brs, 2H); HRMS (ESI) calculated for $C_{38}H_{39}N_4O_4$ ($[M + H]^+$) m/z = 615.2971, found 615.2977. CCDC 1936495.

Synthesis of dibenzyl 5,5'-((1E,1'E)-((4,5-dimethyl-1,2-phenylene)bis(azanylylidene))-bis(methanylylidene))bis(4-ethyl-3-methyl-1H-pyrrole-2-carboxylate) (Me_2Pyrrophen, H_2L^2). Dimethylpyrrophen was synthesized using a modification from a known procedure.[3] To a solution containing compound **3** (0.171 g, 0.63 mmol) dissolved in a minimum amount of methanol, 4,5-dimethyl-o-phenylenediamine (0.041 g, 0.3 mmol) was added as a solid and the mixture stirred at room temperature. Once completely dissolved, one drop of acetic acid was added and the flask closely capped. The reaction was stirred for an additional 30 min and the orange solution was then left to sit capped and undisturbed at room temperature for 48 hrs during which time a large crop of orange-yellow crystals formed, and were collected by vacuum filtration using a short-stemmed pipette and washed with methanol. Prior to filtration, a single crystal suitable for X-ray diffraction was isolated from the solution (Yield: 0.134 g, 69.4%). ^{1}H NMR (600 MHz, $CDCl_3$) δ 1.09 (t, *J* = 7.45 Hz, 6H), 2.30 (d, *J* = 1.72 Hz, 12H), 2.59 (q, *J* = 7.51 Hz), 3.46 (s, 2H), 5.28 (s, 4H), 6.90 (s, 2H), 7.26-7.41 (m, 10H), 8.31 (s, 2H), 10.25 (bs, 2H); HRMS (ESI+) calculated for $C_{40}H_{43}N_4O_6$ ($[M + H]^+$) *m/z* = 643.3284, found 643.3288. CCDC 1971893.

Synthesis of $Zn_2L^1_2$. H_2L^1 (0.100 g, 0.164 mmol) was dissolved in 21 mL of a 20:1 THF/MeOH (v/v) solution in a 50-mL round bottom flask at room temperature and stirred. $Zn(OAc)_2•2H_2O$ (0.043 g, 0.197 mmol, 1.2 equiv.) was added as a solid, causing a color change from bright yellow to intense orange. The flask was loosely capped and stirred at room temperature for 2 h before being reduced to a concentrate using a rotary evaporator, then stored at 0 °C overnight. The complex was collected as a bright orange crystalline powder by vacuum filtration (Yield: 0.070 g, 63%). ^{1}H NMR (400 MHz, $CDCl_3$) δ 1.09 (t, 6H), 2.16 (s, 6H), 2.48 (m, 4H), 4.27 (m, 2H), 5.21 (m, 2H), 6.42 (m, 2H), 6.77 (m, 4H), 6.88 (m, 8H), 7.52 (s, 2H); HRMS (ESI+) calculated for $C_{76}H_{73}N_8O_8Zn_2$ ($[M + H]^+$) *m/z* = 1355.4135, found 1355.4153. CCDC 1983238.

Synthesis of $Cu_2L^1_2$. H_2L^1 (0.100 g, 0.164 mmol) was dissolved in 21 mL of a 20:1 THF/MeOH (v/v) solution in a 50-mL round bottom flask at room temperature and stirred. $Cu(OAc)_2•H_2O$ (0.039 g, 0.197 mmol, 1.2 equiv.) was added as a solid, causing a color change from bright yellow to deep orange-brown. The flask was loosely capped and stirred at room temperature for 2 h before being reduced to a concentrate using a rotary evaporator, then stored at 0 °C overnight. The complex was collected as a bronze powder by vacuum filtration (Yield: 0.103 g, 93%); HRMS (ESI+) calculated for $C_{76}H_{73}N_8O_8Cu_2$ ($[M + H]^+$) *m/z* = 1354.4116, found 1354.4113. CCDC 1936510.

Synthesis of UO_2L^1: H_2L^1 (0.100 g, 0.164 mmol) was dissolved in 21 mL of a 20:1 THF/MeOH (v/v) solution in a 50-mL round bottom flask at room temperature and stirred. $UO_2(OAc)_2•2H_2O$ (0.083 g, 0.197 mmol, 1.2 equiv.) was added as a solid, causing a gradual color

change from bright yellow to deep red-brown. The flask was loosely capped and stirred at room temperature for 3 h before being reduced to a concentrate using a rotary evaporator, then stored at 0 °C overnight. The complex was collected as a bright orange crystalline powder by vacuum filtration (Yield: 0.098 g, 68%). ^{1}H NMR (400 MHz, $CDCl_3$) δ 1.38 (t, *J* = 7.60 Hz, 6H), 2.52 (s, 6H), 2.93 (q, *J* = 7.63 Hz, 4H), 5.89 (s, 4H), 7.36-7.43 (m, 8H), 7.62 (m, 4H), 7.87 (m, 2H), 9.88 (s, 2H); HRMS (ESI+) calculated for $C_{38}H_{37}N_4O_6U$ ($[M + H]^+$) *m/z* = 883.2111, found 883.3192. CCDC 1936509.

Synthesis of UO_2L^2. To a solution containing **H_2L^2** (0.0500 g, 0.0778 mmol) in m mL 9:1 THF:MeOH (v/v) (5 mL), $UO_2(OAc)_2$•$2H_2O$ (0.0330 mg, 0.0778 mmol) was added as a solid. The capped solution was left to stir at room temperature overnight (approximately 12 hrs). The solution was then concentrated via roto evaporator and chilled in a freezer for 48hrs to induce crystallization. Product was collected via vacuum filtration and washed in ether (24 mg, 34%). ^{1}H NMR (600 MHz, $CDCl_3$) δ 1.37 (t, *J* = 6.66 Hz, 6H), 2.43 (s, 6H), 2.51 (s, 6H), 2.92 (q, *J* = 6.43 Hz, 4H), 5.88 (s, 4H), 7.35-7.39 (m, 6H), 7.60 (m, 6H), 9.81 (s, 2H); HRMS (ESI+) calculated for $C_{40}H_{80}N_4O_6NaU$ ($[M + Na]^+$) *m/z* = 933.3353, found 933.3431. CCDC 1971927.

References

1. Pearson, R. G., Hard and soft acids and bases, HSAB, part 1: Fundamental principles. *Journal of Chemical Education* **1968,** *45* (9), 581.

2. Takao, K.; Akashi, S., Exploring the catalytic activity of Lewis-acidic uranyl complexes in the nucleophilic acyl substitution of acid anhydrides. *RSC Advances* **2017,** *7* (20), 12201-12207.

3. Thuéry, P.; Harrowfield, J., Uranyl Ion Complexes with trans-3-(3-Pyridyl)acrylic Acid Including a Uranyl–Copper(II) Heterometallic Framework. *Eur. J. Inorg. Chem.* **2014,** *2014* (28), 4772-4778.

4. DeVore II, M. A.; Kerns, S. A.; Gorden, A. E. V., Characterization of Quinoxolinol Salen Ligands as Selective Ligands for Chemosensors for Uranium. *Eur. J. Inorg. Chem.* **2015,** *2015* (34), 5708-5714.

5. Jeazet, H. B. T.; Gloe, K.; Doert, T.; Mizera, J.; Kataeva, O. N.; Tsushima, S.; Bernhard, G.; Weigand, J. J.; Lindoy, L. F.; Gloe, K., Uranyl(VI) binding by bis(2-hydroxyaryl)diimine and bis(2-hydroxyaryl)diamine ligand derivatives. Synthetic, X-ray, DFT and solvent extraction studies. *Polyhedron* **2016,** *103*, 198-205.

6. Sessler, J. L.; Seidel, D.; Vivian, A. E.; Lynch, V.; Scott, B. L.; Keogh, D. W., Hexaphyrin(1.0.1.0.0.0): An Expanded Porphyrin Ligand for the Actinide Cations Uranyl (UO_2^{2+}) and Neptunyl (NpO_2^{+}). *Angew. Chem. Int. Ed.* **2001,** *40* (3), 591-594.

7. Brewster, J. T.; He, Q.; Anguera, G.; Moore, M. D.; Ke, X.-S.; Lynch, V. M.; Sessler, J. L., Synthesis and characterization of a dipyriamethyrin–uranyl complex. *Chem. Comm.* **2017,** *53* (36), 4981-4984.

8. Andrews, M. B.; Cahill, C. L., Uranyl Bearing Hybrid Materials: Synthesis, Speciation, and Solid-State Structures. *Chem. Rev.* **2013,** *113* (2), 1121-1136.

9. Sessler, J. L.; Vivian, A. E.; Seidel, D.; Burrell, A. K.; Hoehner, M.; Mody, T. D.; Gebauer, A.; Weghorn, S. J.; Lynch, V., Actinide expanded porphyrin complexes. *Coord. Chem. Rev.* **2001,** *216-217*, 411-434.

10. Sessler, J. L.; Melfi, P. J.; Seidel, D.; Gorden, A. E. V.; Ford, D. K.; Palmer, P. D.; Tait, C. D., Hexaphyrin(1.0.1.0.0.0). A new colorimetric actinide sensor. *Tetrahedron* **2004,** *60* (49), 11089-11097.

11. Sessler, J. L.; Gorden, A. E. V.; Seidel, D.; Hannah, S.; Lynch, V.; Gordon, P. L.; Donohoe, R. J.; Drew Tait, C.; Webster Keogh, D., Characterization of the interactions between neptunyl and plutonyl cations and expanded porphyrins. *Inorg. Chim. Acta* **2002,** *341*, 54-70.

12. Brewster, J. T., 2nd; Mangel, D. N.; Gaunt, A. J.; Saunders, D. P.; Zafar, H.; Lynch, V. M.; Boreen, M. A.; Garner, M. E.; Goodwin, C. A. P.; Settineri, N. S.; Arnold, J.; Sessler, J. L., In-Plane Thorium(IV), Uranium(IV), and Neptunium(IV) Expanded Porphyrin Complexes. *J Am Chem Soc* **2019,** *141* (44), 17867-17874.

13. Brewster, J. T.; Zafar, H.; Root, H. D.; Thiabaud, G. D.; Sessler, J. L., Porphyrinoid f-Element Complexes. *Inorg. Chem.* **2020,** *59* (1), 32-47.

14. DeVore, M. A.; Gorden, A. E. V., Copper and uranyl extraction from aqueous solutions using bis-dithiophosphinate ligands have been characterized. *Polyhedron* **2012,** *42* (1), 271-275.

15. DeVore, M. A., II; Kerns, S. A.; Gorden, A. E. V., Characterization of Quinoxolinol Salen Ligands as Selective Ligands for Chemosensors for Uranium. *Eur. J. Inorg. Chem.* **2015,** *2015* (34), 5708-5714.

16. Wu, Z.; Chen, Q.; Xiong, S.; Xin, B.; Zhao, Z.; Jiang, L.; Ma, J. S., Double-Stranded Helicates, Triangles, and Squares Formed by the Self-Assembly of Pyrrol-2-ylmethyleneamines and ZnII Ions. *Angew. Chem. Int. Ed.* **2003,** *42* (28), 3271-3274.

17. Bhowon, M. G.; Li Kam Wah, H.; Dosieah, A.; Ridana, M.; Ramalingum, O.; Lacour, D., Synthesis, Characterization, and Catalytic Activity of Metal Schiff Base Complexes Derived from

Pyrrole-2-carboxaldehyde. *Synthesis and Reactivity in Inorganic and Metal-Organic Chemistry* **2004,** *34* (1), 1-16.

18. Maeda, H., Supramolecular Chemistry of Acyclic Oligopyrroles. *European Journal of Organic Chemistry* **2007,** *2007* (32), 5313-5325.

19. Munro, O. Q.; Joubert, S. D.; Grimmer, C. D., Molecular Recognition: Preorganization of a Bis(pyrrole) Schiff Base Derivative for Tight Dimerization by Hydrogen Bonding. *Chem. Eur. J.* **2006,** *12* (31), 7987-7999.

20. Bacchi, A.; Carcelli, M.; Gabba, L.; Ianelli, S.; Pelagatti, P.; Pelizzi, G.; Rogolino, D., Syntheses, characterization and X-ray structure of palladium(II) and nickel(II) complexes of tetradentate pyrrole containing ligands. *Inorg. Chim. Acta.* **2003,** *342*, 229-235.

21. Yang, L.; Chen, Q.; Li, Y.; Xiong, S.; Li, G.; Ma, Jin S., Self-Assembly of Bis(pyrrol-2-ylmethyleneamine) Ligands with CuII Controlled by Bridging [−(CH2)n−] Spacers and Weak Intermolecular C−H···Cu Hydrogen Bonding. *Eur. J. Inorg. Chem.* **2004,** *2004* (7), 1478-1487.

22. Xu, H.; Xu, D. C.; Wang, Y., Natural Indices for the Chemical Hardness/Softness of Metal Cations and Ligands. *ACS Omega* **2017,** *2* (10), 7185-7193.

23. Shannon, R., Revised effective ionic radii and systematic studies of interatomic distances in halides and chalcogenides. *Acta Crystallographica Section A* **1976,** *32* (5), 751-767.

24. Thyrann, T.; Lightner, D. A., Oxidation of Pyrrole Alpha-Methyl to Formyl with Ceric Ammonium-Nitrate. *Tetrahedron Letters* **1995,** *36* (25), 4345-4348.

25. Bobal, P.; Lightner, D. A., An inexpensive, selective procedure for oxidizing alpha-methyl to alpha-formyl pyrroles. *J Heterocyclic Chem* **2001,** *38* (5), 1219-1221.

26. Allen, W. E.; Gale, P. A.; Brown, C. T.; Lynch, V. M.; Sessler, J. L., Binding of Neutral Substrates by Calix[4]pyrroles. *J. Am. Chem. Soc.* **1996,** *118* (49), 12471-12472.

27. Sathish Kumar, B.; Panda, P. K., 1D water chain stabilized by meso-expanded calix[4]pyrrole. *Crystengcomm* **2014,** *16* (37), 8669-8672.

28. Mayhugh, J. T.; Niklas, J. E.; Forbes, M. G.; Gorden, J. D.; Gorden, A. E. V., Pyrrophens: pyrrole-based macroacyclic hexadentate ligands tailor-made for uranyl (UO_2^{2+}) coordination and molecular recognition. *Inorg. Chem. (Submitted)* **2020**.

29. Anzenbacher, P.; Jursíková, K.; Lynch, V. M.; Gale, P. A.; Sessler, J. L., Calix[4]pyrroles Containing Deep Cavities and Fixed Walls. Synthesis, Structural Studies, and Anion Binding Properties of the Isomeric Products Derived from the Condensation of *p*-Hydroxyacetophenone and Pyrrole. *J. Am. Chem. Soc.* **1999,** *121* (47), 11020-11021.

30. Sessler, J. L.; Vivian, A. E.; Seidel, D.; Burrell, A. K.; Hoehner, M.; Mody, T. D.; Gebauer, A.; Weghorn, S. J.; Lynch, V., Actinide expanded porphyrin complexes. *Coordination Chemistry Reviews* **2001,** *216-217* (Supplement C), 411-434.

31. Noufele, C. N.; Pham, C. T.; Hagenbach, A.; Abram, U., Uranyl Complexes with Aroylbis(N,N-dialkylthioureas). *Inorg. Chem.* **2018,** *57* (19), 12255-12269.

32. Zhang, Q.; Jin, B.; Zheng, T.; Tang, X.; Guo, Z.; Peng, R., Hexadentate β-Dicarbonyl(bis-catecholamine) Ligands for Efficient Uranyl Cation Decorporation: Thermodynamic and Antioxidant Activity Studies. *Inorg. Chem.* **2019**.

33. Hayton, T. W.; Wu, G., Exploring the Effects of Reduction or Lewis Acid Coordination on the U═O Bond of the Uranyl Moiety. *Inorg. Chem.* **2009,** *48* (7), 3065-3072.

34. Niklas, J. E.; Hardy, E. E.; Gorden, A. E. V., Solid-state structural elucidation and electrochemical analysis of uranyl naphthylsalophen. *Chem. Comm.* **2018,** *54* (83), 11693-11696.

35. http://supramolecular.org.

36. Thordarson, P., Determining association constants from titration experiments in supramolecular chemistry. *Chem. Soc. Rev.* **2011,** *40* (3), 1305-1323.

37. Brynn Hibbert, D.; Thordarson, P., The death of the Job plot, transparency, open science and online tools, uncertainty estimation methods and other developments in supramolecular chemistry data analysis. *Chem. Comm.* **2016,** *52* (87), 12792-12805.

38. Ercolani, G., Assessment of Cooperativity in Self-Assembly. *J. Am. Chem. Soc.* **2003,** *125* (51), 16097-16103.

39. Vukovic, S.; Hay, B. P.; Bryantsev, V. S., Predicting Stability Constants for Uranyl Complexes Using Density Functional Theory. *Inorg. Chem.* **2015,** *54* (8), 3995-4001.

40. Rounaghi, G.; Kakhki, R. M. Z., Thermodynamic study of complex formation between dibenzo-18-crown-6 and UO_2^{2+} cation in different non-aqueous binary solutions. *Journal of Inclusion Phenomena and Macrocyclic Chemistry* **2008,** *63* (1), 117.

41. Rounaghi, G. H.; Nazari, E.; Ghaemi, A.; Mohajeri, M., Complexing ability of a macrocyclic ligand, dibenzo-24-crown-8, with UO_2^{2+} in some binary mixed non-aqueous solvents. *J. Coord. Chem.* **2010,** *63* (13), 2349-2359.

42. Baker, R. J., New Reactivity of the Uranyl(VI) Ion. *Chem. Eur. J.* **2012,** *18* (51), 16258-16271.

43. Fillaux, C.; Guillaumont, D.; Berthet, J.-C.; Copping, R.; Shuh, D. K.; Tyliszczak, T.; Auwer, C. D., Investigating the electronic structure and bonding in uranyl compounds by combining NEXAFS spectroscopy and quantum chemistry. *Phys. Chem. Chem. Phys.* **2010,** *12* (42), 14253.

44. Kano, K.; Minamizono, H.; Kitae, T.; Negi, S., Self-Aggregation of Cationic Porphyrins in Water. Can π–π Stacking Interaction Overcome Electrostatic Repulsive Force? *J. Phys. Chem.* **1997,** *101* (34), 6118-6124.

Chapter 5

Conclusions and Future Work

5.1 | Conclusions

Uranyl complexes featuring a variety of imine donor ligands, including those of the tetradentate phen-BIAN, gbha,[1-2] salophen and bis-salophen types,[3] and the hexadentate pyrrole-containing pyrrophen system (**Figure 5.1**),[4] have been prepared and characterized through X-ray diffraction, UV-Vis and IR spectroscopy, and electrochemical techniques. Many of these ligands represent either novel frameworks or new derivatives of existing ligands and are strategically designed for uranyl coordination. This makes them powerful tools with which to study coordination chemistry and redox behavior of f-elements.

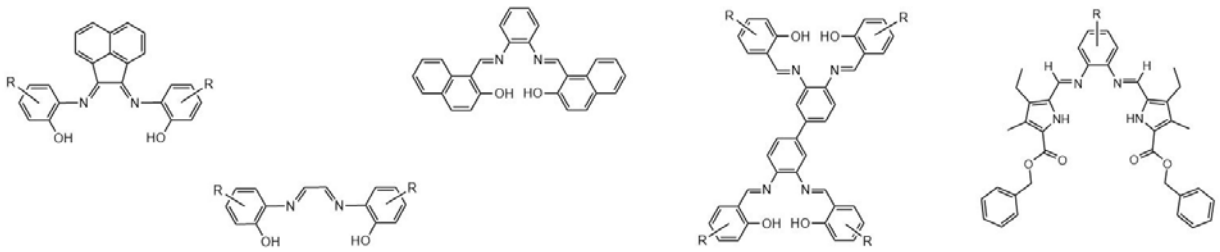

Figure 5.1. Ligand types examined in this work (left to right: phen-BIAN, gbha, naphthylsalophen, bis-salophen, and pyrrophen). phen-BIAN and gbha ligands shown in "open" form.

The phen-BIAN ligands which integrate the redox-active α-diimine and acenaphthene backbone of aryl-BIANs with a more traditional O-N-N-O salen-type pocket were investigated for their potential to more closely examine the redox-chemistry of uranyl complexes. The first uranyl phen-BIAN complex isolated, $[UO_2(t\text{-bu})\text{phen-BIAN})]_2$ (**UO_2-2b**), is a μ-phenolato bridged dimeric species which features interactions between the oxo ligands and CH_2Cl_2 or $CHCl_3$ protons depending on the crystallization conditions.[1] This was the only uranyl phen-BIAN derivate that could be crystallized due to the poor solubility of most of these species; however, four uranyl gbha derivates were crystallized (**UO_2-1b,c,e,f**), all of which engage in similar oxo-proton interactions,

one of which is also associated with an increase in one of the U=O bond lengths from the typical ~1.76-1.78 Å to 1.809 (9) Å.[2] Both the phen-BIAN and gbha uranyl complexes feature redox-activty consistent with stepwise reduction of the complexes (to varying degrees) through a series of formally mixed-valent states. Incorporation of the acenaphthene backbone led to more positive reduction potentials (**UO_2-2b**) than for the less-conjugated gbha species (**UO_2-1b**) and allowed for greater stabilization of the reduced complexes.[1-2] Additionally, the asymmetric stretching frequencies ($\nu_{3,O=U=O}$) of the phen-BIAN complexes (**UO_2-2a-f**) were overall lower than those of the gbha complexes (**UO_2-1a-f**), indicating greater covalent contributions in the equatorial plane for **UO_2a-f**, and in cases where an electron-donating group was positioned *para* to the imine nitrogen (**UO_2-2c,e**), significantly lower stretcher frequencies were observed than for their gbha counterparts, implicating the electronic environment of the imine nitrogen donors as a greater contributor to the covalent character of the metal-ligand interaction than the phenolic oxygen donors.[2] This work represents the addition of a new class of ligands to the current repertoire of redox-active frameworks with which to study the structural and electrochemical properties of uranyl complexes, and highlights the value of ligand conjugation in these systems.

The complex uranyl naphthylsalophen (**UO_2L**) was characterized crystallographically and in solution, and was of interest for its more highly-conjugated framework in particular as compared to standard salophen species.[3] In the solid-state, this complex exists as a water coordinated monomer which hydrogen-bonds to an adjacent unit, and these units pack as pseudo-tetramers via additional hydrogen-bonding and uranyl oxo-proton interactions.[3] Electrochemical studies of the complex revealed that the uranyl U(VI)/U(V) couple was slightly more negative than is typical for uranyl salophen complexes,[5] but also that coordination resulted in a 260 mV positive shift of the ligand reduction potential and sweep-range dependent behavior that indicate significant metal-

ligand communication.[3] Additional investigations into the utility of the salophen framework led to the employment of bis-salophens, which link two salophen units through a biphenyl spacer. The dinuclear uranyl complex of bis-naphthylsalophen (**$(UO_2)_2L1$**) was characterized and compared to its monomeric counterpart. More positive U(VI)/U(V) reduction potentials were observed for the dinuclear complex (**$(UO_2)_2L1$**) than for the mononuclear species **UO_2L**,[3] but the differing solvents and reference electrode types limit the conclusions that can be drawn. Another bis-salophen ligand derivative, bis-diethylaminosalophen (**H_4L2**) was also studied, and upon coordination to Th(IV) was observed to form the trinuclear complex, **$[ThL_2]_3$**, which stands to be the first circular thorium helicate reported.[6] This species features a planar cavity that may be useful for anion or neutral molecule recognition, and studies are under way to determine if this type of actinide helicate complex shows potential on this front. The possibility for further tuning of the salicylidene arms and biphenyl linker could also allow for the formation of higher-order complexes with larger three-dimensional void space. The use of these flexible bis-salophen ligands in actinide coordination chemistry is unprecedented and has many opportunities for further assessment of the properties of polynuclear actinide complexes.

The pyrrophen ligands, which share the mixed imine/pyrrole pocket of macrocyclic expanded porphyrins and the flexible, mixed O/N-donor pocket of salophens were employed to investigate the ability to selectively coordinate uranyl over transition metal and lanthanide ions.[4] The unique structure of pyrrophens allows them to coordinate transition metal ions such as Cu^{2+} and Zn^{2+} as tetradentate N-donor ligands through self-assembly into dinculear helicates, and to completely satisfy the equatorial plane of uranyl as a hexadentate O-N-N-O ligand. In the solid-state, the uranyl complexes **UO_2L^1** and **UO_2L^2** adopt unusually planar conformations and the uranium atoms sit almost perfectly in the center of the pockets indicating that these frameworks are very

well-suited to the size and geometry of the uranyl ion.[4] Additionally, the softer nature of these donor atoms in combination with the ability to delocalize pyrrole electron density throughout the π-system demonstrates favorable interactions between uranyl and softer-donor ligands. The disparate coordination modes of these ligands and the distinct colors of the complexes of the unsubstituted $\mathbf{L^1}$ in solution prompted us to explore the potential of this system to function as a uranyl sensor. While the binding of $\mathbf{H_2L^1}$ to uranyl is unfortunately slow at low concentrations, $\mathbf{H_2L^2}$ does show improved kinetics, demonstrating the potential of this system to be tuned for more favorable coordination of uranyl. Additionally, UO_2^{2+} can displace Zn^{2+} from the complex $\mathbf{Zn_2(L^1)_2}$, which is the only complex with a color that is not visually distinct from that of the uranyl complex. As pyrrophen shows no affinity for Ln^{3+} ions or Th^{4+}, the modularity of this ligand system makes it promising as a new candidate for continued studies in the molecular recognition of uranyl. This work again represents a novel framework with which to examine the fundamental aspects of uranyl coordination and to move towards the development of selective chemosensors.

Much of the focus of this research has been the development of the redox-active ligand "phen-BIAN" and its derivatives along with preparation of the analogous gbhas, and the employment of this suite of ligands to elucidate the impacts of electronic flexibility and extended conjugation in the equatorial plane on the solid-state structural features, reductive chemistry, and covalent interactions in their uranyl complexes.[1-2] The findings of these studies informed investigations into both the salophen and pyrrophen classes of ligands. Careful attention to the results of what evolved into a multi-faceted project has allowed for the valuable visualization of several key trends across this set of related but distinctive complexes, namely the surprising array of redox behavior of these uranyl species, their molecular structures which contain an unusually high presence of

interactions between “inert” uranyl oxo ligands and solvent or other protons, and the relationship between more highly-conjugated equatorial ligands and observations that indicate a higher degree of metal-ligand covalency. Most of these trends emerge for the phen-BIAN, gbha, and salophen-based systems, as these species were examined in the context of better understanding fundamental uranyl chemistry.[1-3] The related pyrrophen studies emphasize the potential of such systems to act as selective or colorimetric uranyl sensors, and while the motivations of this work gravitate towards applications, this is an example where fundamental chemistry and applications overlap. Again, the functionality of a large π-system is highlighted. Each of these imine-containing ligand systems has potential for continued studies of the unique behaviors of actinides.

5.2 | Future Work and Preliminary Findings

As this work consists largely of novel ligand systems for which the groundwork has only begun, there is still considerable work to be done using these systems to explore fundamental actinide chemistry. The ligands presented here may serve as suitable scaffolds for exploring the reduction of uranyl or the coordination of tetravalent uranium and thorium species and their bonding and redox behaviors. In some cases, these could serve as suitable models for characterizing the differences among actinyl ions. Each branch of this research has opportunies for expanding the repertoire of ligand derivatives though which to study the behavior of actinides, as well as for examining these behaviors more deeply as they relate to the reduction of uranyl, lower-valent uranium complexes, and potentially transuranic species.

Modifications to the BIAN Framework and Reductions

The BIAN-type backbone has been shown to be of great utility in exploring the electrochemical behavior of uranyl species.[1-2] The presence of the phenolic-donor/diimine-acceptor units within the same framework presents one opportunity for examining how intraligand charge transfer processes are impacted by coordination to uranyl. This raises the question if there is potentially evidence of non-classical π-backbonding-type interactions. As uranyl phen-BIAN complexes feature a Lewis acidic center trapped between the donor and acceptor moieties, it could be of great value to investigate through computational analysis if the uranium center participates in this charge transfer process, and if so, to what extent. Though this is one feature that may offer additional depth of understanding of fundamental behaviors, it also may be the root of the difficulties in obtaining U(IV) complexes of phen-BIAN.

Efforts to isolate phen-BIAN U(IV) complexes from a variety of U(IV) starting materials (UCl_4, $U[N(SiMe_3)_2]_4$, U^0 metal) have proven unfruitful, even under rigourously air-free conditions—preliminary analysis of the resulting products of such reactions by NMR, IR, and X-ray diffraction have indicated formation of the uranyl species. Reasons for this behavior are unclear as the origin of the oxidation to uranyl has not yet been systematically pursued. It is worth future investigations into the utility of an exclusively nitrogen-donor pocket that may be more robust. Proposed ligand architectures (**L^A1-3**) based on the acenaphthene backbone with which to do this are listed in **Scheme 5.1**. These ligands may also be suitable for uranyl coordination, and would allow for comparisons to be made between the mixed-donor pocket of phen-BIANs and a softer N-donor pocket. Improvement and derivitization of this ligand system may facilitate a wider range of impactful physiochemical data to be obtained on BIAN-type uranyl complexes.

L^{A}1 has been previously reported as the dinuclear zinc chloride complex, but the synthesis of the free ligand has not been achieved.[7] Templation of the ligand around UO_2^{2+}or U(IV) in the presence of triethylamine may prove to be a promising synthetic starting point. 8-Aminoquinoline is air-sensitive, so inert atmosphere techniques would be required for the synthesis of a U(IV) or a uranyl complex. As quinoline-containing species often have useful flourescence properties and have been used as sensors for a variety of metal ions including UO_2^{2+}, a rigid iminoquinoline ligand such as **L^{A}1** would be ideal not only for investigating lower-valent uranium chemistry, but potentially the sensing of uranyl as well. Proposed ligands **L^{A}2** and **L^{A}3** have larger bite angles than **L^{A}1** and the other ligands discussed in this text and may be less suitable for uranyl

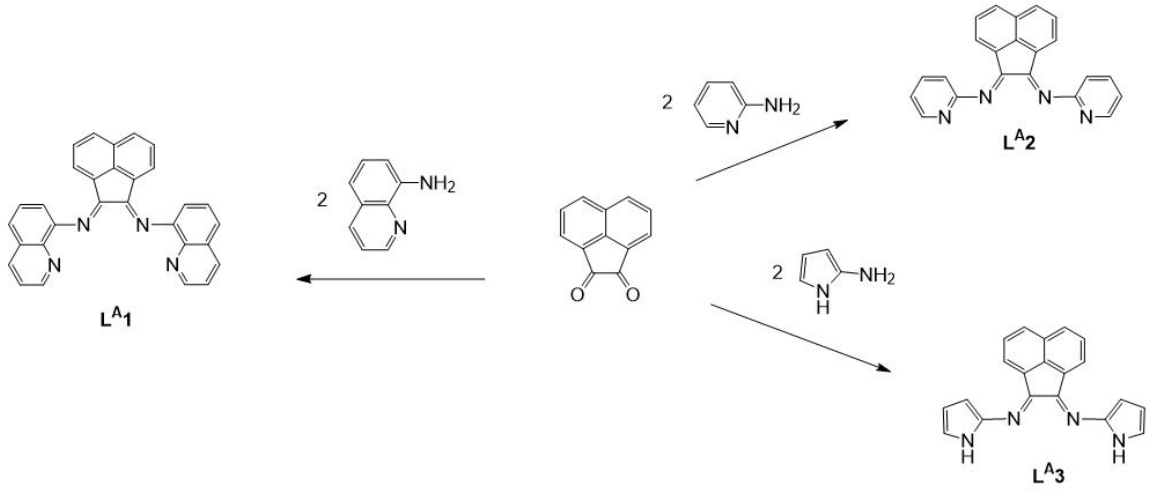

Scheme 5.1. Proposed acenaphthene-based BIAN-type N-donor ligands **L^{A}1-3**, and corresponding amine starting materials (1 – 8-aminoquinoline; 2 – 2-aminopyridine; 3 – 2-aminopyrrole).

coordination; however, they may accommodate the larger ionic radius of U(IV). Neither of these species has been reported previously, but the 3-aminopyridyl derivative of **L^{A}2** has, and is synthesized by the neat reaction of acenaphthenequinone and excess 3-aminopyridine (m.p. 65 °C) at 150 °C,[8] and an analogous preparation should be viable using 2-aminopyridine (m.p. ~60 °C).

In addition to assembling new N-donor tetradentate phen-BIAN derivatives, additional studies on the reduction of existing phen-BIAN ligands and their uranyl complexes should be explored. Two primary routes to accomplish this are through initial reduction of the ligand with alkali metals (Na or K) as done for Ar-BIAN species[9-10] before reaction with uranyl, or by the addition of a one-electron reducing agent such as decamethylcobaltocene (Cp^*_2Co)[11] to the uranyl phen-BIAN complex. Since both the α-diimine and naphthalene π-system can be used for electron storage and to transfer stored electrons to a metal center, [12-13] the use of this system to reduce UO_2^{2+} is promising. The four-step sodium reductions of dpp-BIAN reported by Fedushkin allowed for isolation of mono-, di-, tri- and tetra-anion forms of the ligand,[9] and this sequence should be transferrable to phen-BIAN ligands as well, though the presence of the phenol moieties theoretically allows for access to two additional ligand oxidation states should they be tolerated by the framework. Initial investigations into the sodium reduction of (*t*-bu)phen-BIAN (**2b**) have already been conducted but with limited results. In the course of the reaction of **2b** with excess Na^0 (~50 equiv.) which was washed and dried using hexanes under an inert atmosphere, distinct solution colors were observed upon addition of the ligand (dark violet) and after 2.5 hours (dark green), and NMR of the isolated dark green solid unsurprisingly indicated a paramagnetic material. Also of note is that the reaction of the ligand with one equivalent of anhydrous KH resulted in the formation of a dark red solution, and upon addition of a second equivalent, the dark violet solution observed during sodium reduction. This suggests the red color is associated with the monoanionic form of the ligand, purple with the dianionic form, and green with a further-reduced radical form. Follow-up studies of these ligand species and their reactions with uranyl and U(IV) would be particularly interesting, and the full extent of the redox-activity of these ligands should be explored for lower-valent uranium chemistry.

BIAN-like Salophens

While many of the investigations in this work entailed the use BIAN-type ligands which were designed to coordinate more like salen and salophen species, preliminary studies were also conducted on a salophen-type ligand which was inspired by the BIAN backbone. The two crystal structures are of publishable quality, but have not yet been finalized due to more extensive modeling required for partial-occupancy solvent molecules. These ligands feature an extended acenaphthoquinoxaline backbone, composed of fused acenaphthene and quinoxaline systems, which is intended to impart signficicant fluorescent character to the ligand as well as to support extensive redox chemistry. The diamine, 9,10-diamino-acenaphtho[1,2-*b*]quinoxaline ("daq") is

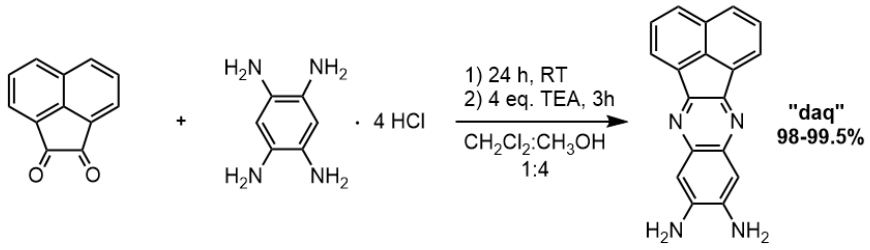

Scheme 5.2. Synthesis of "daq".

synthesized cleanly in near-quantitative yields from acenaphthenequinone and 1,2,4,5-tetraaminobenzene tetrahydrochloride at room temperature (**Scheme 5.2**), and can be reacted with salicylaldehydes to form symmetric and asymmetric Schiff base ligands (**Figure 5.2**). Further optimization of the reaction conditions is necessary in order to form these species reliably and in suitable yields. The poor solubility of the one-arm species drives its formation over the symmetric ligand. This an impediment to isolating the tetradentate species, but is also an opportunity for the synthesis of asymmetric ligands, should those be desired.[14-15] In the attempted synthesis of **1-aq**, the main product formed was **1-aq(NH$_2$)**, as determined by ^{1}H NMR. The symmetric *t*-butyl-

derived ligand **1-aq** was characterized by X-ray diffraction using a single crystal that grew from the reaction filtrate (**Figure 5.4**). The asymmetric unit of this species contains two ligand molecules which π-stack together (plane-to-plane distance: 3.58 Å) and engage in several hydrogen-bonding interactions with associated solvent molecules. Due to the small scale of this preparation, yield and bulk purity could not be established; however, solid-state UV-Vis and

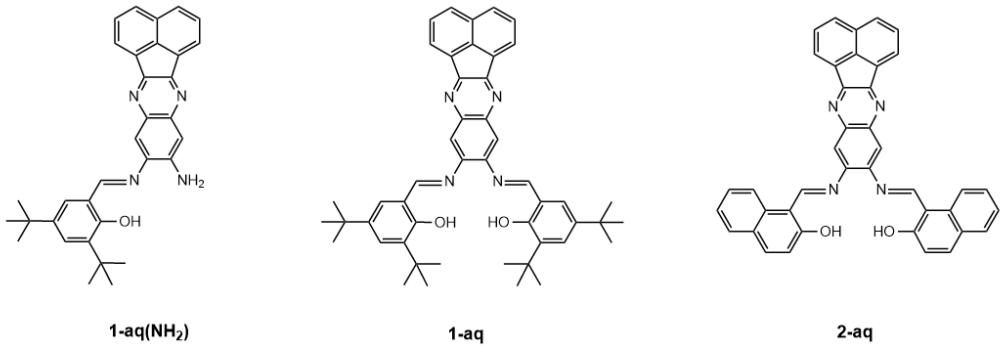

Figure 5.3. Asymmetric and symmetric ligands **1-aq(NH$_2$)** and **1-aq** resulting from the reaction of **daq** with 5.8 equiv. TFA (solid and filtrate, respectively), and proposed ligand **2-aq**.

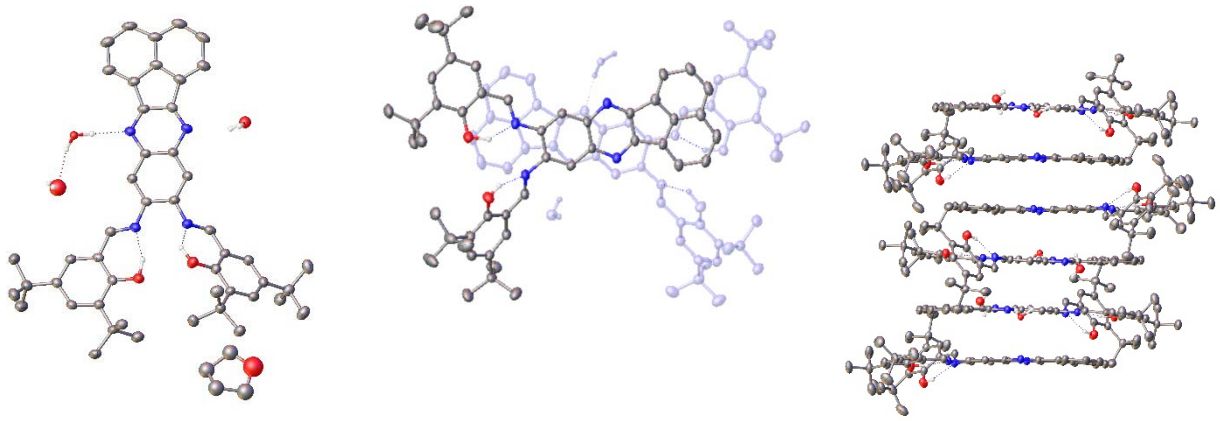

Figure 5.4. (Left to right) Crystal structure of **1-aq**, asymmetric unit, and packing. All non-interacting hydrogen atoms removed for clarity. Thermal ellipsoids at 50%.

fluorescence spectra were recorded using the single-crystalline sample (**Figure 5.5**). **1-aq** features a broad absorption from 325-450 nm and a small shoulder near 555 nm. During data collection, it was evident that some faces of the crystals appeared to have more intense fluorescence that was not solely related to crystal thickness. The emission spectra collected at 365 nm and 546 nm primarily feature a band around 625-630 nm, and were sampled from two side-by-side crystals

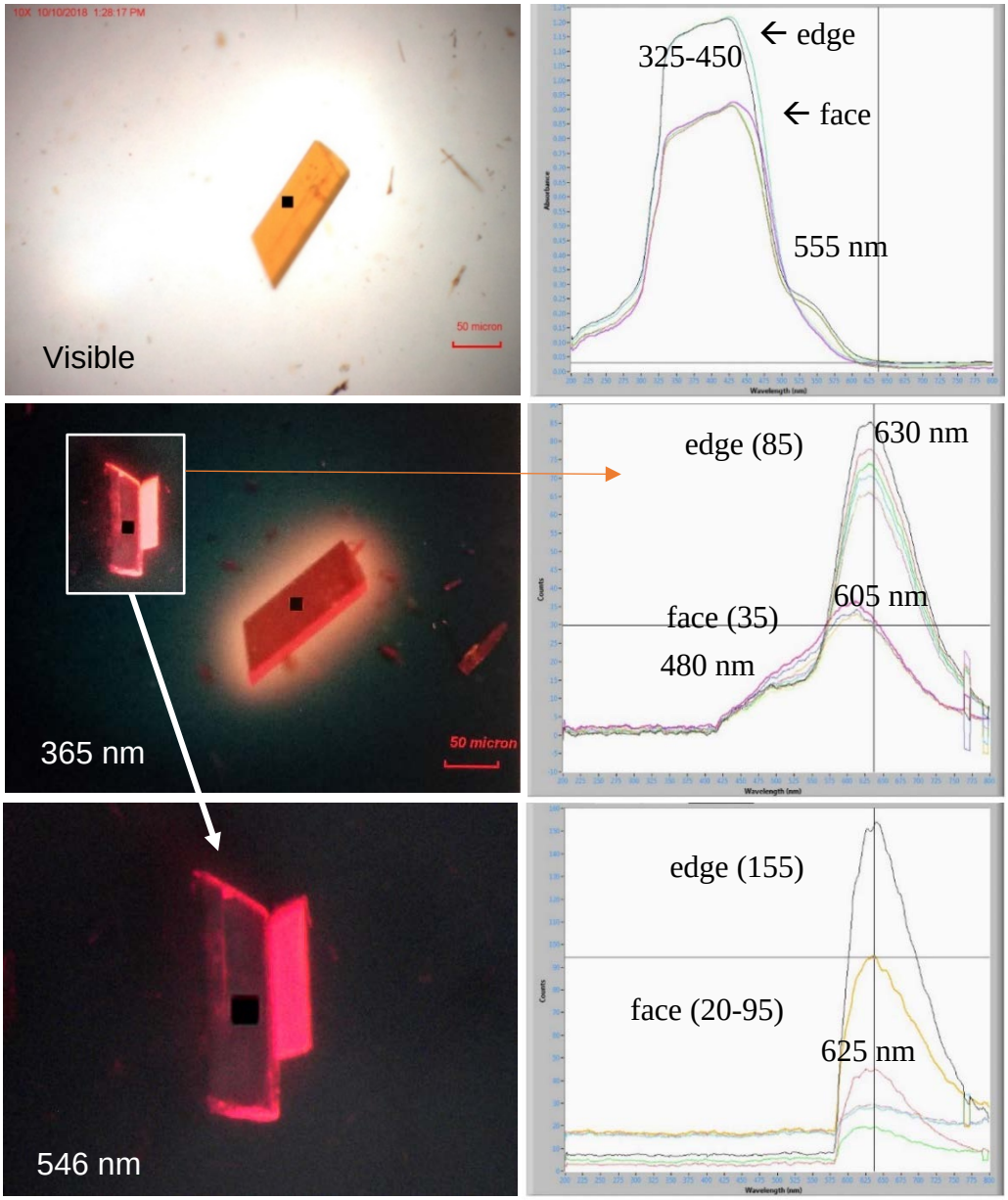

Figure 5.5. Photos of crystals taken under visible, 365 nm, and 546 nm light and corresponding solid-state absorption or emission spectra sampled fromdifferent crystal faces/orientations. Numbers in parentheses denote counts.

which were of approximately the same thickness in the chosen orientations to highlight the large differences in emission along different crystal axes. This is consistent with the π-stacking observed in the extended structure. Through the incorporation of different salicylaldehyde substituents, the fluorescence properties should be tunable, as different steric and electrostatic interactions will influence the distance between the backbones. Fluorescence studies in the solution state have not yet been conducted.

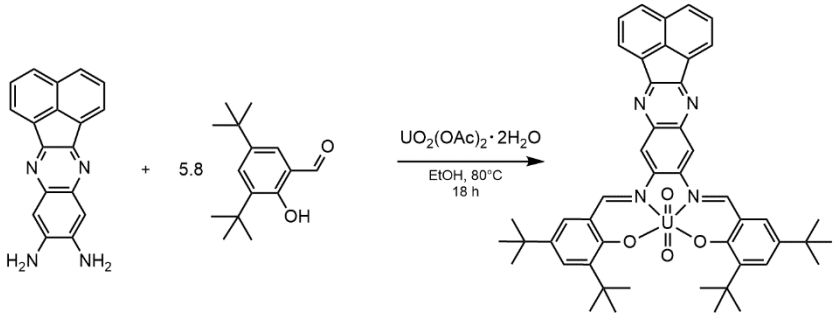

Scheme 5.2. Synthesis of **UO_2(1aq)** by templation.

The uranyl complex **UO_2(1-aq)** was synthesized by templating with uranyl (**Scheme 5.2**), as no substantial amount of the free ligand **1-aq** was isolated. Single crystals suitable for X-ray diffraction were harvested from the concentrated filtrate, giving the structure shown in **Figures 5.6** and **5.7**, which features similar π-stacking to that of the free ligand, with a plant-to-plane distance of 3.80 Å. On coordination, the ligand distorts significantly from the planar structure shown in **Figure 5.4**. Though the acenaphthoquinoxaline backbone remains rigid, it lies at a ~70° angle to the uranyl fragment, likely to maximize π-stacking interactions while accommodating the linear uranyl ion. This is fairly typical behavior for uranyl salophen species (some reported species have angles of 76° and 80°),[3, 16] but this angle is somewhat steeper and appears exaggerated due

to the absurd size of the backbone. No fluorescence was observed for the complex in the solution or solid state.

Syntheses of **2-aq** and its uranyl complex were attempted as well, and their preparations are

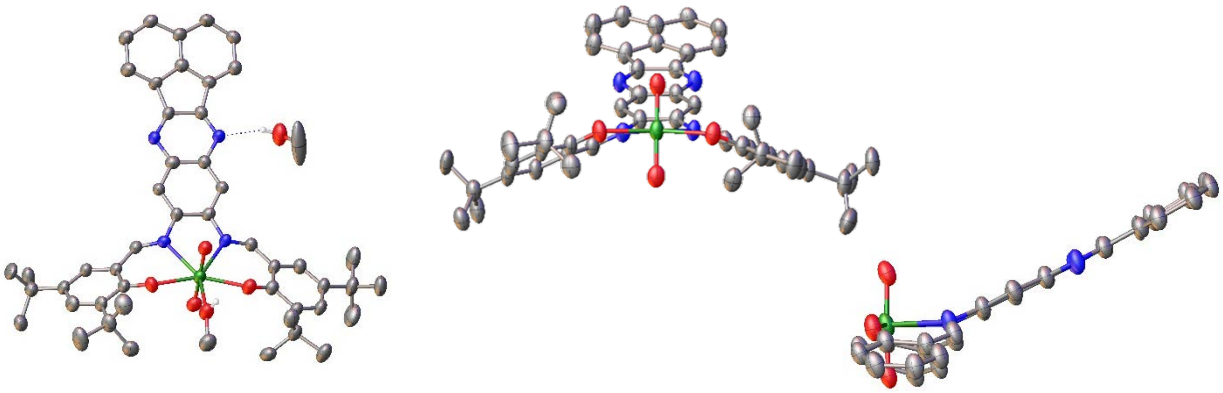

Figure 5.6. Crystal structure of **UO_2(1-aq)**, including view down the O-N-N-O plane (coordinated methanol omitted) and side view down the horizontal plane of the backbone (coordinated methanol and *t*-butyl groups omitted). All non-interacting hydrogen atoms removed for clarity. Thermal ellipsoids at 50%.

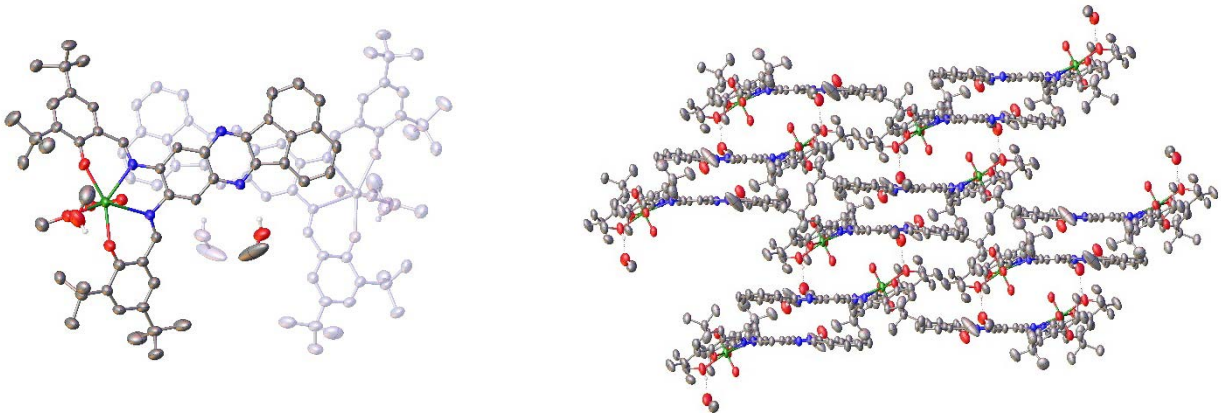

Figure 5.7. Packing of **UO_2(1-aq)**, highlighting stacking of molecules along *c*-axis. All non-interacting hydrogen atoms removed for clarity. Thermal ellipsoids at 50%.

reported; however, these reactions yielded products with very poor solubility, and follow-up characterization has not been done. In general, the synthesis of these ligand frameworks still requires attention and optimization. Though the two-arm ligand **1-aq** has been confirmed crystallographically, the one-arm ligand is the primary product. Nonetheless, the interesting solid-state and fluorescence properties of these species as well as their tunability warrants further

investigation into their use as supporting ligands for uranyl and lower-valent uranium. The immense, conjugated backbone also makes these uranium complexes of interest electrochemically as there is ample electron storage.

Actinide Bis-Salophen Complexes

The isolation of the trinuclear thorium helicate of bis-diethylaminosalophen (**[ThL2]**$_3$) and its unique structure have prompted further study of the supramolecular chemistry of tetravalent actinides. Synthesis of the U(IV) analogue of this complex as well as of a set of Th(IV) and U(IV) bis-salophen derivatives, including those of strictly N-donors (**Figure 5.8**) is ongoing. The

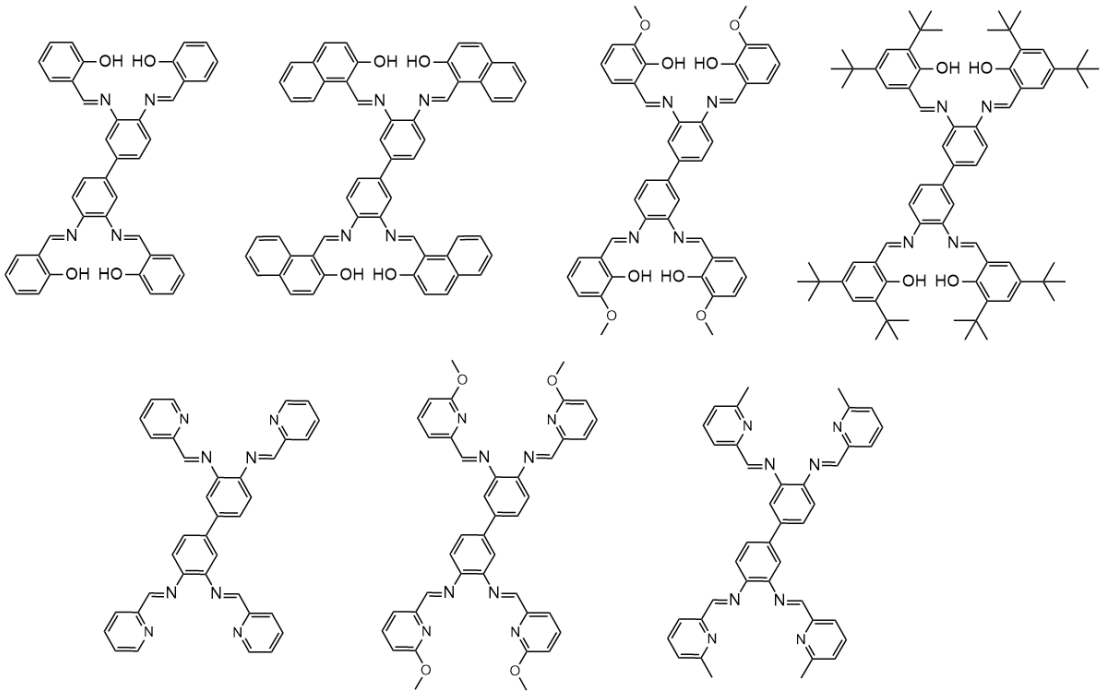

Figure 5.8. Proposed derivatives of the bis-salophen framework.

derivatization of the salicylidene is a potential route to sterically and electronically alter the shape or size of the supramolecular complex formed. Additional opportunities could be found in derivatization of the biphenyl linker; however, this may be more synthetically challenging. Of

interest in the formation of these complexes is the size of the cavity that can be produced, and if the cavity is suitable for trapping anions such as NO_3^- or small molecules. As these discrete supramolecular actinide species are part of a very small class of compounds and are fundamentally interesting for their novelty and possible array of structures. Additionally, the electrochemical behavior of these multi-actinide-center complexes should be investigated, as should their magnetic properties. There is a significant interest in the study of multimetallic lanthanide species for their magnetic relaxation and exchange properties[17]—paramagnetic 5*f* complexes may exhibit similar characteristics.

Pyrrophen Derivatives and Exploration of Transuranic Complexes

The highly modular pyrrophen framework offers many opportunities for derivatization, as a wide range of substituted *o*-phenylenediamines are commercially available, as are substituted acetoacetates. It may be possible to disfavor the formation of transition metal helicates through tuning the peripheral ester substituent to have a steric requirement that prevents helical self-assembly, though this would likely require a bulky group such as *t*-butyl or adamantyl (the latter acetoacetate is not commercially available). Of greater priority is the synthesis of additional pyrrophen derivatives, and examination of how the electronic properties impact their coordination to uranyl and properties of these complexes such as the oxo stretching frequencies, U(VI)/U(V) reduction potentials, and spectroscopic behaviors. Preliminary investigations have indicated that the introduction of electron-withdrawing groups on the phenylene backbone substantially hinders formation of the uranyl complex, whereas the presence of groups that are slightly electron-donating results in improved binding kinetics and a small positive shift in reduction potential. The symmetric and asymmetric diamines listed in **Figure 5.8** represent possible pyrrophen backbones

that are either commercially available or easily synthesized. One of the shortcomings of the unsubstituted pyrrophen **H_2L^1** is the slow binding to uranyl relative to transition metal species. In order to make this system practical for the molecular recognition of uranyl, a much faster response is required. An increase in the deviation of the uranyl complex UV-Vis signal from those of transition metal complexes is also desired, which can be accomplished by extending the conjugation or adding electron-donating groups. Additionally, adding features that elicit distinctive fluorescence responses from their respective complexes may be a route to better distinguish the uranyl complex from transition metal species.

This planar, equatorially coordinating system shows a great deal of potential for examining fundamental behaviors of other actinyl ions such as NpO_2^+ and PuO_2^{2+}, which are structurally analogous to uranyl. Pyrrophen may be a suitable system for colorimetrically distinguishing

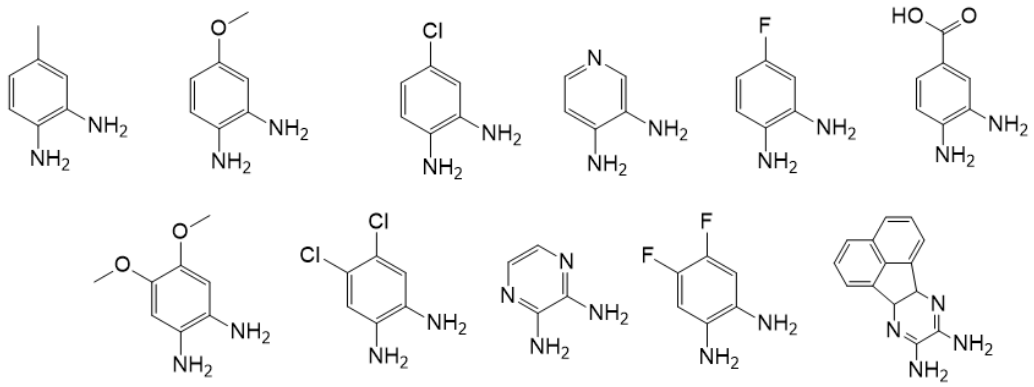

Figure 5.8. Potential diamine starting materials for pyrrophen derivatives.

between these ions in solution and may also allow for detailed characterization of a set of synthetically accessible isostructural actinyl complexes and exploration of their unique electronic properties.

The future directions of this work provide a variety of avenues through which to explore the molecular and supramolecular coordination chemistry of actinides, and to continue to develop studies of their covalent interactions and redox behaviors. Such studies may ultimately provide insight into the development of selective actinyl sensors or extracting agents, or elucidation of the mechanisms of reduction of uranyl. The exploration of these fundamentals allows for the development of a deeper understanding of many of the unique and unusual facets of actinide chemistry and how these translate to more impactful applications.

5.3 | Synthesis of Compounds and Methods

General Considerations

Caution! The uranium metal salt – $UO_2(OAc)_2 \cdot 2H_2O$ – used in this study contained depleted uranium. Standard precautions for handling radioactive materials or heavy metals such as uranyl nitrate and lead sulfate were followed. Organic solvents solvents (EtOH, Pharmco-Aaper; MeOH, anhydrous THF (DriSolv), EMD Millipore; CH_2Cl_2, THF, BDH Chemicals) were used as received without additional purification. Organic reagents (acenaphthenequinone, 2-hydroxynaphthaldehyde, 3,5-di-tert-butylsalicylaldehyde, 4-(diethylamino)salicylaldehyde, 1,2-diaminophenylene, Alfa Aesar; 3,3'-diaminobenzidine and 1,2,4,5-tetraaminobenzene tetrahydrochloride, Matrix Scientific) were used as received. $TBAPF_6$ (Beantown Chemical) and $TBAClO_4$ (electrochemical grade, Sigma-Aldrich) were recrystallized from anhydrous EtOH, and uranyl acetate (Polysciences) was recrystallized from methanol prior to use.

Identity and purity of compounds has been established via NMR where possible, mass and spectrometry (TOF MS, ESI+). 1H and 13C NMR were recorded on a Bruker AV 400 or 600 MHz spectrometer using DMSO-d6, DMF-d7, CDCl3, or THF-d8 (Cambridge Isotope Laboratories). Chemical shifts are reported in parts per million (δ) and referenced against TMS or residual internal solvent signals.

Solid-state UV/Vis and fluorescence data was collected on a CRAIC Technologies 20/20 PV microspectrophotometer using crystals mounted in Paratone-n oil on a glass slide. The exposure time was atuo-optimized by the CRAIC Minerva 8.7.3.12 software, and a background containing the slide and the oil was subtracted before spectra were recorded. The aperture was set manually according to crystal size.

Infrared spectra were obtained in the solid state using an attenuated total reflectance (ATR) method on a Thermo Scientific Nicolet iS50 FT-IR, and normalization of spectra [0, 100] was performed using OriginPro.

X-ray Crystallography

Crystals suitable for single crystal X-ray diffraction were selected and mounted on a 50-micron MiTeGen loop using Paratone-n oil and data set collection was completed on a Bruker D8 VENTURE κ-geometry diffractometer using Cu Kα or Mo K α radiation (Incoatec IμS DIAMOND microfocus sealed tube (λ = 1.54178 Å or 0.71073 Å). Crystals were kept at 100 K during unit cell and data collection. Determination of the unit cell and collection of data were performed using the APEX III software, and determination of integrated intensities and global cell refinement were performed with the Bruker SAINT software package. A multi-scan absorption correction (SADABS) was applied. Structures were solved using Intrinsic Phasing/Direct Methods[18]

(ShelXT) and least-squares refinement was performed using ShelXL in APEX III. Olex2.1.19 was used to mask solvent molecules [ThL2]3 in order to achieve convergence with the lowest possible Rint. Projections were created on Olex2.1.

Electrochemical Measurements

Electrochemical measurements were carried out using a CH Instruments 660 E potentiostat in HPLC-grade CH_3CN (BDH Chemicals), or anhydrous THF (DriSolv, EMD Millipore) with -tetrabutylammonium hexafluorophosphate ($TBAPF_6$) supporting electrolyte (0.1 M). $TBAPF_6$ was recrystallized from EtOH and dried overnight in vacuo at 60 °C immediately before use. Solutions were purged for 30 minutes with N_2 using a pre-purge solution. Potentials were scanned using a three-electrode cell consisting of a glassy carbon disc working electrode, Pt wire counter electrode, and Ag/AgCl/satd. KCl/H_2O reference electrode. For measurements in THF, a non-aqueous reference electrode (Ag/Ag^+ wire in ACN, 0.01 M $AgNO_3$) was used. Data was corrected to versus ferrocene based on values for $E_{1/2}(Fc^{+/0})$ collected using the same three-electrode cell before and after measurements. DPV conditions: Increment: 0.01 V; amplitude: 0.05 V; pulse width: 0.05 s; sample width: 0.0167 s; pulse period: 0.5 s.

Synthesis of 9,10-diamino-acenaphtho[1,2-*b*]quinoxaline ("daq"): Acenaphthenequinone (0.062 g, 0.35 mmol) and 1,2,4,5-tetraaminobenzene tetrahydrochloride (0.100 g, 0.35 mmol) were added to a 100-mL round bottom flask charged with a stir bar and dissolved in 50 mL of 1:4 CH_2Cl_2:MeOH. The resulting dark purple-red solution was stirred at room temperature for 24 h. 4 equivalents of triethylamine (0.190 mL, 1.4 mmol) was added by syringe, resulting in the immediate formation of a bright yellow solid. This suspension was stirred at room temperature for

an additional 3 h, then filtered. Yield: 95-98%. ^{1}H NMR (400 MHz, DMSO-d6): δ 8.17 (d, 2H, J = 6.8), 8.08 (d, 2H, J = 8.0), 7.80 (dd (t), 2H, J = 6.8, 1.2), 7.07 (s, 2H), 5.75 (s, 4 H).

Synthesis of 1-aq(NH_2),10-diamino-acenaphtho[1,2-*b*]quinoxaline (0.035 g, 0.125 mmol) in 50 mL EtOH was heated to 80 °C and stirred until most of the solid had dissolved. 2 drops of trifluoroacetic acid were added, and the orange-yellow solution turned orange-red. 3,5-di-*tert*-butylsalicylaldehyde (0.166 g, 0.725 mmol) was added as a solution in 5 mL EtOH, and the mixture was stirred for 18 h slightly above reflux temperature, affording a fine yellow solid. The suspension was cooled to room temperature, then chilled in the freezer overnight. The yellow solid was collected by filtration (2.5 μm pore size). Yield: 0.026 g, 29.0%. ^{1}H NMR (400 MHz, pyridine-d_5): δ 14.37 (br, 1H), 8.53 (d, 2H, J=7.0), 8.08 (d, 2H, J=8.3), 8.03 (d, 1H, J=2.2), 7.82 (t(dd), 2H, J=7.2), 7.74 (d, 1H, J=2.3), 5.05 (br, NH_2), 1.74 (s, 9H), 1.26 (s, 9H). Single crystals suitable for x-ray diffraction were grown by slow evaporation of an EtOH/THF solution of the filtrate, giving the symmetric ligand. *Note: NMR of the yellow solid collected indicates the 1-arm product, but XRD from the filtrate gives the 2-arm (left). Additionally, the solid is only soluble in pyridine-d_5 for NMR, and one peak is missing, likely obscured by a solvent peak (the integrations are not 2:2:1 for pyridine as they should be) as this peak in the NMR of* daq *is very close to the δ 7.22 pyridine peak.*

Synthesis of UO_2(1-aq): In a 250-mL round bottom flask charged with a stir bar, 0.115 g (0.50 mmol) of 3,5-di-*tert*-butylsalicylaldehyde was dissolved in 45 mL pyridine and heated to 90 °C. $UO_2(OAc)_2{\cdot}2H_2O$ (0.104 g, 0.25 mmol) was added as a solid, and the mixture turned red-pink. 9,10-diamino-acenaphtho[1,2-*b*]quinoxaline (0.071 g, 0.25 mmol) was dissolved in 40 mL hot pyridine and added slowly by pipette over 35 minutes, causing the solution to gradually darken.

The reaction was heated for 48 hours then cooled to room temperature, at which point a small amount of dark residue was removed by filtration. The filtrate was concentrated to near-dryness in vacuo, and solids redissolved in the minimum amount of hot MeOH (~20 mL) and cooled in the freezer for several days. A red-orange solid was collected by filtration (0.084 g), and the filtrate re-concentrated in MeOH and placed in the freezer overnight. An additional crop (0.028 g) of the same solid was collected the next day. Yield: 0.112 g, 45.5%.

Synthesis of 2-aq: In a 100-mL round bottom flask charged with a stir bar, 0.040 g (0.141 mmol) 9,10-diamino-acenaphtho[1,2-*b*]quinoxaline and 0.051 g (0.296 mmol) 2-hydroxynaphthaldehyde were dissolved in 45 mL EtOH and heated to 80 °C. 1 drop of trifluoracetic acid was added, and a solid was produced within 10 minutes. The reaction was allowed to heat and stir overnight, then cooled to room temperature and placed in the freezer for 2 h. A bright red-orange solid was collected by filtration, and the filtrate was dried in vacuo. 10 mL MeOH and 1 mL EtOH were added to the flask to liberate the solids from the sides, and the solution was re-filtered, affording a second crop of red-orange solid. Yield: 0.031 g, 37.3% (assuming product identity and purity).

Synthesis of UO_2(2-aq): In a 100-mL round bottom flask charged with a stir bar, 0.075 g (0.264 mmol) 9,10-diamino-acenaphtho[1,2-*b*]quinoxaline and 0.112 g (0.264 mmol) $UO_2(OAc)_2{\cdot}2H_2O$ were dissolved in 40 mL EtOH and stirred at 80°C for 1.5 hr. 2-hydroxynaphthaldehyde (0.095 g, 0.554 mmol) was added as a 10 mL solution in EtOH, and the yellow reaction mixture darkened to orange over 5 minutes. The solution was stirred for 10 minutes, then 3 drops of glacial acetic acid were added, and the reaction was stirred at 80 °C for 18 hr, the cooled to room temperature, affording an orange-brown solid. This solid was collected by filtration (0.078 g), and the filtrate concentrated and stored in the freezer for several days. An

additional crop of solid (0.070 g) was collected by filtration (lighter in color). Yield: 0.148 g, 65.2% (assuming product identity and purity).

References

1. Niklas, J. E.; Farnum, B. H.; Gorden, J. D.; Gorden, A. E. V., Structural Characterization and Redox Activity of a Uranyl Dimer and Transition-Metal Complexes of a Tetradentate BIAN Ligand. *Organometallics* **2017,** *36* (23), 4626-4634.

2. Niklas, J. E.; Hunter, K. M.; Gorden, A. E. V., Bonding Interactions in Uranyl α-Diimine Complexes: A Spectroscopic and Electrochemical Study of the Impacts of Ligand Electronics and Extended Conjugation. *Inorg. Chem.* **2019**.

3. Niklas, J. E.; Hardy, E. E.; Gorden, A. E. V., Solid-state structural elucidation and electrochemical analysis of uranyl naphthylsalophen. *Chem. Comm.* **2018,** *54* (83), 11693-11696.

4. Mayhugh, J. T.; Niklas, J. E.; Forbes, M. G.; Gorden, J. D.; Gorden, A. E. V., Pyrrophens: pyrrole-based macroacyclic hexadentate ligands tailor-made for uranyl (UO_2^{2+}) coordination and molecular recognition. *Inorg. Chem. (Submitted)* **2020**.

5. Kim, S.-Y.; Tomiyasu, H.; Ikeda, Y., Electrochemical Studies on $[UO_2(DMF)_5](ClO_4)_2$, $UO_2(acac)_2DMF$, and UO_2(salen)DMF (DMF=N, N-dimethylformamide, acac=acetylacetonate, salen=N, N′-disalicylideneethylenediaminate) Complexes in DMF. *J. Nucl. Sci. Technol.* **2002,** *39* (2), 160-165.

6. Niklas, J. E.; Reßnik, F.; Gorden, J. D.; Gorden, A. E. V., Polynuclear actinide bis-salophen complexes. *In Preparation*.

7. Pedras, B.; Rosa, V.; Welter, R.; Lodeiro, C.; Avilés, T., New quinoline α-diimine ligands as fluorescent probes for metal ions: Ultrasound-assisted and conventional synthetic methods. *Inorg. Chim. Acta.* **2012,** *381*, 143-149.

8. Jia, A.-Q.; Liu, F.; Wang, J.-Q.; Liu, D., Synthesis, characterization, and olefin polymerization of half-sandwich Ir, Rh, Ru metallacycle enclosing a nickel in the center. *J. Coord. Chem.* **2017,** *70* (11), 1791-1799.

9. Fedushkin, I. L.; Skatova, A. A.; Chudakova, V. A.; Fukin, G. K., Four-Step Reduction of dpp-bian with Sodium Metal: Crystal Structures of the Sodium Salts of the Mono-, Di-, Tri- and Tetraanions of dpp-bian. *Angew. Chem. Int. Ed.* **2003,** *42* (28), 3294-3298.

10. Fedushkin, Igor L.; Skatova, Alexandra A.; Chudakova, Valentina A.; Cherkasov, Vladimir K.; Fukin, Georgy K.; Lopatin, Mikhail A., Reduction of 1,2-Bis[(2,6-diisopropylphenyl)imino]acenaphthene (dpp-bian) with Alkali Metals − A Study of the Solution Behaviour of $(dpp\text{-}bian)_n{-}[M^+]_n$ (M = Li, Na; n = 1−4) with UV/Vis, ESR and ^1H NMR Spectroscopy. *Eur. J. Inorg. Chem.* **2004,** *2004* (2), 388-393.

11. Pankhurst, J. R.; Bell, N. L.; Zegke, M.; Platts, L. N.; Lamfsus, C. A.; Maron, L.; Natrajan, L. S.; Sproules, S.; Arnold, P. L.; Love, J. B., Inner-sphere vs. outer-sphere reduction of uranyl supported by a redox-active, donor-expanded dipyrrin. *Chem. Sci.* **2017,** *8* (1), 108-116.

12. Vasudevan, K.; Cowley, A. H., Synthesis and structures of 1,2-bis(imino)acenaphthene (BIAN) lanthanide complexes that involve the transfer of zero, one, or two electrons. *Chem. Comm.* **2007,** (33), 3464-3466.

13. Schelter, E. J.; Wu, R.; Scott, B. L.; Thompson, J. D.; Cantat, T.; John, K. D.; Batista, E. R.; Morris, D. E.; Kiplinger, J. L., Actinide Redox-Active Ligand Complexes: Reversible

Intramolecular Electron-Transfer in U(dpp-BIAN)$_2$/U(dpp-BIAN)$_2$(THF). *Inorg. Chem.* **2010,** *49* (3), 924-933.

14. Cheng, J.; Ma, X.; Zhang, Y.; Liu, J.; Zhou, X.; Xiang, H., Optical Chemosensors Based on Transmetalation of Salen-Based Schiff Base Complexes. *Inorg. Chem.* **2014,** *53* (6), 3210-3219.

15. Dalla Cort, A.; De Bernardin, P.; Forte, G.; Yafteh Mihan, F., Metal–salophen-based receptors for anions. *Chem. Soc. Rev.* **2010,** *39* (10), 3863.

16. Klamm, B. E.; Windorff, C. J.; Celis-Barros, C.; Marsh, M. L.; Albrecht-Schmitt, T. E., Synthesis, Spectroscopy, and Theoretical Details of Uranyl Schiff-Base Coordination Complexes. *Inorg. Chem.* **2020,** *59* (1), 23-31.

17. Gao, F.; Yang, F.-L.; Zhu, G.-Z.; Zhao, Y., Syntheses, structures, and magnetic properties of homodinuclear lanthanide complexes based on dinucleating Schiff base ligands. *Dalton Trans.* **2015,** *44* (46), 20232-20241.

18. Sheldrick, G. M., Crystal structure refinement with SHELXL. *Acta Crystallogr., Sect. C: Struct. Chem.* **2015,** *71* (Pt 1), 3-8.

19. Dolomanov, O. V.; Bourhis, L. J.; Gildea, R. J.; Howard, J. A. K.; Puschmann, H., OLEX^2: a complete structure solution, refinement and analysis program. *J. Appl. Crystallogr.* **2009,** *42* (2), 339-341.

Appendix I

Abridged Crystallographic Tables

CIFs for the following structures can be obtained from the Cambridge Crystallographic Data Centre (CCDC) in addition to tables containing the following information: fractional atomic coordinates ($\times 10^4$) and equivalent isotropic displacement parameters ($å^2 \times 10^3$), anisotropic displacement parameters ($å^2 \times 10^3$), bond lengths, bond angles, torsion angles, and hydrogen atom coordinates ($å \times 10^4$) and isotropic displacement parameters ($å^2 \times 10^3$)

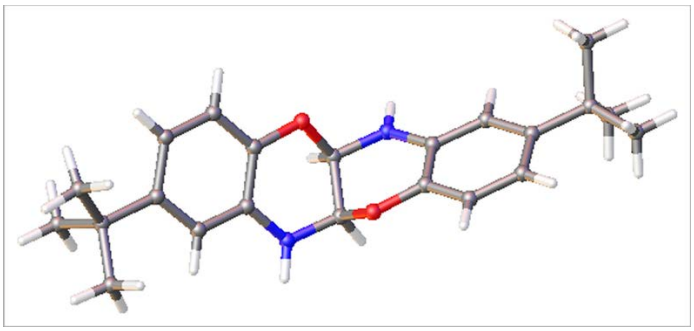

Table A1. Crystal data and structure refinement for 1b.

Identification code	1918535
Empirical formula	$C_{22}H_{28}N_2O_2$
Formula weight	352.46
Temperature/K	100.(2)
Crystal system	monoclinic
Space group	$P2_1/c$
a/Å	16.0253(13)
b/Å	10.8736(8)
c/Å	10.9086(9)
α/°	90
β/°	95.994(4)
γ/°	90
Volume/Å^3	1890.5(3)
Z	4
ρ_{calc}g/cm^3	1.238
μ/mm^{-1}	0.624
F(000)	760.0
Crystal size/mm^3	0.110 × 0.100 × 0.015
Radiation	Cu Kα (λ = 1.54178)
2Θ range for data collection/°	9.84 to 145.14
Index ranges	$-19 \leq h \leq 19$, $-13 \leq k \leq 12$, $-13 \leq l \leq 13$
Reflections collected	40974
Independent reflections	3663 [R_{int} = 0.0991, R_{sigma} = 0.0442]
Data/restraints/parameters	3663/0/249
Goodness-of-fit on F^2	1.270
Final R indexes [I>=2σ (I)]	R_1 = 0.0948, wR_2 = 0.1743
Final R indexes [all data]	R_1 = 0.1186, wR_2 = 0.1858
Largest diff. peak/hole / e Å^{-3}	0.28/-0.36

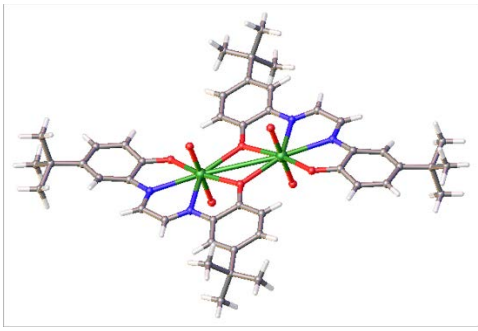

Table A2. Crystal data and structure refinement for UO_2-1b.

Identification code	1918539
Empirical formula	$C_{44}H_{52}N_4O_8U_2$
Formula weight	1240.95
Temperature/K	100.(2)
Crystal system	triclinic
Space group	P-1
a/Å	7.7884(5)
b/Å	9.2145(6)
c/Å	15.6747(11)
α/°	106.675(3)
β/°	93.928(3)
γ/°	102.831(3)
Volume/Å^3	1040.12(12)
Z	1
ρ_{calc}g/cm^3	1.981
μ/mm^{-1}	22.220
F(000)	592.0
Crystal size/mm^3	0.030 × 0.005 × 0.001
Radiation	Cu Kα (λ = 1.54178)
2Θ range for data collection/°	5.94 to 127.76
Index ranges	$-9 \le h \le 9$, $-10 \le k \le 10$, $-18 \le l \le 18$
Reflections collected	6708
Independent reflections	3427 [R_{int} = 0.0764, R_{sigma} = 0.0914]
Data/restraints/parameters	3427/1/256
Goodness-of-fit on F^2	1.161
Final R indexes [I>=2σ (I)]	R_1 = 0.0846, wR_2 = 0.2075
Final R indexes [all data]	R_1 = 0.0964, wR_2 = 0.2157
Largest diff. peak/hole / e Å^{-3}	4.40/-1.45

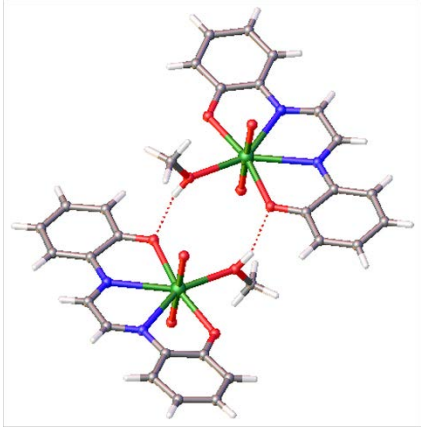

Table A3. Crystal data and structure refinement for UO_2-1c.

Identification code	1918541
Empirical formula	$C_{15}H_{14}N_2O_5U$
Formula weight	540.31
Temperature/K	110.(2)
Crystal system	monoclinic
Space group	$P2_1/c$
a/Å	22.6315(15)
b/Å	6.7145(4)
c/Å	23.1200(15)
α/°	90
β/°	96.962(3)
γ/°	90
Volume/Å^3	3487.4(4)
Z	8
ρ_{calc}g/cm^3	2.058
μ/mm^{-1}	26.432
F(000)	2000.0
Crystal size/mm^3	0.157 × 0.025 × 0.004
Radiation	Cu Kα (λ = 1.54178)
2Θ range for data collection/°	3.94 to 130.16
Index ranges	$-26 \leq h \leq 26$, $-7 \leq k \leq 7$, $-27 \leq l \leq 27$
Reflections collected	83550
Independent reflections	5932 [R_{int} = 0.1073, R_{sigma} = 0.0408]
Data/restraints/parameters	5932/2/419
Goodness-of-fit on F^2	1.164
Final R indexes [I>=2σ (I)]	R_1 = 0.0707, wR_2 = 0.2136
Final R indexes [all data]	R_1 = 0.0771, wR_2 = 0.2224
Largest diff. peak/hole / e Å^{-3}	5.59/-3.68

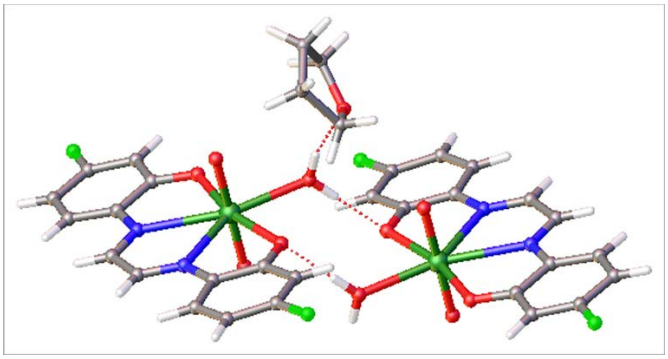

Table A4. Crystal data and structure refinement for UO_2-1e.

Identification code	1921460
Empirical formula	$C_{18}H_{18}F_2N_2O_6U$
Formula weight	634.37
Temperature/K	150.(2)
Crystal system	monoclinic
Space group	$P2_1/c$
a/Å	11.3072(9)
b/Å	19.5295(15)
c/Å	9.2017(7)
α/°	90
β/°	109.758(2)
γ/°	90
Volume/Å^3	1912.3(3)
Z	4
ρ_{calc}g/cm^3	2.203
μ/mm^{-1}	24.430
F(000)	1192.0
Crystal size/mm^3	0.354 × 0.097 × 0.001
Radiation	Cu Kα (λ = 1.54178)
2Θ range for data collection/°	8.3 to 144.22
Index ranges	$-13 \leq h \leq 13$, $-23 \leq k \leq 24$, $-11 \leq l \leq 9$
Reflections collected	31829
Independent reflections	3750 [R_{int} = 0.0524, R_{sigma} = 0.0272]
Data/restraints/parameters	3750/7/267
Goodness-of-fit on F^2	1.057
Final R indexes [I>=2σ (I)]	R_1 = 0.0297, wR_2 = 0.0883
Final R indexes [all data]	R_1 = 0.0314, wR_2 = 0.0905
Largest diff. peak/hole / e Å^{-3}	3.66/-2.15

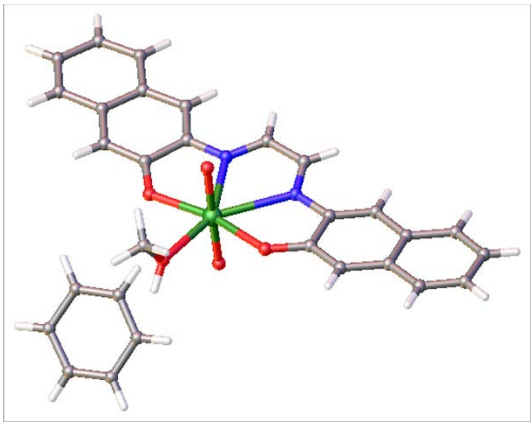

Table A5. Crystal data and structure refinement for UO_2-1f.

Identification code	1918540
Empirical formula	$C_{29}H_{24}N_2O_5U$
Formula weight	718.53
Temperature/K	110.(2)
Crystal system	triclinic
Space group	P-1
a/Å	7.191(4)
b/Å	11.092(5)
c/Å	15.742(8)
α/°	92.05(4)
β/°	98.26(5)
γ/°	93.73(4)
Volume/Å^3	1238.7(11)
Z	2
ρ_{calc}g/cm^3	1.927
μ/mm^{-1}	18.809
F(000)	688.0
Crystal size/mm^3	0.094 × 0.015 × 0.002
Radiation	Cu Kα (λ = 1.54178)
2Θ range for data collection/°	5.68 to 131.3
Index ranges	$-8 \leq h \leq 8$, $-13 \leq k \leq 13$, $-18 \leq l \leq 18$
Reflections collected	29892
Independent reflections	4230 [R_{int} = 0.1055, R_{sigma} = 0.0583]
Data/restraints/parameters	4230/76/339
Goodness-of-fit on F^2	1.125
Final R indexes [I>=2σ (I)]	R_1 = 0.0686, wR_2 = 0.1626
Final R indexes [all data]	R_1 = 0.0732, wR_2 = 0.1664
Largest diff. peak/hole / e Å^{-3}	4.11/-2.63

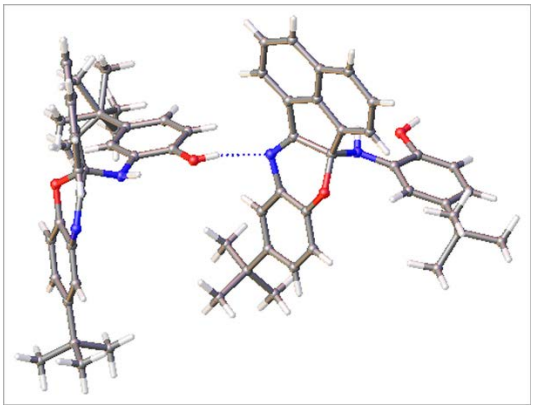

Table A6. Crystal data and structure refinement for 2b.

Identification code	1555320
Empirical formula	$C_{64}H_{64}N_4O_4$
Formula weight	953.25
Temperature/K	180.65
Crystal system	orthorhombic
Space group	Pbca
a/Å	18.5700(7)
b/Å	19.7879(7)
c/Å	29.5769(11)
α/°	90
β/°	90
γ/°	90
Volume/Å^3	10868.4(7)
Z	8
ρ_{calc}g/cm^3	1.1651
μ/mm^{-1}	0.072
F(000)	4065.7
Crystal size/mm^3	0.2 × 0.2 × 0.1
Radiation	Mo Kα (λ = 0.71073)
2Θ range for data collection/°	2.76 to 51.36
Index ranges	$-22 \leq h \leq 22$, $-24 \leq k \leq 23$, $-36 \leq l \leq 36$
Reflections collected	94391
Independent reflections	10320 [R_{int} = 0.0939, R_{sigma} = 0.0557]
Data/restraints/parameters	10320/13/661
Goodness-of-fit on F^2	1.088
Final R indexes [I>=2σ (I)]	R_1 = 0.0676, wR_2 = 0.1290
Final R indexes [all data]	R_1 = 0.1053, wR_2 = 0.1453
Largest diff. peak/hole / e Å^{-3}	0.71/-0.58

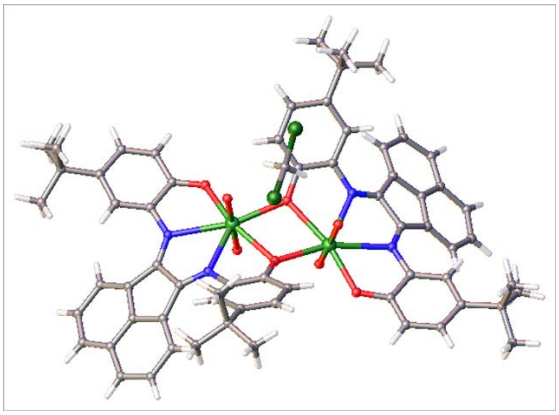

Table A7. Crystal data and structure refinement for UO_2-2b[1].

Identification code	1555904
Empirical formula	$C_{65}H_{62}Cl_2N_4O_8U_2$
Formula weight	1574.20
Temperature/K	181.65
Crystal system	monoclinic
Space group	$P2_1/n$
a/Å	14.683(2)
b/Å	24.897(4)
c/Å	19.990(3)
α/°	90
β/°	105.835(3)
γ/°	90
Volume/Å^3	7030.2(19)
Z	4
ρ_{calc}g/cm^3	1.4872
μ/mm^{-1}	4.729
F(000)	2969.5
Crystal size/mm^3	0.1 × 0.1 × 0.03
Radiation	Mo Kα (λ = 0.71073)
2Θ range for data collection/°	2.68 to 46.56
Index ranges	$-16 \le h \le 16$, $-27 \le k \le 27$, $-22 \le l \le 22$
Reflections collected	62479
Independent reflections	10031 [R_{int} = 0.1417, R_{sigma} = 0.0958]
Data/restraints/parameters	10031/392/736
Goodness-of-fit on F^2	1.073
Final R indexes [I>=2σ (I)]	R_1 = 0.0648, wR_2 = 0.1261
Final R indexes [all data]	R_1 = 0.1094, wR_2 = 0.1451
Largest diff. peak/hole / e Å^{-3}	3.85/-4.68

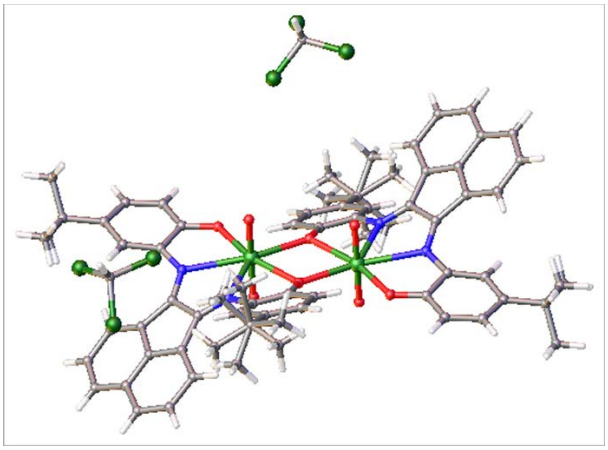

Table A8. Crystal data and structure refinement for UO_2-2b[2].

Identification code	1555319
Empirical formula	$C_{34}H_{32}Cl_6N_2O_4U$
Formula weight	983.39
Temperature/K	180.
Crystal system	monoclinic
Space group	$P2_1/c$
a/Å	16.3570(11)
b/Å	11.6673(8)
c/Å	19.6674(13)
α/°	90
β/°	100.665(1)
γ/°	90
Volume/Å^3	3688.5(4)
Z	4
ρ_{calc}g/cm^3	1.7707
μ/mm^{-1}	4.876
F(000)	1904.0
Crystal size/mm^3	0.2 × 0.1 × 0.05
Radiation	Mo Kα (λ = 0.71073)
2Θ range for data collection/°	2.54 to 51.36
Index ranges	$-19 \leq h \leq 19$, $-14 \leq k \leq 14$, $-22 \leq l \leq 23$
Reflections collected	34449
Independent reflections	6986 [R_{int} = 0.0681, R_{sigma} = 0.0611]
Data/restraints/parameters	6986/6/425
Goodness-of-fit on F^2	1.060
Final R indexes [I>=2σ (I)]	R_1 = 0.0551, wR_2 = 0.1127
Final R indexes [all data]	R_1 = 0.0693, wR_2 = 0.1215
Largest diff. peak/hole / e Å^{-3}	2.76/-1.51

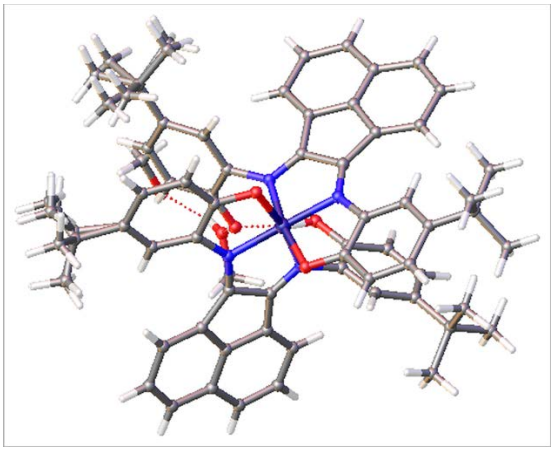

Table A9. Crystal data and structure refinement for Co-2b.

Identification code	1555321
Empirical formula	$C_{66}H_{70}CoN_4O_6$
Formula weight	1074.25
Temperature/K	180.65
Crystal system	triclinic
Space group	P-1
a/Å	13.7849(6)
b/Å	14.5741(7)
c/Å	15.8371(8)
α/°	93.438(2)
β/°	92.014(2)
γ/°	117.784(2)
Volume/Å^3	2802.7(2)
Z	2
ρ_{calc}g/cm^3	1.2729
μ/mm^{-1}	0.363
F(000)	1139.2
Crystal size/mm^3	0.28 × 0.15 × 0.13
Radiation	Mo Kα (λ = 0.71073)
2Θ range for data collection/°	2.58 to 48.8
Index ranges	$-16 \leq h \leq 16$, $-16 \leq k \leq 16$, $-18 \leq l \leq 18$
Reflections collected	51863
Independent reflections	9199 [R_{int} = 0.0552, R_{sigma} = 0.0477]
Data/restraints/parameters	9199/23/711
Goodness-of-fit on F^2	1.083
Final R indexes [I>=2σ (I)]	R_1 = 0.0607, wR_2 = 0.1298
Final R indexes [all data]	R_1 = 0.0810, wR_2 = 0.1394
Largest diff. peak/hole / e Å^{-3}	0.75/-0.58

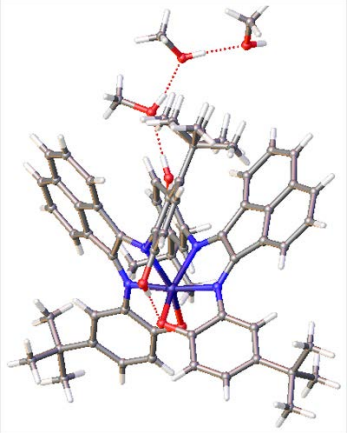

Table A10. Crystal data and structure refinement for Ni-2b.

Identification code	1555322
Empirical formula	$C_{67}H_{74}N_4NiO_7$
Formula weight	1106.05
Temperature/K	180.45
Crystal system	monoclinic
Space group	$P2_1/n$
a/Å	15.0147(12)
b/Å	20.0876(16)
c/Å	19.9220(16)
α/°	90
β/°	99.879(1)
γ/°	90
Volume/Å^3	5919.6(8)
Z	4
ρ_{calc}g/cm^3	1.2410
μ/mm^{-1}	0.385
F(000)	2354.4
Crystal size/mm^3	0.3 × 0.3 × 0.09
Radiation	Mo Kα (λ = 0.71073)
2Θ range for data collection/°	2.9 to 54.2
Index ranges	$-18 \leq h \leq 19$, $-25 \leq k \leq 21$, $-25 \leq l \leq 25$
Reflections collected	57379
Independent reflections	13060 [R_{int} = 0.0515, R_{sigma} = 0.0542]
Data/restraints/parameters	13060/0/761
Goodness-of-fit on F^2	1.215
Final R indexes [I>=2σ (I)]	R_1 = 0.0559, wR_2 = 0.1468
Final R indexes [all data]	R_1 = 0.1140, wR_2 = 0.2052
Largest diff. peak/hole / e Å^{-3}	1.47/-0.95

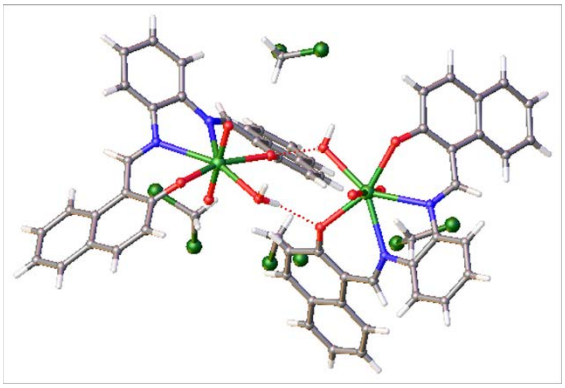

Table A11. Crystal data and structure refinement for UO_2L.

Identification code	1827293
Empirical formula	$C_{60}H_{48}Cl_8N_4O_{10}U_2$
Formula weight	1744.75
Temperature/K	180.0
Crystal system	monoclinic
Space group	$P2_1/n$
a/Å	15.4659(12)
b/Å	19.3294(14)
c/Å	22.2346(16)
α/°	90
β/°	106.655(1)
γ/°	90
Volume/Å^3	6368.1(8)
Z	4
ρ_{calc}g/cm^3	1.8197
μ/mm^{-1}	5.476
F(000)	3269.1
Crystal size/mm^3	0.18 × 0.12 × 0.1
Radiation	Mo Kα (λ = 0.71073)
2Θ range for data collection/°	2.84 to 51.52
Index ranges	$-18 \le h \le 18$, $-23 \le k \le 23$, $-27 \le l \le 27$
Reflections collected	74217
Independent reflections	12168 [R_{int} = 0.0706, R_{sigma} = 0.0463]
Data/restraints/parameters	12168/0/759
Goodness-of-fit on F^2	1.094
Final R indexes [I>=2σ (I)]	R_1 = 0.0440, wR_2 = 0.0935
Final R indexes [all data]	R_1 = 0.0628, wR_2 = 0.1031
Largest diff. peak/hole / e Å^{-3}	3.33/-1.96

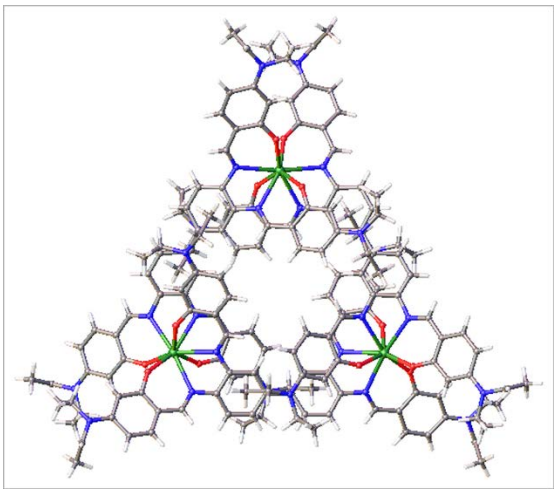

Table A12. Crystal data and structure refinement for $[ThL2]_3$.

Identification code	1964435
Empirical formula	$C_{226}H_{277}N_{53}O_{17}Th_3$
Formula weight	4704.13
Temperature/K	100.(2)
Crystal system	trigonal
Space group	P-3c1
a/Å	24.0247(6)
b/Å	24.0247(6)
c/Å	19.8283(6)
α/°	90
β/°	90
γ/°	120
Volume/Å^3	9911.3(6)
Z	2
ρ_{calc}g/cm^3	1.576
μ/mm^{-1}	7.608
F(000)	3444.0
Crystal size/mm^3	0.239 × 0.040 × 0.020
Radiation	Cu Kα (λ = 1.54178)
2Θ range for data collection/°	4.24 to 130.32
Index ranges	$-28 \leq h \leq 28$, $-28 \leq k \leq 28$, $-23 \leq l \leq 22$
Reflections collected	217785
Independent reflections	5670 [R_{int} = 0.1119, R_{sigma} = 0.0232]
Data/restraints/parameters	5670/0/316
Goodness-of-fit on F^2	1.051
Final R indexes [I>=2σ (I)]	R_1 = 0.0364, wR_2 = 0.0993
Final R indexes [all data]	R_1 = 0.0434, wR_2 = 0.1046
Largest diff. peak/hole / e Å^{-3}	1.93/-1.12

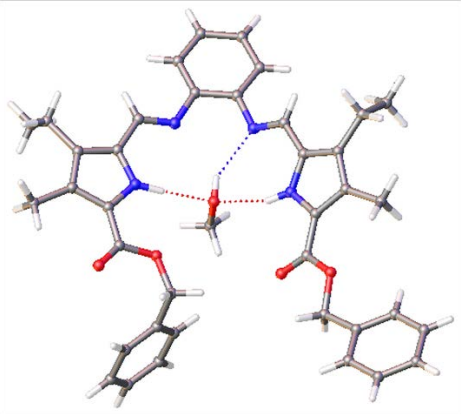

Table A13. Crystal data and structure refinement for H_2L^1.

Identification code	1936495
Empirical formula	$C_{39}H_{42}N_4O_5$
Formula weight	646.76
Temperature/K	100.(2)
Crystal system	monoclinic
Space group	$P2_1/n$
a/Å	18.5869(5)
b/Å	7.8296(2)
c/Å	23.2772(6)
α/°	90
β/°	91.9290(10)
γ/°	90
Volume/Å^3	3385.56(15)
Z	4
ρ_{calc}g/cm^3	1.269
μ/mm^{-1}	0.679
F(000)	1376.0
Crystal size/mm^3	0.211 × 0.080 × 0.045
Radiation	Cu Kα (λ = 1.54178)
2Θ range for data collection/°	5.98 to 140.38
Index ranges	$-22 \le h \le 22$, $-9 \le k \le 8$, $-28 \le l \le 28$
Reflections collected	62317
Independent reflections	6455 [R_{int} = 0.0778, R_{sigma} = 0.0295]
Data/restraints/parameters	6455/0/447
Goodness-of-fit on F^2	1.047
Final R indexes [I>=2σ (I)]	R_1 = 0.0409, wR_2 = 0.0881
Final R indexes [all data]	R_1 = 0.0526, wR_2 = 0.0942
Largest diff. peak/hole / e Å^{-3}	0.20/-0.23

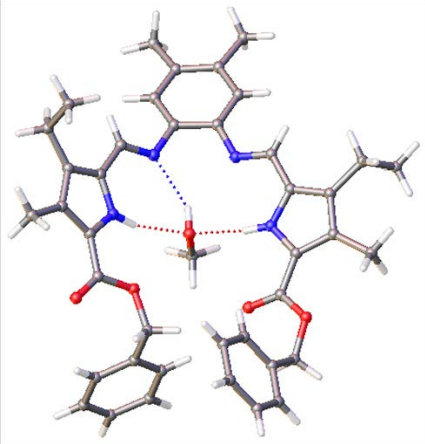

Table A14. Crystal data and structure refinement for H_2L^2.

Identification code	1971893
Empirical formula	$C_{41}H_{46}N_4O_5$
Formula weight	674.82
Temperature/K	100.(2)
Crystal system	triclinic
Space group	P-1
a/Å	10.7587(4)
b/Å	13.6898(5)
c/Å	13.7875(5)
α/°	86.0290(10)
β/°	67.3370(10)
γ/°	74.2830(10)
Volume/Å^3	1802.42(12)
Z	2
ρ_{calc}g/cm^3	1.243
μ/mm^{-1}	0.658
F(000)	720.0
Crystal size/mm^3	0.238 × 0.145 × 0.144
Radiation	Cu Kα (λ = 1.54178)
2Θ range for data collection/°	6.72 to 140.12
Index ranges	-13 ≤ h ≤ 13, -16 ≤ k ≤ 16, -16 ≤ l ≤ 16
Reflections collected	59485
Independent reflections	6804 [R_{int} = 0.0212, R_{sigma} = 0.0114]
Data/restraints/parameters	6804/0/467
Goodness-of-fit on F^2	1.038
Final R indexes [I>=2σ (I)]	R_1 = 0.0335, wR_2 = 0.0819
Final R indexes [all data]	R_1 = 0.0343, wR_2 = 0.0824
Largest diff. peak/hole / e Å^{-3}	0.24/-0.20

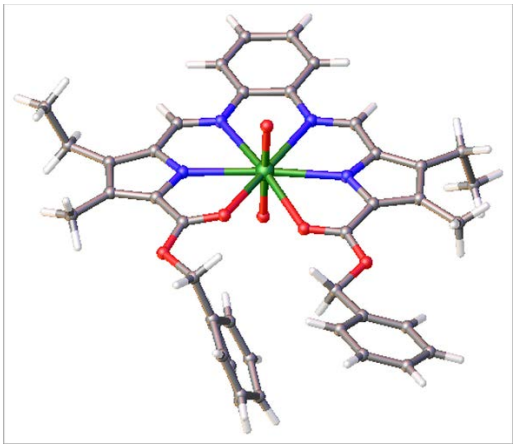

Table A15. Crystal data and structure refinement UO_2L^1.

Identification code	1936509
Empirical formula	$C_{39}H_{38}Cl_2N_4O_6U$
Formula weight	967.66
Temperature/K	110.(2)
Crystal system	monoclinic
Space group	C2/c
a/Å	26.1188(11)
b/Å	13.3574(5)
c/Å	21.5144(8)
α/°	90
β/°	99.526(2)
γ/°	90
Volume/Å^3	7402.4(5)
Z	8
ρ_{calc}g/cm^3	1.737
μ/mm^{-1}	4.582
F(000)	3792.0
Crystal size/mm^3	0.265 × 0.242 × 0.005
Radiation	Mo Kα (λ = 0.71073)
2Θ range for data collection/°	4.96 to 58.26
Index ranges	$-35 \leq h \leq 35$, $-18 \leq k \leq 18$, $-29 \leq l \leq 29$
Reflections collected	107359
Independent reflections	9946 [R_{int} = 0.0896, R_{sigma} = 0.0392]
Data/restraints/parameters	9946/0/477
Goodness-of-fit on F^2	1.038
Final R indexes [I>=2σ (I)]	R_1 = 0.0219, wR_2 = 0.0464
Final R indexes [all data]	R_1 = 0.0338, wR_2 = 0.0477
Largest diff. peak/hole / e Å^{-3}	1.09/-0.61

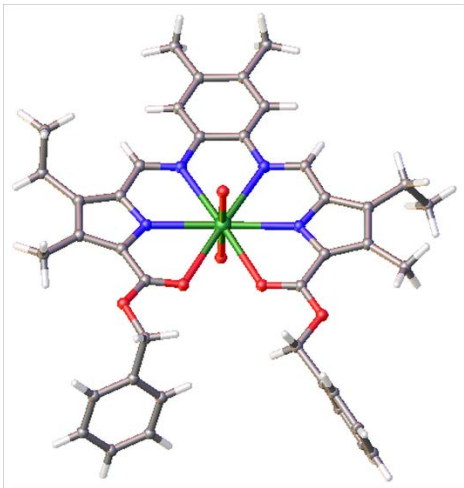

Table A16. Crystal data and structure refinement for UO_2L^2.

Identification code	1971927
Empirical formula	$C_{40}H_{40}N_4O_6U$
Formula weight	910.79
Temperature/K	100.(2)
Crystal system	triclinic
Space group	P-1
a/Å	11.2188(5)
b/Å	12.3197(6)
c/Å	14.8423(7)
α/°	99.161(2)
β/°	97.761(2)
γ/°	101.886(2)
Volume/Å^3	1951.66(16)
Z	2
ρ_{calc}g/cm^3	1.550
μ/mm^{-1}	12.106
F(000)	896.0
Crystal size/mm^3	0.134 × 0.090 × 0.021
Radiation	Cu Kα (λ = 1.54178)
2Θ range for data collection/°	6.12 to 144.64
Index ranges	-13 ≤ h ≤ 13, -14 ≤ k ≤ 15, -18 ≤ l ≤ 18
Reflections collected	81640
Independent reflections	7703 [R_{int} = 0.0461, R_{sigma} = 0.0203]
Data/restraints/parameters	7703/0/466
Goodness-of-fit on F^2	1.051
Final R indexes [I>=2σ (I)]	R_1 = 0.0203, wR_2 = 0.0514
Final R indexes [all data]	R_1 = 0.0209, wR_2 = 0.0518
Largest diff. peak/hole / e Å^{-3}	1.98/-0.81

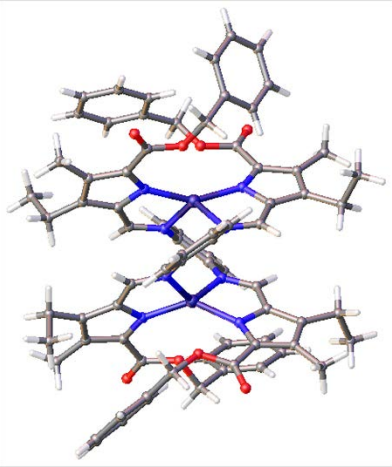

Table A17. Crystal data and structure refinement for $Zn_2(L^1)_2$.

Identification code	1983238
Empirical formula	$C_{76}H_{72}N_8O_8Zn_2$
Formula weight	1356.15
Temperature/K	100.(2)
Crystal system	monoclinic
Space group	$P2_1/c$
a/Å	21.6904(6)
b/Å	14.6578(4)
c/Å	20.8658(5)
α/°	90
β/°	96.2850(10)
γ/°	90
Volume/Å^3	6594.1(3)
Z	4
ρ_{calc}g/cm^3	1.366
μ/mm^{-1}	0.792
F(000)	2832.0
Crystal size/mm^3	0.280 × 0.102 × 0.050
Radiation	Mo Kα (λ = 0.71073)
2Θ range for data collection/°	3.78 to 66.32
Index ranges	$-33 \leq h \leq 33$, $-22 \leq k \leq 22$, $-32 \leq l \leq 32$
Reflections collected	361295
Independent reflections	25155 [R_{int} = 0.1365, R_{sigma} = 0.0440]
Data/restraints/parameters	25155/0/855
Goodness-of-fit on F^2	1.032
Final R indexes [I>=2σ (I)]	R_1 = 0.0324, wR_2 = 0.0920
Final R indexes [all data]	R_1 = 0.0440, wR_2 = 0.0963
Largest diff. peak/hole / e Å^{-3}	0.54/-0.96

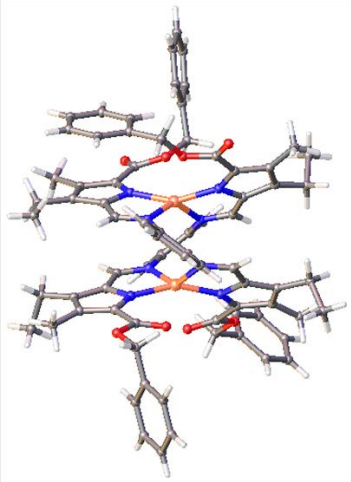

Table A18. Crystal data and structure refinement for $Cu_2(L^1)_2$.

Identification code	1936510
Empirical formula	$C_{76}H_{72}Cu_2N_8O_8$
Formula weight	1352.49
Temperature/K	100.(2)
Crystal system	triclinic
Space group	P-1
a/Å	12.8717(5)
b/Å	14.2601(6)
c/Å	17.9034(8)
α/°	84.458(2)
β/°	88.658(3)
γ/°	80.978(2)
Volume/Å^3	3230.3(2)
Z	2
ρ_{calc}g/cm^3	1.391
μ/mm^{-1}	1.340
F(000)	1412.0
Crystal size/mm^3	0.137 × 0.084 × 0.013
Radiation	Cu Kα (λ = 1.54178)
2Θ range for data collection/°	4.96 to 130.16
Index ranges	$-15 \leq h \leq 15$, $-16 \leq k \leq 16$, $-21 \leq l \leq 21$
Reflections collected	91399
Independent reflections	11002 [R_{int} = 0.0870, R_{sigma} = 0.0469]
Data/restraints/parameters	11002/0/855
Goodness-of-fit on F^2	1.017
Final R indexes [I>=2σ (I)]	R_1 = 0.0428, wR_2 = 0.0883
Final R indexes [all data]	R_1 = 0.0672, wR_2 = 0.0984
Largest diff. peak/hole / e Å^{-3}	0.44/-0.41

Miscellaneous Structures

Note:

The following structures were the products of many attempts to make derivatized phen-BIAN ligands (2a, 2c, 2e, and 2f) from acenaphthenequinone and aminophenol starting materials under a variety of conditions, as well as from the attempted synthesis of a copper-phen-BIAN complex of 2b. These compounds have not been characterized further; however, their characterization provides some insight as to why isolation of many of the desired phen-BIAN derivatives was not successful. Though they were note characterized, they have been uploaded to the Cambridge Crystallographic Data Centre and are included in this dissertation as they are relevant to the synthesis of phen-BIAN ligands, and their unexpected structures may be of interest or inspiration down the line. These structures have been uploaded to the CCDC and are under embargo until the end of 2020. They are referred to by their 7-digit identification code (CCDC entry number) in the table titles.

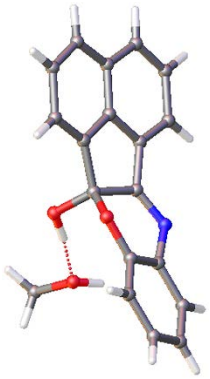

Table A19. Crystal data and structure refinement for 1886893.

Identification code	1886893
Empirical formula	$C_{19}H_{15}NO_3$
Formula weight	305.32
Temperature/K	100.(2)
Crystal system	triclinic
Space group	P-1
a/Å	8.1562(3)
b/Å	8.4038(3)
c/Å	11.4691(4)
α/°	70.5880(10)
β/°	77.2110(10)
γ/°	83.9660(10)
Volume/Å^3	722.62(5)
Z	2
ρ_{calc}g/cm^3	1.403
μ/mm^{-1}	0.095
F(000)	320.0
Crystal size/mm^3	0.100 × 0.060 × 0.040
Radiation	Mo Kα (λ = 0.71073)
2Θ range for data collection/°	5.34 to 52.22
Index ranges	$-10 \leq h \leq 10$, $-10 \leq k \leq 10$, $-14 \leq l \leq 14$
Reflections collected	29344
Independent reflections	2866 [R_{int} = 0.0216, R_{sigma} = 0.0130]
Data/restraints/parameters	2866/0/217
Goodness-of-fit on F^2	1.048
Final R indexes [I>=2σ (I)]	R_1 = 0.0331, wR_2 = 0.0868
Final R indexes [all data]	R_1 = 0.0340, wR_2 = 0.0876
Largest diff. peak/hole / e Å^{-3}	0.37/-0.21

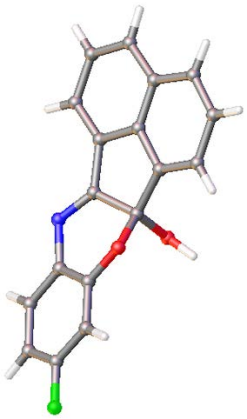

Table A20. Crystal data and structure refinement for 1886892.

Identification code	1886892
Empirical formula	$C_{18}H_{10}FNO_2$
Formula weight	291.27
Temperature/K	100.(2)
Crystal system	monoclinic
Space group	$P2_1/c$
a/Å	11.0114(4)
b/Å	10.6453(4)
c/Å	11.1461(4)
α/°	90
β/°	99.7050(10)
γ/°	90
Volume/Å^3	1287.84(8)
Z	4
ρ_{calc}g/cm^3	1.502
μ/mm^{-1}	0.902
F(000)	600.0
Crystal size/mm^3	0.190 × 0.080 × 0.080
Radiation	Cu Kα (λ = 1.54178)
2Θ range for data collection/°	8.14 to 148.92
Index ranges	$-13 \leq h \leq 13$, $-12 \leq k \leq 13$, $-13 \leq l \leq 13$
Reflections collected	30604
Independent reflections	2588 [R_{int} = 0.0497, R_{sigma} = 0.0241]
Data/restraints/parameters	2588/0/201
Goodness-of-fit on F^2	1.063
Final R indexes [I>=2σ (I)]	R_1 = 0.0422, wR_2 = 0.0958
Final R indexes [all data]	R_1 = 0.0456, wR_2 = 0.0988
Largest diff. peak/hole / e Å^{-3}	0.33/-0.22

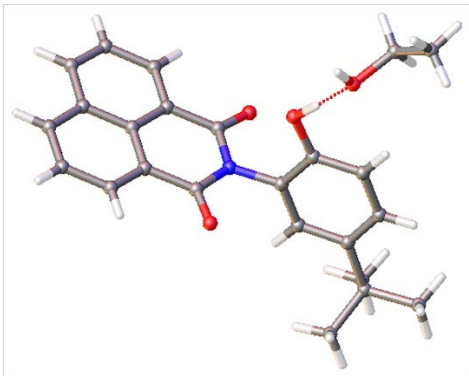

Table A21. Crystal data and structure refinement for 1986125.

Identification code	1986125
Empirical formula	$C_{24}H_{25}NO_4$
Formula weight	391.45
Temperature/K	182.(2)
Crystal system	triclinic
Space group	P-1
a/Å	7.6493(7)
b/Å	9.3682(9)
c/Å	15.2254(14)
α/°	88.3360(10)
β/°	89.5410(10)
γ/°	69.2070(10)
Volume/Å^3	1019.56(16)
Z	2
ρ_{calc}g/cm^3	1.275
μ/mm^{-1}	0.087
F(000)	416.0
Crystal size/mm^3	0.380 × 0.210 × 0.090
Radiation	Mo Kα (λ = 0.71073)
2Θ range for data collection/°	4.66 to 58.26
Index ranges	-10 ≤ h ≤ 10, -12 ≤ k ≤ 12, -20 ≤ l ≤ 20
Reflections collected	27759
Independent reflections	5486 [R_{int} = 0.0441, R_{sigma} = 0.0347]
Data/restraints/parameters	5486/0/274
Goodness-of-fit on F^2	1.073
Final R indexes [I>=2σ (I)]	R_1 = 0.0552, wR_2 = 0.1211
Final R indexes [all data]	R_1 = 0.0704, wR_2 = 0.1329
Largest diff. peak/hole / e Å^{-3}	0.31/-0.24

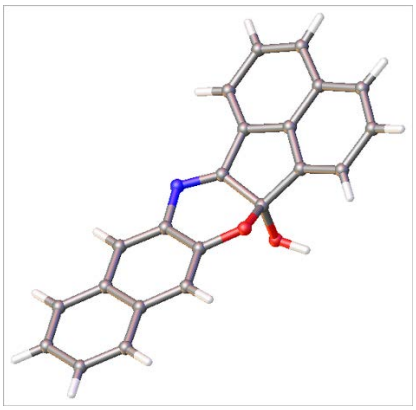

Table A22. Crystal data and structure refinement for 1886891.

Identification code	1886891
Empirical formula	$C_{22}H_{13}NO_2$
Formula weight	323.33
Temperature/K	100.(2)
Crystal system	monoclinic
Space group	$P2_1/c$
a/Å	8.9472(5)
b/Å	11.4780(6)
c/Å	14.7503(8)
α/°	90
β/°	95.515(2)
γ/°	90
Volume/Å^3	1507.78(14)
Z	4
ρ_{calc}g/cm^3	1.424
μ/mm^{-1}	0.734
F(000)	672.0
Crystal size/mm^3	0.170 × 0.040 × 0.020
Radiation	Cu Kα (λ = 1.54178)
2Θ range for data collection/°	12.58 to 145.18
Index ranges	$-11 \leq h \leq 10$, $-14 \leq k \leq 14$, $-18 \leq l \leq 17$
Reflections collected	27451
Independent reflections	2933 [R_{int} = 0.0580, R_{sigma} = 0.0304]
Data/restraints/parameters	2933/0/228
Goodness-of-fit on F^2	1.085
Final R indexes [I>=2σ (I)]	R_1 = 0.0449, wR_2 = 0.1311
Final R indexes [all data]	R_1 = 0.0460, wR_2 = 0.1325
Largest diff. peak/hole / e Å^{-3}	0.28/-0.28

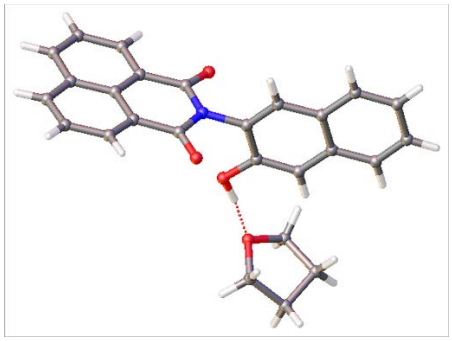

Table A23. Crystal data and structure refinement for 1886894.

Identification code	1886894
Empirical formula	$C_{26}H_{21}NO_4$
Formula weight	411.44
Temperature/K	100.(2)
Crystal system	triclinic
Space group	P-1
a/Å	7.9269(6)
b/Å	9.3762(7)
c/Å	15.1725(11)
α/°	102.052(4)
β/°	95.205(4)
γ/°	114.471(3)
Volume/Å^3	983.67(13)
Z	2
ρ_{calc}g/cm^3	1.389
μ/mm^{-1}	0.760
F(000)	432.0
Crystal size/mm^3	0.100 × 0.100 × 0.010
Radiation	Cu Kα (λ = 1.54178)
2Θ range for data collection/°	6.08 to 144.94
Index ranges	$-9 \le h \le 9$, $-11 \le k \le 11$, $-18 \le l \le 18$
Reflections collected	26937
Independent reflections	3860 [R_{int} = 0.0963, R_{sigma} = 0.0544]
Data/restraints/parameters	3860/0/283
Goodness-of-fit on F^2	1.093
Final R indexes [I>=2σ (I)]	R_1 = 0.0747, wR_2 = 0.2061
Final R indexes [all data]	R_1 = 0.0942, wR_2 = 0.2362
Largest diff. peak/hole / e Å^{-3}	0.41/-0.44